“Polymerizations in Surfactant-free Mesostructured Liquids”

Dissertation

zur Erlangung des Doktorgrades der Naturwissenschaften (Dr. rer. nat)

der Fakultät für Chemie und Pharmazie

der Universität Regensburg

vorgelegt von

Jonas Blahnik

aus Cham/Opf.

September 2023

"The most elementary and valuable statement in science, the beginning of wisdom, is 'I do not know.'"

Commander Data
in Star Trek: The Next Generation

The practical work of this thesis was performed from October 2019 to July 2023 at the Institute of Physical and Theoretical Chemistry at the University of Regensburg in the working group of Prof. Dr. Werner Kunz.

This work was supervised by Prof. Dr. Werner Kunz

Submission of the PhD thesis: 26.09.2023

Date of the oral exam: 15.11.2023

Examination Committee:

Chairman: Prof. Dr. Oliver Tepner

1st Examiner: Prof. Dr. Werner Kunz

2nd Examiner: Prof. Dr. Rainer Müller

3rd Examiner: Prof. Dr. Frank-Michael Matysik

Acknowledgments

The achievements made in the course of this PhD thesis would not have been possible without the valuable aid and support of numerous people:

First of all, I want to thank **Prof. Werner Kunz** for giving me the opportunity to carry out this interesting thesis at his institute and for his support during the work, whenever needed. Thanks for the possibility to work in his company SKH GmbH during my thesis, which gave me the opportunity to not only finance my thesis but also to learn a lot!

I want to thank also **Prof. Rainer Müller** for being my second referee and for his help with BET measurements. Thanks to **Prof. Frank-Michael Matysik** and **Prof. Oliver Tepner** for completing the examination board.

Furthermore, I want to thank **Dr. Eva Müller** for getting a second mentor during the time of this thesis concerning all kinds of questions. Thanks for many fruitful discussions and for an open ear whenever needed.

Thanks go to **Dr. Sebastian Krickl** for his help introducing the topic to me and for his advice and help during the writing of publications and our patent.

Further thanks belong to **Dr. Klaus Schmid** for all his help, concerning not only initiators, but also for bringing an industrial perspective to the topic. Thanks for numerous lunch and dinner meetings and our good discussions!

Thanks go to **Dr. Theresa Eder**, **Eva Schmid**, and **Prof. John Lupton** for the possibility to use their GPC device, and to **Prof. Reinhard Rachel** for letting me use his SEM.

I am deeply grateful to my colleagues **Dr. Theresa Höß**, **Dr. Marcel Flemming**, **Dr. Eva Müller,** and **Theresa Ferstl** from SKH GmbH for a great working atmosphere and their support whenever needed!

Thanks go to all members of the go2green network for interesting meegins, discussions, fruitful cooperations and their industrial perspective, which was sometimes very helpful. In particular, I would like to mention **Dr. Toine Biemans**, **Thomas Rathschlag**, and **Michael Kiehnel.**

I am thankful to my master and bachelor student sand research interns: **Jennifer Schuster**, **Chantal Walser**, **Selina Reigl**, **Diana Funkner**, **Natalie Olitzscher**, **Sebastian Bösl-Bichlmeier**, **Antonia**

Schmalhofer, **Sebastian Hof**, **Chiara Schmid**, **David Hennek**, **Andreas Kanygin**, **Hornela-Emma Mortoum-Defo**, **Yanyu Chen**, **Moritz Schweiger**, **Lea Sammet** and **Benedict Hofmann.**

I am grateful to the permanent and former members of our institute, namely our perfectly organized secretaries **Bianca Heiligtag, Steffi Meinel** and **Rosemarie Röhrl**, **Prof. Rainer Müller, Prof. Richard Buchner, Prof. Hubert Motschmann, Prof. Dominik Horinek, Dr. Didier Touraud Dr. Eva Müller, Dr. Johnny Hioe, Dr. Thomas Herl, Georg Berger, Hellmuth Schönsteiner**, **Theresa Ferstl, Daria Nieder** and **Franziska Wolf** for their help when needed and the pleasant working chlimate during the time I spent there.

Of course, I want to thank all my collegues at the chair of solution chemistry: **Moritz, Selina, Vanessa, Manu, Adrien, Lea, Nadja, Eva, Lena, Johannes, Johannes, Franz, Jutta, Patrick** and especially my former office collegues **Pierre**, **Max**, **Flo**, **Basti**, and **Jenny**.

I am especially grateful to all my friends who supported me whenever it was needed. In particular, I want to thank **Philipp Schmid**, **Evamaria Hofmann**, and **Nicole Heigl** for their friendship and constant support during our studies, from the first semester of the Bachelor course to the PhD.

Last but not least, my deepest thanks belong to my family for their love, care, and never-ending support. Especially to my father **Alfred,** his partner **Beate**, my girlfriend **Alina**, and in particular, I want to dedicate this work to my deceased mother **Sieglinde** in never-ending loving memory to her.

Thank you all very much!

Abstract

In industry, polymerizations are widely performed in conventional microemulsion systems. Using microemulsion or microsuspension techniques allows gaining control over the polymerization kinetics and polymer morphologies while undesirable effects can be suppressed. However, a drawback might be that the surfactant or auxiliaries remain in the polymer and can impact the resulting product. In this dissertation, surfactant-free microemulsions (SFMEs) are investigated as simple, mesostructured reaction media for free-radical polymerizations. The idea behind this approach is to work only with water and simple alcohols as hydrotropes that can be completely removed after the polymerization process (*e.g.,* by distillation).

After an introduction to the topic in the first chapter, a general proof-of-concept for surfactant-free microemulsion or microsuspension polymerization is presented using the monomer methyl methacrylate (MMA). It could be shown that by choosing surfactant-free, mesostructured systems, one can impact the polymerization kinetics and thus the conversion and weight average molar mass of the latter polymer. The third chapter expands the work to other industrial-relevant polymers and co-polymers, as well as longer-chain hydrotropes and polymerizable hydrotropes.

While chapters two and three focus mainly on polymerization kinetics, conversions, and obtained molar masses, the fourth chapter gives an overview of morphologies obtained. MMA and 2-hydroxyethyl methacrylate (HEMA) are used as monomers. It is proven that SFMEs can work as templates not only for powder-like but also for porous polymers. The obtained polymer morphologies are comparable to results from surfactant-based microemulsions.

Chapter five bridges the gap to surfactant-based microemulsions and first examines the effect of low surfactant concentrations on the phase behavior of SFMEs. Anionic surfactants like surfactant sodium dodecylsulfate (SDS) are shown to decrease the binodal significantly at quite low concentrations when mesostructuring is already present before addition. Nonionic surfactants, on the other side, do not impact the location of the binodal. On the contrary, the interplay between water, hydrotrope, and oil seems to determine the type of structuring (oil-in-water, bicontinuous, or inverse). Secondly, the impact of SDS and several electrolytes on polymerizable SFME systems and the derived polymers are investigated. The last chapter comprises a pre-study of the use of natural phenols and amino acids as photoinitiators. Some combinations of benzoic- or cinnamic acid derivates and amino acids show promising results for their use as Type II photoinitiators.

Zusammenfassung

Microemulsionen sind als Reaktionsmedium für freie radikalische Polymerisationen in der Industrie weit verbreitet. Suspensions- oder Emulsionsmethoden erlauben Kontrolle über die Polymerisationskinetik und die Morphologie der synthetisierten Polymere, während unerwünschte Effekte während der Polymerisation unterdrückt werden können. Ein Nachteil ist allerdings, dass die genutzten Tenside oder Hilfsstoffe im Polymer verbleiben und die Eigenschaften des späteren Produkts beeinträchtigen können. In dieser Dissertation werden tensidfreie Mikroemulsionen (SFMEs) als einfaches, mesostrukturiertes Reaktionsmedium für radikalische Polymerisationen untersucht. Die Idee hinter diesem Ansatz ist, nur mit Wasser und einfachen Alkoholen als Hydrotropen zu arbeiten, die nach der Polymerisation vollständig entfernt werden können (z.B. durch Destillation).

Nach einer Einführung in das Thema im ersten Kapitel wird ein Proof-of-Concept für die tensidfreie Mikroemulsions- oder Mikrosuspensionspolymerisation des Monomers Methylmethacrylat (MMA) vorgestellt. Durch die Wahl des SFME-Systems kann die Polymerisationskinetik und damit der Umsatz und die Molmasse des späteren Polymers beeinflusst werden. Das dritte Kapitel weitet den Proof-of-Concept auf andere industriell relevante Polymere und Co-Polymere sowie auf längerkettige Hydrotrope und polymerisierbare Hydrotrope aus.

Während sich die Kapitel zwei und drei hauptsächlich auf die Polymerisationskinetik konzentrieren, gibt das vierte Kapitel einen Überblick über die verschiedenen erreichbaren Morphologien. Als Monomere wurden MMA und 2-Hydroxyethylmethacrylat (HEMA) verwendet. Es konnte gezeigt werden, dass SFMEs nicht nur für pulverförmige, sondern auch für poröse Polymere als Template dienen können. Die Polymermorphologien sind mit denen aus klassischen, tensidbasierten Mikroemulsionen vergleichbar.

Das fünfte Kapitel schließt die Lücke zu konventionellen Mikroemulsionen und untersucht zunächst die Auswirkungen niedriger Tensidkonzentrationen auf das Phasenverhalten von SFMEs. Es wurde gezeigt, dass anionische Tenside wie Natriumdodecylsulfat (SDS) die Phasengrenze bereits bei niedrigen Konzentrationen deutlich verringern, wenn zuvor bereits ein mesostrukturiertes System vorhanden war. Nichtionische Tenside hingegen haben keinen Einfluss auf die Lage der Mischungslücke. Im Gegenteil, es scheint sogar, als ob das Zusammenspiel aus Wasser, Hydrotrop und Öl die Art der Strukturierung (Öl-in-Wasser, bikontinuierlich oder invers) bestimmt. Desweiteren wurde der Einfluss von SDS und verschiedenen Elektrolyten auf polymerisierbare SFME-Systeme und die darin hergestellten Polymere untersucht. Das letzte Kapitel

umfasst eine Vorstudie zur Nutzung von natürlichen Phenolen und Aminosäuren als Photoinitiatoren. Einige Kombinationen von Benzoesäure- oder Zimtsäurederivaten und natürlichen Aminosäuren zeigen vielversprechende Ergebnisse für deren Verwendung als Typ II-Photoinitiatoren.

List of Abbreviations

AA	Acrylic acid
ABS	Acrylonitrile-Butadiene-Styrene (Copolymer)
AC	Acrylonitrile
ATRP	Atom transfer radical (polymerization)
AZDN	Azobisisobutyronitrile
BCC	Di(4-*tert*-butyl-cyclohexyl)-peroxydicarbonate
BDE	Bond dissociation enthalpies
BET	Brunner-Emmett-Teller (Modell)
CMC	Critical micellar concentration
CP	Critical point
C12E10	Polyoxyethelene(10) dodecyl ether
COSMO-RS	Conductor like screening model for real solvents
CPR	Controlled living (polymerization)
Da	Dalton (= g mol^{-1})
DEGME	Diethylene glycol monomethyl ether
DCE	Dichloroethane
DGB	Diethylene glycol butyl ether
DLS	Dynamic light scattering
DLVO	Derjaguin-Landau-Verwey-Overbeek (Theory)
DPM	Dipropylene glycol methyl ether
ESI-MS	Electrospray ionization mass spectrometry
EtOH	Ethanol
GC	Gas chromatography
GPC	Gel permeation chromatography
HEMA	2-Hydroxyethyl methacrylate
IPA	*iso*-Propanol
IUPAC	International Union of Pure and Applied Chemistry
LED	Light emitting diode
MD	Molecular dynamics (simulation)
MEEKC	Microemulsion electrokinetic chromatography
MHC	Minimal hydrotropic concentration
MIB	Methyl isobutyrate
MMA	Methyl methacrylate
NADES	Natural deep eutectic solvents
NMR	Nuclear magnetic resonance (spectroscopy)
NPA	*n*-Propanol
O/W	Oil-in-water
P-	Poly- (to use together with monomer abbreviations)
PE	Polyethylene
PET	Polyethyleneterephthalate

PP	Polypropylene
PS	Persulfate
PTFE	Polytetrafluoroethylene
PUR	Polyurethane
RAFT	Reversible addition-fragmentation chain-transfer (polymerization)
RI	Refractive index
SANS	Small angle neutron scattering
SBME	Surfactant-based microemulsion
SDS	Sodium dodecyl sulfate
SEC	Size exclusion chromatography
SEM	Scanning electron microscopy
SFME	Surfactant-free microemulsion
SLES	Sodium lauryl ether sulfate
SLS	Static light scattering
SWAXS	Small/wide angle x-ray scattering
TBA	*tert*-Butyl alcohol
TEM	Transmission electron microscopy
THF	tetrahydrofurane
UV	Ultraviolett (wavelength)
VA	Vinyl alcohol
VAc	Vinyl acetate
VC	Vinyl chloride
VOC	Volatile Organic Compound
VIS	Visual (wavelength)
W/O	Water-in-oil

Contents

Acknowledgments i

Abstract iii

Zusammenfassung iv

List of Abbreviations vi

1 General Background 1

1.1 Preface 1

1.2 Microemulsions and Emulsions 4

1.2.1 Conventional Microemulsions and Emulsions 4

1.2.2 Surfactant-free Microemulsions and Emulsions 5

1.3 Radical Polymerizations 11

1.3.1 Polymers – An Overview 11

1.3.2 Free-radical Polymerizations 12

1.3.3 Advantages of Polymerizations in Organized Media 14

1.4 State of the Art 18

1.4.1 Applications of Surfactant-free Microemulsions 18

1.4.2 Polymerizations in Surfactant-free, Organized Media 19

1.5 Important Techniques Applied in this Thesis 21

1.5.1 Dynamic Light Scattering (DLS) 21

1.5.2 Conductivity Measurements and the Percolation Model 24

1.5.3 Gel Permeation Chromatography (GPC) 25

1.6 Bibliography 27

2 Surfactant-free Microemulsion and Microsuspension Polymerization of Methyl Methacrylate 31

2.1 Abstract and Preface 31

2.2 Introduction 33

2.3 Materials and Methods 35

2.3.1 Materials 35

2.3.2 Ternary Phase Diagrams 35

2.3.3 Critical Point Determination 35

2.3.4 Tie Line Determination 35

2.3.5 Dynamic Light Scattering (DLS) in SFME Systems 36

2.3.6 Conductivity Measurements 36

2.3.7 Microemulsion Polymerizations Followed by DLS 36

2.3.8 Microsuspension Polymerizations Followed by DLS 37

2.3.9 Further Polymerizations and Yield of Thermal Microsuspension Polymerizations ... 37
2.3.10 Gel Permeation Chromatography (GPC) ... 38
2.3.11 Viscosity and Density Measurements ... 38
2.3.12 Light Microscopy ... 38
2.4 Results ... 39
2.4.1 Structural Investigations of the Ternary System Water/Alcohols/MMA ... 39
2.4.2 Microemulsion Polymerization with PS and UV-initiated Microsuspension Polymerization with AZDN ... 41
2.4.3 Thermally Initiated Microsuspension Polymerization with BCC ... 42
2.5 Discussion ... 46
2.5.1 Structural Investigation of the Ternary Systems ... 46
2.5.2 Dissecting the Different Effects on Mean Molar Masses of Microsuspension Polymers ... 48
2.5.3 Conversion Yield ... 52
2.5.4 Impact of Mesostructuring ... 53
2.6 Conclusion and Outlook ... 55
2.7 Appendix ... 57
2.7.1 Composition of all Samples ... 57
2.7.2 Critical Points ... 57
2.7.3 Viscosity and Density Data and Calculated Hydrodynamic Radii ... 58
2.7.4 Ternary Phase Diagrams in Mol Fractions ... 59
2.7.5 Autocorrelation Functions derived by DLS ... 60
2.7.6 Conductivity Data ... 61
2.7.7 Macroscopic and Microscopic Images of Dried Polymers ... 63
2.7.8 Exemplary Evaluation of M_w by GPC ... 66
2.7.9 Exemplary Tie Line Determination ... 67
2.8 Bibliography ... 68
3 Industrially Relevant (Co)polymers and Hydrotropes for Use in SFME Polymerization ... 71
3.1 Abstract and Preface ... 71
3.2 Introduction ... 73
3.3 Materials and Methods ... 74
3.3.1 Materials ... 74
3.3.2 Ternary Phase Diagrams ... 74
3.3.3 Dynamic Light Scattering (DLS) of SFME Systems ... 74
3.3.4 Polymerizations ... 74

3.3.5 Gel Permeation Chromatography (GPC) 75
3.3.6 Monomer Ratios in the Copolymers by Nuclear Magnetic Resonance Spectroscopy (NMR) 75
3.4 Results and Discussion 76
3.4.1 Poly(vinyl acetate-co-acrylic acid) 76
3.4.2 Poly(vinyl acetate-co-methyl methacrylate) 81
3.4.3 Proof-of-concept: Vinyl Chloride (VC) 84
3.4.4 Proof-of-concept: Styrene and Acrylonitrile (AN) 86
3.4.5 Glycol Ethers as Hydrotropes for SFME Polymerizations 88
3.5 Conclusions 91
3.6 Appendix 92
3.6.1 System Poly(acrylic acid-co-vinyl acetate) 92
3.6.2 System Poly(vinyl acetate-co-methyl methacrylate) 94
3.6.3 System Vinyl Chloride/Dichloroethane 95
3.6.4 System Poly(styene-co-acrylonitrile) 96
3.6.5 System with Glycolethers as Hydrotropes 96
3.7 Bibliography 98
4 Surfactant-free Microemulsions (SFMEs) as a Template for Porous Polymer Synthesis .. 101
4.1 Introduction 103
4.2 Materials and Methods 105
4.2.1 Materials 105
4.2.2 Ternary Phase Diagrams 105
4.2.3 Critical Point Determination 105
4.2.4 Compositions of Phases and Tie Lines 106
4.2.5 Dynamic Light Scattering (DLS) of SFME Systems 106
4.2.6 Conductivity Measurements 106
4.2.7 Polymerizations 106
4.2.8 Light Microscopy 106
4.2.9 Scanning Electron Microscopy (SEM) 106
4.2.10 BET Adsorption Isotherms 107
4.3 Results 108
4.3.1 Structural Investigations of Ternary and Pseudo-ternary SFME Systems 108
4.3.2 Structural Investigations of the Reference Systems 113
4.3.3 Investigation of PMMA Polymers 113
4.3.4 Investigation of Poly(MMA-co-HEMA) Copolymers 115

4.4 Discussion 117
4.4.1 The Role of HEMA in Pseudo-ternary Systems 117
4.4.2 Investigation of (Pseudo-)Ternary Systems Before Polymerization 118
4.4.3 PMMA Polymers 119
4.4.4 PMMA-HEMA-Copolymers 121
4.4.5 Comparison of Polymerizations in SFME and Surfactant-based Microemulsions 122
4.5 Conclusions and Outlook 123
4.6 Appendix 124
4.6.1 Compositions of Samples Investigated in this Work 124
4.6.2 Ternary Phase Diagrams Given in Mol Fractions 126
4.6.3 DLS and Conductivity Data of the Pseudo-ternary Systems with HEMA 127
4.6.4 Investigation of the Reference System without HEMA 128
4.6.5 Polymers Derived from Ternary SFME Systems 129
4.6.6 Polymers Derived from Pseudo-ternary SFME Systems 133
4.6.7 Polymers Derived from Surfactant-based Reference Systems 137
4.7 Bibliography 140
5 The Impact of Additives on Surfactant-free Microemulsions and Polymerizations in Those 143
5.1 Preface and Abstract 143
5.2 Introduction 145
5.3 Materials and Methods 148
5.3.1 Materials 148
5.3.2 Ternary Phase Diagrams 148
5.3.3 Dynamic Light Scattering (DLS) 148
5.3.4 Critical Point Determination 148
5.3.5 Small-and-wide-angle X-ray Scattering (SWAXS) 149
5.3.6 Polymerizations and Yield Determination 149
5.3.7 Gel Permeation Chromatography (GPC) 149
5.4 Results and Discussion 150
5.4.1 Impact of SDS on SFMEs 150
5.4.2 Discussion – Impact of Surfactants on SFME 157
5.4.3 Impact of SDS and Electrolytes on Polymerizations in SFME 162
5.4.4 Discussion – Impact of SDS and Electrolytes on Polymerizations in SFME 174
5.5 Conclusion and Outlook 177
5.6 Bibliography 179

6 Natural Photoinitiator Systems for Polymerizations in SFMEs 181
6.1 Preface and Abstract 181
6.2 Introduction 183
6.3 Materials and Methods 184
6.3.1 Materials 184
6.3.2 Polymerizations 184
6.3.3 UV/Vis Spectroscopy 185
6.3.4 Gel Permeation Chromatography (GPC) 185
6.3.5 Bond Dissociation Enthalpies (BDE) 185
6.4 Results and Discussion 186
6.4.1 Screening of Different Phenols and Amines 186
6.4.2 Irradiation of Curcumin and Riboflavin with Visual Light 189
6.4.3 Further Investigation of More Effective Initiators with Different Amines 189
6.4.4 Comparison of Bond Dissociation Enthalpies (BDE) 190
6.5 Conclusion and Outlook 192
6.6 Appendix 193
6.6.1 Structures of Phenols and Amines Tested as Photoinitiators 193
6.6.2 UV/Vis Spectra of Investigated Phenols, Polyphenols, and Vitamins 195
6.7 Bibliography 197
7 Epilogue 199
7.1 Conclusion and Outlook 199
7.2 List of Scientific Contributions 205
7.2.1 List of Publications and Patents 205
7.2.2 List of Conference Contributions 205
7.3 Eidesstattliche Erklärung 207

1 General Background

1.1 Preface

Nowadays, polymers and plastics have a bad reputation among the public. [1; 2] Hardly a week passes without articles about “bad” plastics in newspapers. Those reports range from microplastics, pollution of plastic packaging in the oceans, bad chlorinated or fluorinated polymers, and so on. These reports are supplemented by demands where plastic should be banned or will even be banned. [3; 4] After all these reports, one could come to the conclusion that the world will be free of plastics in a couple of years.

This is obviously far from the reality in the industry and possibly wishful thinking of some non-scientists. From 2016 to 2021, the global demand for plastics increased from 350 Mt to 390 Mt. [5] Due to the fact that the Corona pandemic had still a major impact on the industry in the year 2021, this is especially remarkable. [6; 7]

While it certainly makes sense to replace disposable plastics (*e.g.,* shopping bags, staw necks, or packaging of takeaway food), future life will not be possible without more specialized polymers. This applies to goals like the energy transition and climate neutrality (*e.g.,* wind turbines or battery technology), but also to modern medical or high-tech products. But also packaging or coatings will not be possible without plastics or polymers in the near future. [8; 9]

Nevertheless, our use of plastics must become more sustainable. This defines a list of main challenges for modern research on polymers (without claiming to be complete): [10–13]

- Finding bio-based alternatives to petrol-based polymers and reducing the energy demand
- Recycling of used polymers, with the goal of coming close to a rate of 100%
- Designing less hazardous materials and production techniques
- Reducing pollution in the environment

This thesis aims to address all points mentioned above, except for the recycling of polymers. When dispersed or powder-like polymers are required, (micro-)emulsion or (micro-)suspension polymerizations in water are state-of-the-art (for a further description, see section 0). Dispersing the monomers and the growing polymers is either very energy-intensive or requires the addition of auxiliaries, surfactants, or protective colloids. Removing those substances is nearly impossible and extremely costly. Impurities like surfactants influence the properties of the subsequent polymer, which can have a negative effect on the desirable properties. In addition to the surfactants or protective colloids themselves, these contaminants can also enhance the release of small molecules, used as softeners, into the environment. [14; 15]

By making use of surfactant-free microemulsions (SFME) as a reaction medium for free-radical polymerizations, this thesis aims to show a surfactant- and protective-colloid-free alternative to conventional microemulsion or microsuspension polymerizations. By using simple and non-toxic alternatives like small-chain alcohols as hydrotropes, all substances are easily separated, *e.g.,* through distillation, and could be recycled up to 100% in an industrial process. This reduces pollution by process additives. Since surfactant-free microemulsions are thermodynamically stable, only a small amount of energy is required for homogenization. [16]

This thesis shows the use and influence of SFMEs as reaction media for free-radical polymerizations with different acrylic monomers. Even though the studies build on each other, the chapters are written in such a way that they can be read independently of each other. Thus, each Chapter is divided according to usual conventions into a Preface and Abstract, Introduction, Results, Discussion, and Conclusion part.

- **Chapter 1** provides an overview of surfactant-based as well as surfactant-free microemulsions, free-radical polymerizations, and important techniques and methods used in this work. A part of the work concerning SFME and their potential applications was published in the review article J. Blahnik, E. Müller, L. Braun, P. Denk, and W. Kunz, "Nanoscopic microheterogeneities or pseudo-phase separations in non-conventional liquids," *Current Opinion in Colloid & Interface Science,* **2022**, *57*, 101535 [16]

- **Chapter 2** presents the proof-of-concept on the use of SFME as a reaction medium for surfactant-free microemulsion and microsuspension polymerization of methyl methacrylate. Redox-induced, thermal, and UV-induced initiators are used. The interplay of mesostructuring, different hydrotropes, and the polymerization kinetics, as well as the latter polymer properties, are studied. This work was published in J. Blahnik, S. Krickl,

K. Schmid, E. Müller, J. Lupton, and W. Kunz, "Microemulsion and microsuspension polymerization of methyl methacrylate in surfactant-free microemulsions (SFME)," *Journal of Colloid and Interface Science* **2023**, *648*, 755-767. [17] Furthermore, the work is part of the patent W. Kunz, S. Krickl, J. Blahnik, and K. Schmid, "Microemulsion or microsuspension process for the production of a polymer dispersion, and polymer particles obtained by the process" *EP 20210203.4,* **2021**. [18]

- **Chapter 3** extends the proof-of-concept to further monomers and co-polymers, and other hydrotropes, with a focus on industrially relevant systems.
- **Chapter 4** gives a deeper insight into the morphologies of polymers derived from SFMEs and studies the use of SFMEs as reaction templates for porous polymeric material with potential use as filtration material. The study compares the results to polymers derived from conventional, surfactant-based microemulsions as templates. This work was published as J. Blahnik, J. Schuster, R. Müller, E. Müller, and W. Kunz, "Surfactant-free microemulsions (SFMEs) as a template for porous polymer synthesis," *Journal of Colloid and Interface Science* **2023**, *655*, 371-382. [19]
- **Chapter 5** studies the influence of different surfactants and electrolytes on SFMEs and the polymerization of methyl methacrylate in a microsuspension polymerization process. Parts of this work are considered to be published in the future.
- **Chapter 6** provides a proof-of-concept regarding the potential use of natural mono- and polyphenols as UV-initiators and natural amines as synergists. The work was a preliminary study, from which the ZIM project "bioinit" from the network "go2green" resulted, aiming toward a more sustainable and less toxic future in the coatings industry.
- **Chapter 7** gives a conclusion and an outlook of potential future work on this topic.

1.2 Microemulsions and Emulsions

1.2.1 Conventional Microemulsions and Emulsions

A conventional surfactant-based microemulsion (SBME) consists of water, oil, and a surfactant (and mostly also a cosurfactant). An amphiphilic substance is needed since water and oil are not miscible by themselves. Amphiphilic substances like surfactants have both hydrophilic and hydrophobic parts in their molecular structure. By accumulating at the oil-water interface, they are able to stabilize it. [20]

Above a certain surfactant concentration, monophasic, thermodynamically stable, and optically transparent microemulsions are formed (cf. **Figure 1.1** markings I-V). Multi-phasic systems, *e.g.,* emulsions, can be observed below this surfactant concentration (marking I). By adding a surfactant, an emulsion can be stabilized kinetically for a certain time period, mainly due to steric and/or electrostatic barrier effects. To create an emulsion, stirring is required. The structures formed are typically in a size range between 1 µm and 100 µm. However, the system is not thermodynamically stable, leading to coalescence and, thereby, phase separation of the emulsion after a certain period of time. A well-known example of an emulsion is vinaigrette, consisting of oil, vinegar (water-phase), mustard (containing amphiphiles), salt, and spices like pepper. [21–23]

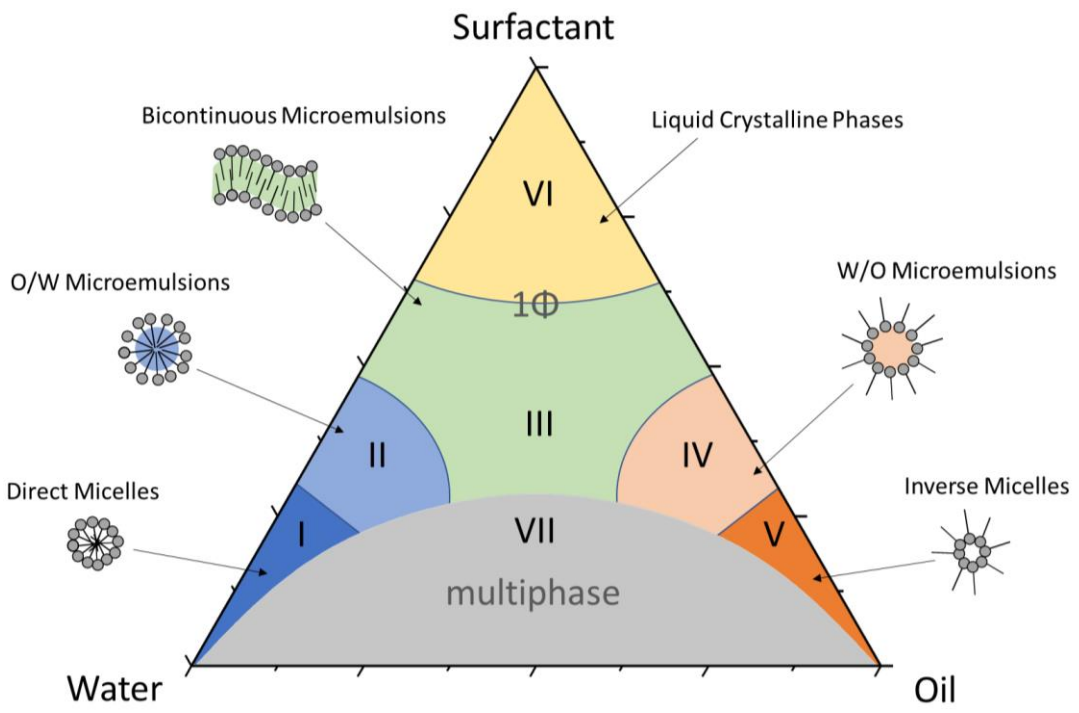

Figure 1.1 *Schematic drawing of a ternary phase diagram of water, oil, and a surfactant with different regions of structured solutions. A further description is provided in the text. The figure is inspired by S. Krickl. [24]*

The size range of structures in microemulsions is much lower compared to emulsions, typically between 5 nm and 100 nm. This is in the so-called mesoscopic scale (between molecular and macroscopic scale). Depending on the exact composition, several well-known types of structured liquids can be observed. As in emulsions, water- and oil-rich regions as well as bicontinuous structures, are known (cf. **Figure 1.1**). The probably most common morphology is the oil-in-water (O/W) microemulsion (cf. region II in **Figure 1.1**). Here, oil droplets are dispersed in an outer aqueous pseudo-phase. The analog region with water droplets dispersed in an outer pseudo-oil phase is called water-in-oil (W/O) microemulsion (cf. region IV in **Figure 1.1**). In between, a bicontinuous region can be found (cf. region III in **Figure 1.1**). Large three-dimensional networks of oil-rich and water-rich channels are observed. The transition between O/W, bicontinuous, and W/O microemulsions is fluent. By adding oil to O/W microemulsions, the droplets swell and get elongated until the first "infinite" channel can be observed. For all types of microemulsions, the surfactants are located at the oil-water interface, preventing both pseudo-phases from coalescing. It has to be noted that those structures in microemulsions are not static but very fluctuating. All structures disaggregate and re-form permanently. The interfaces have to be quite flexible to form a stable microemulsion. [24; 21–23]

Other mesoscale structures can be observed in the corners of the ternary phase diagram. On the water-rich side (cf. region I in **Figure 1.1**), micelles are built above the critical micelle concentration (CMC) of the surfactant due to self-organization. With increasing oil content, the micelles incorporate the hydrophobic molecules, and O/W microemulsions are formed. The corresponding aggregates in the oil-rich corner (cf. region V in **Figure 1.1**) are called inverse micelles (W/O microemulsions). In the region of high surfactant concentration, several liquid crystalline phases are known (existing in region VI in **Figure 1.1**). [24; 21–23] As those liquid crystals are not relevant to this work, it is renounced to go further into detail.

1.2.2 Surfactant-free Microemulsions and Emulsions

In surfactant-free microemulsions (SFMEs), hydrotropes are used as amphiphiles instead of surfactants. The term hydrotrope was introduced by Carl Neuberg in 1916 for a substance that is able to increase the solubilty of another organic compound in water. [25; 26] The transition between hydrotrope and surfactant is not clear-cut, which makes it difficult to draw a definite line. Commonly, substances with a carbon chain length of 8 or more is considered a surfactant. In the context of SFMEs, however, much shorter hydrotropes are conventinally used. Although there have been hints at mesoscopically structured mixtures of water, a hydrotrope and an oil since the 1970s [27–30], the colloidal community largely disregarded them. It was either argued

that the hydrotropes are already slightly amphiphilic and therefore structuring as real surfactants (in our opinion, a bad argument, *e.g.,* in the case of ethanol or propanol) or that this cannot be true because there is no molecule present to create a defined interfacial layer between the two pseudo-phases. The last argument is true; however, it was overlooked that even simple hydrotropes can accumulate at the interface between continuous pseudo-phase and mesoscopic aggregates formed by the second liquid that is not or only purely miscible with the first liquid. [31] As a result, the interface is not stabilized by the amphiphilic molecules and is thus highly dynamic and fluctuates. This can be of interest, *e.g.*, when compartmentation is required, for example, for chemical or biochemical reactions, but without hindering the transport of reacting species through the interface. That this is a favorable case is demonstrated for several enzymatic reactions. [32; 33]

Sometimes, the effect of mesoscopic compartmentation in water-oil-hydrotrope systems was called the "pre-Ouzo" effect. The "Ouzo effect" has been well-known for many years. [34–36] In fact, a mixture of water, anethole (the oil), and ethanol (the hydrotrope) can form very stable emulsions over a long time (up to months) when enough water is added to enter into the biphasic region of the phase diagram. Surprisingly, stability is achieved without any (or only very few) surfactants. While this effect today is more or less understood (in fact, there are several mechanisms that can be responsible for it [37; 38]), it was challenging to understand what happens in the ternary mixture when the composition is still in the monophasic region, *just before adding enough water* to see the Ouzo effect. Since, in this *pre-*Ouzo region, SFME has been detected, the effect has been termed the "pre-Ouzo" effect. It was only very recent that the relation between the pre-Ouzo and the Ouzo effect was described. [38]

Several studies were done to investigate the mechanism behind the stabilization in SFMEs. In the 1970s, SFMEs were postulated to explain observations like enzyme activities and the appearance of three optically clear domains in an analytical ultracentrifuge. [27; 28; 32] Only since more recent methods like dynamic (DLS) and static light scattering (SLS), density contrast variation in small-angle neutron scattering (SANS) combined with small-wide angle high-resolution X-ray scattering (SWAXS) as well as molecular dynamics (MD) simulation have found their way into SFME research, a structural determination was possible. [31; 39]

The system composed of water, ethanol (EtOH), and 1-octanol is, amongst others (cf. **Table 1.1**), currently the best-studied SFME system. It was investigated in detail in the last decade. Klossek *et al.* started research on this system by performing SLS and DLS experiments. They

found aggregates and calculated a size range of 2 nm (assuming spherical micelles). [40] Diat *et al.* found fatty alcohol-rich domains in the pre-Ouzo region in the exact same size using combined SANS and SWAXS measurements. [41] Schöttl *et al.*, as well as Lopian and coworkers, were able to check the previous results by predicting very similar scattering intensity data by MD simulations. [42; 43]

Table 1.1 *Overview of all SFME systems discussed in this section and methods used to characterize the systems.*

System	Methods	Reference
1-Hexane|2-Propanol|Water	Conductivity, fluorescence, Ultracentrifugation, ^{1}H-NMR, enzymatic activity	[27; 28; 30; 32; 44]
Toluene|2-Propanol|Water	Conductivity, ^{13}C-NMR, Light scattering, Ultracentrifugation	[29]
1-Octanol|Ethanol|Water	SANS, SWAXS, MD, SLS, DLS	[31; 40; 41; 43; 42]
Citriodiol|2-Propanol|Water	DLS, SLS	[31]
1-Hexane|1-Propanol|Water	Enzymatic activity	[33]
1-Hexane|*tert*-Butyl alcohol|Water	Enzymatic activity	[33]
Oleic acid|Solketal|Water	DLS	[45]
Triethyl citrate|Ethanol|Water	DLS	[45]
Eugenol|Ethanol|Water	DLS	[46]
Safflower oil|1-Octanol|Ethanol	DLS, SWAXS, Conductivity	[47]
Ethyl acetate|Sodium salicylate|Water	DLS, SWAXS, SANS	[48]
Limonene|Ethanol, 1-Propanol, 2-Propanol, *tert*-Butanol|Water	DLS, SWAXS, SANS, Conductivity	[49]
Benzyl alcohol|Ethanol, 1-Propanol, 2-Propanol, *tert*-Butyl alcohol|Water	DLS, SWAXS, SANS, Conductivity	[49]
Limonen|Aceton|Acetonitrile	DLS, COSMO-RS	[50]
Anisol|Ethanol, Aceton, Tetrahydrofurane|Water	DLS, COSMO-RS	[50]
Triacetin|Ethanol|Water	DLS, COSMO-RS	[51]
Triacetin|Diacetin|Water	DLS, COSMO-RS	[51]
1-Octen-3-ol|Ethanol|Water	Conductivity, Optical Density, DLS, TEM	[52]
Ethyl acetate|2-Propanol|Water	Conductivity, UV-VIS	[53]
Chlorobenzene|Methanol|Ethyleneglycol	Optical Microscopy	[54]
Dichloromethan|Ethanol|Water	-	[55]

As a side effect, those simulations lead to the probably most descriptive model image of mesoscale structures in SFME. **Figure 1.2** depicts the location of the pre-Ouzo region in the water/ethanol/octanol system and gives an insight into the distribution of the three different components in solution, leading to the mesoscale structures. As can be seen, the aggregates are much less well structured and geometrically defined as the micelles in classical microemulsions. This is a consequence of the much weaker or nearly absent stabilization of the interface due to the absence of true surfactants. As a consequence, the interfaces and the whole structures are even much more fluctuating than surfactant-based microemulsion pseudo-phases. This can be of interest for chemical reactions, where the diffusion of molecules through the "interfaces" must not be hindered.

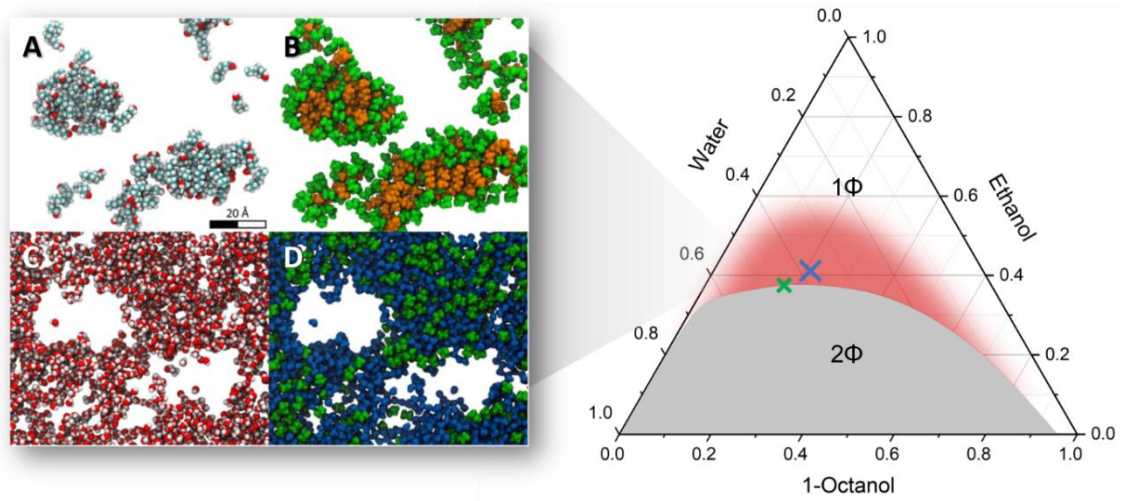

Figure 1.2 *Snapshots from molecular dynamics (MD) (left side) in the pre-Ouzo region. The red zone of the phase diagram (right side) marks the area where we can expect more or less defined SFME structures around the critical point (green cross). All MD snapshots are made at the marked blue point (octanol weight fraction x_E=0.2, water weight fraction x_W=0.39, ethanol weight fraction x_W=0.41). On the upper left (A), only octanol molecules are shown (white/red). On the upper right (B), the ethanol molecules (green) are printed, which interact strongly with the octanol molecules (orange), building the dispersed pseudo-phase. On the lower left (C), only water molecules are shown. The external water-rich pseudo-phase, consisting of water (blue) and ethanol (EtOH, green), is shown on the lower right (D). Snapshots from MD simulations are re-printed by Zemb et al. [31; 42]*

To describe the system thermodynamically, an extended Derjaguin, Landau, Verwey, Overbeek (DLVO) approach was chosen. [31] In a classical DLVO approach, van der Waals vs. electrostatics is considered. For microemulsions, entropic terms caused by fluctuations of diluted monolayers, considered solids [56], are included. Furthermore, by assuming vanishing interfacial film thickness, ultra-flexible microemulsions can be described. [57] Nevertheless, this state-of-the-art approach is not applicable to SFME. Neither electrostatic repulsion nor surfactants at the interface exist, which could control the water-oil interface. Thus, other driving forces have to be considered. Zemb *et al.* found an accurate model by comparing two contributions to the free energy

of the system: the mixing entropy, driving the system to smaller domains, with a term resulting from hydration forces between surfaces, using Gaussian random field theory. They found that the contribution of van der Waals forces is negligibly low (factor of 20 lower than the hydration-free energy) in the case of SFME, leading to a comparatively simple thermodynamic description. [31]

Even though first attempts were made using a model based on COSMO-RS theory, it is still not possible to predict the existence of pre-Ouzo clusters in ternary systems in every case. Up to now, many examples of ternary systems are known, which do – or do not – include a pre-Ouzo region. Examples of systems with a distinct pre-Ouzo region are water/ethanol/eugenol, water/solketal/oleic acid, or even water-free systems like ethanol/octanol/safflower oil. [45–47] On the other hand, in the system water/ethanol/ethyl acetate, which shows excellent solubility properties, no pre-Ouzo region, and no Ouzo effect either could be found. [48] It was thought that the organic solvent needs to be quite polar, and the biphasic region must not be too large. This is probably not true. When we compare the systems water/solketal/oleic acid to the system water/ethanol/ethyl acetate (cf. **Figure 1.3 a** and **b**), the first system with a large two-phase system shows distinct correlation functions in the expected pre-Ouzo region in DLS, whereas the second one with a small two-phase system does not. In the latter system, ethanol was replaced by the hydrotrope sodium salicylate. It comprises a second, liquid-solid biphasic region on the hydrotrope-rich corner of the phase diagram. While no pre-Ouzo region can be found in this system either, a new domain of density anomaly with pre-nucleation clusters can be observed in the one-phasic region near the liquid-solid phase border. [48]

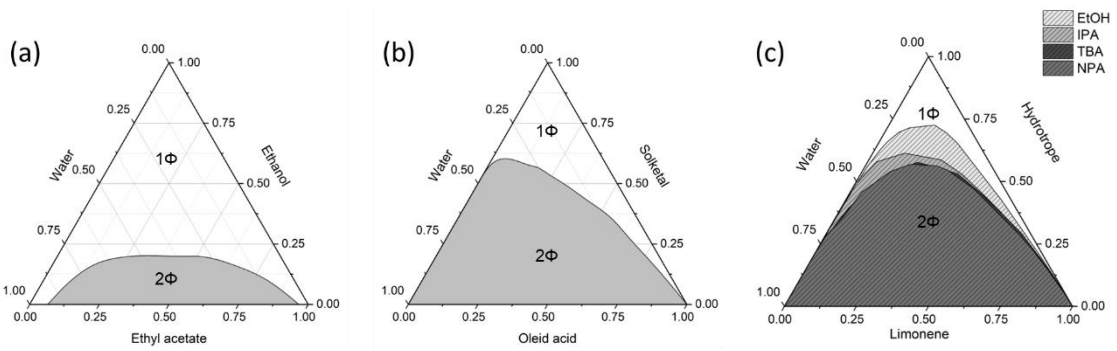

Figure 1.3 *Comparison of different ternary systems: (a) water/ethanol/ethyl acetate with a small two-phase region but no pre-Ouzo region, (b) the system water/solketal/oleic acid with a distinct pre-Ouzo region and (c) water/hydrotrope/limonene, where the hydrotrope Ethanol is not strong enough to form a pre-Ouzo region, whereas the hydrotropes iso-propanol, 1-propanol, and tert-Butyl alcohol do. All compositions are given in percent by weight. [45; 48; 49]*

Buchecker, Krickl *et al.* [49] studied the impact of the pre-structuring of alcohol-water mixtures on the mesoscale solubilization of a third hydrophobic component. EtOH and also *iso*-propanol (IPA) do not show structuring in binary mixtures with water, while *n*-propanol (NPA) and *tert*-butyl alcohol (TBA) do. The authors compared the four hydrotropes in ternary systems containing water and the oils benzyl alcohol and limonene, respectively. In the case of benzyl alcohol, the solubilization efficiency is best with ethanol as the hydrotrope. In other words, the two-phase region increases from EtOH to TBA. This fits with previous thoughts that structuring is induced by the addition of a third, poorly water-miscible component and that this is crucial for a pronounced solubilization power of the hydrotrope.

However, for limonene, it was found to be the other way around. While even no pre-Ouzo and a large two-phase region can be found for the hydrotrope ethanol, less hydrotrope is needed to solubilize limonene in water with tert-butyl alcohol or n-propanol (see **Figure 1.3 c**). Here, the distinct pre-structuring boosts the solubilization. Obviously, this is based on different mechanisms. It is proposed that the solubilization can take place either in a pseudo-bulk phase or in the pre-structured hydrotrope-water mixtures. This might be the case for more hydrophobic compounds like limonene. The second mechanism might be interface solubilization in the case of hydrophobic but still slightly amphiphilic compounds like benzyl alcohol or octanol. [49] Recently, a system was published which is not even able to form hydrogen bonds but still forms SFME. [50] This finding strengthens the assumption that different mechanisms can be responsible for mesoscale structuring.

Finally, a special feature of such SFME has to be pointed out: their structuring is very subtle, and the interactions responsible for it are of the order of 1 k_BT or even less. This point was extensively discussed in a special volume of COCIS. [58] Of course, such subtleties are difficult to grasp, to model, and to apply. On the other hand, we believe that this is one of the big challenges for modern science. Applications of SFMEs will be discussed in section 1.4.1.

1.3 Radical Polymerizations

1.3.1 Polymers – An Overview

The term "polymer" originates from the two Greek words *polys,* meaning "many," and *meros* meaning "part." J. Berzelius first used it in 1833 [59] but in the context of the novel concept of isomerism. In the 1840s and 1850s, organic chemistry started to develop. During this time, the word polymer was also used in the context of large molecules consisting of repeating subunits. Due to the muddle, H. Staudinger [60] introduced the word "macromolecule" in 1922. [61] Nowadays, the terms "polymer" and "macromolecule" are clearly defined by IUPAC [62] but are sometimes wrongly used as synonyms. A polymer is *"a substance composed of macromolecules"* by the definition of IUPAC. A macromolecule is defined as a *"molecule of high relative molecular mass."* It has a *"structure of which essentially comprises the multiple repetitions of units derived, actually or conceptually, from molecules of low relative molecular mass."* [62] Thus, a polymer is created by the reaction of many small molecules (called monomers). A polymer can be composed of macromolecules that consist of only one kind of monomer, whereas a copolymer consists of two or even more different monomers. A special case can be found in nature. Natural proteins can contain up to 20 different amino acids (called proteinogenic). The definition of a polymer includes a lot of different kinds of molecules of synthetic as well as of natural origin. Natural macromolecules include proteins, polysaccharides, polyisoprenes, nucleic acids, or melanin. Examples of synthetic polymers are nylons, synthetic rubber, fibrous glass, poly(ethylene) (PE), poly(styrene), poly(vinyl chloride) (PVC), or poly(methyl methacrylate) (PMMA). [63; 64] In this work, the focus will be on the latter group.

There are various techniques for the production of industrial polymers. In the following, we will shortly mention the most common ones. PE and poly(propylene) (PP) are produced by insertion polymerization. In this method, the polymerization is catalyzed by a metalorganic complex. This polymerization technique was investigated in 1953 by Karl Ziegler for ethylene and extended to propylene by Giulio Natta. Both received the Nobel Price in the year 1963 for their work. [65; 66] Polycondensation is a method that is even common in nature in the production of proteins, for example. Condensation reactions produce at least one side product, *e.g.*, water, ammonium, or HCl. [63] The first completely synthetic produced polymer, Bakelite, is a condensation polymer developed by Adolph von Baeyer in 1872. [67] Other industrially relevant examples are Nylon, Perlon, or polyethylene terephthalate (PET). [68; 69] Polyaddition forms polymers via individual independent addition reactions that will form a polymer chain at high conversions. In contrast to polycondensation, no side products are produced. Famous examples are

polyurethane (PUR), formed from isocyanates and alcohols, [70] or epoxy resins. [71] The last polymerization type worth mentioning is chain-growth polymerization, which is suitable for many vinyl monomers. The polymerization can take place radically or ionically. Examples of common polymers produced by chain-growth polymerizations are poly(styrene), PVC, PMMA, poly(vinyl acetate) (PVAc) or its cleaving product poly(vinyl alcohol) (PVA), as well as numerous copolymers or rubbers. [72; 63] Nowadays, many novel variants are known, *e.g.*, controlled radical polymerizations (CRP), living polymerization, atom transfer radical polymerization (ATRP), or reversible addition-fragmentation chain-transfer (RAFT) polymerization. [73] However, classical free-radical polymerization is still the most common one, which will be explained in more detail in the following section 1.3.2.

1.3.2 Free-radical Polymerizations

Free-radical polymerizations require the formation of initial radicals in the first step. Radicals are highly reactive compounds possessing an unpaired electron, produced by the decomposition of a starting reagent (called radical starter or initiator). Usually, at least one less stable bond is homolytically cleaved, forming radicals (see **Table 1.2 a**). Temperature-dependent decompositions follow a simple first-order kinetics, giving the decomposition rate k_d, which can be found in handbooks. [74] In industrial data sheets, mainly half-life temperatures are given instead of rate constants, commonly for 10 h, 1 h, and 10 min. [75] Industrial relevant initiators comprise peroxide-, peroxy carbonate-, or azo-functionalizations. While peroxides decompose directly, peroxy carbonates release CO_2, and azo-compound N_2 during decomposition. Other kinds of initiators produce radicals, *e.g.*, by irradiation with UV light or by a redox process.

A novel chain growth starts when the radical attacks the double bond of a vinylic monomer. A novel σ-bond is formed between the radical and one electron of the former π-bond of the monomer (cf. **Table 1.2 b**). The second electron of the former π-bond is now a radical, which can attack and add another monomer. (cf. **Table 1.2 c**). Some (mostly unwanted) side reactions may occur during a free-radical polymerization process. A recombination reaction forms a sigma bond between two radical species (see **Table 1.2 e**) and counts thus to termination reactions.

Transfer reactions (see **Table 1.2 f**), abstract an H-atom from any other molecule (*i.e.,* other polymer chains, solvents, monomers, and any other additive present in a polymerization process), leaving a radical on the second molecule where the H-atom was bound to formerly. The novel radical species may start further propagation reactions (which can lead to branched polymer chains when another polymer chain has been attacked) or react with other molecules

(which terminates the reaction). The rate of transfer reactions and the kind of reactions of the novel radical is extremely dependent on the environment in which the polymerization takes place. Additives with high transfer constants lead to shorter chain lengths due to many transfer reactions to the additive. This is called a chain regulating effect. [76; 74; 77]

Table 1.2 *Example reaction mechanisms of radical formation, propagation, termination, and transfer reactions that can occur during a free-radical polymerization process.*

Reaction	Reaction Mechanism	
Radical Formation	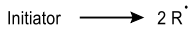	(a)
Propagation	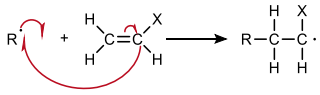	(b)
	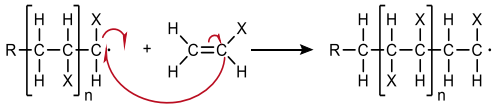	(c)
Termination	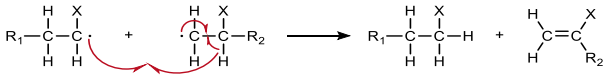	(d)
	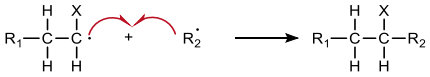	(e)
Transfer	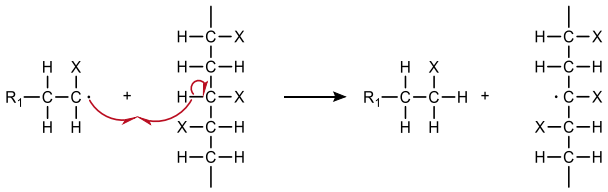	(f)

A special form of transfer reaction is elimination, which counts to termination reactions. When the H-atom is abstracted in α-position to an already existing radical, both radicals can form a novel π-bond on the molecule on which the proton has been abstracted (see **Table 1.2 e**). [74]

When more than one monomer is involved in the polymerization process, the variety of possible reactions will get higher. Even though most chemists will expect a statistical distribution of all monomers in a polymer chain, this is often not the case. Instead, gradient copolymers (with significant enrichment of one monomer either on one side of the polymer chain or at a certain

time of the polymerization process) can be formed due to different reactivities of the monomers. Other copolymers, like perfectly alternating ones, graft copolymers (with side chains consisting of another monomer), or block copolymers, are hardly produced by a one-step-one-batch free-radical mechanism. [78]

Table 1.3 *Reaction kinetics and rate constants for radical formation (k_d), propagation (k_p), termination (k_t), and transfer reactions ($k_{tr,X}$) that can occur during a free-radical polymerization process.*

Reaction	**Reaction kinetics and rate constant**	
Radical Formation	$v_d = -\frac{d[\text{initiator}]}{dt} = k_d \cdot [\text{initiator}]$	(1.1)
Propagation	$v_p = -\frac{d[\text{monomer}]}{dt} = k_p \cdot [\text{monomer}] \cdot [\text{radical species}]$	(1.2)
Termination	$v_t = -\frac{d[\text{radical species}]}{dt} = k_t \cdot [\text{radical species}]^2$	(1.3)
Transfer	$v_{tr} = \sum v_{tr,\ X} = \sum k_{tr,X} \cdot [\text{radical species}] \cdot [\text{transfer species X}]$ Transfer possible to X = monomers, polymers, initiators, solvents, additives,…	(1.4)

The kinetics of the most relevant reactions are listed in **Table 1.3** for radical decomposition (equation (1.1)), propagation (equation (1.2)), termination (equation (1.3)), and transfer (equation (1.4)). Rate constants for decomposition (k_d), propagation (k_p), termination (k_t), and transfer (k_{tr}), as well as copolymerization parameters, were a topic of many research works and can be found summarized in polymer handbooks. [74; 79]

1.3.3 Advantages of Polymerizations in Organized Media

The easiest way to carry out a polymerization process is in bulk, which works for liquid or liquified monomers. A huge problem of bulk polymerization is the so-called autoacceleration, gel effect, or Trommsdorff effect. [80–82] The exothermic polymerization, in combination with increasing viscosity due to the growing polymer chains, leads to inadequate heat dissipation, causing a fast increase in temperature. The increasing temperature increases both initiator decomposition and the polymerization reaction itself. Thus, the effect is – as the name autoacceleration suggests – amplifying itself and can, in the worst case, lead to reactor damage and even to explosions. [83; 78]

Thus, most free-radical polymerizations in industry need to be done either in solution or in aqueous media to avoid gel effects. Using unstructured, organic solutions would be the simplest way to overcome gel effects. However, many suitable solvents are toxic or at least environmentally questionable. If the polymer is not further processed in solution, separation from the solvent is usually very energy-intensive. [84] A special case of solution polymerization is precipitation polymerization, which occurs when the monomer is soluble in the solvent while the resulting polymer is not. [85]

Emulsions or microemulsions comprise very interesting compartments for polymerization. The oil-rich droplets act like little bulk reactors, in which the polymerization can proceed relatively undisturbed while the surrounding water ensures good heat dissipation (see schematic drawing in **Figure 1.4**). [63] Polymerization in emulsions is the most important process for producing polyacrylates and their copolymers in industry nowadays. [84]

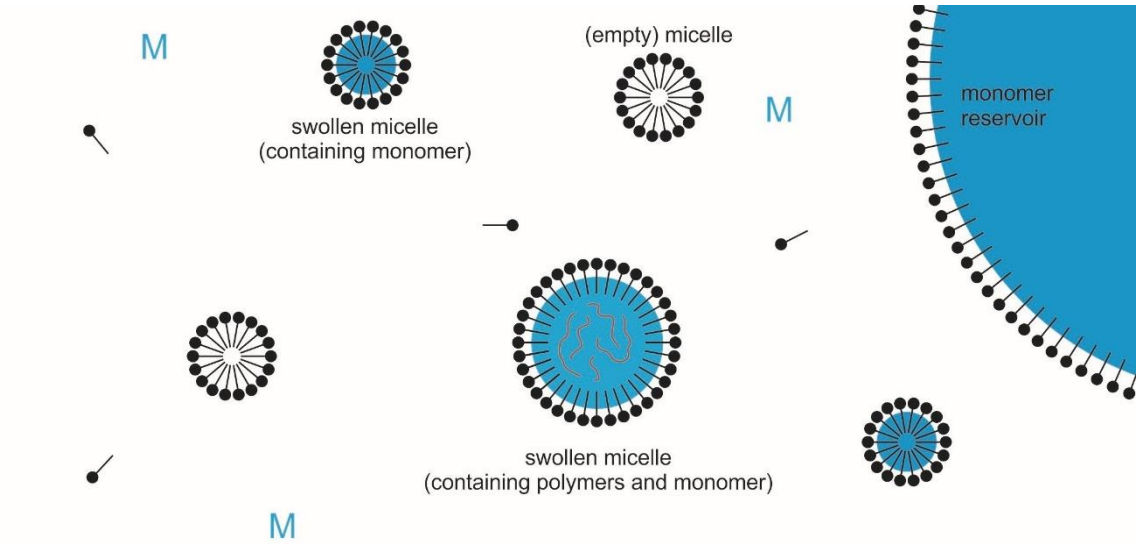

Figure 1.4 *A schematic drawing of an emulsion or suspension polymerization process with monomer reservoirs, empty micelles, and swollen micelles (containing both monomers and polymers). as well as free monomers (M) and surfactants in the aqueous phase. For microemulsion or microsuspension, the monomer reservoir is omitted. The graphic was inspired by Arshady et al. [85]*

We distinguish between emulsion, microemulsion, suspension, and microsuspension polymerizations, even though the systems in which the polymerizations take place are not too different. Emulsion and suspension polymerizations take place in thermodynamically unstable systems, which are mostly kinetically stabilized by surfactants or auxiliary colloids (*e.g.,* PVA, poly(ethylene oxide)/poly(propylene oxide)-(co)polymers, or cellulose esters, just to name a few). [84; 64] These systems require a high effort in homogenizing the reaction mixture. There are also processes without auxiliaries, which require even more stirring. The difference between emulsion and suspension processes lies in the chemical nature of the initiator used. When the

initiator is oil-soluble (*e.g.,* organic peroxides, percarbonates, or azo compounds), the process is called suspension polymerization, with direct conversion of the monomer droplets. In an emulsion process, the initiator is soluble in the water-rich phase (*e.g.,* inorganic persulfates), which divides the polymerization process into nucleation and growth, in which the active radical needs to diffuse from the water-rich to the monomer-rich phase. [85]

When the systems are thermodynamically stable before polymerization, they are called microemulsion or microsuspension polymerization, in line with the difference between emulsions and microemulsions in colloidal science. [74] It must be noticed that even microemulsion and microsuspension polymerizations will become thermodynamically unstable during the process due to growing polymer chains by 7-10 k_BT. [86; 87] It must, however, be noticed that emulsion, suspension, microsuspension, and microemulsion processes lead to polymers with different sizes and morphologies. In industry, it is, above all, the further use of the polymers that decides which process of manufacturing is chosen. While bulk or additive-free emulsion or suspension processes provide relatively pure polymers, these generally result in relatively coarse polymer granules. Suspension reactions also lead to relatively coarse material, while emulsions as well as microemulsions, and microsuspensions produce a finer morphology. [86; 88] From an industrial point of view, the morphology and size are especially relevant if the polymer is processed as plastisol (a colloidal dispersion of small polymer particles, liquid plasticizers, and additives like pigments, fillers, or propellants, if necessary). PVC must be mentioned as the most relevant polymer in this context. [88] Of course, processing the polymer as a polymer dispersion or latex itself requires the production in an emulsion or microemulsion, as well (*e.g.*, for paints). [84; 89]

From a scientific point of view, using self-organized media for polymerizations was a huge topic in the 1990s and 2000s and has slightly decreased since the 2010s. However, the topic is still of interest. Using self-organized media does not only impact polymerization kinetics, including the average molar mass (distribution) but impacts especially the morphology. Many systems like microemulsions, vesicular solutions or dispersions, lyotropic mesophases, or even inorganic compounds were already tested as templates for polymerizations. [90; 91] The variety of microemulsions (O/W, bicontinuous, or W/O, cf. section 1.2) alone is of interest. Even though a conventional microemulsion breaks during polymerization, the resulting polymer has a remarkable memory of the initial kind of template but in a larger size range (several hundred nanometers up to some micrometer instead of 5-50 nm for a typical microemulsion. [91; 86] This can be prevented when both the surfactant and cosurfactant are polymerizable and take place in the polymerization process. [92; 86] O/W microemulsions have been widely used in the polymer

industry for many years. Derived morphologies and particle sizes can be extremely important for application, as already mentioned above. [84] Template syntheses with bicontinuous or inverse microemulsions, on the other hand, have been discussed for producing porous material for filtration applications since the first publications but are not yet industrially applied to a large scale to our knowledge. However, using conventional microemulsions will always have the disadvantage of residues of surfactants or auxiliaries in the latter product, which can have an impact on the latter properties. [14] Imitating such a process in a surfactant-free environment might thus be advantageous for producing purer polymer and, thus, high-value products.

1.4 State of the Art

1.4.1 Applications of Surfactant-free Microemulsions

Surfactant-free microemulsions do already have some applications, although mesoscopic structuring has not been identified as the main prerequisite. The use of hydrotropes to solubilize pharmaceuticals was already mentioned back in 1916 by Carl Neuberg in the same paper in which he introduced the term "hydrotropy". [26; 25]

A common use of pre-Ouzo systems is providing a structured reaction medium for enzymatic reactions (cf. section 1.2.2). The most investigated system in this context consists of *n*-hexane, *iso*-propanol, and water. Several enzymes like trypsin, lipases or oxidases, and peroxidases have been used so far, just to name a few. [32; 33; 93] But also greener systems containing limonene and the hydrotropes NPA and TBA show a favorable correlation between mesoscale structuring in the SFME and the enzyme activity. [94]

Since SFMEs are known as potent solubilization media, their use for plant extraction suggests itself. Even though classical, organic, and petrol-based solvents like cyclohexane are still widely present, some first greener alternatives have been shown in the last years. [51; 52; 95; 96]

The first examples of the use of SFME for inorganic nanoparticle syntheses were recently published. [53–55] Nevertheless, there are hardly any examples known of the use of SFME as a mesostructured reaction medium for organic reactions [97], except for enzymatic ones. Hofmann [98] investigated the use of mesostructured media for catalyzed reactions. For many reactions, not mesostructuring itself but a balanced solubility might be the crucial factor. Krickl *et al.* showed that mesostructuring might even hinder some reactions. [99] However, SFME can also have advantages, especially in coupled reactions. Vanillin was recently produced in a process with only food-grade chemicals using a combination of the high extraction power of SFMEs in combination with photochemistry. [100] For the first time, a cascade reaction of a Heck reaction followed by an enzyme-catalyzed reaction could be reported in a surfactant-free system recently, performing better than a specially designed micellar system. [101]

A special application used SFMEs for microemulsion electrokinetic chromatography (MEEKC), a powerful analytical tool to separate neutral species. Using SFMEs instead of conventional microemulsions allowed the combination of MEEKC with electrospray ionization mass spectrometry (ESI-MS) for the first time, which is not compatible with conventional surfactants. [102]

As those first examples show, SFME can be a very promising alternative to conventional, surfactant-based microemulsions in many applications where subtle compartmentation is sufficient. By this, several advantages can be achieved: In comparison to surfactants, hydrotropes are usually not or only slightly surface-active and thus easy to separate (*e.g.*, by distillation in the case of short-chain alcohols). Considerably pure reaction products can be achieved without pollution by reaction auxiliaries. Hydrotropes are usually cheap, available in large amounts, and may avoid the possible ecotoxicity of surfactants. [103] Classical surfactant-based microemulsions are still mandatory when a structured reaction medium is needed with a well-defined and well-stabilized interface. [104] In the future, we expect that applications of SFME will develop in parallel to those of classical surfactant-containing microemulsions, depending on the importance of well-defined interfaces and depending on the possibly perturbing role of surfactants in them. We also note that there is a continuous cross-over from typical ternary hydrotropic mixtures to SFME and finally to classical microemulsions.

1.4.2 Polymerizations in Surfactant-free, Organized Media

Surfactant-free processes for polymerizations are not a completely new idea. Aside from solution processes, emulsion or suspension polymerizations can be performed completely without any surfactants or auxiliaries at all. However, these systems are extremely unstable and require high energy impacts to avoid instant coagulation of monomer droplets to complete phase separation. [88; 77] Using polymeric auxiliaries like PVA, poly(ethylene oxide)/poly(propylene oxide)-(co)polymers or cellulose esters might not be exactly the same as using a surfactant. However, also polymeric auxiliaries are somehow amphiphilic, stabilizing the interface and remaining in the final product, just like surfactants do. [78; 84]

Surfactant-free polymer dispersions are the first real surfactant-free systems that do not require intense homogenization or auxiliaries. However, having a closer look, these systems comprise a high amount of water-soluble monomers. Using monomers like acrylic acid, which can even be neutralized during or after polymerization, or sodium styrene sulfonate adds electrostatic stabilization. [105; 106] Thus, these polymers are amphiphilic and self-dispersing, acting similarly to surfactants and only suitable for special applications.

Recently, a surfactant-free Pickering system using cellulose nanocrystals as emulsifiers was reported. [107] This system does not comprise surfactants or polymeric amphiphiles and does also not produce those during the process. Thus, using a Pickering system might be the first real surfactant-free system, which comprises an organized medium and which is applicable for many industrially relevant monomers. Even though cellulose nanocrystals are biobased and non-toxic,

they will be incorporated in the polymeric material just like conventional auxiliaries, which reduces the advantage of being free of surfactants.

Ouzo and even the pre-Ouzo systems were already used to prepare polymeric materials. In most cases, this was done in a top-down instead of a bottom-up method. By dissolving the polymer in a suitable solvent, followed by solvent shifting, drop-like polymer particles can be generated. [37; 108–110] In the Ouzo region, a bottom-up method was recently published. [111]

Concerning SFMEs, there are a few first approaches to use them as a surfactant-free, organized medium for polymerizations. However, all these studies are very special and may not be generalizable. Yan *et al.* and Yao *et al.* deal with nanoencapsulation using polymerizable hydrotropes and non-polymerizable oils. The idea behind this work is to encapsulate hydrophobic drugs for pharmaceutical applications. [112; 113] Peng *et al.* synthesized PMMA nanodroplets in a system with water, MMA, and EtOH. [114] Two things make this work questionable: At first, they discussed that they used the Ouzo effect, even though the polymerization was done in the pre-Ouzo region. Secondly, they introduced a quite hydrophobic surface, onto which the (very few) formed nano lenses should adsorb. Even though this system is the closest to the ones used in this thesis, the outcome was extremely different. Mirhoseini *et al*. recently published an SFME system for the synthesis of PMMA/Ag nanocomposites. [115] The used system with 1-butanol as a hydrotrope is not really a balanced SFME system anymore, in our opinion, as the hydrotrope is not fully water-miscible. Finally, the probably oldest contribution of Raj *et al*. might be one of the most interesting ones concerning the idea of polymerizations in surfactant-free microemulsions. [116] They compared a system with MMA, acrylic acid (AA), water, and a cross-linker with and without a surfactant for the synthesis of porous materials.

In summary, there are already some examples of studies aiming to perform free-radical polymerizations in surfactant-free media. The few examples that are surfactant-free, mesostructured, using only hydrotropes as additives, are all for special applications. None of these publications so far claim to take a more general look at the subject or to even replace classical, industrial-relevant microemulsion or microsuspension polymerization processes.

1.5 Important Techniques Applied in this Thesis

1.5.1 Dynamic Light Scattering (DLS)

Dynamic light scattering (DLS) is a rapid method to determine aggregates, macromolecules, or mesoscale inhomogeneities in solution. [117–123] With the refractive index of the dispersed pseudo-phase and the viscosity of the continuous phase only, it is possible to determine the size of the dispersed particles or inhomogeneities. A typical size range is in the sub-micron region. [124] The measurement principle is based on the scattering of mostly monochromatic, coherent, and vertically polarised laser light on the dispersed pseudo-phase. This is due to the different refractive indices of the two phases. The incoming light is scattered in all directions in direct proportion to the refractive index difference. Due to Brownian motion, scattering centers move relatively to each other. This leads to time-dependent constructive and destructive interference, resulting in a fluctuation in the scattering intensity. [118] The smaller the particles, the faster they move and the more rapid the fluctuations.

The resulting Doppler-shift-spectrum is used in its Fourier-transformed form (autocorrelation form). Direct detection of the frequency shift (usually 10 Hz to several 1000 Hz) compared to the high frequency of the laser light (10^{14} Hz) is not trivial. Thus, the variations of the scattered light are analyzed by using the normalized autocorrelation function of intensity $g^2(\tau)$ by Fourier transformation.

The calculation is based on the theory of noise: [122]

$$g^2(\tau) = \frac{\langle I(t) \cdot I(t+\tau) \rangle}{\langle |I(t)| \rangle^2} \tag{1.5}$$

In **Equation (1.5)**, $I(t)$ and $I(t+\tau)$ are the measured intensities at an arbitrary time t and $t+\tau$ with the so-called decay time τ. Information about the size of the dispersed phases is accessible by the field correlation function $g^1(\tau)'$. It is related to the normalized autocorrelation function by the Siegert relation: [118]

$$g^2(\tau) - 1 = \beta \cdot |g^1(\tau)|^2 + C \tag{1.6}$$

Here, C and β are fit parameters to correct minor baseline drifts and account for the deviation from the ideal correlation. By assuming a large number of monodisperse particles, the correlation function $g^1(\tau)$ can be described as a single exponential decay function:

$$g^1(\tau) - 1 = A \cdot [1 + B \cdot exp(-2\Gamma\tau)] \tag{1.7}$$

In **Equation (1.7)**, variable A represents the baseline of the correlation function and B the intercept of the correlation function. The decay rate Γ is defined by the translational diffusion coefficient D and the scattering vector q: [118]

$$\Gamma = Dq^2 \tag{1.8}$$

$$q = \frac{4\pi n}{\lambda_0} sin\left(\frac{\theta}{2}\right) \tag{1.9}$$

In **Equation (1.9)** n is the refractive index, λ_0 is the wavelength of irradiated laser light, and θ is the scattering angle. Assuming spherical geometry of the dispersed particles, the diffusion coefficient calculated from **Equations (1.8)** and **(1.9)** can be related to the hydrodynamic radius R_H by using the Stokes-Einstein equation: [24]

$$D = \frac{k_B T}{6\pi\eta R_H} \tag{1.10}$$

Aside from this mono-exponential fitting procedure, the scattering data can be evaluated by cumulant analysis using a polynomial function in the exponent: [117; 118; 122]

$$ln\left(g^1(\tau)\right) = ln(B) + \sum_{n=0}^{N} K_n \frac{(-\tau)^n}{n!} \tag{1.11}$$

To avoid over-resolving the data, polynomials with n = 1, 2 or 3 are used in a standard cumulant analysis procedure. The cumulants K_n are directly related to the moments of the distribution function: K_1 describes the mean intensity, K_2 the width and K_3 the wryness of the distribution. The polydispersity index as a quality criterion for size distribution can be assumed by the fraction $\frac{K_2}{K_1}$. [24] The calculation of hydrodynamic radii via the Stokes-Einstein approach is scientifically correct. However, the assumption of spherical particles will only reflect the real system on very limited occasions. In contrast, the cumulant analysis is no scientifically accurate formula but a powerful tool to approximate the size and even the size distribution of the dispersed pseudo-phase.

Aggregates in SFMEs are usually highly fluctuating and of no well-defined shapes. Thus, both approaches have to be used carefully in this context. Results obtained measuring an SFME by means of DLS should be evaluated more qualitatively with regard to their decomposition rate

and decay time. As a rule of thumb, a higher intercept of the correlation function and larger lag times are assumed to represent more time-stable and more pronounced structures in solution. [49]

The schematic measurement principle of DLS is depicted in **Figure 1.5**. The left side **(a)** shows the measurement setup of a goniometer system. The laser light is focussed through a lens system towards a simple and the laser intensity is optimized by an attenuator. The laserbeam hits the sample in a thermostatted measurement cell, filled with toluene (as its refractive index is similar to glass). One or more detectors can be set to a certain angle θ referring to the incident beam of laser light, which is often 90° in DLS setups. The measured intensities of a medium to poorly scattering sample **(b)** and a strongly scattering sample **(d)** are depicted on the right side in **Figure 1.5**. Those fluctuations are automatically evaluated by the connected autocorrelator. Both, the intensity and the Fourier-transformed autocorrelation function **(c)** and **(e)** are transmitted from the autocorrelator to a computer.

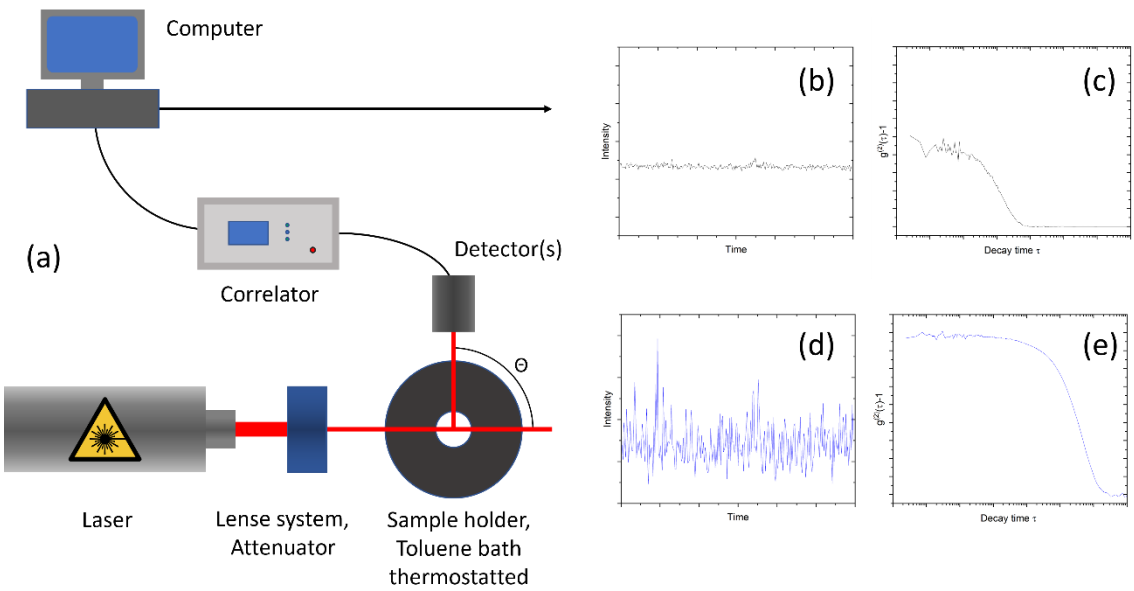

Figure 1.5 *Schematic measurement principle of DLS. (a) Instrument setup consisting of a laser, lense system, attenuator, sample holder, detectors, correlator, and computer. (b) Fluctuation intensity over a certain time scale and (c) the Fourier-transformed autocorrelation function of a medium to poorly scattering sample (black). (d) Fluctuation intensity and (e) Fourier-transformed autocorrelation function of a strongly scattering sample (blue).*

1.5.2 Conductivity Measurements and the Percolation Model

SBMEs as well as SFMEs can be of the three types O/W, bicontinuous, and W/O, as described in section 1.2.1. In any microemulsion, the charges of counterions of ionic surfactants as well as dissolved salts, will almost completely stay in the water-rich pseudo-phase. The oil-rich pseudo-phase is – depending on the nature of the ions – nearly free of charge. Surfactants – ionic and non-ionic – will stay at the interface between the water and the oil-rich pseudo-phase. The ion mobility in the water-rich pseudo-phase is essential for the electrical conductivity in a solution. Due to this fact, conductivity measurements are a good method to determine the structuring of microemulsions.

Figure 1.6 shows an example of the specific conductivity of a microemulsion as a function of the water volume fraction. This behavior was intensively studied in the late 1970s and can be explained with a percolation model. [125–129] Starting with a minimal water volume fraction and a fixed oil-to-surfactant ratio, only swollen, inverse micelles are existent. With increasing water content, spherical W/O microemulsions start to form. The ions are inside those swollen micelles.

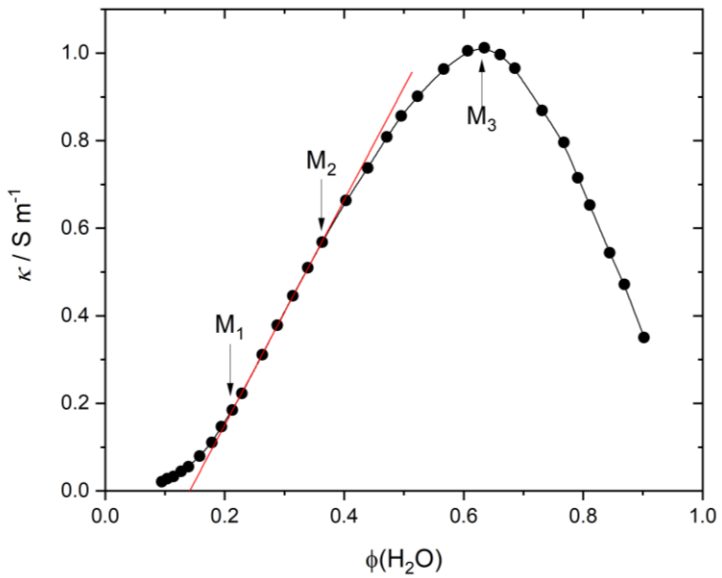

Figure 1.6 *Specific conductivity of a classical anionic SBME as a function of the water volume fraction.*

The exchange of charges can hardly exist because the micelles are far away from each other in the continuous oil phase. The only possibility of conducting electrical charge is the collision and regeneration of the inverse micelles. This behavior begins at point M_1. Up to point M_2, the micelles are swelling and approach a wormlike form. The outer phase is still oil, and the conductivity is still dependent on the collision and regeneration of those micelles. In this region, the specific conductivity is directly proportional to the water volume fraction and, thus the collision

cross-section of the elongated micelles. At water volume fractions above M_2, the slope starts to decrease. This indicates the first formation of an “infinite” cluster and the transition to bicontinuous structures. Beginning at this concentration, the ions are able to move directly through the formed water channels. The bicontinuous structures are enlarged up to the maximum conductivity at point M_3. From here, the dilution of the ions impacts the conductivity more than the enlarged water-rich structures. With water volume fractions above M_3, water-rich O/W microemulsions are formed. [130–134]

The first conductivity measurements of surfactant systems were performed using charged surfactants, which already provide sufficient load carriers. The concept was adapted soon to uncharged systems, adding small amounts of simple salts like NaCl or NaBr to ensure electric conductivity. [135] Buchecker *et al.* showed that conductivity measurements are an applicable technique for surfactant-free binary or ternary mixtures, as well. As the surfactant-free systems do not already bring charge carriers, additional electrolytes need to be added, like for conventional, nonionic microemulsions. It is not clarified yet whether a more detailed analysis (e.g., the existence of a percolation point) is possible in surfactant-free systems. However, conductivity curves lead to similar curves as for conventional systems, and a discussion based on the location of the maximum of the conductivity curve is surely reliable. [49]

1.5.3 Gel Permeation Chromatography (GPC)

Gel permeation chromatography (GPC) (also called size exclusion chromatography (SEC)) is a powerful tool for characterizing the molecular weights and molecular weight distribution of polymeric materials. [136; 137] Like any chromatographic method, GPC has a mobile and a stationary phase. The separation takes place due to the interaction between the diluted polymers in the mobile phase and the stationary phase. The stationary phase consists of porous polymer material. The smaller the hydrodynamic volume of a dissolved polymer, the higher is its ability to go inside the porous material. Thus, smaller polymers are slowed down more than larger polymers and shifted to higher retention volumes. This behavior is nearly linear over a high molecular mass range for modern GPC/SEC-columns. The column material can be chosen to fit the exact purpose. For example, styrene-divinylbenzene-copolymers are common for polymers in organic solvents, methylmethacrylate is used for water-soluble solvents, and silica columns are used for the separation of proteins. For determining the retention volume, an additional detector is required. Established detectors measure, for example, refractive index (RI), UV/VIS, viscosity, light scattering or electrical conductivity. The calibration of a GPC is realized by the measurement of polymers (usually polystyrene or PMMA standards for organic polymers) with well-

known, narrow size distributions. [138; 139] Thereby, the received data is evaluated, and three different mass values are given:

- M_n (number average molar mass) gives the number average value of the molecular masses. It is calculated simply by the arithmetic mean:

$$M_n = \frac{\sum_i N_i \, M_i}{\sum_i N_i} \tag{1.12}$$

- M_w (mass average molar mass) gives the weight average value of the molecular masses. It is calculated by the following equation:

$$M_w = \frac{\sum_i N_i M_i^2}{\sum_i N_i \, M_i} \tag{1.13}$$

- M_p (mass peak value) gives the molecular weight of the highest signal intensity of the chromatogram.

A schematic drawing of an exemplary GPC setup is depicted in **Figure 1.7**. The eluent is taken from the storage vessel and pumped into the computer-controlled autosampler. The sample can be injected through a loop, allowing a split injection. From there, the eluent is pumped through a pre-filter into the GPC/SEC-column system to prevent the column from being clogged by pollutions or badly dissolved polymers. One or more detectors are placed directly after the column. The different parts are connected by capillaries.

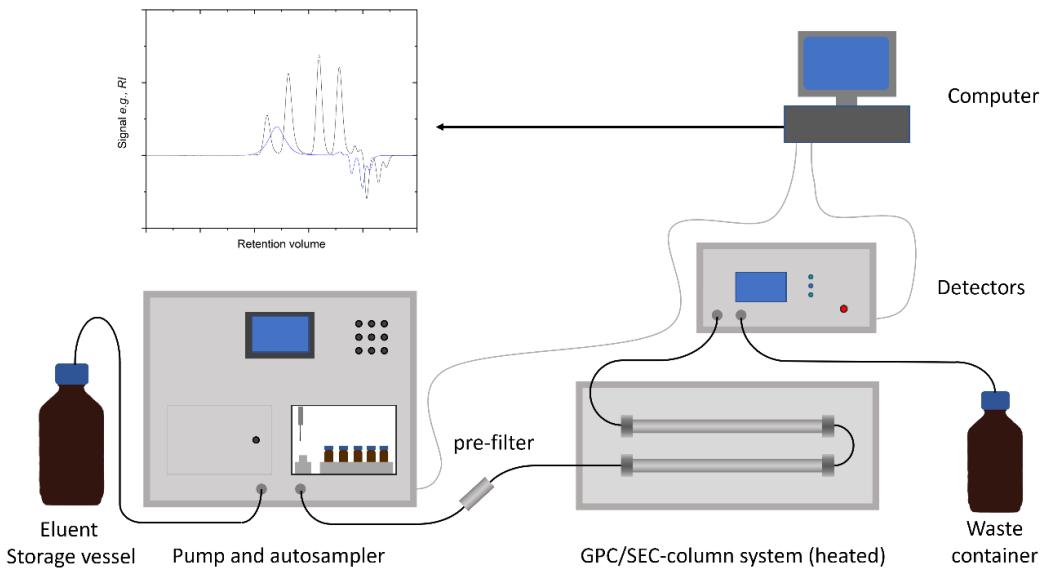

Figure 1.7 *Schematic drawing of a GPC setup consisting of an eluent storage vessel, pump and autosampler system, pre-filter, heated GPC/SEC-column system, detectors, and a waste container, as well as an example of two chromatograms.*

1.6 Bibliography

[1] J. L. Meikle, *Environmental History* **1997**, *2,* 278–300.
[2] S. Kahlert, and C. R. Bening, *Resour. Conserv. Recycl.* **2022**, *181,* 106279.
[3] T. Herberz, C. Y. Barlow, and M. Finkbeiner, *Sustainability* **2020**, *12,* 3746.
[4] *Turning the tide on single-use plastics,* Publications Office of the European Union, Luxembourg, **2021**.
[5] Plastics Europe, *Plastics - the Facts 2022,* www.plasticseurope.org, **2022**.
[6] *Impacts of the COVID-19 pandemic on EU industries,* **2021**.
[7] M. Iqbal, N. Ahmad, M. Waqas, and M. Abrar, *BJO&PM* **2021**, *18,* 1–17.
[8] S. Rhein, and M. Schmid, *Resour. Conserv. Recycl.* **2020**, *162,* 105063.
[9] *Sustainability in the plastics industry: concerns, issues, and strategies,* **2012**.
[10] J. Hopewell, R. Dvorak, and E. Kosior, *Philos. Trans. R. Lond., B, Biol. Sci.* **2009**, *364,* 2115–2126.
[11] Y. Chen, and S. Selvinsimpson, in: *Plastic and Microplastic in the Environment,* John Wiley & Sons, Ltd, **2022,** 205–221.
[12] R. M. Cywar, N. A. Rorrer, C. B. Hoyt, G. T. Beckham, and E. Y.-X. Chen, *Nat. Rev. Mater.* **2022**, *7,* 83–103.
[13] R. P. Babu, K. O'Connor, and R. Seeram, *Prog. Biomater.* **2013**, *2,* 8.
[14] S. Sakai, S. Urano, and H. Takatsuki, *Waste Management* **2000**, *20,* 241–247.
[15] E. L. Teuten, J. M. Saquing, D. R. U. Knappe, M. A. Barlaz, S. Jonsson, A. Björn, S. J. Rowland, R. C. Thompson, T. S. Galloway, R. Yamashita, D. Ochi, Y. Watanuki, C. Moore, P. H. Viet, T. S. Tana, M. Prudente, R. Boonyatumanond, M. P. Zakaria, K. Akkhavong, Y. Ogata, H. Hirai, S. Iwasa, K. Mizukawa, Y. Hagino, A. Imamura, M. Saha, and H. Takada, *Philos. Trans. R. Lond., B, Biol. Sci.* **2009**, *364,* 2027–2045.
[16] J. Blahnik, E. Müller, L. Braun, P. Denk, and W. Kunz, *COCIS* **2022**, *57,* 101535.
[17] J. Blahnik, S. Krickl, K. Schmid, E. Müller, J. Lupton, and W. Kunz, *J. Colloid. Interface Sci.* **2023**, *648,* 755–767.
[18] W. Kunz, S. Krickl, J. Blahnik, and K. Schmid. WO2022112481A1, **26.11.2021**.
[19] J. Blahnik, J. Schuster, R. Müller, E. Müller, and W. Kunz, *J. Colloid. Interface Sci.* **2024**, *655,* 371–382.
[20] D. Langevin, *Annu. Rev. Phys. Chem.* **1992**, *43,* 341–369.
[21] D. F. Evans und H. Wennerström, *Thecolloidal domain,* 2. Aufl., Wiley-VCH, New York, **op. 1999**.
[22] *Handbook of microemulsion science and technology,* CRC Press, Boca Raton, Florida, USA, **2019**.
[23] H.-D. Dörfler, *Grenzflächen und kolloid-disperse Systeme,* Springer, Berlin, **2002**.
[24] S. Krickl. Dissertation, Universität Regensburg, Regensburg, **2021**.
[25] J. Mehringer, and W. Kunz, *Adv. Colloid Interface Sci.* **2021**, *294,* 102476.
[26] C. Neuberg, *Biochem. Z.* **1916,** 107–108.
[27] N. F. Borys, S. L. Holt, and R. E. Barden, *J. Colloid. Interface Sci.* **1979**, *71,* 526–532.
[28] B. A. Keiser, D. Varie, R. E. Barden, and S. L. Holt, *J. Phys. Chem.* **1979**, *83,* 1276–1280.
[29] G. Lund, and S. L. Holt, *J. Am. Oil Chem. Soc.* **1980**, *57,* 264–267.
[30] G. D. Smith, C. E. Donelan, and R. E. Barden, *J. Colloid. Interface Sci.* **1977**, *60,* 488–496.
[31] T. N. Zemb, M. Klossek, T. Lopian, J. Marcus, S. Schöettl, D. Horinek, S. F. Prevost, D. Touraud, O. Diat, S. Marčelja, and W. Kunz, *Proc. Natl. Acad. Sci. U. S. A.* **2016**, *113,* 4260–4265.
[32] Y. L. Khmelnitsky, R. Hilhorst, and C. Veeger, *Eur. J. Biochem.* **1988**, *176,* 265–271.

[33] M. Zoumpanioti, M. Karali, A. Xenakis, and H. Stamatis, *Enzyme Microb.* **2006**, *39,* 531–539.
[34] S. A. Vitale, and J. L. Katz, *Langmuir* **2003**, *19,* 4105–4110.
[35] Z. Lu, H. Xu, H. Zeng, and X. Zhang, *Langmuir* **2015**, *31,* 12120–12125.
[36] F. Ganachaud, and J. L. Katz, *ChemPhysChem* **2005**, *6,* 209–216.
[37] R. Botet, and K. Roger, *COCIS* **2016**, *22,* 108–112.
[38] S. Prévost, S. Krickl, S. Marčelja, W. Kunz, T. Zemb, and I. Grillo, *Langmuir* **2021**, *37,* 3817–3827.
[39] K.-V. Schubert, R. Strey, S. R. Kline, and E. W. Kaler, *J. Chem. Phys.* **1994**, *101,* 5343–5355.
[40] M. L. Klossek, D. Touraud, T. Zemb, and W. Kunz, *ChemPhysChem* **2012**, *13,* 4116–4119.
[41] O. Diat, M. L. Klossek, D. Touraud, B. Deme, I. Grillo, W. Kunz, and T. Zemb, *J. Appl. Crystallogr.* **2013**, *46,* 1665–1669.
[42] S. Schöttl, J. Marcus, O. Diat, D. Touraud, W. Kunz, T. Zemb, and D. Horinek, *Chem. Sci.* **2014**, *5,* 2949–2954.
[43] T. Lopian, S. Schöttl, S. Prévost, S. Pellet-Rostaing, D. Horinek, W. Kunz, and T. Zemb, *ACS Cent. Sci.* **2016**, *2,* 467–475.
[44] Y. L. Khmelnitsky, A. van Hoek, C. Veeger, and A. J. W. G. Visser, *J. Phys. Chem.* **1989**, *93,* 872–878.
[45] S. Krickl, L. Jurko, K. Wolos, D. Touraud, and W. Kunz, *J. Mol. Liq.* **2018**, *271,* 112–117.
[46] A. Lucia, P. G. Argudo, E. Guzmán, R. G. Rubio, and F. Ortega, *Colloids Surf. A.* **2017**, *521,* 133–140.
[47] T. Shenavaei Zare, A. Khoshsima, and B. ZareNezhad, *Energy Fuels* **2020**, *34,* 4643–4659.
[48] A. El Maangar, P. Degot, V. Huber, J. Causse, P. Berthault, D. Touraud, W. Kunz, and T. Zemb, *J. Mol. Liq.* **2020**, *310,* 113240.
[49] T. Buchecker, S. Krickl, R. Winkler, I. Grillo, P. Bauduin, D. Touraud, A. Pfitzner, and W. Kunz, *Phys. Chem. Chem. Phys.* **2017**, *19,* 1806–1816.
[50] M. Hahn, S. Krickl, T. Buchecker, G. Jošt, D. Touraud, P. Bauduin, A. Pfitzner, A. Klamt, and W. Kunz, *Phys. Chem. Chem. Phys.* **2019**, *21,* 8054–8066.
[51] P. Degot, V. Huber, E. Hofmann, M. Hahn, D. Touraud, and W. Kunz, *Food chemistry* **2021**, *336,* 127660.
[52] X. Zhang, M. Song, J. Chai, X. Cui, and J. Wang, *J. Mol. Liq.* **2020**, *300,* 112278.
[53] X. Cui, J. Wang, X. Zhang, Q. Wang, M. Song, and J. Chai, *Langmuir* **2019**, *35,* 9255–9263.
[54] H. S. Tarkas, D. M. Marathe, M. S. Mahajan, F. Muntaser, M. B. Patil, S. R. Tak, and J. V. Sali, *Mater. Res. Express* **2017**, *4,* 25018.
[55] Y. Wu, L. Tang, Q. Zhang, F. Kong, and Y. Bi, *Materials Letters* **2021**, *285,* 129053.
[56] W. Helfrich, *J. Phys. France* **1985**, *46,* 1263–1268.
[57] S. A. Safran, D. Roux, M. E. Cates, and D. Andelman, *Phys. Rev. Lett.* **1986**, *57,* 491–494.
[58] T. Zemb, and W. Kunz, *COCIS* **2016**, *22,* 113–119.
[59] J. Berzelius, *Jahresbericht über die Fortschritte der physischen Wissenschaften* **1833**, *1833,* 63–67.
[60] H. Staudinger, and J. Fritschi, *Helv. Chim. Acta* **1922**, *1922,* 785–806.
[61] W. B. Jensen, *J. Chem. Educ.* **2008**, *85,* 624.
[62] V. Gold, *The IUPAC Compendium of Chemical Terminology,* IUPAC, Research Triangle Park, NC, **2019**.
[63] M. Brahm, *Polymerchemie kompakt,* 3. Aufl., S. Hirzel Verlag, Stuttgart, **2016**.
[64] M. D. Lechner, K. Gehrke und E. H. Nordmeier, *Makromolekulare Chemie,* Springer Berlin Heidelberg, Berlin, Heidelberg, **2014**.

[65] L. L. Böhm, *Angew. Chem. Int. Ed.* **2003**, *42,* 5010–5030.
[66] K. Soga, *Prog. Polym. Sci.* **1997**, *22,* 1503–1546.
[67] D. Crespy, M. Bozonnet, and M. Meier, *Angew. Chem. Int. Ed.* **2008**, *47,* 3322–3328.
[68] U. K. Thiele, *Int. J. Polym. Mater* **2001**, *50,* 387–394.
[69] J. Jewkes, D. Sawers, and R. Stillerman, in: *The Sources of Invention,* Palgrave Macmillan, London, **1969,** 275–278.
[70] J. O. Akindoyo, M. D. H. Beg, S. Ghazali, M. R. Islam, N. Jeyaratnam, and A. R. Yuvaraj, *RSC Adv.* **2016**, *6,* 114453–114482.
[71] F.-L. Jin, X. Li, and S.-J. Park, *J. Ind. Eng. Chem.* **2015**, *29,* 1–11.
[72] S. Koltzenburg, *Polymere: Synthese, Eigenschaften und Anwendungen,* Springer Spektrum, Berlin, Heidelberg, **2014**.
[73] K. Parkatzidis, H. S. Wang, N. P. Truong, and A. Anastasaki, *Chem* **2020**, *6,* 1575–1588.
[74] *Polymer handbook,* 4. Aufl., Wiley, New York, **1999**.
[75] PERGAN, *PEROXAN BCC Technical Datasheet,* **2022**.
[76] M. R. Billany, K. Khatib, M. Gordon, and J. K. Sugden, *Int. J. Pharm.* **1996**, *137,* 143–147.
[77] D. Colombani, *Prog. Polym. Sci.* **1997**, *22,* 1649–1720.
[78] H. Tobita, in: *Ullmann's encyclopedia of industrial chemistry,* Wiley-VCH, Weinheim, Wiley online library, **2010,** 1–50.
[79] *Modern plastics handbook,* McGraw-Hill Education; McGraw Hill, New York, N.Y., **2000**.
[80] B. O'Shaughnessy, and J. Yu, *Macromolecules* **1994**, *27,* 5067–5078.
[81] R. G. W. NORRISH, and R. R. SMITH, *Nature* **1942**, *150,* 336–337.
[82] V. E. Trommsdorff, H. Köhle, and P. Lagally, *Makromol. Chem.* **1948**, *1,* 169–198.
[83] G. A. O'Neil, M. B. Wisnudel, and J. M. Torkelson, *Macromolecules* **1996**, *29,* 7477–7490.
[84] E. Penzel, in: *Ullmann's encyclopedia of industrial chemistry,* Wiley-VCH, Weinheim, Wiley online library, **2010**.
[85] R. Arshady, *Colloid. Polym. Sci.* **1992**, *270,* 717–732.
[86] M. Antonietti, R. Basten, and S. Lohmann, *Macremol. Chem. Phys.* **1995**, *196,* 441–466.
[87] F. M. Pavel, *J. Dispers. Sci. Technol.* **2004**, *25,* 1–16.
[88] *PVC handbook,* 1. Aufl. (Hrsg.: C. E. Wilkes, J. W. Summers, C. A. Daniels und M. T. Berard), Hanser Gardner; Hanser, Cincinnati, Ohio, Munich, **2005**.
[89] *Wässrige Polymerdispersionen,* Wiley-VCH, Weinheim, **1999**.
[90] H.-P. Hentze, and E. W. Kaler, *COCIS* **2003**, *8,* 164–178.
[91] H. Hentze, and M. Antonietti, *Curr. Opin. Solid State Mater Sci.* **2001**, *5,* 343–353.
[92] T. D. Li, L. M. Gan, C. H. Chew, W. K. Teo, and L. H. Gan, *Langmuir* **1996**, *12,* 5863–5868.
[93] A. Xenakis, M. Zoumpanioti, and H. Stamatis, *COCIS* **2016**, *22,* 41–45.
[94] S. Krickl, D. Touraud, P. Bauduin, T. Zinn, and W. Kunz, *J. Colloid. Interface Sci.* **2018**, *516,* 466–475.
[95] V. Huber, L. Muller, P. Degot, D. Touraud, and W. Kunz, *Food chemistry* **2021**, *355,* 129624.
[96] V. Huber, L. Muller, J. Hioe, P. Degot, D. Touraud, and W. Kunz, *Molecules* **2021**, *26*.
[97] B. A. Keiser, and S. L. Holt, *Inorg. Chem.* **1982**, *21,* 2323–2327.
[98] E. Hofmann. Dissertation, Universität Regensburg, Regensburg, **2023**.
[99] S. Krickl, T. Buchecker, A. U. Meyer, I. Grillo, D. Touraud, P. Bauduin, B. König, A. Pfitzner, and W. Kunz, *Phys. Chem. Chem. Phys.* **2017**, *19,* 23773–23780.
[100] E. Hofmann, P. Degot, D. Touraud, B. König, and W. Kunz, *Food chemistry* **2023**, *417,* 135944.
[101] E. Hofmann, L. Schmauser, J. Neugebauer, D. Touraud, F. Gallou, and W. Kunz, *J. Chem. Eng.* **2023,** 144599.

[102] U. Mohorič, A. Beutner, S. Krickl, D. Touraud, W. Kunz, and F.-M. Matysik, *Anal. Bioanal. Chem.* **2016**, *408,* 8681–8689.
[103] W. Hou, and J. Xu, *COCIS* **2016**, *25,* 67–74.
[104] M. Giedyk, R. Narobe, S. Weiß, D. Touraud, W. Kunz, and B. König, *Nat. Catal.* **2020**, *3,* 40–47.
[105] M. Elrebii, and S. Boufi, *J. Ind. Eng. Chem.* **2014**, *20,* 3631–3638.
[106] S. Bilgin, S. Bahraeian, M. L. Liew, R. Tomovska, and J. M. Asua, *Prog. Org. Coat.* **2022**, *162,* 106591.
[107] J. Glasing, P. G. Jessop, P. Champagne, W. Y. Hamad, and M. F. Cunningham, *Langmuir* **2020**, *36,* 796–809.
[108] B. Guo, E. Middha, and B. Liu, *ACS Nano* **2019**, *13,* 2675–2680.
[109] J. Aubry, F. Ganachaud, J.-P. Cohen Addad, and B. Cabane, *Langmuir* **2009**, *25,* 1970–1979.
[110] M. Beck-Broichsitter, J. Nicolas, and P. Couvreur, *Nanoscale* **2015**, *7,* 9215–9221.
[111] H. Kempe, and M. Kempe, *J. Colloid. Interface Sci.* **2022**, *616,* 560–570.
[112] X. Yan, P. Alcouffe, G. Sudre, L. David, J. Bernard, and F. Ganachaud, *Chem. Commun. (Camb.)* **2017**, *53,* 1401–1404.
[113] Y. Yao, C. Li, F. Liu, P. Zhao, Z. Gu, and S. Zhang, *Phys. Chem. Chem. Phys.* **2019**, *21,* 10477–10487.
[114] S. Peng, C. Xu, T. C. Hughes, and X. Zhang, *Langmuir* **2014**, *30,* 12270–12277.
[115] B. Sadat Mirhoseini, and A. Salabat, *J. Mol. Liq.* **2021**, *342,* 117555.
[116] W. R. P. Raj, M. Sasthav, and H. M. Cheung, *Langmuir* **1991**, *7,* 2586–2591.
[117] R. Pecora, *J. Nanopart. Res.* **2000**, *2,* 123–131.
[118] L. Øgendal, *Light Scattering Demystified Theory and Practice,* **2013**.
[119] T. Nicolai, W. Brown, and R. Johnsen, *Macromolecules* **1989**, *22,* 2795–2801.
[120] Å. Jamting, J. Cullen, V. A. Coleman, M. Lawn, J. Herrmann, J. Miles, and M. J. Ford, *Adv. Powder Technol.* **2011**, *22,* 290–293.
[121] C. M. Hoo, N. Starostin, P. West, and M. L. Mecartney, *J. Nanopart. Res.* **2008**, *10,* 89–96.
[122] P. A. Hassan, S. Rana, and G. Verma, *Langmuir* **2015**, *31,* 3–12.
[123] L. M. Gugliotta, Vega, JR, and G. R. Meira, *J. Colloid. Interface Sci.* **2000**, *228,* 14–17.
[124] Malvern Instruments, *Dynamic Light Scattering: An Introduction in 30 Minutes,* **2017**.
[125] M. Clausse, L. Nicholas-Morgantini, A. Zradba, and D. Touraud, in: *Surfactant Science Series* (Hrsg.: M. Dekker), New York, **1987,** 15–62.
[126] B. Lagourette, J. Peyrelasse, C. Boned, and M. Clausse, *Nature* **1979**, *281,* 60–62.
[127] M. Clausse, J. Peyrelasse, J. Heil, C. Boned, and B. Lagourette, *Nature* **1981**, *293,* 636–638.
[128] M. Laguës, *J. Phyique Lett.* **1979**, *40,* 331–333.
[129] M. Lagües, R. Ober, and C. Taupin, *J. Phyique Lett.* **1978**, *39,* 487–491.
[130] J. Marcus. Dissertation, Universität Regensburg, **2016**.
[131] M. L. Klossek, D. Touraud, and W. Kunz, *Green Chem.* **2012**, *14,* 2017.
[132] M. L. Klossek, J. Marcus, D. Touraud, and W. Kunz, *Colloids Surf. A.* **2013**, *427,* 95–100.
[133] A. Ponton, T. K. Bose, and G. Delbos, *J. Chem. Phys.* **1991**, *94,* 6879–6886.
[134] M. Lagues, and C. Sauterey, *J. Phys. Chem.* **1980**, *84,* 3503–3508.
[135] R. MacKay, and R. Agarwal, *J. Colloid. Interface Sci.* **1978**, *65,* 225–231.
[136] Z. Grubisic, P. Rempp, and H. Benoit, *J. Polym. Sci. B Polym. Lett.* **1967**, *5,* 753–759.
[137] J. C. Moore, *J. Polym. Sci. A Gen. Pap.* **1964**, *2,* 835–843.
[138] J. Porath, *J. Protein Chem.* **1997**, *16,* 463–468.
[139] B. Trathnigg, *Prog. Polym. Sci.* **1995**, *20,* 615–650.

2 Surfactant-free Microemulsion and Microsuspension Polymerization of Methyl Methacrylate

2.1 Abstract and Preface

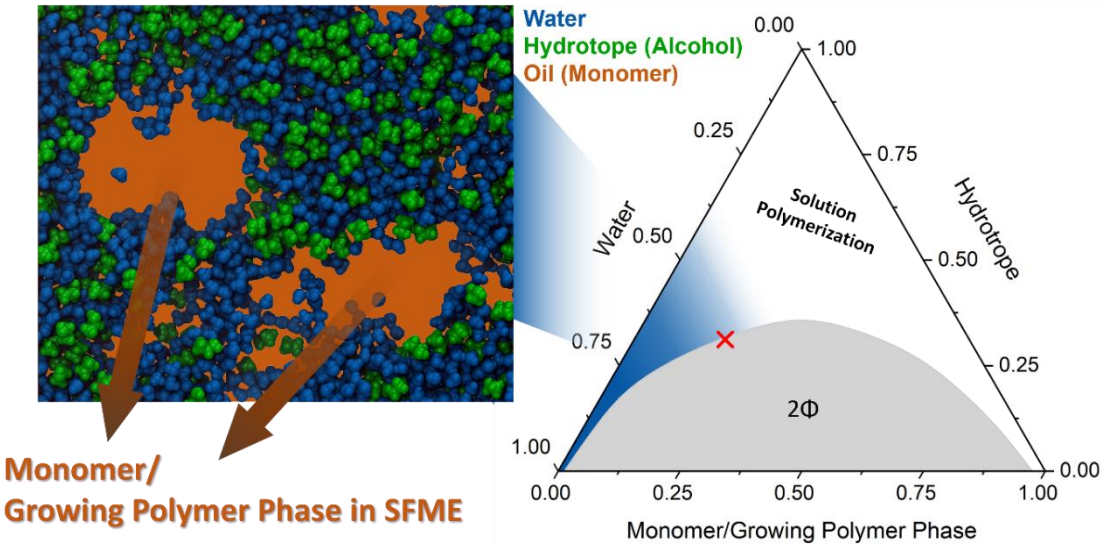

Figure 2.1 *Graphical Abstract: Right side: Schematic drawing of a phase diagram expected for an SFME system and the region, which is suitable for polymerization in SFMEs. Left side: MD simulations of an SFME. Polymerization reactions take place in the oil-rich domains (marked orange).*

This chapter presents a free-radical polymerization method in a mesostructured system – free of any surfactants, protective colloids, or other auxiliary agents. It is applicable for a large variety of industrially relevant vinylic monomers. The aim of this work is to study the impact of surfactant-free mesostructuring on the polymerization kinetics and the polymer derived.

So-called surfactant-free microemulsions (SFME) are investigated as reaction media with a simple composition comprising water, a hydrotrope (ethanol, *n*-propanol, *iso*-propanol, *tert*-butyl alcohol), and the monomer as the reactive oil phase (methyl methacrylate). Polymerization

reactions are performed using oil-soluble, thermal- and UV-active initiators (surfactant-free microsuspension polymerization) and water-soluble, redox-active initiators (surfactant-free microemulsion polymerization). Structural analysis of the SFMEs used and the polymerization kinetics are followed by dynamic light scattering (DLS). Dried polymers are analyzed with regard to their conversion yield by mass balance, the corresponding molar masses were determined using gel permeation chromatography (GPC), and the morphology is investigated by light microscopy.

All alcohols are suitable hydrotropes to form SFMEs, except for ethanol, which forms a molecularly disperse system. We observe significant differences in the polymerization kinetics and the molar masses of the polymers obtained. Ethanol leads to significantly higher molar masses. Within a system, higher concentrations of the other alcohols investigated give rise to less pronounced mesostructuring, lower conversions, and lower average molar masses. It is demonstrated that the effective concentration of alcohol in the oil-rich pseudo-phases as well as the repulsive effect of the surfactant-free, alcohol-rich interphases constitute the relevant factors influencing polymerization. Concerning the morphology, the polymers derived range from powder-like polymers in the so-called “pre-Ouzo region” over porous-solid polymers in the bicontinuous region to dense, almost compacted, transparent polymers in unstructured regions, comparable to the findings for surfactant-based systems reported in the literature. Polymerizations in SFMEs comprise a new intermediate between well-known solution (*i.e.*, molecularly dispersed) and microemulsion, respectively, microsuspension polymerization processes.

This chapter has been published in *Journal of Colloids and Interface Science* (J. Blahnik, S. Krickl, K. Schmid, E. Müller, J. Lupton, and W. Kunz, *Microemulsion and microsuspension polymerization of methyl methacrylate in surfactant-free microemulsions (SFME)*, JCIS, **2023**, *648,* 755-767) [1] and are a part of the patent application W. Kunz, S. Krickl, J. Blahnik, K. Schmid, *Microemulsion or microsuspension process for the production of a polymer dispersion, and polymer particles obtained by the process,* **2022,** WO 2022112481 A. [2]

Contributions to the experimental work:

- Jonas Blahnik: Conceptualization, experimental work, data evaluation
- Sebastian Krickl: Experimental work of initial kinetics (**Figure 2.4**)
- Jennifer Schuster: Experimental work of some phase diagrams (**Figure 2.2**)
- Andreas Kanygin and Lea Sammet helped with the conversion kinetics (**Figure 2.6**)

2.2 Introduction

For radically polymerizable monomers, various reaction methods are known, such as bulk, solution, suspension or emulsion polymerization. [3] Polymerization in emulsions and microemulsions offers particularly attractive techniques for the synthesis of aqueous polymer dispersions. [4–6] (Micro)suspension and (micro)emulsion polymerizations do have the technical advantage of providing the option of size-tunability, while yields and heat dissipation in industrial plants are usually within the desired range. In addition, unwanted gelation effects during the reaction can be effectively suppressed. [7] However, surfactants or auxiliary colloids like poly(vinyl alcohol) (PVA), poly(ethylene oxide)/poly(propylene oxide)-(co)polymers or cellulose esters, just to name a few, partly remain in the product, which can have a negative impact on the desired properties. For example, surfactants were shown to accelerate the release of smaller molecules (*e.g.*, plasticizers) from a polymeric workpiece. [8; 9] Techniques for the separation of long-chain amphiphiles are mostly inadequate, complex, and costly. Surfactants have a considerable foaming behavior and adhere strongly to the polymer phase, making them difficult to separate from the product. [10; 11] A mesoscale-structured medium, free of surfactants or auxiliary colloids, could help to overcome such problems – and at the same time maintain all advantages of suspension and emulsion techniques, in particular, size control of the polymers produced.

Surfactant-free microemulsions (SFMEs) are ternary, mesostructured liquids consisting of oil, water, and a hydrotrope. [12] The first publications about SFMEs date back to the late 1970s. [13; 14] Khmelnitsky *et al.* were the first to investigate an SFME as a reaction medium for enzymatic reactions. [15–17] Nonetheless, it took some time until SFMEs found wider interest in the colloidal research community. [18] In the past two decades, several studies have been reported in order to understand the structural and (reaction) mechanistic effects of and within SFMEs. [19] To emphasize the properties of a more poorly defined interface, the term “ultra-flexible microemulsions” has been commonly used in parallel. [20] Meanwhile, more examples have been published about the use of SFMEs for organic reactions [21] as well as some methods for inorganic nanoparticle synthesis. [22–24] Whereas the use of Ouzo-like systems (surfactant-free emulsions) has been discussed more frequently in literature in the context of polymerizations [25–28], only a few examples have been presented dealing with SFMEs in this context. [29–32] Other commonly discussed surfactant-free polymerization techniques still require additives that are hard to separate, such as Pickering systems. [10]

In this context, the present contribution reports on simple surfactant-free methods for the preparation of polymer latices by microemulsion or microsuspension polymerization. We investigate

SFMEs containing water, the vinylic monomer methyl methacrylate, and various short-chain alcohols as hydrotropes (ethanol (EtOH), *iso*-propanol (IPA), *n*-propanol (NPA), *tert*-butyl alcohol (TBA)). The structure of the SFMEs is investigated using dynamic light scattering (DLS) and conductivity measurements. UV-, redox-, and thermally activated initiator systems are used to start the polymerization. The initial polymer growth is tracked using DLS measurements. The conversion yield is determined by precise mass-balance measurements, and the molar mass of the dried polymers is determined using gel-permeation chromatography (GPC). The morphology of dried polymers is studied with light microscopy.

2.3 Materials and Methods

2.3.1 Materials

Methyl methacrylate (MMA, 99% purity, stabilized with 4-methoxyphenol ≤ 30 ppm), ethanol (EtOH, 99.8%), *n*-propanol (NPA, 99.5%), sodium sulfite (98%), sodium bromide (99%), potassium peroxodisulfate (PS, for analysis), CombiTitrant 5, methanol (anhydrous for analysis, max. 0.003% H_2O) and dimethyl sulfoxide-d_6 (DMSO-d_6, 99.5 atom % D) are obtained from Merck (Darmstadt, Germany). *tert*-Butyl alcohol (TBA, 99%) are purchased from Carl Roth (Karlsruhe, Germany). Tetrahydrofuran (THF, analytical reagent grade) and *iso*-propanol (IPA, 99.8%) are bought from Fisher Scientific (Schwerte, Germany). Poly(methyl methacrylate) standards (ReadyCal-Kit PSS-mmkitr1) are obtained from PSS Polymer Standards Service (Mainz, Germany). Azobisisobutyronitrile (AZDN, 98%) and *bis*-(4-*tert*-butylcyclohexyl) peroxy dicarbonate (BCC, 95%) are provided by PERGAN (Bocholt, Germany).

Prior to use, MMA is distilled at 40 °C and 60 mbar to remove the stabilizer. Aqueous solutions are prepared using deionized water with a resistivity of 18 MΩcm. All other chemicals are used without further purification.

2.3.2 Ternary Phase Diagrams

Phase diagrams are recorded at 25 °C ± 1 °C and 45 °C ± 1 °C according to the method of Clausse *et al.* [33] Binary mixtures of water/alcohol and alcohol/oil (each 3 g, at least 12 data points per diagram) are prepared in sealable tubes made of borosilicate glass. The third component is added dropwise until a visible change in the phase behavior occurred. The phase transition is determined by the naked eye. Weight fractions are calculated from the masses of the individual components by precise weight measurements.

2.3.3 Critical Point Determination

To determine the critical point of the SFME, ternary mixtures (within the two-phase region close to the phase boundary) ae centrifuged in 15 mL, volume-scaled centrifuge tubes at 13,000 g for 90 minutes to achieve a complete phase separation (T = 25 °C ± 1 °C and 45 °C ± 1 °C; Sigma 1-18KS centrifuge, Osterode am Harz, Germany). The critical point is allocated by approximation to sample compositions yielding a volume ratio of 50:50 the two phases after centrifugation. [34]

2.3.4 Tie Line Determination

Tie lines are determined by centrifuging ternary mixtures in the two-phase region. Samples of 10 g each are centrifuged in 15 mL centrifuge tubes for 20 minutes at 13,000 g (T = 25 °C ± 1 °C)

using a Sigma 3-18KS centrifuge (Osterode am Harz, Germany). The upper, oil-rich phase is diluted in DMSO-d_6 and analyzed by ^{1}H-NMR using a Bruker Avance III HD 400 (400 MHz) spectrometer. The MMA to alcohol ratio is calculated by comparing the corresponding integrals. MMA-rich compositions of the tie-lines is allocated to compositions in the MMA-rich region with MMA/alcohol ratios determined by ^{1}H-NMR. The water content of the lower, water-rich phase is determined by an average of five volumetric Karl Fischer titrations using a KF Titrino plus by Metrohm (Herisau, Switzerland). The compositions of the water-rich phase of the tie-lines are calculated by extrapolating from the above-determined MMA-rich compositions in the phase boundary in the water-rich region with equal water contents as determined by Karl Fischer titration. An example data evaluation is provided with **Figure S 2.10** in the appendix.

2.3.5 Dynamic Light Scattering (DLS) in SFME Systems

DLS experiments are performed using a temperature-controlled CGS-3 goniometer system from ALV (Langen, Germany), connected to an ALV-7004/FAST Multiple Tau digital correlator and a vertically polarized 22 mW HeNe laser (λ=632.8 nm). All measurements are performed at a scattering angle of 90°. Samples are filtrated into dust-free cylindrical measurement cells with an outer diameter of 10 mm using 0.2 µm PTFE membrane filters and closed with a cap. Data are collected for 300 s to determine the autocorrelation of the intensity fluctuations at temperatures of 25 ± 1 °C and 45 ± 1 °C.

2.3.6 Conductivity Measurements

Conductivity measurements are performed in a temperature-controlled measurement cell under permanent stirring at 25 ± 0.2 °C using a low-frequency WTW inoLab Cond 730 conductivity meter with a WTW TetraCon 325 electrode (Weilheim, Germany), as described by Buchecker *et al.* [35] Binary MMA/alcohol mixtures are prepared with an addition of 0.2 wt% sodium bromide to ensure the presence of a sufficient amount of charge carriers and a minimal amount of water necessary to allow for complete dilution of the salt. 20 g of each sample are filled into the measurement cell and successively diluted with pure water.

2.3.7 Microemulsion Polymerizations Followed by DLS

Further DLS experiments are performed to monitor the polymerization kinetics of the initial growth of microemulsion polymers. The polymerizations are redox-induced, using potassium persulfate and sodium sulfite (each 2 mol% referring to the monomer). The same instrumental setup is used as described in section 2.3.5. The polymerizable solution is filtered in special

cylindrical tubes with a septum, and the oxygen is removed by flushing the reaction mixture with nitrogen for one minute through a cannula. Polymerizations are performed at 25 ± 1 °C.

Data are collected for 30 s every minute *in situ* during the polymerization, which is performed directly in the DLS setup. Hydrodynamic radii are evaluated by 2nd order cumulant analysis, using the ALV-7004 Correlator Software provided and assuming the viscosity of the alcohol-water mixtures (without monomers) and the refractive index of the pure monomer to be approximately constant throughout the reaction.

2.3.8 Microsuspension Polymerizations Followed by DLS

Microsuspension polymerizations are performed using the thermal initiator BCC (0.2, 0.1, and 0.04 mol% referring to the monomer) at 45 °C ± 1 °C and the UV-sensitive initiator AZDN (0.2 mol% referring to the monomer) at 25 °C ± 1 °C. In both cases, the initiator is mixed with distilled monomer (precooled in an ice bath) and added to the water-alcohol mixtures. The polymerizable solution is filtered in special cylindrical tubes with a septum, and the oxygen is replaced by flushing the reaction mixture with nitrogen for one minute through a cannula. Polymerizations with AZDN (0.2 mol% referring to the monomer, dissolved in the monomer phase) are initiated by UV light, using a sample holder equipped with six UV-LEDs (CUNA66A1B, λ=365 nm, 900 mW each). Each vial is irradiated by exactly one UV-LED for four minutes. Polymerizations with BCC are initiated by heating the samples to 45 °C. The instrumental setup to track the polymerization reaction via DLS and the corresponding data analysis is identical to the procedure described in section 2.3.7.

2.3.9 Further Polymerizations and Yield of Thermal Microsuspension Polymerizations

Microsuspension polymerizates are investigated further regarding reaction yields. To this purpose, the reaction mixtures (approx. 6 g) are prepared and filled into rolled-rim bottles which are closed with crimp caps. 0.2 mol% BCC (referring to the monomer) is added by mixing with the monomer. Oxygen is removed by flushing the reaction mixture with nitrogen for one minute through a cannula. The sample containers are put into a temperature-controlled bath (45 ± 0.2 °C) to start the polymerization and maintain temperature control during the reaction. The polymerized mixtures are frozen in liquid nitrogen after different reaction times in order to stop the polymerization reaction. Frozen mixtures are freeze-dried under reduced pressure (< 10 mbar). To ensure complete drying, the polymers are stored at 130 °C until constant weight is reached. Dried polymers are weighed on an analytical balance, and the conversion yield is determined by comparison to the weight of the monomer present in the initial sample.

2.3.10 Gel Permeation Chromatography (GPC)

GPC is used to determine the mean molar mass of microsuspension poly(methyl methacrylate) (PMMA) particles synthesized by thermal initiation using a Viscotek 270-03 setup equipped with two GPC1000 columns and a RImax refractive index detector from Malvern (Malvern, United Kingdom). Dried polymers are dissolved in THF (approx. 1.5 mg mL^{-1}) and filtered into 1.5 mL GC (gas chromatography) vials using 0.2 µm PTFE membrane filters. 150 µL of each sample are injected in a ratio of 1:45 split by an autosampler. The measurement is performed at a flow rate of 1 mL min^{-1}. The evaluation of mass-weighted (M_w) molar mass is performed by the software provided with a conventional homopolymer calibration, using PMMA ReadyCal kit PSS-mmrkitr1 from PSS Polymer Standards Service (Mainz, Germany) as a reference. Refractive index (RI) vs. retention volume of the Ready Cal kit and an example measurement curve are depicted in **Figure S 2.9** in the appendix.

2.3.11 Viscosity and Density Measurements

Dynamic viscosities are measured with a temperature-controlled, automated rolling-ball-Microviscosimeter from Anton Paar (AMVn Graz, Austria) equipped with a glass capillary (1.6 mm inner diameter) and a stainless-steel ball (diameter 1.5 mm, density 7.7 g cm^{-3}). The rolling time is measured at angles of 30° and 70° ten times each (T = 25/45 ± 0.01 °C). The viscosity is calculated as a mean value of all measurements in total. Between each setup, the instrument constant is controlled with deionized water. Density measurements are performed with a temperature-controlled oscillating tube densimeter from Anton Paar (DMA 5000M, Graz, Austria).

2.3.12 Light Microscopy

Light microscopy images of dried microsuspension polymers are taken using an Eclipse E400 Microscope equipped with Plan 4×/0.10, 10×/0.30, and 20×/0.30 lenses by Nikon (Tokio, Japan). Illumination from above is established by a KL 1500 electronic light source by Schott (Mainz, Germany) by using two lighting cables. Pictures are taken with a Canon DS126371 camera mounted directly on the microscope. Size scales are determined by measuring a 2 mm scale divided into 200 parts by E. Leitz (Wetzlar, Germany) with the same optical settings as the samples.

2.4 Results

2.4.1 Structural Investigations of the Ternary System Water/Alcohols/MMA

Ternary phase diagrams comprising water, MMA, and EtOH/IPA/NPA/TBA for 25 °C and 45 °C are depicted in **Figure 2.2** (including reaction mixtures, as described below).

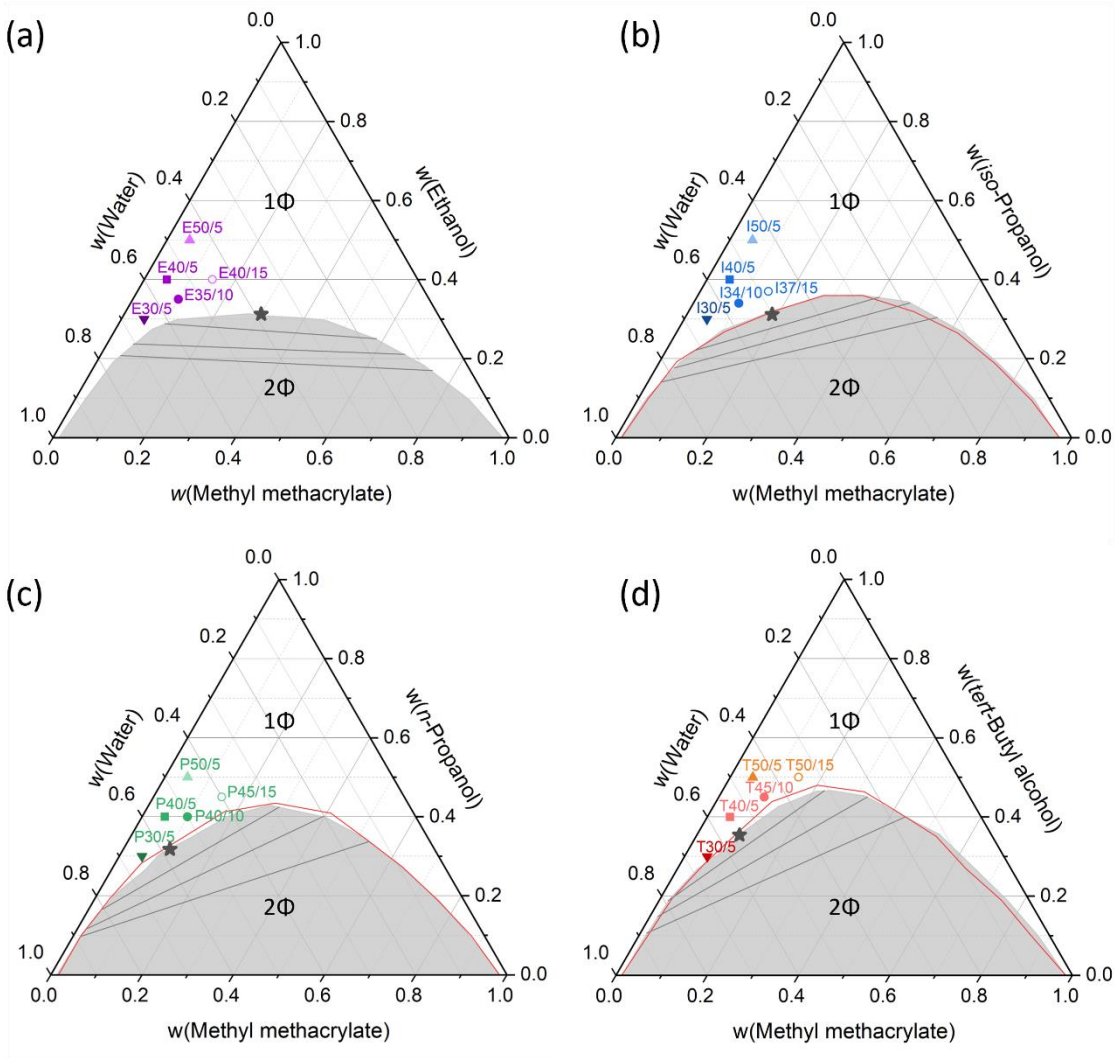

Figure 2.2 *Ternary phase diagrams of MMA, water, and the hydrotropes (a) ethanol (samples E), (b) iso-propanol (samples I), (c) n-propanol (samples P), and (d) tert-butyl alcohol (samples T) given in weight fractions. The phase boundary is determined at 25 °C (grey area biphasic) and 45 °C (biphasic below the red line). The critical point is marked as a black star. Tie lines are drawn as dark grey lines. Further compositions studied are marked with different symbols and their sample names.*

We observe phase diagrams with miscibility gaps that can be commonly expected for rather balanced SFME systems. [18] An increase in temperature from 25 °C to 45 °C does not significantly affect the location of the phase separation border. The two-phase region increases in the order EtOH < IPA < NPA < TBA (by area). When drawing the phase diagram in terms of molar ratios, still the same order is observed (see **Figure S 2.1** in the appendix). The critical point is

shifted to compositions with lower MMA concentrations when moving from EtOH to TBA (exact compositions **Table S 2.1** in the appendix). Tie lines are tilted slightly to the MMA-rich side in the EtOH system. The slope of the tie lines moves more and more towards the water-rich side when going via IPA and NPA to TBA, indicating more alcohol in the oil-rich phase.

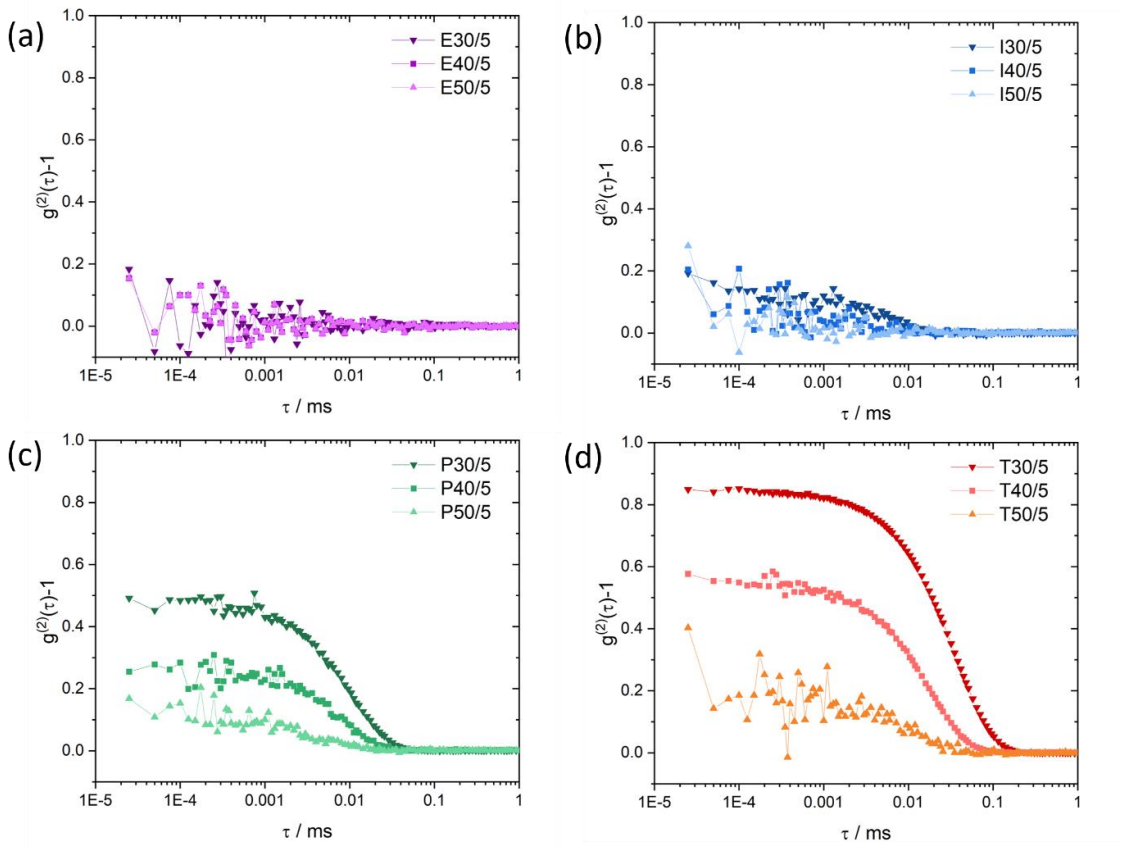

Figure 2.3 *Autocorrelation functions obtained from DLS measurements at 45 °C for the ternary systems with (a) EtOH, (b) IPA, (c) NPA, and (d) TBA for reaction mixtures as marked in* ***Figure 2.2****, containing a fixed MMA content of 5 wt% and 30, 40, and 50 wt% alcohol, respectively.*

Figure 2.3 shows autocorrelation functions of samples with each 5 wt% MMA for reaction mixtures marked in **Figure 2.2**. Autocorrelation functions for samples with higher MMA concentrations can be found in **Figure S 2.2** in the appendix. For EtOH-based mixtures autocorrelation functions fluctuate strongly on the baseline level and no defined shape can be discerned (see **Figure 2.3 a** and **Figure S 2.2 b**). For the other alcohols, the quality of the autocorrelation functions (*i.e.,* the higher lag times and higher y-axis intercepts) increases in the order IPA < NPA < TBA. In general, we observe a trend of a less pronounced autocorrelation function when increasing the alcohol content at a fixed MMA concentration of 5 wt% (*e.g.,* T30/5 > T40/5 > T50/5, see **Figure 2.3 b**, **c**, and **d**). When increasing the MMA content close to the phase boundary, the quality of the autocorrelation functions increases for IPA (from I30/5 over I34/10 to I37/15, see

Figure S 2.2 d) and decreases for NPA and TBA (*e.g.*, from T30/5 over T45/10 to T50/15, see **Figure S 2.2 f** and **h**). For the oil-rich domains, hydrodynamic radii of up to 5 nm are reached by 2nd order cumulant analysis (exact values are given in **Table S 2.3** in the appendix).

2.4.2 Microemulsion Polymerization with PS and UV-initiated Microsuspension Polymerization with AZDN

The initial growth of the polymers – or the response of the SFME system to the growing polymers – is tracked by the hydrodynamic radii derived from DLS measurements. **Figure 2.4 a** shows the first 35 minutes of the microemulsion polymerization process. One can observe that the hydrodynamic radii grow much faster and further with increasing alcohol content when moving from P30/5 to P50/5 in the NPA system. The initial growth of the EtOH system shows the same trend (increasing hydrodynamic radii when moving from E30/5 to E50/5), but the hydrodynamic radii for EtOH are higher by a factor of at least five compared to NPA, reaching the range of microns after just a few minutes.

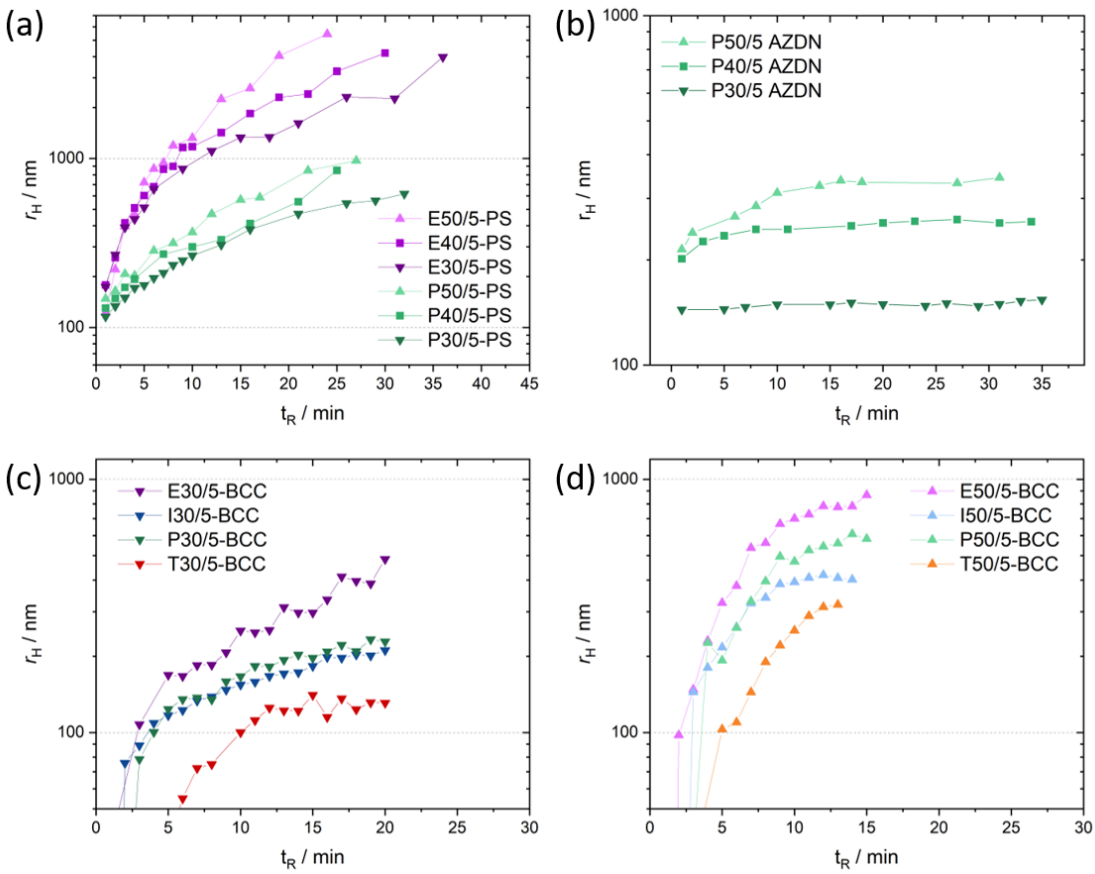

Figure 2.4 *Initial polymerization kinetics followed by DLS. (a) Microemulsion polymerization, initiated with 2 mol% persulfate, activated by 2 mol% sulfite, and (b) microsuspension polymerization, UV-initiated with 0.2 mol% AZDN, and microsuspension polymerizations initiated thermally with 0.04 mol% BCC. (c) Samples with 30 wt% alcohol and 5% MMA and (d) samples with 50 wt% alcohol and 5 wt% MMA. Please note that the first measuring points of (a) and (b) are recorded only a few minutes after the start of polymerization due to the experimental setup.*

The results of the first microsuspension polymerizations, where we expect the initiator to be in the oil-rich instead of the water-rich pseudo-phase, show basically the same trends (see **Figure 2.4 b**). The slope of the increase in the hydrodynamic radii is less steep, and the absolute values differ. However, we find the same consistent trend P30/5 < P40/5 < P50/5.

2.4.3 Thermally Initiated Microsuspension Polymerization with BCC

2.4.3.1 Initial Growth Tracked by DLS

The initial polymerization kinetics in the thermal system with BCC for all four alcohols with 5 wt% MMA and 30 wt% alcohol are depicted in **Figure 2.4 c**, and the corresponding kinetics with 50 wt% alcohol are shown in **Figure 2.4 d**. For all four alcohols, the hydrodynamic radii grow with increasing alcohol contents. We observe, as for the microemulsion polymerizations (cf. section 2.4.2), that particle sizes in EtOH-based mixtures grow most rapidly. The order EtOH-IPA-NPA-TBA as determined from the structuring results in nonpolymerized ternary systems (cf. section 2.4.1) can also be identified for the hydrodynamic radii, but in reverse order, with EtOH leading to the largest and TBA to the smallest particle sizes. There is one slight difference in the ordering, with IPA and NPA samples apparently swapping places. The absolute difference between IPA and NPA samples is not significantly great, especially for the formulations containing 30 wt% alcohol. Comparing the results of 30 wt% alcohol and 50 wt% alcohol, the slope of the kinetic experiments (see **Figure 2.4 c** and **d**) is steeper for 50 wt% alcohol, almost reaching the micron range in the case of E50/5 after 15 minutes. The samples derived from the other alcohols stay in the region of 100-600 nm in radius after this time. In contrast, in the systems containing 30 wt% alcohols, the radii are determined to be between 100 and 250 nm for TBA, NPA, and IPA after 20 minutes, and merely pass 500 nm in the system E30/5. The impact of the initiator concentration is tested only in the system T30/5 with 0.2, 0.1, and 0.04 mol% BCC. A slight increase in the hydrodynamic radius with increasing initiator concentration is observed (see **Figure S 2.5** in the appendix).

2.4.3.2 Further Progress in Polymerization – Molar Masses after 7 Hours

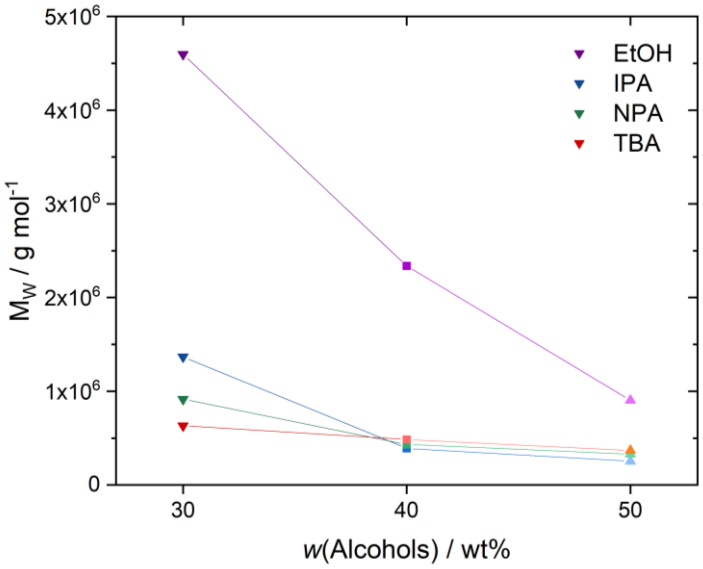

Figure 2.5 *Weight average molar masses (M_w) of microsuspension polymers thermally initiated by 0.2 mol% BCC derived by GPC for systems with the four different alcohols and the mixtures containing 5 wt% MMA and 30, 40, and 50 wt% alcohol.*

The weight average molar weights of freeze-dried polymers derived from polymerization with BCC after 7 hours are depicted in **Figure 2.5**. The molar mass in the EtOH-based reaction mixtures, especially with 30 wt% EtOH, is significantly higher than the others, reaching almost 5 MDa. The average molar masses for the other three alcohols for samples with 30 wt% alcohol range from around 600 kDa (for T30/5) to around 1.4 MDa (for I30/5). Thus, we can again confirm the order EtOH > IPA > NPA > TBA not only with respect to the diameter of the particles synthesized but also for the average molar mass of the polymers. The samples with 40 and 50 wt% IPA, NPA and TBA lead to quite similar molar masses of around 500 kDa. The difference of samples with different alcohol concentrations is lowest for the TBA samples and increases for NPA and IPA. The mean molar masses of polymers originating from samples with 40 and 50 wt% EtOH drastically decrease from around 4.6 MDa (E30/5) to 2.3 MDa (E40/5) and 1 MDa (E50/5).

2.4.3.3 Kinetics of the systems with IPA and TBA

Figure 2.6 shows the kinetics of the systems containing TBA and IPA. These two alcohols are chosen for further investigations, as TBA leads to the most pronounced SFMEs and IPA to the weakest, but with the critical point containing higher amounts of monomer (see section 2.4.1). When we compare the conversion for the TBA system (see **Figure 2.6 a**) and the IPA system (see **Figure 2.6 b**), we observe clear similarities. The samples close to the phase boundary (I30/5, I34/10, I37/15, respectively, T30/5, T45/10, and T50/15) show better conversions, yielding

> 90% after approximately 15 h in the case of the IPA sample and after approximately 20-22 h in the case of the TBA system. Comparing these samples, the conversion of compositions with 15 wt% MMA (I37/15, T50/15) is slightly higher and faster than those with 10 wt% and 5 wt%. The kinetics of samples containing all 5 wt% MMA and different amounts of alcohol (I30/5, I40/5, I50/5, respectively, T30/5, T40/5, and T50/5) show more pronounced differences. We observe a clear trend that for both alcohols, the kinetic is slower and leads to a lower conversion with increasing alcohol content. Concerning molar masses (see **Figure 2.6 c** and **d**), we observe some fluctuations with time for both alcohols. For IPA (see **Figure 2.6 d**), molar masses of the three samples close to the phase boundary (I30/5, I34/10, I37/15) are quite similar and stay more or less constant in the range of 0.6-0.8 MDa after three hours. Molar masses of the samples with further distance to the phase boundary are lower and appear to saturate after around 2 hours, in the range of 0.3 MDa (I40/5) and 0.2 MDa (I50/5). In the TBA system, molar masses fluctuate much more strongly and show a high similarity, with T30/5 having higher masses than all the other samples.

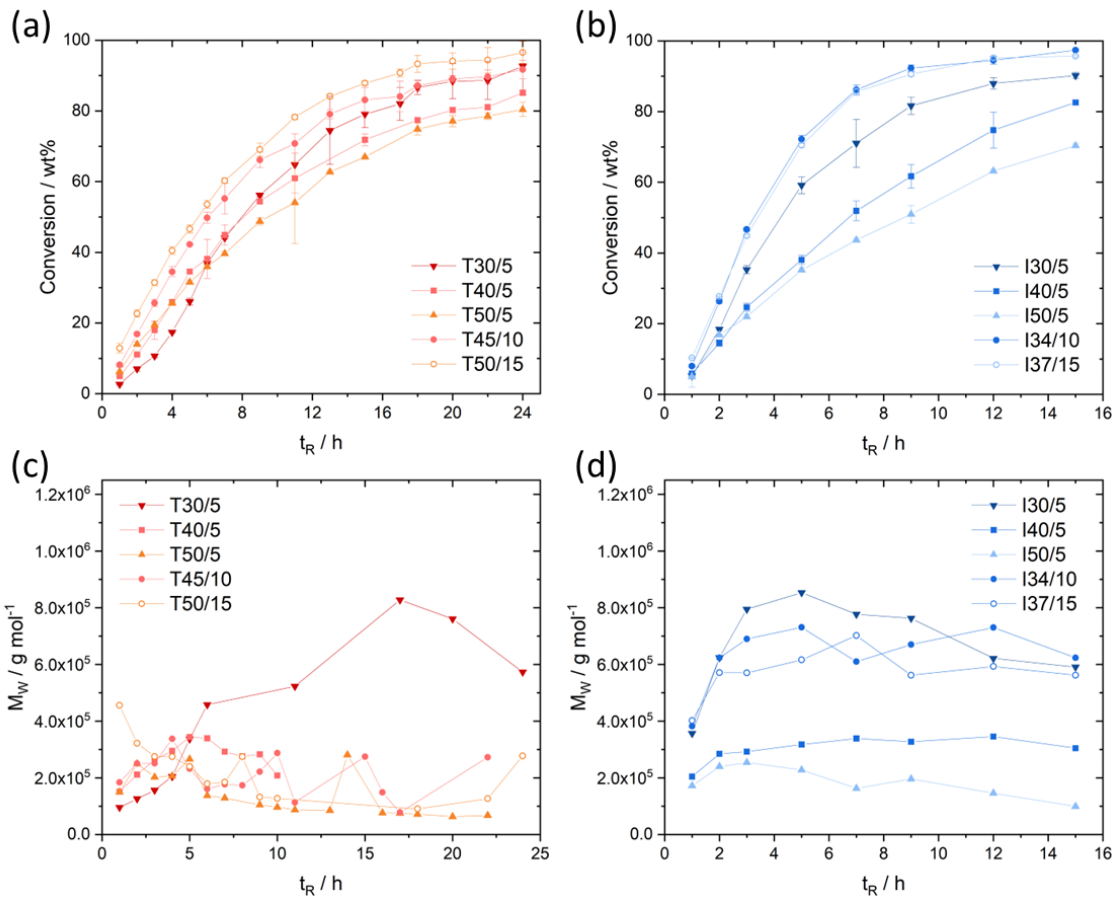

Figure 2.6 *Conversion of mass in the (a) TBA system (N=3) and (b) IPA system (N=3) with time and the corresponding molar masses M_w of the (c) TBA system (N=1) and (d) IPA system (N=1).*

2.4.3.4 Morphology of the Microsuspension Polymerizations with TBA and IPA

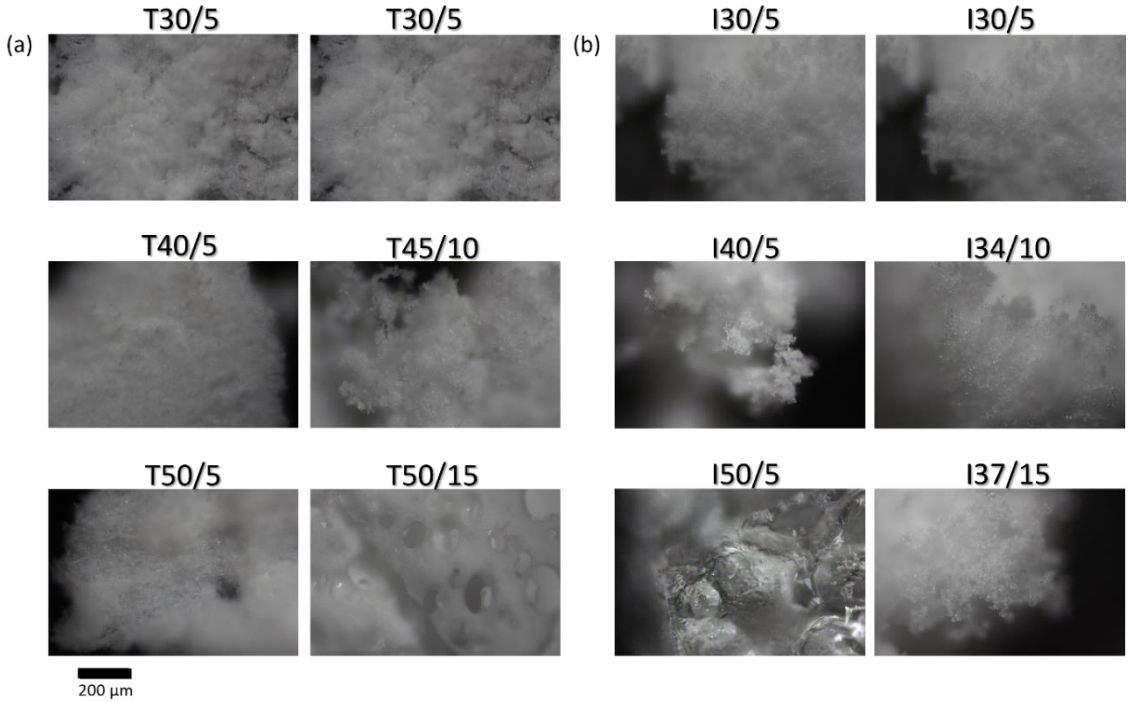

Figure 2.7 *Light microscope images of dried microsuspension polymers originating from systems with (a) TBA (after 22 h growth) and (b) IPA (after 15 h growth). All images have the same magnifications, a scale bar is given in the bottom left.*

A clear difference can be seen in the morphology of the freeze-dried samples (see **Figure 2.7**). More microscope pictures with different magnification factors and macroscopic images of all polymers can be found in **Figure S 2.6, Figure S 2.7, and Figure S 2.8** in the appendix. For both alcohols, TBA and IPA, a powder-like, fluffy morphology is found in the sample originating from the composition that arises from the water-rich corner of the phase diagram (T30/5 and I30/5). When moving away from the phase boundary towards compositions with higher alcohol contents at a fixed MMA content of 5 wt% (*e.g.*, from T30/5 to T50/5), we observe a decrease in the polymer volume and, thus, a more solid polymer. For all three polymers resulting from TBA (T30/5, T40/5, and T50/5), we still observe a powder-like morphology, and no significant morphological differences can be detected in bright-field microscopy. For I40/5, we still observe the same, but for I50/5, a compacted, almost transparent polymer phase with some bubbles embedded are present (see **Figure 2.7 b**). Comparing the results of the samples close to the phase boundary, we observe, in any case, a powder-like morphology for IPA samples (I30/5, I34/10, and I37/15). For TBA, a change towards a more compact, yet nontransparent polymer can be observed for the sample T50/15. Intercalated, some larger cavities (in the 100 µm range) are observable, and many regularly distributed, much smaller cavities, which are in the size range of the resolution limit of the light microscope (*i.e.,* a few microns or less).

2.5 Discussion

2.5.1 Structural Investigation of the Ternary Systems

As SFMEs are highly dynamic systems and do not have well-defined shapes, the DLS measurements (see **Figure 2.3** and **Figure S 2.2** in the appendix) are evaluated semi-quantitatively with regard to their correlation function and compared in their y-axis intercept and lag time as described by Buchecker *et al.* [35] Based on this interpretation, the size of domains of mesoscale structures detected by DLS generally increases in the order EtOH < IPA < NPA < TBA for comparable compositions (w/w/w). Even though a similar phase behavior can be found for all systems investigated (see **Figure 2.2**), virtually no structuring is observed in the case of EtOH. All other SFME systems show distinct autocorrelation functions, indicating mesoscopic separation of hydrophobic and hydrophilic domains on a nanometer scale (up to 5 nm for TBA). As one can expect, mesoscale structuring decreases with increasing distance to the phase separation boundary (see **Figure 2.2** and **Figure 2.3 b**, **c**, and **d**). [36; 37; 18] Along the phase boundary, mesoscale structures become less pronounced with increasing MMA concentration in the TBA (T30/5 > T45/10 > T50/15) and the NPA (P30/5 > P40/10 > P45/15) system. The IPA system behaves the other way around, which is apparent from the fact that the composition I37/15 has a more pronounced autocorrelation amplitude than compositions I34/10 and I30/5. All in all, the most defined mesoscale structured compositions can be concluded to be present in proximity to the critical point [18], which is shifted more to the oil-rich side and thus closest to I37/15 in the IPA system. However, some structuring remains present at larger distances to the critical point, as expected for “pre-Ouzo” systems. [19] The critical point of the system also marks the region in which the system should form bicontinuous SFMEs, whereas O/W-like mesostructures are expected to form on the water-rich side of the critical point. Conductivity measurements of the samples (see **Figure S 2.3 and Figure S 2.4** in the appendix) support this assumption.

The mesoscopic separation in an SFME into an oil- and water-rich pseudo-phase is closely related to the tie lines of the two-phase regions of the SFME-system, as recent research revealed. [38–40] In accordance with these findings, the mesoscopic phase separation should follow the tilt of the (extrapolated) tie lines, similar to centrifugation maps, which are recently published for similar systems. [40; 39] The mesoscopic separation can thus be described by mesoscale separation lines in the monophasic region (similar to tie lines in the two-phase region), which will decrease with increasing distance to the phase boundary. When the molecularly disperse region is reached, no mesoscale separation and thus no separation line is any longer present. A schematic

of how the separation lines are expected to be located in the EtOH and TBA systems is shown in **Figure 2.8**.

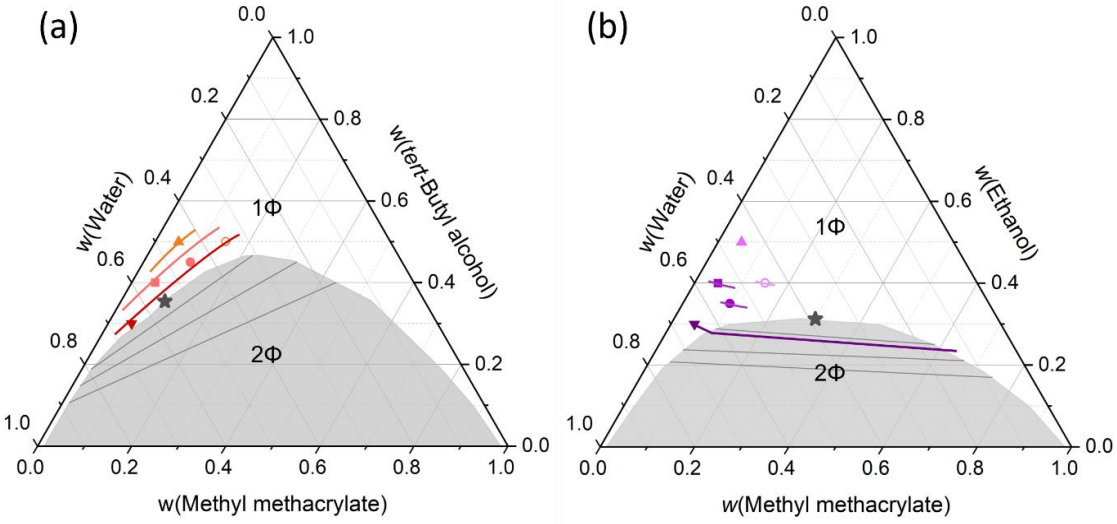

Figure 2.8 *Expected tilt and length of mesoscale phase separation lines for samples in the systems with (a) TBA and (b) EtOH, following the tilt of tie lines. The tilt and length of separation lines are estimated in accordance with the results of centrifugation maps in similar systems. [40; 39]*

Adapting this concept to our ternary systems, oil-rich phases in the TBA (and also the NPA) system are assumed to be alcohol-rich, as the tie lines are predominantly tilted the most to the water-rich corner of the phase diagram (cf. **Figure 2.2**). Due to the continuously strong structuring for all samples of the TBA system, the mesoscopic separation lines should be quite similar. Thus, we expect the separation lines to be quite large and tilted towards the water-rich side, leading to quite high TBA concentrations in the MMA-rich domains (cf. **Figure 2.8 a**) and a low TBA concentration in the water-rich phase. For the IPA system, with more different structuring and less tilted tie lines, a lower alcohol content in the oil-rich phase and simultaneously a higher difference concerning the exact compositions of the oil-rich domains of the four different samples can be assumed. If phase separation also occurs in the EtOH system (although possibly not before polymerization has started but rather triggered by the increase in local structuring with growing polymer chain length), the hydrophobic phase would be overwhelmingly MMA-rich with lower EtOH content in contrast to the other alcohols. This is particularly the case for the composition E30/5, as in this case the tie line through the two-phase region must be followed for mesoscale separation (cf. **Figure 2.8 b**). Such a triggered separation is expected to only be present close to the two-phase region. With greater distance to the binodal, the length of the separation lines will decrease, also in the case of triggered pseudo-phase separation, until the compositions of both pseudo-phases converge to a molecularly dispersed mixture. [39; 40]

2.5.2 Dissecting the Different Effects on Mean Molar Masses of Microsuspension Polymers

Three factors should be considered for the mean molar mass: the initiator decomposition; the environment and its impact on the reaction with regards to propagation, transfer, and termination; and steric or repulsive effects on the growing polymer chains due to the structuring, forcing the polymer to coil.

2.5.2.1 Impact of the Alcohols on the Initiator Decomposition

According to fundamental theory described in literature, molar masses are expected to depend on the radical concentration, with higher radical ratios leading to smaller average molar masses. [41] For all polymerization reactions studied in detail in the present work, the thermal initiator BCC is used to generate reactive radicals in a microsuspension method. In contrast, using the UV-initiated AZDN or even persulfate in a microemulsion technique, the generation of radicals will work differently.

The decomposition of organic peroxides is known to be dependent on the chemical environment. [42] The more polar the solvent, the faster the decomposition to free radicals to promote the polymerization reaction. At the same time, molar masses decrease, due to an increase in the number of polymer chains competing with each other for monomer supply. As BCC is soluble in the alcohols and in MMA but not significantly in water, the composition of the oil-rich pseudophase – if present in the system – will be the decomposition rate impacting factor. Even though no relevant data on the decomposition of BCC could be found in the literature, decomposition rates of other peroxides such as acetyl peroxide, and also for the thermal decomposition of AZDN, are reported. [43; 44] In both examples, the rates decrease slightly when moving from EtOH to longer-chain alcohols. This would suggest that the largest average molar masses arise for TBA and the lowest for EtOH, which obviously is not the case (cf. **Figure 2.5**), indicating that different initiator decomposition rates due to the different alcohols are not a relevant factor in explaining the different molar masses in our systems.

Following the discussion concerning the compositions of the MMA-rich domains (cf. section 2.5.1), we would expect the lowest alcohol contents for the E30/5 sample and the highest one for the T30/5 sample within monomer-rich domains. Faster decomposition due to increased alcohol concentration, similar to a higher initiator concentration, could explain a lower molar mass found in this work, *e.g.*, for sample T30/5 compared to sample E30/5. In the case of initiator decomposition, the effect should already occur at the onset of polymerization. In addition,

the effect would have to be similar for samples with a higher initiator concentration. When comparing the initial kinetics followed by DLS, hydrodynamic radii increase from sample T30/5 to sample E30/5 (cf. **Figure 2.3**). Higher initiator concentrations in the composition T30/5 (see **Figure S 2.5** in the appendix), on the other hand, lead to slightly increased hydrodynamic radii. This observation suggests that the different hydrodynamic radii in the two examples have different causes, which will be discussed later with the impact of mesostructures (see section 2.5.4). For all systems investigated, hydrodynamic radii follow the same trends, independently of the initiation methods (UV, thermal, redox). In summary, the initiator decomposition does not seem to be the rate determining step in the polymerization kinetics and growth, and therefore cannot explain the differences found in the weight average molar masses. The fact that the decomposition rate of AZDN in MMA is reported to be rather similar to the case of the alcohols strengthens this conclusion. [43]

2.5.2.2 Impact of the Alcohols on the Reaction Kinetics

Another way of tuning the molar mass is by adding chain-regulating agents, such as small-chain alcohols. These are known to influence chain propagation, chain termination, and chain transfer reactions. [45] Unfortunately, not much kinetic data for polymerizations in alcohols can be found in the literature. Available data are often inconsistent, presumable because of the different measurement techniques used. However, as a general rule of thumb, rates increase with the polarity of the solvent. [43] For propagation, termination, and chain transfer, corresponding rate constants are higher in alcohols than in nonpolar solvents. The most important rate constant for alcohols is reported to be the chain termination. [46] Several different alcohols were present in the first attempts at microemulsion or microsuspension polymerization, as they were used as cosurfactants. [47] Accordingly, the impact of alcohols also came into the focus of polymer research, both in terms of chain regulators and with regards to modifying the microemulsion interphase. [48] It is found that molar weights are dependent on the nature of the alcohol, the location in the case of microemulsions (*i.e.*, bulk or interphase), and also the alcohol concentration in the formulation. [46]

In the context of the present work, the relevant alcohol concentration is the effective concentration of alcohol in the monomer-rich pseudo-phase, where the polymerization takes place. The impact of the interphase will be discussed later on in section 2.5.2.3. Nie *et al.* tested the radical scavenging effect of different alcohols on the polymerization rate of ultrasonication-initiated, surfactant-based emulsion polymerization without initiators. [49] They found that the polymerization rate increases with increasing alcohol concentration. When comparing different

alcohols, they found the order methanol < EtOH < NPA < *n*-butanol. [49] Compared to our system, we could find a similar behavior, coming to the order EtOH < IPA < NPA < TBA. This is the same order as already found with regards to the SFME properties, which is also dependent on the balance in hydrophilicity and, thus, polarity.

Combining these literature findings with our system, we can draw the interim conclusion that the chemical nature of the alcohol and the composition of the MMA-rich pseudo-phase might have an impact on the molar mass due to the effects discussed. Returning to the results of the structuring in the ternary systems (see section 2.5.1), the compositions of the pseudo-phases differ most in EtOH and least in TBA. In the TBA system, we observe good structuring with quite similar tilts of the separation lines along with comparable compositions of the oil-rich pseudo-phases for samples T30/5, T40/5 and T50/5. For EtOH, no structuring is detectable in the ternary mixtures, but a microphase separation occurs during polymerization due to the growing chains following the tie lines is conceivable, most pronounced close to the phase boundary. Consequently, most alcohol-rich pseudo-phases should be present for TBA and the least alcohol-rich ones for EtOH, with compositions aligning more closely with the alcohol concentration for a molecularly-disperse solution possibly for sample E40/5 but certainly for sample E50/5. Here, we expect molecularly-dispersed solution polymerization to be the dominant mechanism. The systems with NPA and IPA should have intermediate properties. Due to the resulting alcohol concentration in the pseudo-phases, a higher termination rate with increasing alcohol concentration will be present. This conclusion is compatible with the molar masses found (cf. **Figure 2.5** and **Figure 2.6**). If all mixtures behaved like entirely molecularly-disperse solutions, we would expect a steady decrease in molar mass with increasing alcohol content, comparable for all systems due to their similar alcohol contents and showing only minor differences due to the different nature of the alcohols. This is obviously not the case, when comparing the negligible differences found for the TBA systems to the significant differences found for the EtOH samples (cf. **Figure 2.5**). Concerning masses with different MMA concentrations close to the phase border in the example of IPA (see **Figure 2.6**), rather similar mean molar masses are observed for samples I30/5, I34/10 and I37/15. For all three samples, the composition of the pseudo-phases should be not too different. Comparing I30/5 with I40/5 and I50/5, the mean molar mass decreases more rapidly. For TBA, with all systems comprising a well-pronounced mesostructuring and probably quite similar separation lines, only small and variable differences in weight average molar masses are found. However, one remarkable behaviour with regards to the molar masses cannot be explained at the moment in the sample T30/5 after around 7-10 h, which shows higher

molar masses. We assume a higher tendency for chain transfer reactions in this particular composition very close to the phase boundary, which, however, could not be clarified.

2.5.2.3 Impact of the Interphase

The alcohol concentration in MMA-rich pseudo-phases alone might explain the findings regarding molar masses but not the initial kinetics followed by DLS. The largest hydrodynamic radii are observed with increasing alcohol concentration within one system, and hydrodynamic radii increase with constant alcohol concentration from EtOH to TBA (see **Figure 2.4**). Results are similar for all three initiator systems, indicating that the impacts on the initiator play a minor role. Also, the impact of the alcohol concentration, which boosts both propagation and termination, does not explain the findings by DLS in this early stage of polymerization. This is particularly the case with termination reactions, as their influence becomes more important with longer reaction times, but not in the first minutes. If only the nature of the alcohol and its effective concentration had an impact, especially on the propagation, polymerizations in the E30/5 sample would lead to the lowest radii due to the slowest propagation.

As mentioned in the discussion in section 2.5.2.2, the interphase and its steric effects were shown to have an impact in the literature. Antonietti described a thermodynamic model for polymerizations in classical, surfactant-based microemulsions. The permeability of interphases was identified to play a major role. [48] The microemulsions are reported to become thermodynamically unstable due to the growth of the polymer particle. The contribution is calculated to be 3-10 k_BT per polymer molecule for linear polymers (like PMMA) in contrast to microgels. [48] However, even though the microemulsion becomes unstable, we still observe different kinetics and higher molar masses compared to polymerizations in emulsions. [48; 46] The thermodynamic stability of SFMEs is calculated to be only of the order of a few k_BT. [19] Thus, the SFMEs are likely to be similarly disturbed during the polymerization. The relevant thermodynamic factors for SFME stability are the entropy of mixing versus the free energy of hydration. The repulsive force is the latter one, which comes from the OH-group density at the interphases. [19] As the “pre-Ouzo” and the “Ouzo effect” are closely linked [34], the same stabilizing effect as in the interface of Ouzo droplets, which are remarkably stable, should also occur in the growing polymers in this work. We can expect the repulsive force to be the strongest in the case of TBA-based systems and the lowest in the case of the EtOH-based system, where the entropically driven term wins in the ternary system before the polymerization reaction has started. The interphase generated will lead to two effects during the polymerization growth: on the one hand, the polymer experiences a repulsive force, forcing it to coil inside the monomer-rich aggregate. On the

other hand, it bounces to a very alcohol-enriched interphase, which will again favor termination reactions, increasing the effects discussed in section 2.5.2.2. In contrast, we expect the polymer to have a more expanded appearance and thus a lower tendency to coil in formerly molecularly disperse solutions due to a lower repulsive force. This leads to higher hydrodynamic radii, as found in the DLS kinetics (cf. **Figure 2.4**).

Another factor in the overall kinetics not discussed so far is diffusion. Diffusion of monomers to the active polymerizing centers is, of course, easier in a monomer-rich environment compared to a molecularly disperse solution. [1] Particularly with increasing polymerization time, propagation (and thus also the average molar mass) is higher when a higher monomer concentration is available near the polymerizing centers. Yet, gel effects, as known to influence bulk polymerizations, are not a relevant factor in diffusion and kinetics in polymerizations in SFMEs. [41]

2.5.3 Conversion Yield

Conversion yield and molar mass are closely linked parameters of polymerization reactions. Hence, most factors concerning the molar mass (discussed in section 2.5.2) also influence the conversion reaction and yield. A higher termination reaction rate will lead to lower conversion and molar mass provided that the same number of growing polymer chains is present initially. Most relevant for the conversion yield, especially for advanced polymerization reaction times, is the available monomer concentration. The monomer concentration favors propagation versus termination or transfer reactions. As mentioned in section 2.5.2.3, the diffusion and, thus, availability of monomers are important factors for the conversion. The conversion is expected to drop with decreasing quality of the mesostructures. For a solution-like polymerization, conversion yields should be in the region of 60%. [3] The conversion yield of IPA and TBA samples with 5 wt% MMA each indeed decreases with increasing alcohol content (*e.g.*, from sample I30/5 to sample I50/5, see **Figure 2.6 a** and **b**). This decrease can be explained by a transformation from surfactant-free microemulsion to a molecularly dispersed solution and thus from a microsuspension-like-polymerization to a more solution-like-polymerization. Higher alcohol contents will also lead to more termination reactions, as already discussed in section 2.5.2.2. On closer inspection, we observe that the differences between the conversion of the samples I40/5 and I50/5 are greater in the IPA system than in the TBA system in samples T40/5 and T50/5. This observation fits to the overall less pronounced structuring found in the IPA system compared to the TBA system. The same applies to the I30 sample compared to the I40 and I50 samples, which are closer to the critical point with better mesostructuring.

2.5.4 Impact of Mesostructuring

The impact of mesostructuring with regards to the morphology of the dried polymers can already be seen by the naked eye. Many different microemulsions and their impact on the polymer morphology formed have been discussed in the literature. Oil-in-water microemulsion and microsuspension polymerizates are usually powder-like and have different microstructures. [48] But also inverse and bicontinuous structures have been discussed: the latter ones, for example, as templates for porous membrane material. [50; 51] Powder-like polymers are observed for most of the samples formed from the IPA and TBA systems (see **Figure 2.7** and **Figure S 2.6, Figure S 2.7,** and **Figure S 2.8** in the appendix), but this applies especially to the polymers obtained in the SFME-mixtures I30/5 and T30/5. To distinguish the impact of mesostructuring on the samples, we have to look particularly at samples with the highest alcohol contents (I50/5 and T50/5) and both samples with 15 wt% MMA (T50/15 and I37/15). While the polymer derived from sample I50/5 is a compact, almost transparent material, we still observe porous polymer structures originating from sample T50/5. This can be rationalized as sample T50/5 still showing mesostructure formation, while for sample I50/5, a solution-like character appears to dominate. If both systems are molecularly disperse, we would not expect significant differences between both alcohols at a similar composition. Comparing the samples close to the binodal (*i.e.*, samples I30/5, I34/10, and I37/15), hardly any difference can be seen. All three compositions are on the water-rich side of the critical point (cf. **Figure 2.2**). Consequently, they are most probably O/W-like SFMEs, leading to fine, powder-like polymer morphologies. For the TBA system, however, the critical point lies between sample T30/5 and sample T45/10. Sample T50/15 is already quite far removed from the oil-rich side of the critical point, possibly already indicating W/O-like structures (see also the conductivity data, **Figure S 2.3** in the appendix). The polymer derived from sample T50/15 is solid, containing micropores similar to the structures expected in W/O-microemulsions. Such morphologies can also be found for polymerizations in conventional microemulsions, with porous but disjointed structures for O/W and W/O-microemulsions and an open, interconnected morphology for bicontinuous microemulsions. Literature results indicate that the morphology of such a polymer retains some memory of the initial structure, even with a larger length scale than that of the initial microemulsions, with only a few nanometers in diameter. [46; 48] The reason for this memory lies in the repulsive force on the thermodynamically unstable polymer particles (see section 2.5.2.3). Obviously, the same is also found in the surfactant-free system of this study.

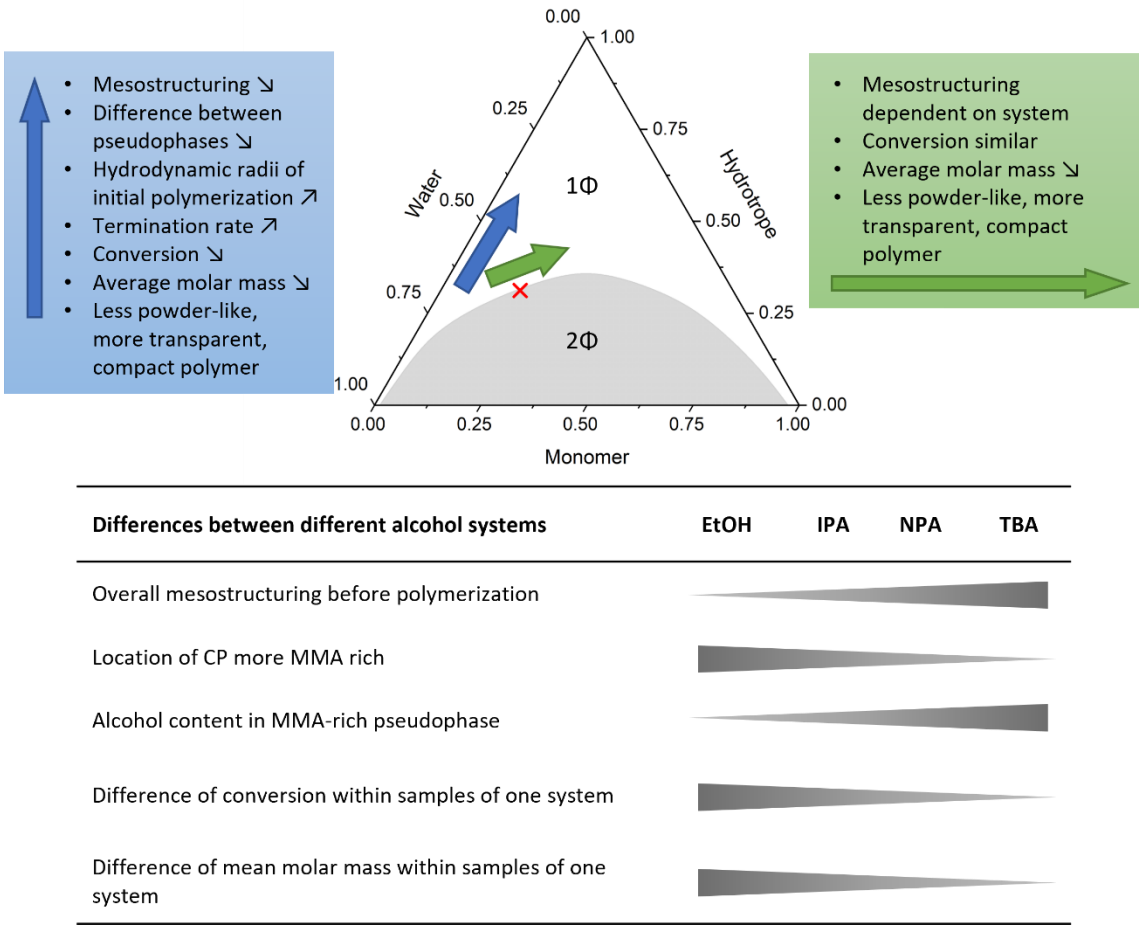

Figure 2.9 *Schematic overview of the results and factors discussed influencing the polymerizations.*

The mesostructuring is also relevant for all the other effects discussed above. The transition to a solution-like polymerization leads to an overall lower conversion and is thus linked to structuring (see section 2.5.3). Molar masses are discussed to be mainly dependent on two factors. The effective concentration of alcohol in the MMA-rich pseudo-phases is an indirect effect of mesostructuring (see section 2.5.2.2). A sterical effect due to the interphase itself is a direct effect of the balance forces, which were previously responsible for the formation of SFMEs (see section 2.5.2.1). A schematic overview over the results discussed and the resulting effects is depicted in **Figure 2.9**.

2.6 Conclusion and Outlook

Microemulsion systems comprise an interesting reaction medium for polymerizations, allowing precise control of the polymerization kinetics and morphologies. [48; 46] However, surfactants can remain in the polymer and influence its properties. [8] A new method has been presented for the preparation of poly(methyl methacrylate) (PMMA) in surfactant-free microemulsions (SFMEs). It allows to gain control over polymer sizes, molar masses, kinetics, and macroscopic polymer morphologies without the help of any surfactants. In contrast to previous approaches aiming to avoid the use of surfactants, the present work is also free of protective colloids. [10] Although a tiny amount of examples of polymerizations in SFME are reported so far, they worked with a polymerizable hydrotrope instead of a polymerizable oil [30; 29] designed for special applications with a tiny number of suitable monomers. The presented technique, in contrast, is likely to be applicable to a large number of acrylic monomers. It is different from the classifications of polymerization reactions in conventional (surfactant- or protective colloid-based or solution based) reaction media [48; 52; 46] and joins a series of innovative applications of surfactant-free microemulsions as reaction media. [53; 36; 37; 54]

Molar masses and conversions range in the same size region as PMMA particles derived from conventional microsuspension polymerizations. [52] As expected, ethanol-based reaction mixtures, in which no mesostructures could be found in the initial starting mixture, lead to much higher molar masses and lower yields compared to the SFME systems used. It is found that the composition of the MMA-rich pseudo-phase, as well as the alcohol-rich interphase and its repulsive force, plays a decisive role for conversion and mean molar mass. The macroscopic morphology is likely to be a direct result of mesostructuring, providing a kind of mesoscale template (comparable to conventional microsuspension polymerizations [55; 51]). The transition to solution polymerization and the composition of the reaction mixture relative to the critical point are decisive (the latter corresponds generally to the type of structuring, *i.e.*, oil-in-water (O/W), bicontinuous or water-in-oil (W/O)). We could also demonstrate that moving away from the phase separation boundary towards an unstructured system lowers the conversion yield and changes the morphology to a more compact polymer structure (as expected for structurally uncontrolled solution polymerizations [3]).

Polymerizing in an O/W-based SFME system can provide an attractive alternative to classical microemulsion- and microsuspension polymerizations, especially if polymers without impurities are of interest. Before thinking of an application in an industrial context (*e.g.*, for poly(vinyl chloride) (PVC) or poly(vinyl acetate) (PVAc)), further studies will be required after this proof-of-

concept, with a focus on the material properties. Taking advantage of the sponge-like morphology obtained by polymerizations at the oil-rich side (relative to the critical point) can be interesting for producing porous material, such as used for filters. Copolymerizations in relevant systems, *e.g.,* MMA-2-hydroxyethacrylate (HEMA), which were already discussed for filtration applications [51; 55], could be compared to polymers derived from conventional systems. Furthermore, this study might also be relevant for surfactant- and cosurfactant-based polymerizations in microemulsions, as the impact of different alcohols as possible cosurfactants or process additives is explored.

All in all, we have been able to demonstrate that simple, short-chain alcohols (using them as easily removed hydrotropes) are suitable for polymer synthesis within a controlled surfactant-free microemulsion/suspension polymerization – a new intermediate in-between the well-known solution (*i.e.,* molecularly dispersed) and microemulsion/-suspension polymerization processes.

2.7 Appendix

2.7.1 Composition of all Samples

Table S 2.1 *Exact compositions of the investigated ternary systems.*

Sample ID	MMA / wt%	Water / wt%	EtOH / wt%	IPA / wt%	NPA / wt%	TBA / wt%
E30/5	5	65	30	-	-	-
E40/5	5	55	40	-	-	-
E50/5	5	45	50	-	-	-
E35/10	10	55	35	-	-	-
E40/15	15	45	40	-	-	-
I30/5	5	65	-	30	-	-
I40/5	5	55	-	40	-	-
I50/5	5	45	-	50	-	-
I34/10	10	56	-	34	-	-
I37/15	15	48	-	37	-	-
P30/5	5	65	-	-	30	-
P40/5	5	55	-	-	40	-
P50/5	5	45	-	-	50	-
P40/10	10	50	-	-	40	-
P45/15	15	40	-	-	45	-
T30/5	5	65	-	-	-	30
T40/5	5	55	-	-	-	40
T50/5	5	45	-	-	-	50
T45/10	10	45	-	-	-	45
T50/15	15	35	-	-	-	50

2.7.2 Critical Points

Table S 2.2 *Compositions of the critical points found by approximation experiments in the four ternary systems.*

Hydrotrope	MMA / wt%	Water / wt%	EtOH / wt%	IPA / wt%	NPA / wt%	TBA / wt%
EtOH	30.0	38.7	31.3	-	-	-
IPA	18.7	50.1	-	31.2	-	-
NPA	10.2	58.0	-	-	31.8	-
TBA	9.4	55.2	-	-	-	35.4

2.7.3 Viscosity and Density Data and Calculated Hydrodynamic Radii

Table S 2.3 *Viscosity and density data and calculated hydrodynamic radii by 2nd order cumulant analysis. "n.d." stands for not determined. For samples in which no size could be determined as the autocorrelation function is too weak for calculation, 0 is given as a value.*

Sample ID	ρ (25 °C) / g mL^{-1}	ρ (45 °C) / g mL^{-1}	η (25 °C) / Pa s	η (45 °C) / Pa s	r_H (25 °C) / nm	r_H (45 °C) / nm
E30/5	0.949146	0.935219	2.19	0.97	0	0
E40/5	0.935219	0.913071	2.37	1.06	0	0
E50/5	0.913071	0.928803	2.31	1.05	0	0
E35/10	0.928803	0.904188	2.33	1.03	n.d.	0
E40/15	0.904188	0.887408	2.36	1.06	n.d.	0
I30/5	0.945066	0.947869	2.67	1.33	0.69	1.11
I40/5	0.921132	0.904841	n.d.	1.48	n.d.	n.d.
I50/5	0.896327	0.879443	n.d.	1.56	n.d.	n.d.
I34/10	n.d.	n.d	n.d.	n.d.	n.d.	n.d.
I37/15	n.d.	n.d	n.d.	n.d.	n.d.	n.d.
P30/5	0.907784	0.907785	2.61	1.17	1.51	1.84
P40/5	0.907785	0.922513	2.70	1.23	0.96	1.41
P50/5	0.922513	0.901559	2.60	1.18	0.61	0.78
P40/10	0.901559	0.88621	2.67	1.21	n.d.	1.47
P45/15	0.941748	0.926507	3.26	1.32	n.d.	1.04
T30/5	0.926507	0.900059	3.26	1.51	2.21	5.04
T40/5	0.900059	0.91649	3.77	1.73	1.48	2.17
T50/5	0.91649	0.89576	4.51	1.69	0.75	0.25
T45/10	0.89576	0.878934	4.38	1.78	n.d.	2.43
T50/15	0.879645	0.862528	4.72	1.78	n.d.	0.98

2.7.4 Ternary Phase Diagrams in Mol Fractions

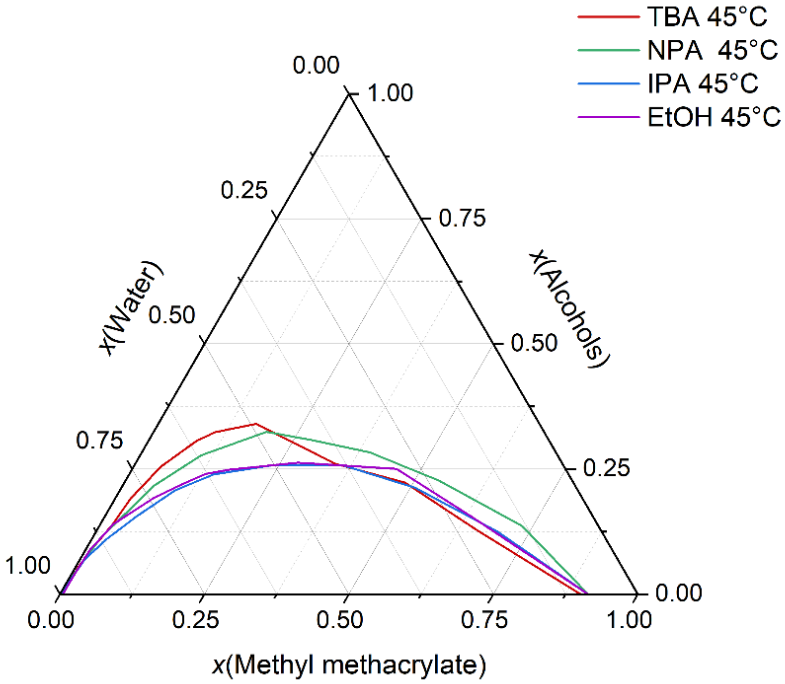

Figure S 2.1 *Ternary phase diagrams at 45 °C, given in molar fractions*

2.7.5 Autocorrelation Functions derived by DLS

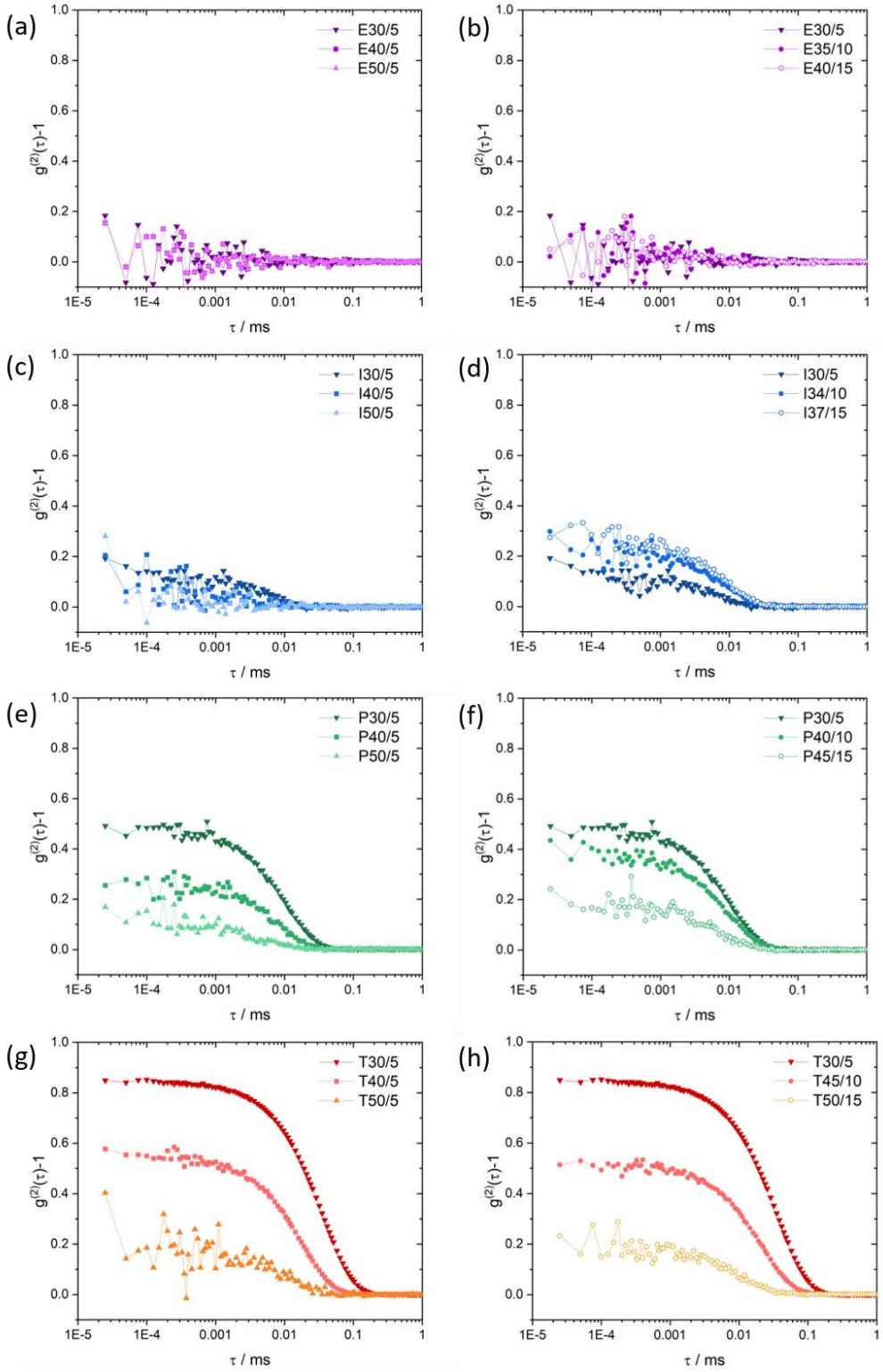

Figure S 2.2 *Autocorrelation functions obtained from DLS measurements at 45 °C for the ternary systems with EtOH (a) and (b), IPA (c) and (d), NPA (e) and (f), TBA (g) and (h) for reaction mixtures as marked in* ***Figure 2.2****. Panels (a), (c), (e), and (g) show the samples containing a fixed MMA content of 5 wt% and 30, 40, and 50 wt% alcohol, respectively; (b), (d), (f), and (h) show the samples with MMA contents of 5, 10, and 15 wt% and different alcohol contents, depending on the position of the binodal line.*

2.7.6 Conductivity Data

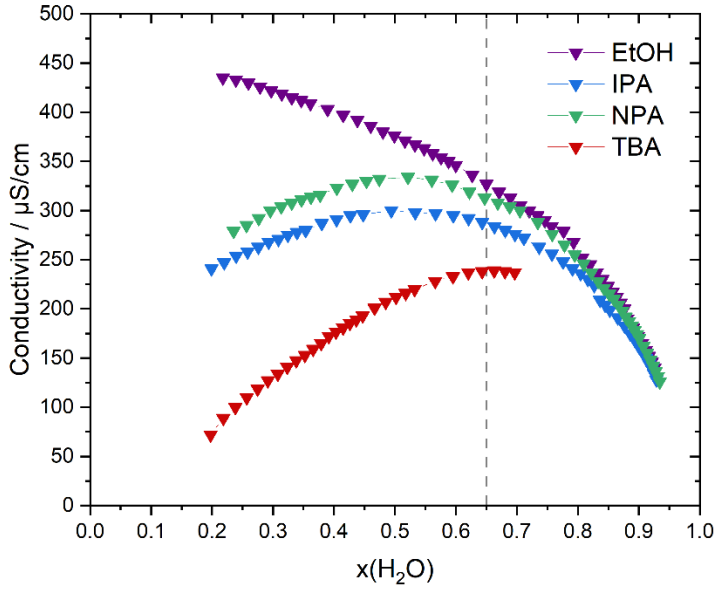

Figure S 2.3 *Conductivity versus water content curves for the systems EtOH (purple), IPA (blue), NPA (green), and TBA (orange). The curves cut the samples containing 5 wt% MMA and 30 wt% alcohol (X30/5) at the dashed lines. A small amount of NaBr is used as the charge carrier.*

Conductivity measurements are performed to further investigate the kind of structuring of our four systems. The small amount of 0.2 wt% NaBr did not noticeably change the phase behavior, as already proven by Buchecker *et al.* [35] The conductivity curves are diluted along the dashed lines in the phase diagrams and cut the composition X30/5 for every system (see dashed lines, figure S3). We observe percolation curves for IPA, NPA, and TBA, which are expected for micro-emulsion systems and can also be applied to SFME [35] For EtOH, a continuous decrease in conductivity can be observed during dilution. For both propanols, the samples I30/5, respectively P30/5, lay in the decreasing branch, indicating an oil-in-water-like structure of the SFME. This could also be expected from the location of the critical point. For the TBA sample, the location of T30/5 is at the turning point of the conductivity curve, indicating a bicontinuous-like or worm-like SFME. As tert-butanol forms chain-like aggregates in binary mixtures with water, this behavior could be expected even when low concentrations of a hydrophobic compound are inserted into the pre-structure. [56; 35]

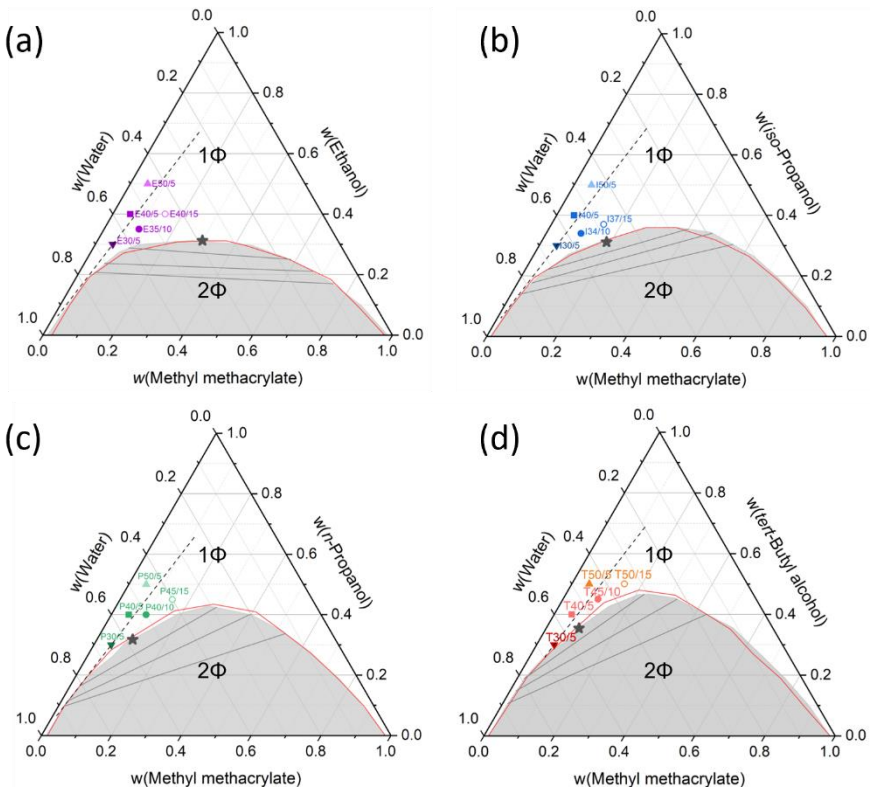

Figure S 2.4 *Ternary phase diagrams of MMA, water, and the hydrotropes (a) ethanol (samples E), (b) iso-propanol (samples I), (c) n-propanol (samples P), and (d) tert-butyl alcohol (samples T) given in weight fractions. The phase boundary is determined at 25 °C (grey area biphasic) and 45 °C (biphasic below the red line). The dilution line of conductivity experiments (see**Figure S 2.3**) is marked black dashed.*

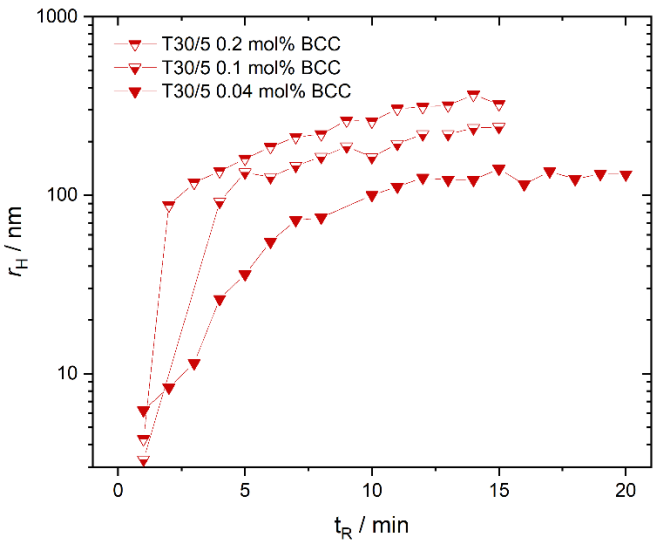

Figure S 2.5 *Initial polymerization kinetics of microsuspension polymerizations initiated thermally with 0.2, 0.1, and 0.04 mol% BCC followed by DLS. All samples have the composition T30/5.*

2.7.7 Macroscopic and Microscopic Images of Dried Polymers

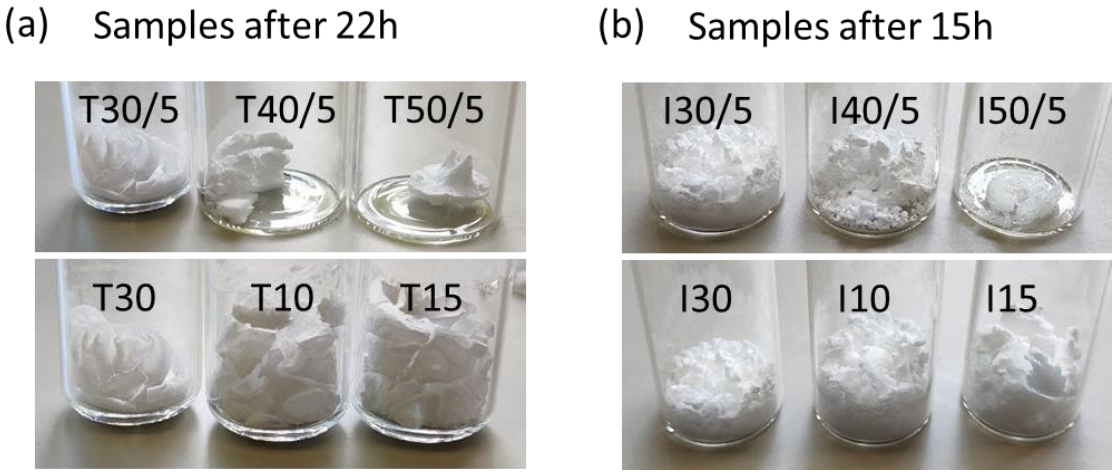

Figure S 2.6 *Appearance of freeze-dried microsuspension polymers (a) with the hydrotrope TBA after 22h and (b) with the hydrotrope IPA after 15h.*

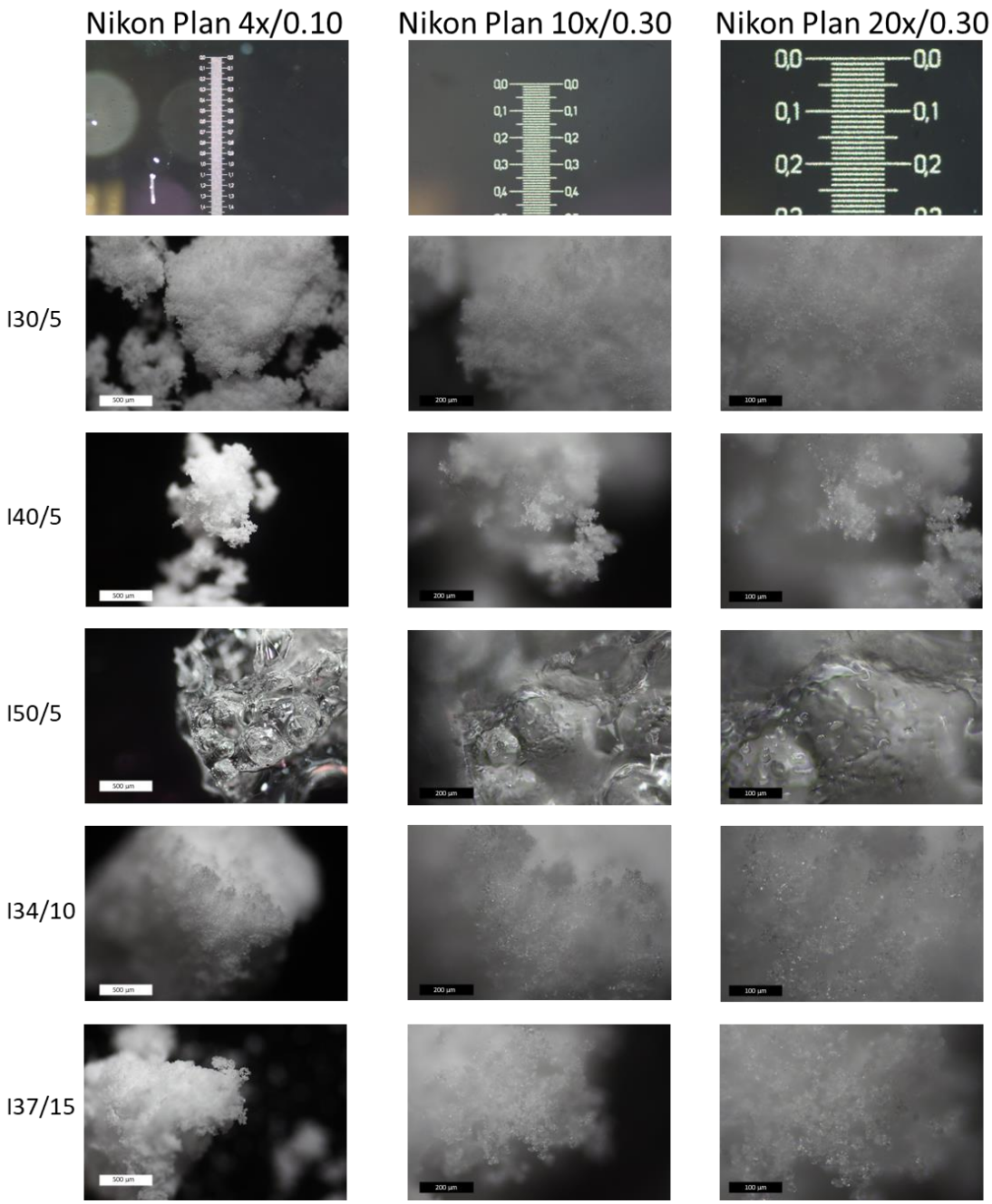

Figure S 2.7 *Light microscope images with different magnification factors of freeze-dried microsuspension polymers with the hydrotrope IPA after 15h.*

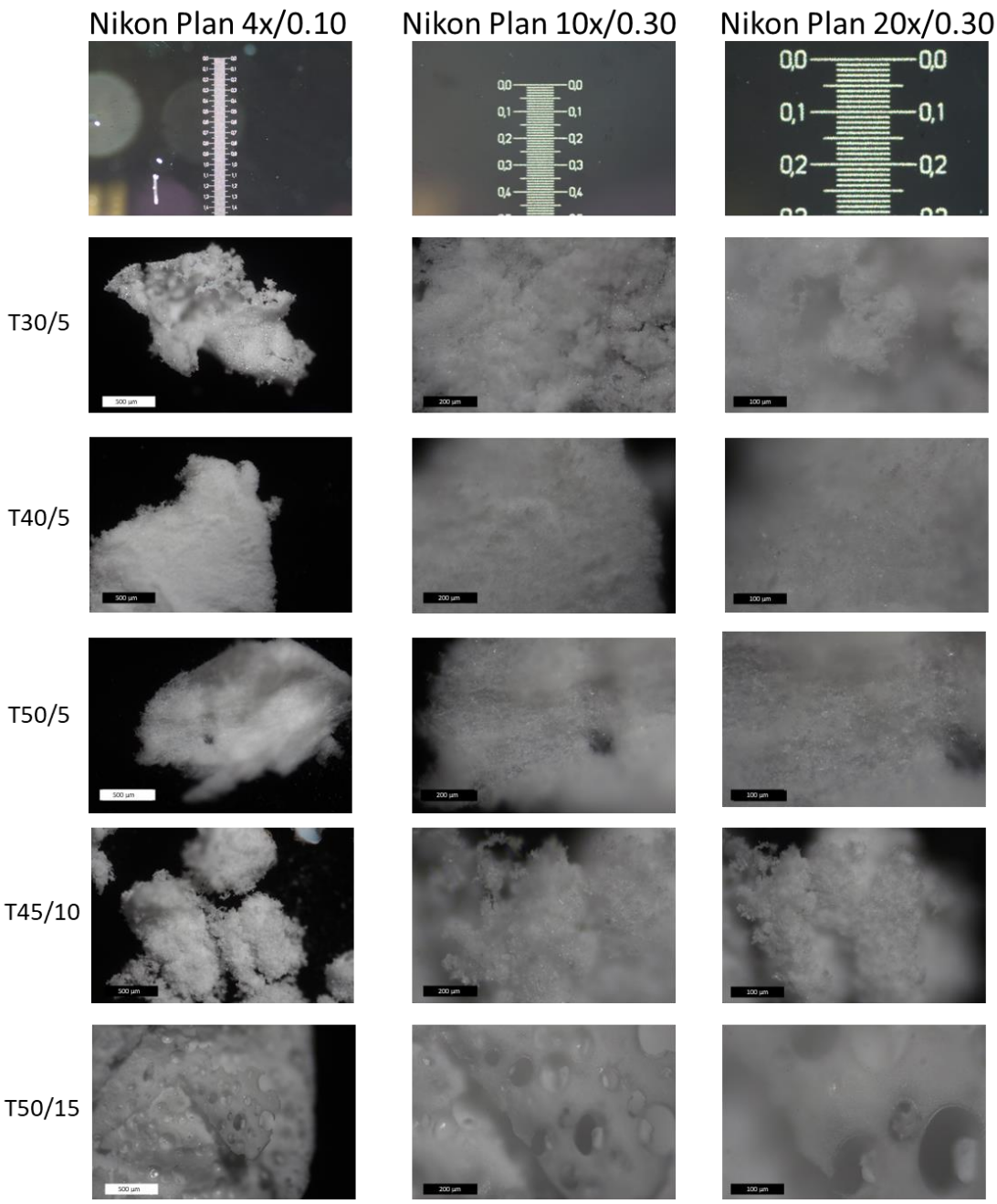

Figure S 2.8 *Light microscope images with different magnification factors of freeze-dried microsuspension polymers with the hydrotrope TBA after 22h.*

2.7.8 Exemplary Evaluation of M_w by GPC

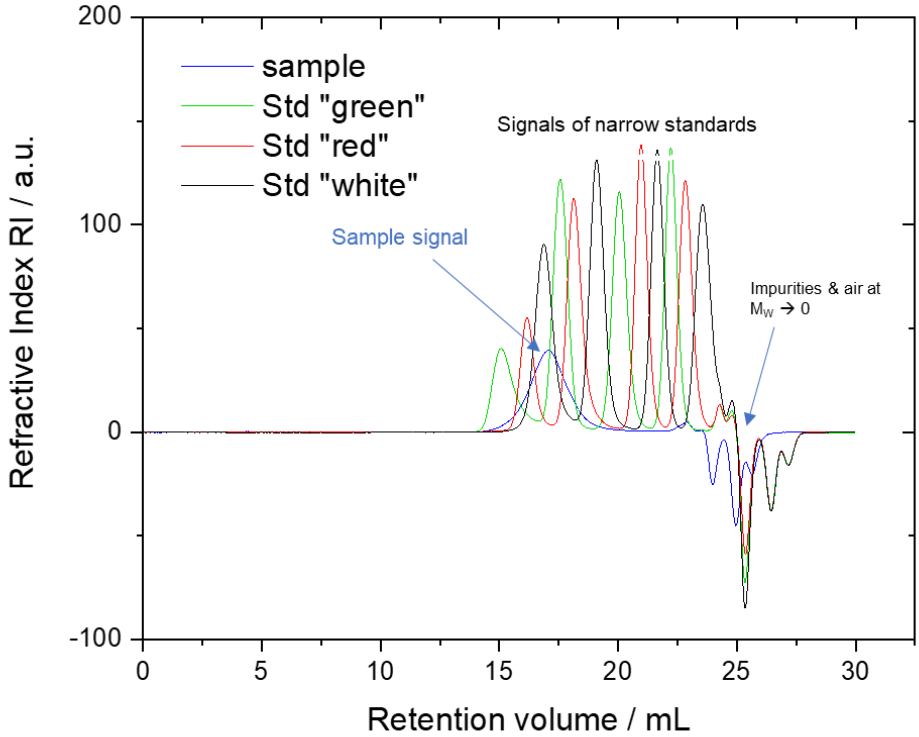

Figure S 2.9 *Exemplary raw-data for M_w-determination on the example T50/5 5h (blue) and three narrow MMA-Standards (Std) from PSS, containing each four different molar masses.*

2.7.9 Exemplary Tie Line Determination

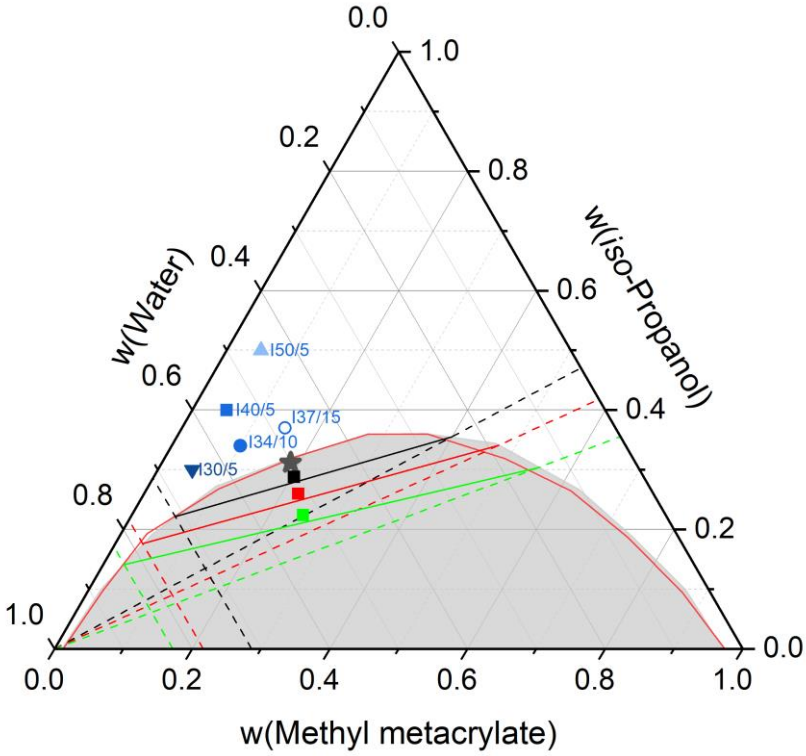

Figure S 2.10 *Exemplary tie line determination. The MMA-rich end of the tie lines is identified as the intercept in between the line of constant MMA to alcohol ratio derived by NMR and the binodal line. The water-rich end of the tie lines is identified as intercept in between the line of constant water ratio as derived by Karl Fischer experiments and the binodal line (marked as black, red and green dashed lines for both sides). The tie lines arise from the connection of the determined oil- and water-rich ends (solid lines). The initial sample compositions before centrifugation (marked as squares) are slightly more alcohol-rich compared to the determined tie lines. This is due to the alcohol-enrichment in the interphase in between the oil- and water-rich phases, which is rejected in the tie-line determination process.*

2.8 Bibliography

[1] J. Blahnik, S. Krickl, K. Schmid, E. Müller, J. Lupton, and W. Kunz, *J. Colloid. Interface Sci.* **2023**, *648,* 755–767.

[2] W. Kunz, S. Krickl, J. Blahnik, and K. Schmid. WO2022112481A1, **26.11.2021**.

[3] D. Colombani, *Prog. Polym. Sci.* **1997**, *22,* 1649–1720.

[4] B. M. Louie, G. M. Carratt, and D. S. Soong, *J. Appl. Polym. Sci.* **1985**, *30,* 3985–4012.

[5] A. M. van Herk, and R. G. Gilbert, in: *Chemistry and Technology of Emulsion Polymerisation* (Hrsg.: A. M. van Herk), John Wiley & Sons Ltd, Oxford, UK, **2013,** 43–73.

[6] J. M. Asua, *J. Polym. Sci. A Polym. Chem.* **2004**, *42,* 1025–1041.

[7] A. Rudin und P. Choi, *The elements of polymer science and engineering,* 3. Aufl., Elsevier Academic Press, San Diego, Calif., **2013**.

[8] S. Sakai, S. Urano, and H. Takatsuki, *Waste Management* **2000**, *20,* 241–247.

[9] E. L. Teuten, J. M. Saquing, D. R. U. Knappe, M. A. Barlaz, S. Jonsson, A. Björn, S. J. Rowland, R. C. Thompson, T. S. Galloway, R. Yamashita, D. Ochi, Y. Watanuki, C. Moore, P. H. Viet, T. S. Tana, M. Prudente, R. Boonyatumanond, M. P. Zakaria, K. Akkhavong, Y. Ogata, H. Hirai, S. Iwasa, K. Mizukawa, Y. Hagino, A. Imamura, M. Saha, and H. Takada, *Philos. Trans. R. Lond., B, Biol. Sci.* **2009**, *364,* 2027–2045.

[10] J. Glasing, P. G. Jessop, P. Champagne, W. Y. Hamad, and M. F. Cunningham, *Langmuir* **2020**, *36,* 796–809.

[11] S. Nishimura, K. Nishida, S. Shiomoto, and M. Tanaka, *Mater. Adv.* **2022**, *3,* 5043–5054.

[12] O. Diat, M. L. Klossek, D. Touraud, B. Deme, I. Grillo, W. Kunz, and T. Zemb, *J. Appl. Crystallogr.* **2013**, *46,* 1665–1669.

[13] N. F. Borys, S. L. Holt, and R. E. Barden, *J. Colloid. Interface Sci.* **1979**, *71,* 526–532.

[14] B. A. Keiser, D. Varie, R. E. Barden, and S. L. Holt, *J. Phys. Chem.* **1979**, *83,* 1276–1280.

[15] Y. L. Khmelnitsky, I. N. Zharinova, I. V. Berezin, A. V. Levashov, and K. Martinek, *Ann. N. Y. Acad. Sci.* **1987**, *501,* 161–164.

[16] Y. L. Khmelnitsky, R. Hilhorst, and C. Veeger, *Eur. J. Biochem.* **1988**, *176,* 265–271.

[17] Y. L. Khmelnitsky, A. K. Gladilin, I. N. Neverova, A. V. Levashov, and K. Martinek, *Collect. Czech. Chem. Commun.* **1990**, *55,* 555–563.

[18] J. Blahnik, E. Müller, L. Braun, P. Denk, and W. Kunz, *COCIS* **2022**, *57,* 101535.

[19] T. N. Zemb, M. Klossek, T. Lopian, J. Marcus, S. Schöettl, D. Horinek, S. F. Prevost, D. Touraud, O. Diat, S. Marčelja, and W. Kunz, *Proc. Natl. Acad. Sci. U. S. A.* **2016**, *113,* 4260–4265.

[20] S. Prevost, T. Lopian, M. Pleines, O. Diat, and T. Zemb, *J. Appl. Crystallogr.* **2016**, *49,* 2063–2072.

[21] B. A. Keiser, and S. L. Holt, *Inorg. Chem.* **1982**, *21,* 2323–2327.

[22] H. S. Tarkas, D. M. Marathe, M. S. Mahajan, F. Muntaser, M. B. Patil, S. R. Tak, and J. V. Sali, *Mater. Res. Express* **2017**, *4,* 25018.

[23] X. Cui, J. Wang, X. Zhang, Q. Wang, M. Song, and J. Chai, *Langmuir* **2019**, *35,* 9255–9263.

[24] Y. Wu, L. Tang, Q. Zhang, F. Kong, and Y. Bi, *Materials Letters* **2021**, *285,* 129053.

[25] S. T. Camli, F. Buyukserin, O. Balci, and G. G. Budak, *J. Colloid. Interface Sci.* **2010**, *344,* 528–532.

[26] C. G. Dobie, and K. V. Boodhoo, *Chem. Eng. Process* **2010**, *49,* 901–911.

[27] H. Kempe, and M. Kempe, *J. Colloid. Interface Sci.* **2022**, *616,* 560–570.

[28] E. Lepeltier, C. Bourgaux, and P. Couvreur, *Adv. Drug Deliv. Rev.* **2014**, *71,* 86–97.

[29] W. R. P. Raj, M. Sasthav, and H. M. Cheung, *Langmuir* **1991**, *7,* 2586–2591.

[30] Y. Yao, C. Li, F. Liu, P. Zhao, Z. Gu, and S. Zhang, *Phys. Chem. Chem. Phys.* **2019**, *21,* 10477–10487.
[31] B. Sadat Mirhoseini, and A. Salabat, *J. Mol. Liq.* **2021**, *342,* 117555.
[32] S. Peng, C. Xu, T. C. Hughes, and X. Zhang, *Langmuir* **2014**, *30,* 12270–12277.
[33] M. Clausse, L. Nicholas-Morgantini, A. Zradba, and D. Touraud, in: *Surfactant Science Series* (Hrsg.: M. Dekker), New York, **1987,** 15–62.
[34] S. Prévost, S. Krickl, S. Marčelja, W. Kunz, T. Zemb, and I. Grillo, *Langmuir* **2021**, *37,* 3817–3827.
[35] T. Buchecker, S. Krickl, R. Winkler, I. Grillo, P. Bauduin, D. Touraud, A. Pfitzner, and W. Kunz, *Phys. Chem. Chem. Phys.* **2017**, *19,* 1806–1816.
[36] S. Krickl, L. Jurko, K. Wolos, D. Touraud, and W. Kunz, *J. Mol. Liq.* **2018**, *271,* 112–117.
[37] S. Krickl, D. Touraud, P. Bauduin, T. Zinn, and W. Kunz, *J. Colloid. Interface Sci.* **2018**, *516,* 466–475.
[38] M. Hahn, S. Krickl, T. Buchecker, G. Jošt, D. Touraud, P. Bauduin, A. Pfitzner, A. Klamt, and W. Kunz, *Phys. Chem. Chem. Phys.* **2019**, *21,* 8054–8066.
[39] S. Stemplinger, S. Prévost, T. Zemb, D. Horinek, and J.-F. Dufrêche, *J. Phys. Chem. B* **2021**, *125,* 12054–12062.
[40] H. Cölfen, R. Rosenberg, D. Haffke, S. Stemplinger, T. Zemb, and D. Horinek, *Research* **2023**, *6*.
[41] F. Rodriguez, *Principles of polymer systems,* 4. Aufl., Taylor & Francis, Washington, DC, **1996**.
[42] W. A. Strong, *Ind. Eng. Chem.* **1964**, *56,* 33–38.
[43] *Polymer handbook,* 4. Aufl., Wiley, New York, **1999**.
[44] K. W. Dixon, in: *Database of Polymer Properties Online* (Hrsg.: J. Brandrup, E. H. Immergut and E. A. Grulke), Wiley, **2003**.
[45] M. R. Billany, K. Khatib, M. Gordon, and J. K. Sugden, *Int. J. Pharm.* **1996**, *137,* 143–147.
[46] F. M. Pavel, *J. Dispers. Sci. Technol.* **2004**, *25,* 1–16.
[47] J. O. Stoffer, and T. Bone, *J. Dispers. Sci. Technol.* **1980**, *1,* 37–54.
[48] M. Antonietti, R. Basten, and S. Lohmann, *Macremol. Chem. Phys.* **1995**, *196,* 441–466.
[49] M. Nie, Q. Wang, and G. Qiu, *Ultrason. Sonochem.* **2008**, *15,* 222–226.
[50] C. H. Chew, T. D. Li, L. H. Gan, C. H. Quek, and L. M. Gan, *Langmuir* **1998**, *14,* 6068–6076.
[51] T. H. Chieng, L. M. Gan, W. K. Teot, and K. L. Pey, *Polymer* **1996**, *37,* 5917–5925.
[52] M. F. Cunningham, *Polym. React. Eng.* **1999**, *7,* 231–257.
[53] E. Hofmann, P. Degot, D. Touraud, B. König, and W. Kunz, *Food chemistry* **2023**, *417,* 135944.
[54] A. Xenakis, M. Zoumpanioti, and H. Stamatis, *COCIS* **2016**, *22,* 41–45.
[55] T. H. Chieng, L. M. Gan, C. H. Chew, and S. C. Ng, *Polymer* **1995**, *36,* 1941–1946.
[56] K. Yoshida, T. Yamaguchi, A. Kovalenko, and F. Hirata, *J. Phys. Chem. B* **2002**, *106,* 5042–5049.

3 Industrially Relevant (Co)polymers and Hydrotropes for Use in SFME Polymerization

3.1 Abstract and Preface

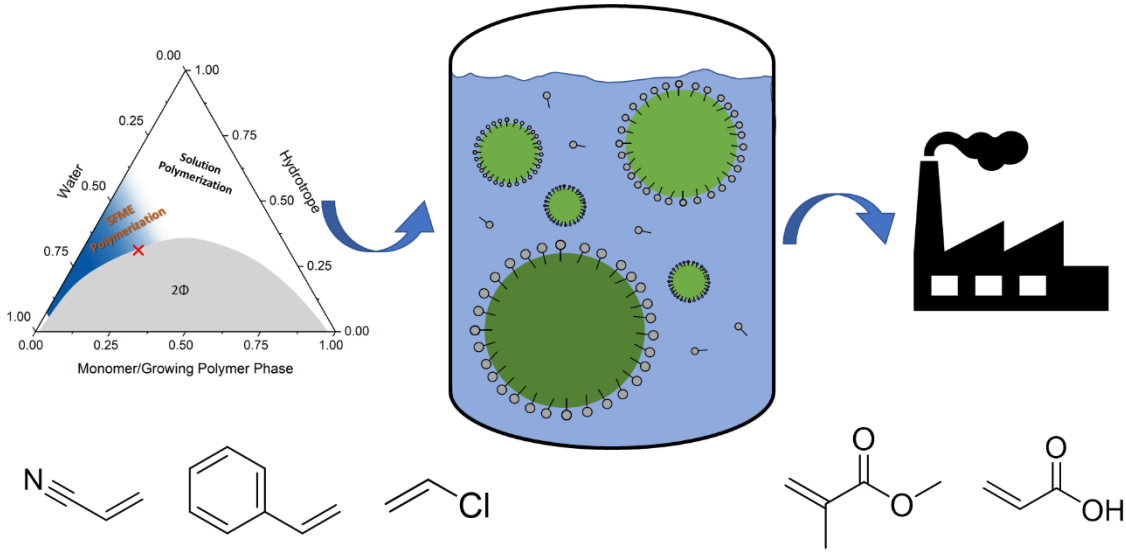

Figure 3.1 *Graphical abstract schematically illustrating the use of extending the concept of polymerizations in SFME to industrially relevant (co)polymers.*

In the previous chapter 2, the concept of polymerizations in surfactant-free microemulsions (SFMEs) with the model monomer methyl methacrylate (MMA) is introduced. Chapter 3 aims to extend the concept of microsuspension polymerizations in SFME to further industrially relevant polymers and copolymers, namely poly(vinyl chloride) (PVC), poly(vinyl acetate-co-acrylic acid), and poly(vinyl acetate-co-methyl methacrylate), and poly(styrene-co-acrylonitrile). Furthermore, some glycol ethers are tested for their suitability as a hydrotrope. For some systems, polymerizations are performed, and resulting polymers are characterized, while for poly(styrene-co-acrylonitrile), only investigations of the pseudo-ternary systems before polymerizations

are done. It is found that, in principle, SFME polymerization should be possible for all investigated systems. In the system poly(acrylic acid-co-methyl methacrylate), which is investigated in more detail, it is observed that the choice of the SFME system impacts not only the conversion but also the copolymer composition.

Contributions to the experimental work:

- Jonas Blahnik: Conceptualization, experimental work, data evaluation
- Chantal Walser: Experimental Work, data evaluation (copolymers)
- David Hennek: Experimental work (glycol ethers)

3.2 Introduction

Poly(methyl methacrylate) (PMMA) is an industrial-relevant polymer famous for its optical transparent properties. [1] Due to its properties (not harmful, easy to handle), it's monomer MMA is a model monomer often used for polymerizations in research. [2–5] Pure PMMA is mainly produced by bulk, suspension, or emulsion techniques. [1] In terms of microsuspension or microemulsion particles, other polymers seem industrially more relevant. However, in copolymers, MMA is sometimes used as one of the monomers. Relevant substances made by microsuspension processes include, *e.g.*, poly(vinyl chloride) (PVC) [6] or co-polymers like poly(styrene-co-acrylonitrile) or acrylates, which are often used in different compositions. [7] An important monomer is vinyl acetate (VAc), which is mostly used for the synthesis of poly(vinyl alcohol) (PVA), but also for PVAc itself. [8; 9] An example of numerous applications of acrylic or vinyl acetate-based copolymers are binders used, *e.g.,* in paints, glues, or mortals, and are mostly produced by emulsion or suspension methods. [10]

An advantage of the method of microemulsion or microsuspension polymerization in an surfactant-free microemulsion (SFME) might be the purity of the derived polymers, free of any surfactants or auxiliary colloids [11–13] as claimed in chapter 2. However, it might also have some drawbacks: Usually, the solvent (water and alcohols) must be removed in order to access the microemulsion or microsuspension polymers, *e.g.*, by distillation or spray-drying. If the (co)polymer will finally be formulated in a liquid product, it might be a big advantage if the hydrotrope can remain for the final application. Thus, the separation of the polymer or water and hydrotrope could be avoided partly or even completely. Relevant solvents in the context of paints are, *e.g.*, glycols, which can have amphiphilic properties. [10]

This chapter aims to extend the concept of polymerizations in SFMEs to further industrially relevant polymers and copolymers, and other hydrotropes. Thus, the phase behavior of VAc/acrylic acid (AA), VAc/MMA, styrene/AN, and 1,2-dichloroethane (DCE) as precursor and model molecule for vinyl chloride is investigated using the hydrotropes *iso*-propanol (IPA), *n*-propanol (NPA), and *tert*-butyl alcohol (TBA). Poly(VAc-co-AA) and poly(VAc-co-MMA) are investigated in more detail concerning conversion, weight average molar mass by gel permeation chromatography (GPC), polymer composition, and glass transition temperature. The glycols diethylene glycol butyl ether (DEG), diethylene glycol monomethyl ether (DEGME), and dipropylene glycol methyl ether (DPM) are tested as hydrotropes for their use with the monomer MMA.

A short introduction about the industrial relevance of each investigated system will be given in each section of the Results and Discussion part.

3.3 Materials and Methods

3.3.1 Materials

Methyl methacrylate (MMA, 99% purity, stabilized with 4-methoxy phenol ≤ 30 ppm), vinyl acetate (VAc, 99%, stabilized with hydroquinone > 1 ppm), styrene (99%, stabilized with 4-tert-butyl catachol, < 15 ppm), acrylonitrile (AN, 99%, stabilized with monomethyl ether hydroquinone, 35-45 ppm), *n*-propanol (NPA, 99.5%), diethylene glycol methyl ether (DEGME, 99%), diethylene glycol butyl ether (DGB, 99%), dipropylene glycol methyl ether (DPM, 99%, mixture of isomers) and dimethyl sulfoxide-d_6 (DMSO-d_6, 99.5 atom % D) are obtained from Merck (Darmstadt, Germany). *tert*-Butyl alcohol (TBA, 99%) is purchased from Carl Roth (Karlsruhe, Germany). Tetrahydrofuran (THF, analytical reagent grade), Acrylic acid (AA, 98%, stabilized with 4-methoxy phenol, 180-220 ppm), and *iso*-propanol (IPA, 99.8%) are bought from Fisher Scientific (Schwerte, Germany). Poly(methyl methacrylate) standards (ReadyCal-Kit PSS-mmkitr1) are obtained from PSS Polymer Standards Service (Mainz, Germany). *Bis*-(4-*tert*-butylcyclohexyl) peroxy dicarbonate (BCC, 95%) is provided by PERGAN (Bocholt, Germany). Dichloroethane (DCE, technical grade) is provided by Vestolit GmbH (Marl, Germany).

Prior to use, MMA is distilled at 40 °C and 60 mbars, AA is distilled at 40 °C and 10 mbars, and VAc is distilled at 40 °C and 240 mbars to remove the stabilizer. Distilled monomers are stored up to 3 weeks in the fridge. Prepacked columns for removing inhibitors (Merck, Darmstadt, Germany) are used to purify styrene and AN directly before use. Aqueous solutions are prepared using deionized water with a resistivity of 18 MΩcm. All other chemicals are used without further purification.

3.3.2 Ternary Phase Diagrams

Phase diagrams are determined as described in section 2.3.2. For pseudo-ternary phase diagrams, one or more substances are mixed previously at a fixed mixing ratio and considered as a single component in the phase diagram.

3.3.3 Dynamic Light Scattering (DLS) of SFME Systems

DLS experiments of SFME systems are performed as described in section 2.3.5.

3.3.4 Polymerizations

Approximately 6 g of the components (water, hydrotrope, monomer(s), 0.4 mol% BCC referring to the monomers as initiator) are mixed in a 20 mL glass vial and closed with an aluminum crimp cap with polytetrafluoroethylene (PTFE) septum. Air is displaced by flushing with nitrogen via a

cannula for 90 s. Polymerizations are stopped after a certain time by immediately freezing them in liquid nitrogen. Afterward, polymers are freeze-dried.

3.3.5 Gel Permeation Chromatography (GPC)

GPC is performed as described in section 2.3.10.

3.3.6 Monomer Ratios in the Copolymers by Nuclear Magnetic Resonance Spectroscopy (NMR)

^{1}H-NMR spectra are recorded on a Bruker Avance 300 NMR spectrometer (Billerica, MA, USA) at 300 MHz. For VAc-AA copolymers, DMSO-d_6 is used as a solvent. Data evaluation is done by using MestReNova (version 6). Calculations of compositions are done by comparing integrals of peaks that can be clearly assigned to a single molecule.

3.4 Results and Discussion

3.4.1 Poly(vinyl acetate-co-acrylic acid)

3.4.1.1 Characterization of the SFME System

Both VAc and AA are commonly used monomers in industry. VAc is a monomer that is slightly more hydrophilic than, *e.g.*, MMA, which is structurally related. This can be seen as the water-solubility is 0.20 g L^{-1} for VAc and 0.15 g L^{-1} for MMA, and the K_{OW} (*n*-octanol-water partition coefficient) value is 1.38 for MMA and 0.6 for VAc. [14; 15] The reactivity of VAc is overall lower than that of MMA and especially of AA. [16] A main application of VAc – next to the production ov PVAc and its copolymers for themselves – is the production of poly(vinyl alcohol) via the hydrolysis of PVAc, which removes the acetate groups. [17] The direct approach from the theoretical monomer vinyl alcohol is nearly impossible due to tautomerization to acetaldehyde. [17; 18] AA is a quite hydrophilic monomer, which is completely water-miscible. It comprises a quite high reactivity in comparison to other vinylic monomers. [16] AA is mainly used as a polyelectrolyte by neutralization after the polymerization, making it extremely hydrophilic. Pure PAA is used as a superabsorbent polymer. By adding AA to a dispersion polymer, the hydrophilicity can be fine-tuned, whereby both the AA content and the degree of neutralization play a role. [19]

Poly(VAc-co-AA) is a commercially relevant polymer, *e.g.*, for the production of paints, stickers, in the textile industry, agriculture, cosmetics, water clarification, oil recovery or paper industry. [8; 9]

As AA is completely water-miscible, the question arises, how to treat it in terms of ternary phase diagrams. In the year 1991, it is first published that AA acts as a hydrotrope in SFME systems with MMA and the cross-linker ethyleneglycoldimethacrylate (even though the term hydrotropy is not used). [20] In another example, AA is used for encapsulation of hydrophobic, pharmaceutically active substances by forming an SFME in the presence of water. [21] Both approaches are indeed interesting but cannot be directly applied to industrially relevant systems.

Figure 3.2 depicts pseudo-ternary phase diagrams of VAc, AA, water, and alcohol (TBA, NPA, or IPA) as an additional hydrotrope. TBA is used twice as a hydrotrope, but with AA being both part of the oil phase (**Figure 3.2 a**) and of the hydrotrope (**Figure 3.2 b**). Interestingly, the phase diagrams of AA and TBA show a comparable binodal, indicating that AA has indeed hydrotropic behavior. On the other side, samples with AA as part of the oil phase still show a quite symmetric biphasic region without decreasing the biphasic region too much. As this approach has the advantage of a fixed AA to VAc ratio for each individual phase diagram and also for different

samples, it is decided to focus on diagrams with AA as part of the oil phase, even though the classification as part of the hydrotropes would be more correct from a colloid chemist's view. When moving from TBA to NPA (cf. **Figure 3.2 d**) and IPA (cf. **Figure 3.2 c**), the biphasic region further decreases, like already described for MMA. [13]

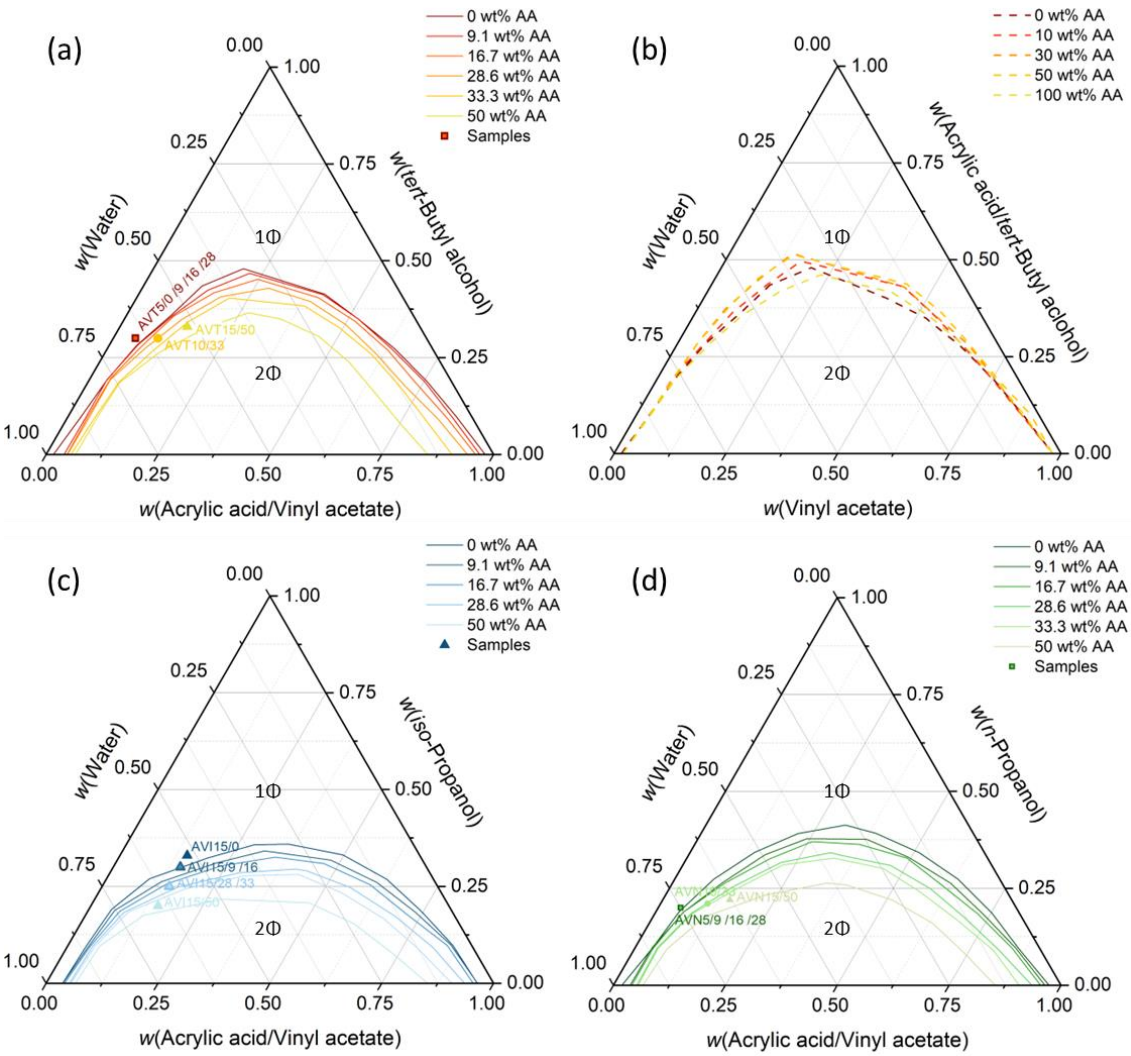

Figure 3.2 *Pseudo-ternary phase diagrams of the system AA/VAc at 45°C: (a) AA/VAc as oil-phase and TBA as hydrotrope, (b) VAc as oil phase and AA/TBA as hydrotropes, (c) AA/VAc as oil-phase and IPA as hydrotrope, (d) AA/VAc as oil-phase and NPA as hydrotrope. Samples which are further investigated are marked and designated. Sample compositions can be found in* ***Table S 3.1*** *in the appendix.*

Samples investigated further are chosen with approximately equidistance to the phase diagram for each system. In the system with IPA, all samples contain a fixed monomer ratio of 15 wt% (each 7.5 wt% AA and VAc) and a varying IPA content. In the systems with NPA and TBA, the alcohol and monomer ratios are slightly changed in order to stay at a similar location on the water-rich side of the binodal. The location of samples is printed in the phase diagrams in **Figure 3.2**. The exact compositions are given in **Table S 3.1** in the appendix. **Figure 3.3** depicts the

autocorrelation functions derived by DLS for all samples. Most pronounced autocorrelation functions can be observed for the sample containing 16 wt% AA for IPA, 50 wt% AA for NPA, and 28 wt% AA for TBA. However, distinct autocorrelation functions can be observed for all investigated samples, which indicates mesostructuring. Thus, all samples should be suitable for polymerization in SFME.

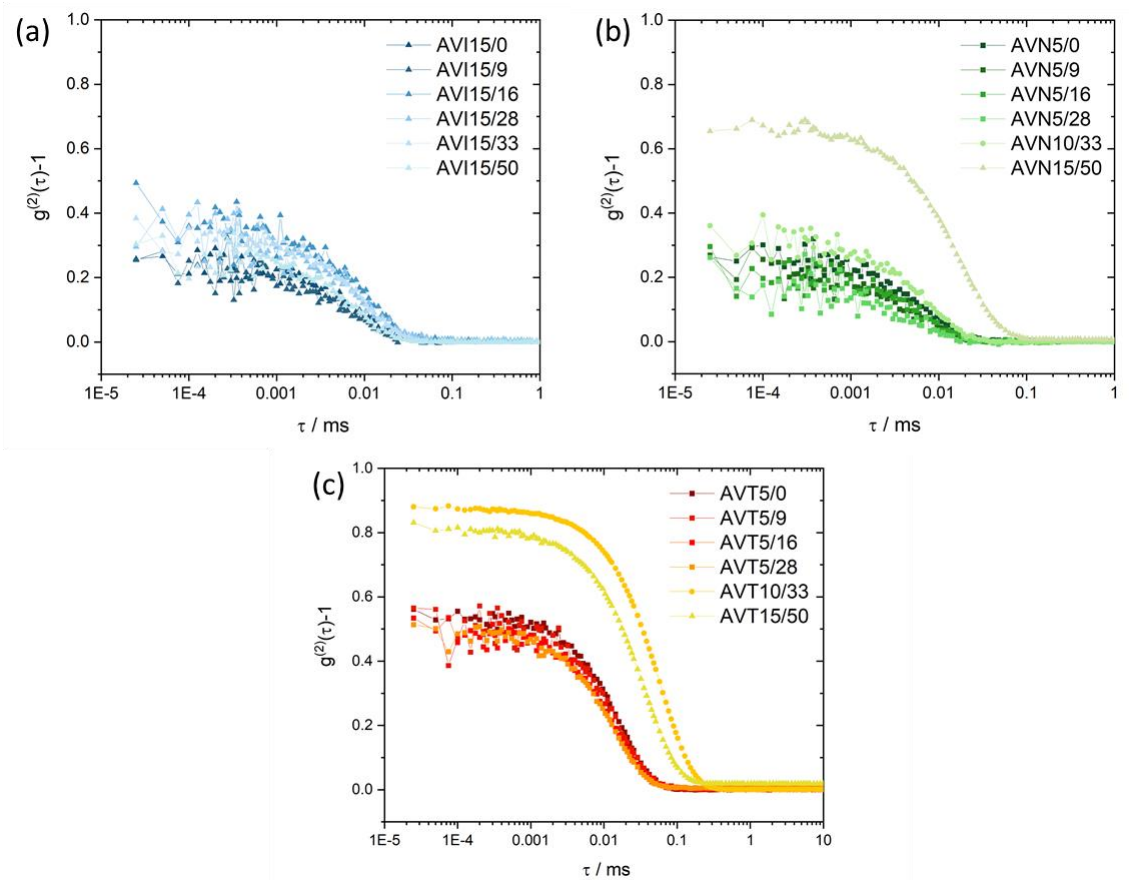

Figure 3.3 *Autocorrelation functions derived by DLS for the systems Water, Acrylic acid//VAc, and the hydrotropes (a) IPA, (b) NPA, (c) TBA at 45 °C.*

3.4.1.2 Polymerizations

Figure 3.4 depicts the conversion of samples with 0.4 mol% BCC as initiator. For all three alcohols, the conversion increases over time and does not seem to be completed after the observation time of 7 h. Conversions for samples with higher AA contents reach 60 wt% after 7h for all three alcohols. However, especially for samples with lower AA contents and with NPA as hydrotrope, conversions are quite bad. This behavior seems to be somehow correlating to the quality of mesostructuring, which is worst for most NPA samples (except for AVN15/50, which shows by far the best structuring and the highest conversions, cf. **Figure 3.3**). However,

structuring alone might not completely explain the differences, but also the reactivities of the alcohols, as already discussed in section 2.5. [13]

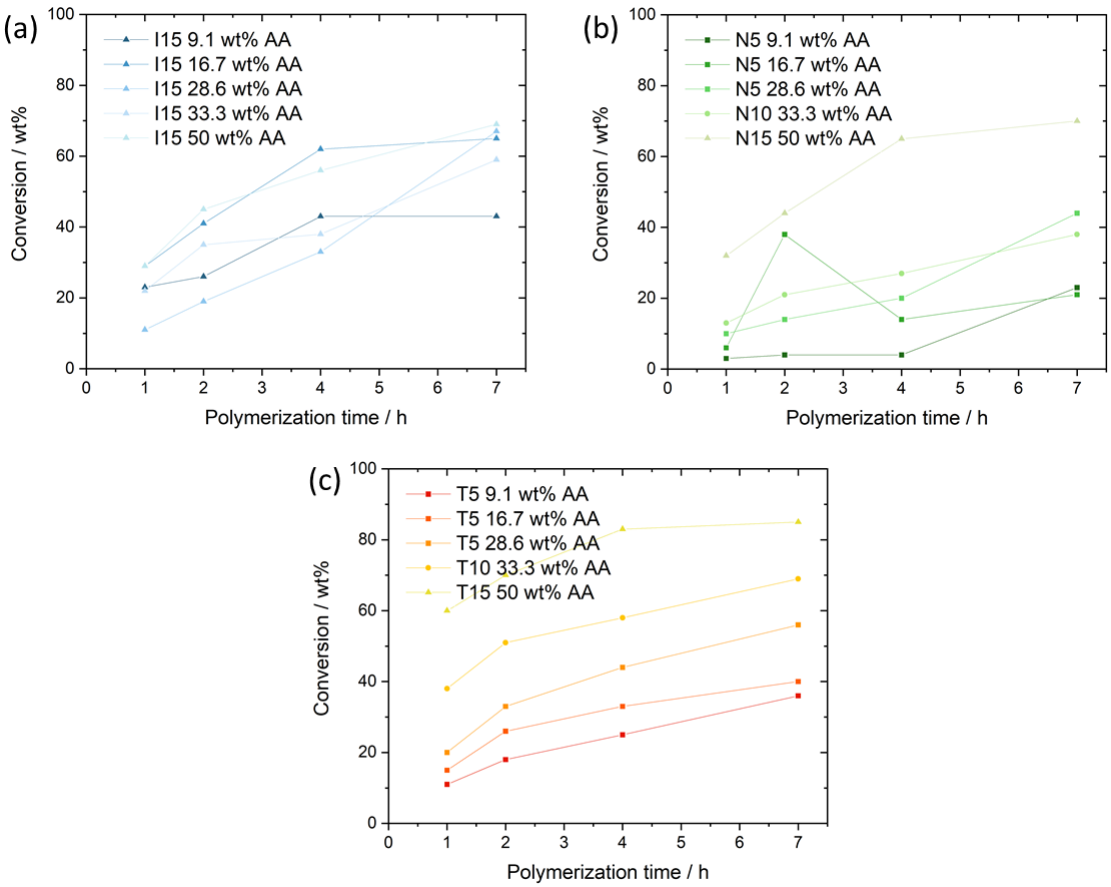

Figure 3.4 *Conversion during the first 7 hours of the polymerization of VAc and AA in different weight ratios with the hydrotropes (a) IPA, (b) NPA, and (c) TBA. 0.4 mol% BCC corresponding to the monomer phase is used as initiator at 45 °C.*

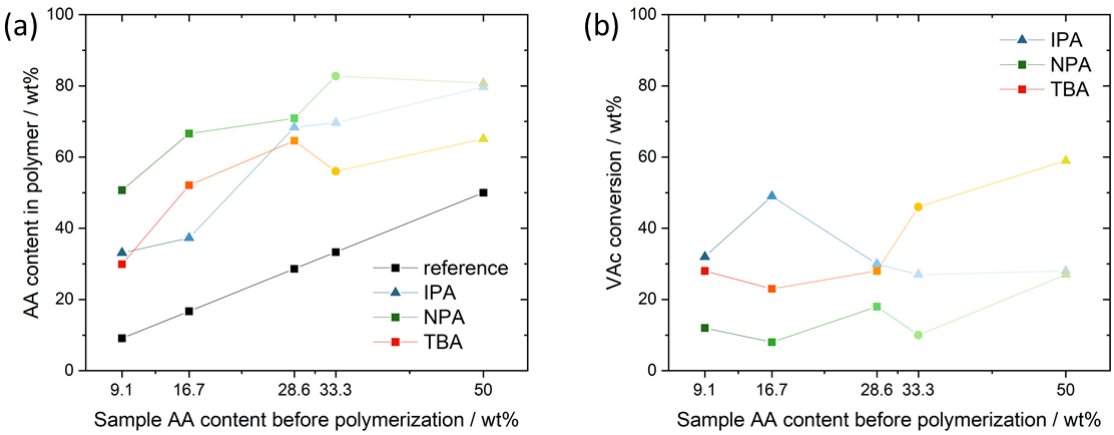

Figure 3.5 *(a) Acrylic acid content in the derived polymer after 7 h plotted against the acrylic acid concentration in the reaction mixtures before polymerization, the black line gives the concentration before as reference. (b) Vinyl acetate conversion after 7 h against the acrylic acid concentration in the reaction mixtures. The acrylic acid conversion can be expected to be 100%. Colors and markings correspond to the phase diagram in* ***Figure 3.2****.*

The AA to VAc ratio in the derived polymer is determined by NMR. **Figure 3.5 a** shows the AA to Vac ratio in the polymer after 7 h plotted against the initial AA content in the reaction mixture. The initial concentrations are plotted as a black line as reference. The ratios in the latter polymer are overall higher than before, which confirms the significantly higher reactivity of AA in comparison to VAc and the fact that VAc is considered as one of the vinylic monomers with the lowest reactivity. [22] Reactivity ratios between AA and VAc for copolymerization are given as 8.66 (for AA) to 0.021 (for VAc). [16] Thus, and also based on NMR data, AA conversion can be assumed to be almost complete after 7 h. **Figure 3.5 b** depicts the VAc conversion, which is calculated from NMR data and the overall conversion. NPA samples, which already showed the lowest overall conversion, show the highest AA contents and thus the lowest VAc conversions for all samples.

The polymerizations with TBA and IPA differ in their course. While for TBA the VAc conversion increases with increased AA content in the reaction mixture, the behavior is opposite for IPA samples. Thus, at lower AA contents, IPA leads to optimal conversions. TBA seems to be favored at higher AA contents, beginning to perform better beginning around 30 wt% AA.

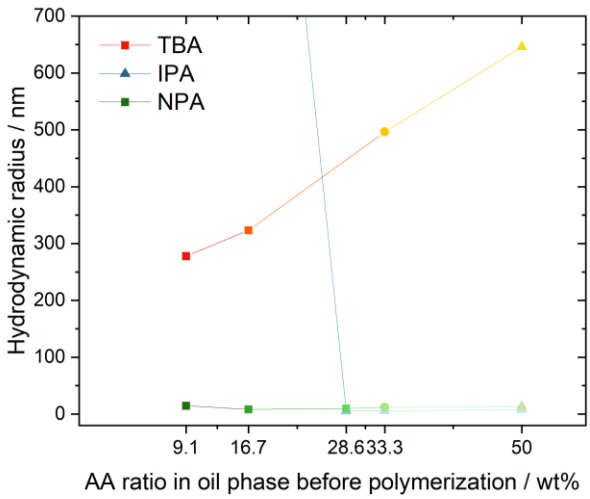

Figure 3.6 *Hydrodynamic radii of VAc/AA copolymers after 7 h polymerization time as a function of the initial AA concentration before the polymerization started, dispersed in EtOH at 25 °C.*

Hydrodynamic radii of polymers dispersed in EtOH are depicted in **Figure 3.6**. Samples that perform best in terms of conversion are now the ones that comprise quite high radii, with IPA samples of low AA contents going to the micron range. This is, on the other side, not astonishing, as higher VAc conversions come along with increased hydrophobicity and, thus, probably also lower solubility in EtOH. This is especially relevant for NPA, showing overall low hydrodynamic radii in the range of 10-20 nm. For IPA, the radii drop from the micron range to the same size

range as NPA particles for samples with initial AA contents of 28.6 wt% or more. For TBA, a steady increase from around 280 nm to over 650 nm in hydrodynamic radius can be observed with increasing initial AA content.

Overall, it can be concluded that by the use of the hydrotropes IPA, NPA, or TBA, AA-VAc-copolymers with different properties and especially different AA contents can be synthesized. This is especially of interest, as reactivity ratios of both monomers seem to be differently strongly affected by the SFME/alcohol environment. This is proven, as not only the absolute conversion changes but also the VAc contents in the resulting polymer. Thus, by optimizing the system, it might be possible to improve the low reactivity of VAc in contrast to AA. [22]

A problem might be the low conversion of VAc, which could possibly be optimized by either higher temperatures, longer polymerization times, or other, maybe combined, initiator systems. The choice of the system obviously has an impact on the polymer itself and the hydrodynamic radii when dispersed. The average molar mass could not be determined due to the high AA content and, thus, the bad solubility of the copolymer in the solvent THF, which is used in the available GPC setup. Of course, the average molar mass would be a relevant property to know before application. Another important property that remains to be investigated is the distribution of the two monomers in the copolymer. Due to the clearly different reactivities, it is assumed that AA and VAc are not homogeneously distributed in the polymer. It is assumed that both properties explain the differences in the hydrodynamic radii (cf. **Figure 3.6**). This should therefore be checked in the future.

3.4.2 Poly(vinyl acetate-co-methyl methacrylate)

3.4.2.1 Characterization of the SFME System

MMA and VAc have already been used in other experiments before (cf. chapter 2 for MMA and section 3.4.1 in this chapter for VAc), but not combined so far. Both monomers can be counted as hydrophilic oils with not very different properties, and both are suitable for SFMEs, as discussed in section 3.4.1. [14; 15] Thus, in contrast to VAc-AA-copolymers, MMA and VAc must certainly be considered as shared oil phases in pseudo-ternary phase diagrams. Poly(VAc-co-MMA) is considered for use as membrane material or for nanoparticles for medical use. [23; 24] Other relevant applications, not only for poly(VAc-co-MMA) but further copolymers, are the field of adhesives or paints. [22]

Figure 3.7 depicts pseudo-ternary phase diagrams with water, the alcohols IPA, NPA, and TBA as hydrotropes, and MMA/VAc-mixtures with different compositions as the oil phase at 45 °C.

As both monomers are not very different concerning their properties, as already discussed, also the phase behavior does not seem to be significantly different.

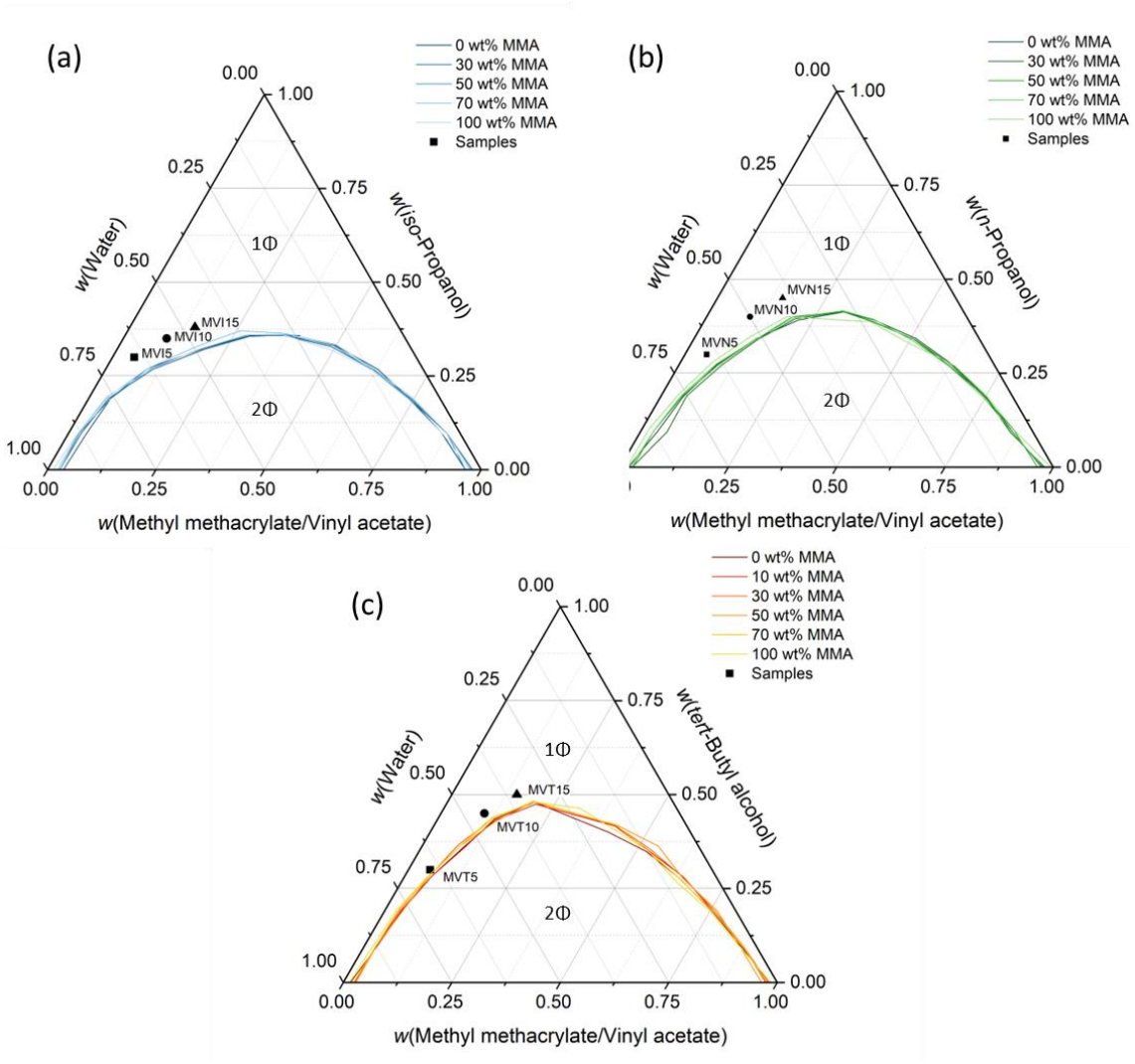

Figure 3.7 *Pseudo-ternary phase diagrams of the system MMA/VAc at 45°C with different MMA to VAc ratios using the hydrotropes (a) IPA, (b) NPA, and (c) TBA.*

For all three alcohols, only little changes can be observed when changing the VAc to MMA ratio. For MMA, the biphasic region might be slightly larger on the water-rich side of the phase diagram and slightly lower on the oil-rich side. Thus, the binodal seems to be shifted slightly to the water-rich side. However, these changes are really small and probably neglectable. As already found for the MMA system (cf. chapter 2), [13] the biphasic region increases from IPA via NPA to TBA. Due to the similarity of phase diagrams with different VAc/MMA-ratios, the same three sample compositions with 5 wt%, 10 wt%, and 15 wt% monomers are chosen for all VAc/MMA-ratios in approximate equidistance to the binodal for the three alcohols. Exact sample compositions are given in **Table S 3.3** in the appendix.

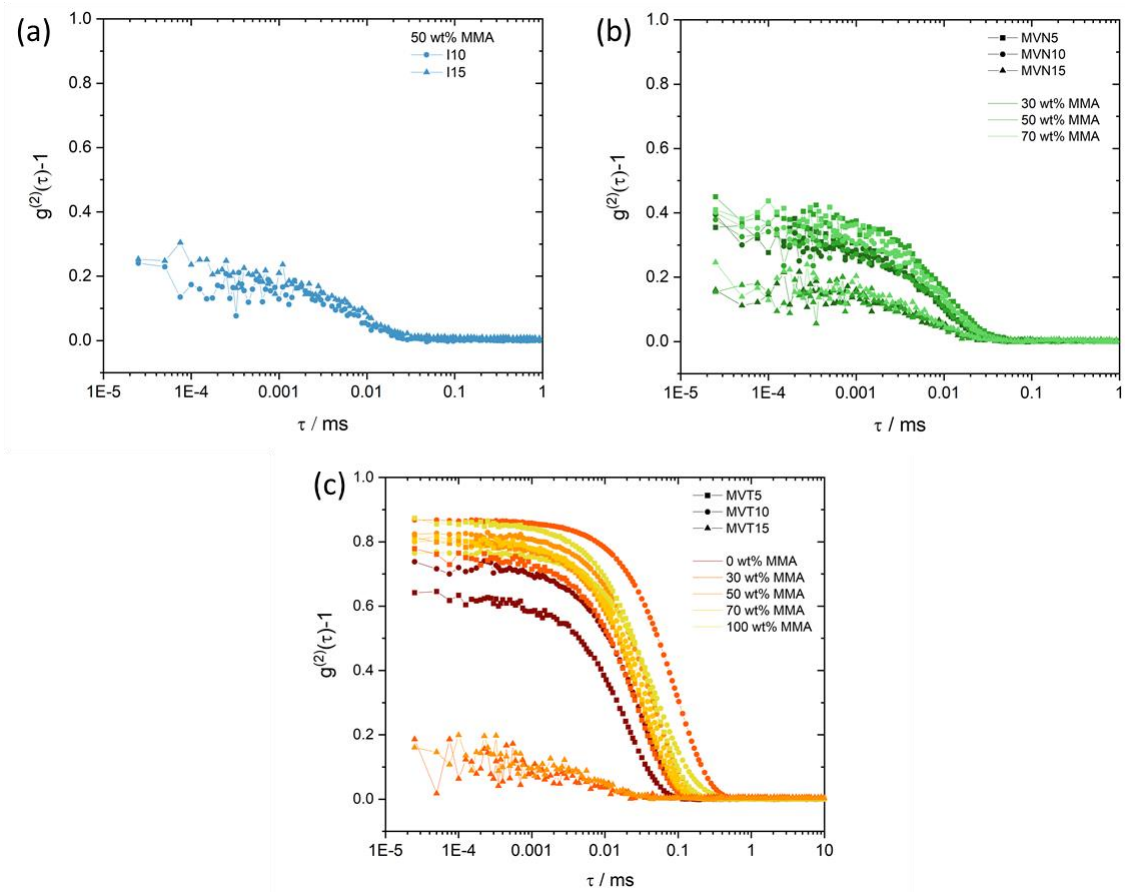

Figure 3.8 *Autocorrelation functions derived by DLS for the systems water, MMA/VAc, and the hydrotropes (a) IPA, (b) NPA, (c) TBA at 45 °C.*

Autocorrelation functions of some samples are given in **Figure 3.8**. For TBA (**Figure 3.8 c**), compositions with MMA contents of 0, 30, 50, 70, and 100 wt% are tested. Distinct autocorrelation functions can be observed for samples with 5 wt% and 10 wt% monomers. For 15 wt% monomers, the autocorrelation function decreases drastically, similar as described for pure MMA (cf. section 2.4). Samples with pure VAc (which is moderately more hydrophilic than MMA) show slightly lower mesostructuring. For mixtures, a clear trend towards better structuring with increasing MMA content cannot really be observed. Also, for NPA (cf. **Figure 3.8 b**), where only mixtures with 30, 50, and 70 wt% MMA are tested, the trends between the ratios are neglectable. One can observe a drop in the quality of autocorrelation functions from 5 wt% and 10 wt% to 15 wt% monomer content for NPA, as well. For IPA, only two samples with 50 wt% MMA and 10 wt% or 15 wt% total monomer concentration are tested (cf. **Figure 3.8 a**). Both autocorrelation functions do not significantly differ. In comparison to NPA and TBA, the quality of the autocorrelation function for 10 wt% monomer phase is worse, and the one for 15 wt% is better. The same is found for pure MMA (cf. section 2.4.1).

3.4.2.2 Polymerizations

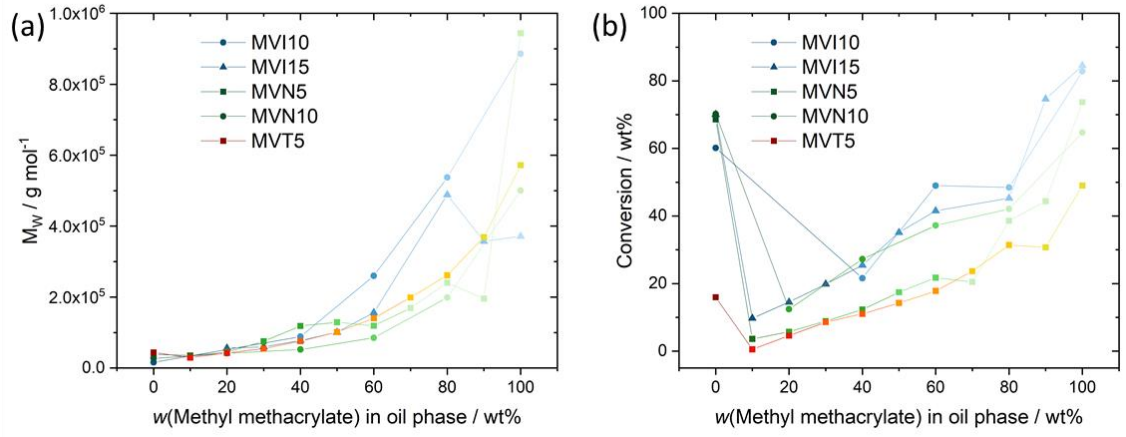

Figure 3.9 *(a) Weight average molar masses and (b) conversions of poly(MMA-co-VAc) after 7 h polymerization time at 45 °C, initiated by 0.4 wt% BCC.*

Figure 3.9 depicts the weight average molar mass and overall conversion of reaction mixtures with all three different hydrotropes and different MMA/VAc ratios. The conversion (**Figure 3.9 b**) drops drastically from pure VAc (0 wt% MMA) from around 60 wt% for IPA and NPA samples and 20 wt% for MVT5 when adding just 10 wt% MMA. From 10 wt% MMA, the conversion is continuously and almost linearly increasing towards pure MMA. The weight average molar mass (**Figure 3.9 a**) is increasing from 0 to 100 wt% MMA but with a lower slope for lower MMA contents and a higher one towards pure MMA. This data suggests that the copolymerization of MMA and VAc in SFME is not favorable. In contrast to the VAc-AA system (cf. section 3.4.1.2), NMR experiments are not possible as the signals are not separable and clearly attributable to MMA or VAc. Thus, the VAc conversion cannot not be calculated likewise. However, due to the very low conversions, we can expect very high MMA ratios in the copolymer. For this system, possibly another initiator system or higher temperatures could be worth trying.

3.4.3 Proof-of-concept: Vinyl Chloride (VC)

PVC is an extremely important polymer in industry. In the year 2022, PVC accounted for 12.9% of the total global plastics production. [25] Next to solution and bulk polymerization, especially emulsion and suspension techniques, are relevant polymerization methods in the industry. [26; 27] This makes it surely worth trying to use the method of polymerization in SFME for the production of PVC. The monomer VC has, however, the drawback of being gaseous, slightly water-soluble cancerogenic, and toxic. [28] Thus, VC is not the easiest molecule to handle in a standard laboratory, especially without suitable autoclaves.

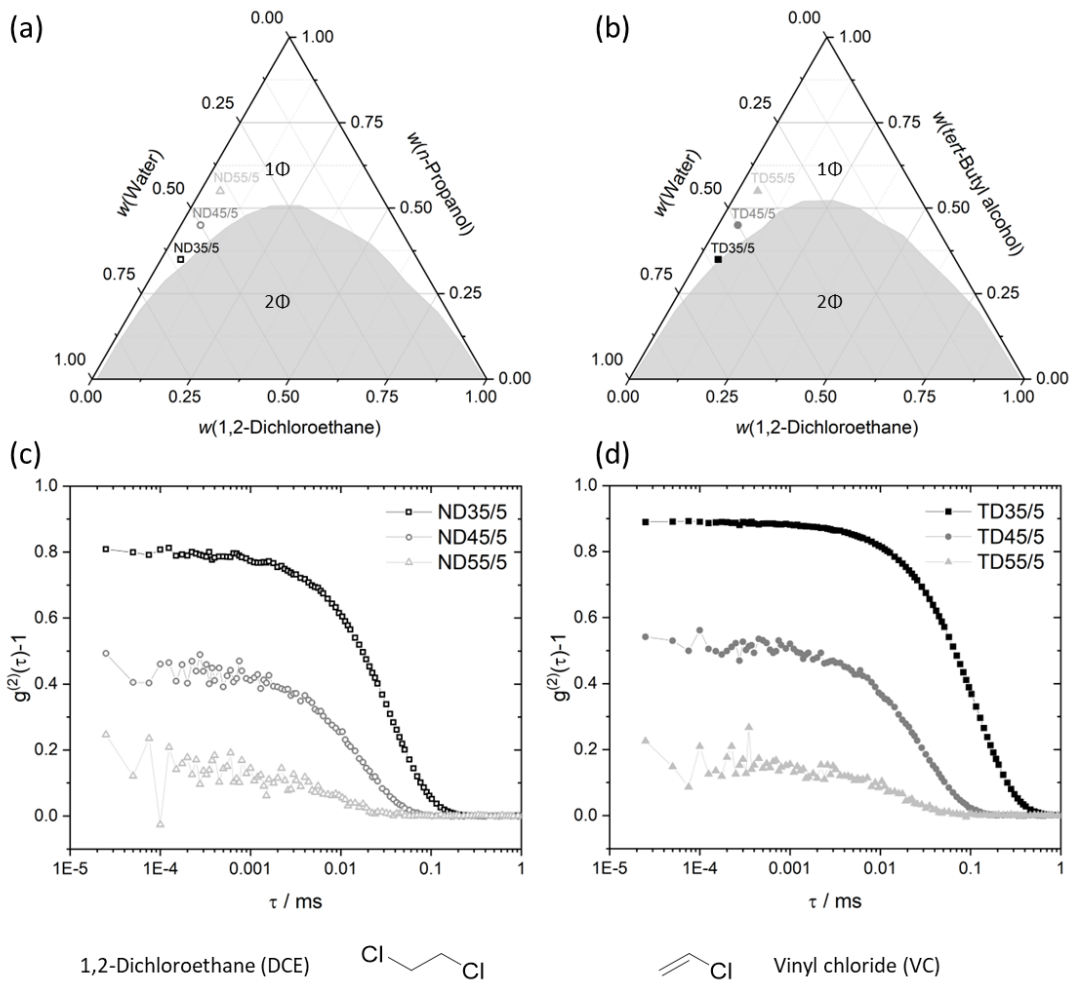

Figure 3.10 *Phase diagrams of water, DCE, the industrial precursor of VC, and the hydrotropes (a) NPAl and (b) TBA at 25 °C and autocorrelation functions of samples from the phase diagrams derived by DLS of the systems (c) NPA and (d) TBA at 25 °C. On the bottom, the structural formula of DCE and VC are given.*

To nevertheless obtain a proof-of-concept also for VC, its industrial precursor 1,2-dichloroethane (DCE) is used for structural investigation. In the process of VC synthesis, DCM is dehydrochlorinated, resulting in VC. [29] DCE is a toxic substance as well and requires appropriate protective measures. However, DCE is liquid at standard conditions in contrast to VC, making its handling much easier. Using this precursor as a model substance is also common in industry. [30] **Figure S 3.2** in the appendix shows that using a similar model substance without double bonding in terms of SFME is acceptable, as it could be shown that MMA and methyl isobutyrate (MIB) behave quite identically concerning their phase behavior and mesostructuring.

Figure 3.10 depicts ternary phase diagrams of water, DCE, and the hydrotropes NPA and TBA. Phase diagrams are found that can be expected for rather balanced SFME systems. TBA leads to a slightly higher biphasic region than NPA, which is commonly observed for other monomers

already (cf. section 2.4.1). Autocorrelation functions are remarkably pronounced and decrease with increasing distance to the binodal, as expected for an SFME system.

Thus, the basic conditions for attempting SFME polymerizations of VC are given. The increased pressure is not expected to cause a problem regarding structuring, as SFME-like aggregates are also reported in systems with supercritical CO_2, [31] which is commonly known to require significantly higher pressures than the polymerization of VC.

3.4.4 Proof-of-concept: Styrene and Acrylonitrile (AN)

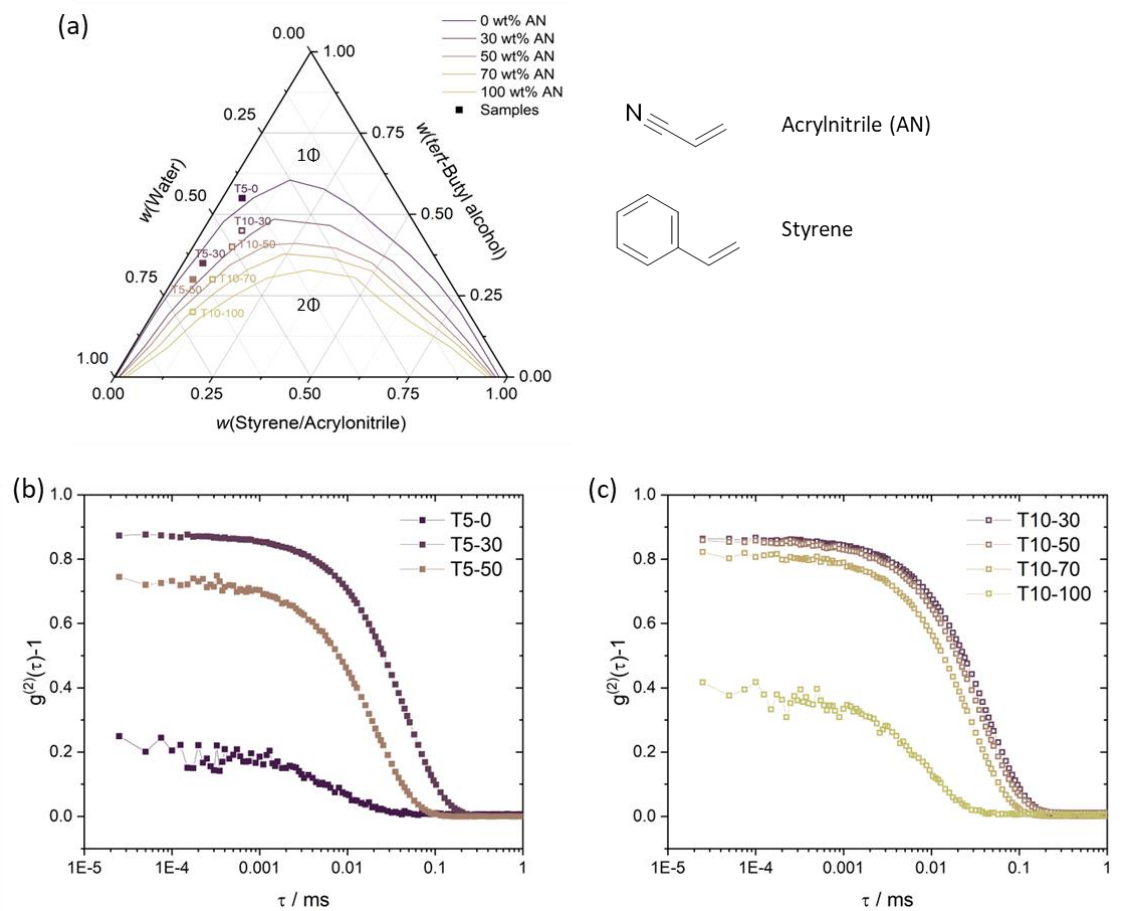

Figure 3.11 *(a) Phase diagram of water, different mixtures of styrene and AN, and the hydrotrope TBA, (b) and (c): autocorrelation functions of samples from the phase diagram derived by DLS of the systems. On the top right, the structural formula of AN and styrene are given.*

Poly(styrene-co-AN) (SAN) is a common copolymer of styrene, which usually comprises compositions around 20-30 wt% acrylonitrile and 70-80 wt% styrene. [32] The addition of acrylonitrile to pure styrene improves the mechanical properties and chemical resistance of the polymer. [33] Important in the context of SAN is also the terpolymer Acrylonitrile butadiene styrene (ABS), which is produced by adding SAN-based side chains to a butadiene main chain. This creates a grafted, branched copolymer. [34] ABS, in contrast to pure SAN, has an improved impact

strength. Technically, often a blend of SAN and ABS is used. [35] Both SAN and ABS are produced by free-radical polymerization in bulk, emulsion, or suspension. [36] However, acrylonitrile is discussed as very toxic. [37–39] Thus, also the system styrene-acrylonitrile is only shown concerning its SFME system, but the resulting polymers are not studied further.

Pseudo-ternary phase diagrams of water, TBA, and different styrene/AN ratios are drawn in **Figure 3.11 a**. The biphasic region of pure styrene is quite high, while AN comprises a rather low biphasic region. The styrene/AN mixtures lay steadily in between, whereby the distance between 0 and 30 wt% AN is higher than between 70 and 100 wt% AN. **Figure 3.11 b** depicts autocorrelation functions of compositions consisting of each 5 wt% monomer(mixture) in the systems with 0 wt%, 30 wt%, and 50 wt% AN in styrene in approximate equidistance to the binodal. While pure styrene (T5-0) comprises a quite low pronounced autocorrelation function in this area, the autocorrelation functions of both pseudo-ternary systems indicate quite pronounced structuring. Samples containing 10 wt% monomer(mixture) in the systems with 30 wt%, 50 wt%, and 70 wt% AN comprise all very similar and well-pronounced autocorrelation functions, while the sample with pure AN shows way less pronounced structuring. Interestingly, both AN and styrene comprise way less pronounced autocorrelation functions compared to the mixed system. Probably, AN and styrene mark the two limits for monomers to form a suitable SFME. An SFME has to be a balanced system with an oil which is neither too hydrophobic nor too hydrophilic. [40] Styrene comprises no other atoms but carbon and hydrogen, making the molecular very unpolar with a low water solubility of 0.2 g L^{-1}. Styrene is probably one of the most hydrophobic oils, which still forms an SFME. A similar, literature-known example is limonene, which also consists only of H and C atoms. While limonene has a extremely high miscibility gap in the system with EtOH and water, it forms an SFME with a comparably large biphasic region with TBA. [41] AN, on the other side, is much more hydrophilic, with a water solubility of 73 g L^{-1}. In the system with TBA, AN still shows some structuring indicated by DLS. The system ethyl acetate (which is even slightly more soluble in water [42]), EtOH, and water has a slightly lower biphasic region. DLS measurements in this system do not indicate structuring anymore. [40] However, the pseudo-ternary system with styrene and AN seems to form very balanced systems, especially for mixtures around 30 wt% and 50 wt% AN, which would be the relevant ones for application. Thus, the formation of an SFME system is given, which is the first step for considering the method of polymerization in SFME.

3.4.5 Glycol Ethers as Hydrotropes for SFME Polymerizations

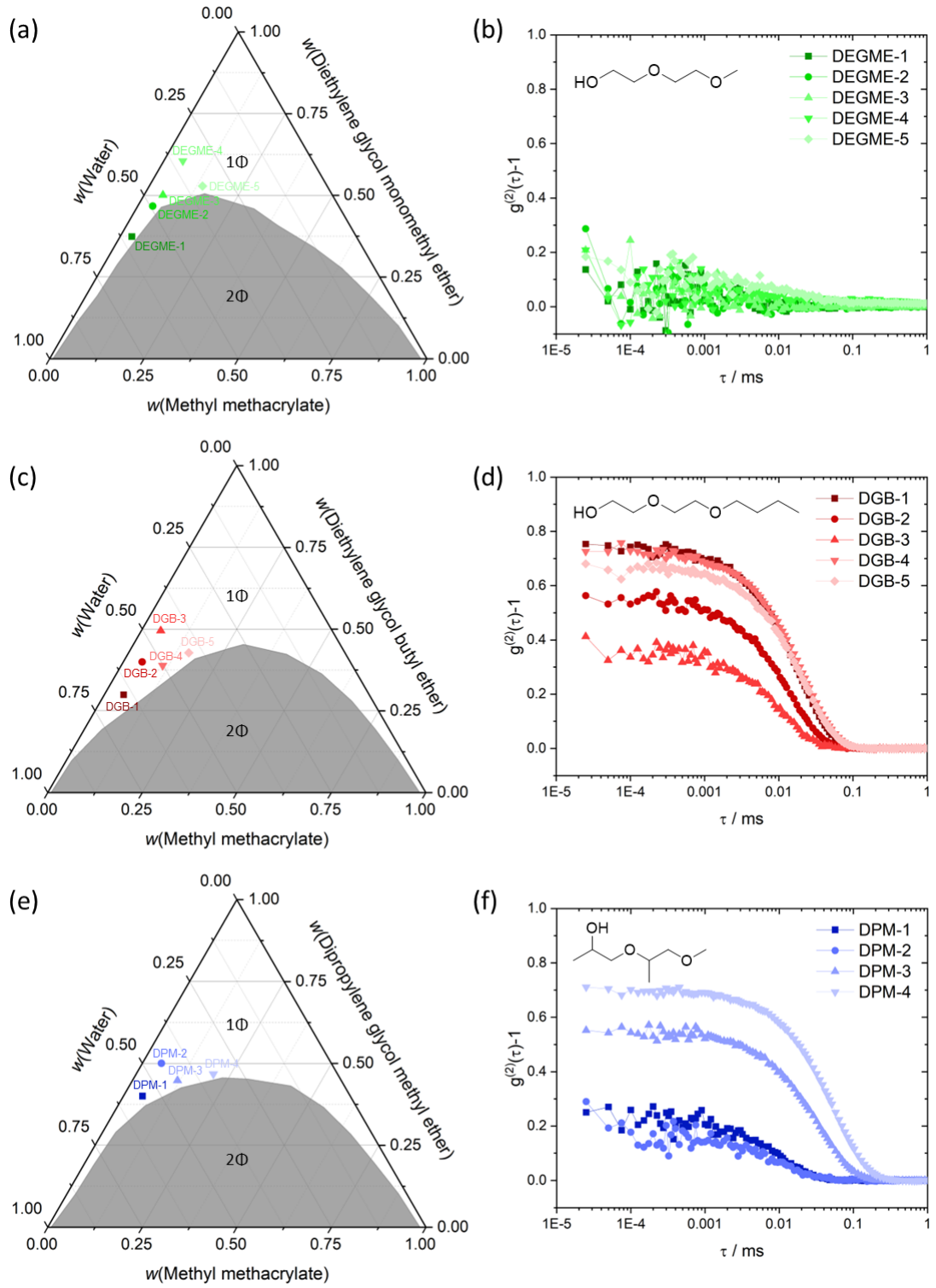

Figure 3.12 *Investigation of the use of glycol ethers as hydrotropes in SFME with MMA as oil phase. (a) Phase diagram and (b) autocorrelation functions derived by DLS for with diethylene glycol monomethyl ether, (c) phase diagram and (d) autocorrelation functions derived by DLS with diethylene glycol butyl ether, and (e) phase diagrams and (f) autocorrelation functions derived by DLS for dipropylene glycol methyl ether. All measurements are performed at 25 °C.*

Glycol ethers are industrially relevant solvents with many applications, but especially in the coatings industry. [43] They are especially famous for their good solubility properties and their overall low toxicity. [44] Many manufacturers produce glycol ethers nowadays, but especially Dow Chemical Company is famous for producing glycerol ethers under the trade name “Dowanol”. [45] We tested three different glycol ethers for their suitability as hydrotropes in SFMEs with MMA: Diethylene glycol monomethyl ether (DEGME) and diethylene glycol butyl ether (DGB) as ethylene glycol ethers, and dipropylene glycol methyl ether (DPM) as representative of the propylene glycols.

Figure 3.12 depicts ternary phase diagrams and autocorrelation functions derived by DLS for systems with water, MMA, and the hydrotropes (a) and (b) DEGME, (c) and (d) DGB, and (e) and (f) DPE at 25 °C. All ternary phase diagrams show biphasic regions that can be expected for rather balanced SFME systems. [40] However, there are differences in the shape of the binodals, which is quite symmetrical for DPM, tilted to the water-rich side for DEGME, and tilted towards the oil-rich side for DGB (cf. **Figure 3.12 a**, **c**, and **e**). Differences can also be found in the autocorrelation functions. For each phase diagram, four to five samples on the water-rich side are prepared, where the pre-Ouzo region is expected to be located. In the system with DEGME (cf. **Figure 3.12 b**), no distinct autocorrelation functions can be observed in this region. For the sample DEGME-5, which contains the highest MMA content (above the highest point of the binodal), one can observe a very less pronounced shift in the y-axis intercept for low lag times.

It may be possible that the quality of autocorrelation functions indicating structuring would increase by going further toward the oil-rich side of the phase diagram (to where a larger monophasic region is due to the asymmetricity of the biphasic region). However, this region is not of interest for surfactant-free microemulsion or microsuspension polymerizations, as surely water-in-oil-like structures would be present.

In both other systems, using DGB (**Figure 3.12 d**) or DPM (**Figure 3.12 f**), distinct autocorrelation functions can be observed, indicating the presence of mesostructures. While the most pronounced structuring can be observed in the most water-rich sample for the system with DGB, the most oil-rich sample comprises the highest y-axis intercept in the system with DPM.

Polymerizations are performed in all three systems for 7 h at 45 °C with 0.4 mol% BCC as initiator. Freeze-dried samples still contained large amounts of the others, so further investigations by weighting the conversion or determining average molar masses by GPC are impossible. For all systems, the reaction mixtures turned milky, and polymers could be observed visually after freeze drying, which show different appearances. For DEGME, where no distinct

mesostructuring could be observed by DLS (cf. **Figure 3.12**), much less polymer seems to be present, sticking to the glass of the sample container. In contrast, it seems that more PMMA could be synthesized visually for DPM and DBG (cf. **Figure S 3.3** in the appendix).

3.5 Conclusions

In this chapter, different, industrially relevant (co)polymers and hydrotropes are tested for their suitability of polymerizations in SFME. The system vinyl(acetate) (VAc) – arylic acid (AA) is composed of a hydrophobic (VAc) and a very hydrophilic monomer (AA), which is completely water-miscible and acts as a hydrotrope. The system shows interesting results, especially due to the fact that the choice of the surfactant-free microemulsion (SFME) system (both the hydrotrope as well as the location in the phase diagram) seems to influence the copolymerization reactivity and parameter, resulting in different VAc ratios in the polymer produced. The system VAc – methyl methacrylate (MMA) has two hydrophobic monomers, which can definitely both be counted to the oil phase of a pseudo-ternary phase diagram. Even though both monomers are not too different concerning their polarity and phase behavior, their reactivity is significantly different. Unfortunately, conversions are bad for MMA/VAc mixtures and especially drastically dropping when adding the first 10 wt% MMA to pure VAc. Even if the proof-of-concept does not look too promising, this does not mean that acceptable results could possibly be achieved, *e.g.*, by changing the initiator system or the reaction temperature. For dichloroethane (DCE) as a model substance for vinyl chloride and the system styrene – acrylonitrile (AN), only the phase behavior is investigated. Both systems form SFME systems with distinct mesostructuring. Thus, the first step towards using SFME polymerization for those systems is done. Glycol ethers are used as hydrotropes for the polymerization of MMA. While dipropylene glycol methyl ether (DPM) and diethylene glycol butyl ether (DGB) show mesostructuring, the autocorrelation functions of diethylene glycol monomethyl ether (DEGME) derived by dynamic light scattering (DLS) do not really indicate distinct structures. Polymerizations are performed in this system. However, the resulting polymers are not further investigated, as the glycol ethers are hard to separate.

Since choice of the system has an influence on the reaction kinetics and the properties of the polymer, using an SFME as reaction medium might give access to copolymers that are hardly formed due to bad copolymerization rates. VAc-AA copolymers worked well, while VAc-MMA copolymers did not seem very promising. However, in both cases, VAc is the one problematic monomer with lower reactivity. To compare polymers from SFME and from classical suspension methods, the target properties of the polymer should first be defined. Unfortunately, these are properties that are mostly hidden as know-how in the industry. Even if it might still be a long way until these (co)polymers might be synthesized in SFME in industry, the first steps are done: It could be proved that many industrially relevant monomers can form SFMEs. First polymerization experiments led to polymers with different properties, which makes further research on this topic interesting.

3.6 Appendix

3.6.1 System Poly(acrylic acid-co-vinyl acetate)

Table S 3.1 *Compositions of samples investigated in the system vinyl acetate-co-acrylic acid.*

Sample	*w*(Vac) / wt%	*w*(AA) / wt%	*w*(Water) / wt%	*w*(IPA) / wt%	*w*(NPA) / wt%	*w*(TBA) / wt%
AVI15/0	15.00	0.00	52.00	33.00		
AVI15/9	13.64	1.37	55.00	30.00		
AVI15/16	12.50	2.51	55.00	30.00		
AVI15/28	10.71	4.29	60.00	25.00		
AVI15/33	10.01	5.00	60.00	25.00		
AVI15/50	7.50	7.50	65.00	20.00		
AVN5/0	5.00	0.00	75.00		20.00	
AVN5/9	4.55	0.46	75.00		20.00	
AVN5/16	4.17	0.84	75.00		20.00	
AVN5/28	3.57	1.43	75.00		20.00	
AVN10/33	7.00	3.50	68.45		21.05	
AVN15/50	7.50	7.50	63.00		22.00	
AVT5/0	5.00	0.00	65.00			30.00
AVT5/9	4.55	0.46	65.00			30.00
AVT5/16	4.17	0.84	65.00			30.00
AVT5/28	3.57	1.43	65.00			30.00
AVT10/33	6.67	3.33	60.00			30.00
AVT15/50	7.50	7.50	52.00			33.00

Table S 3.2 *Data of molar and weight ratio of AA to VAc before polymerization and in the polymer after 7 h polymerization time as well as the conversion after 7 h polymerization times.*

before polymerization		**after 7h of polymerization**		**conversion of monomers**	
***w*(AA) / wt%**	***x*(AA) / mol%**	***w*(AA) / wt%**	***x*(AA) / mol%**	**conversion of VAc / wt%**	**total conversion / wt%**
IPA					
9.1	10.7	33.1	37	26	43
16.7	19.3	37.3	42	25	65
28.6	32.4	68.4	72	56	67
33.3	37.4	69.6	73	54	59
50	54.4	79.7	82	59	69
NPA					
9.1	10.7	50.7	55	46	23
16.7	19.3	66.6	70	60	21
28.6	32.4	70.9	74	59	44
33.3	37.4	82.7	85	74	38
50	54.4	80.8	83	62	70
TBA					
9.1	10.7	29.9	34	23	36
16.7	19.3	52.1	57	43	40
28.6	32.4	64.6	69	50	56
33.3	37.4	56	60	34	69
50	54.4	65.1	69	30	85

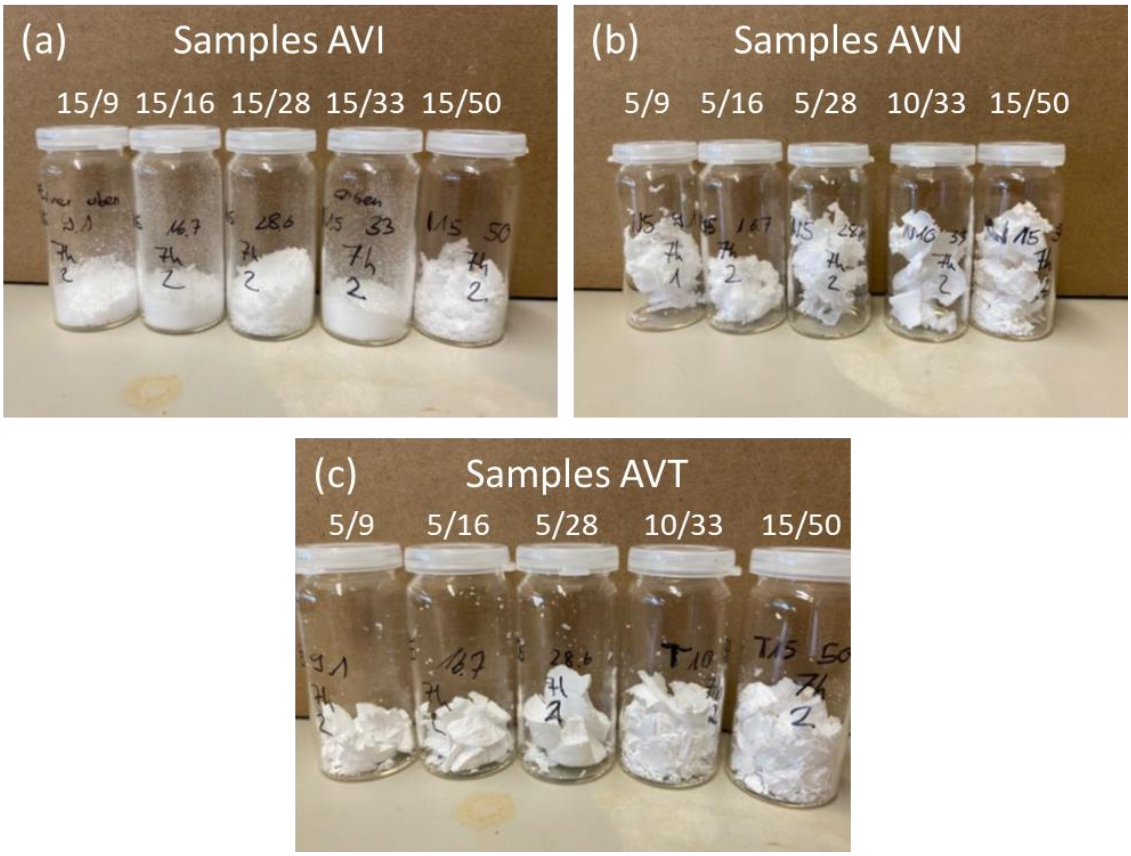

Figure S 3.1 *Macroscopic appearance of poly(vinyl acetate-co-acrylic acid) polymers derived from systems with the hydrotropes (a) IPA, (b) NPA, and (c) TBA.*

3.6.2 System Poly(vinyl acetate-co-methyl methacrylate)

Table S 3.3 *Compositions of samples investigated in the system vinyl acetate-co-methyl methacrylate.*

Sample	MMA content / wt%	w(VAc) / wt%	w(MMA) / wt%	w(Water) / wt%	w(IPA) / wt%	w(NPA) / wt%	w(TBA) / wt%
MVI10	50%	5.00	5.00	65.00	30.00	-	-
MVI15	50%	7.50	7.50	47.00	38.00	-	-
	30%	3.50	1.50				
MVN5	50%	2.50	2.50	65.00	-	30.00	-
	70%	1.50	3.50				
	30%	7.00	3.00				
MVN10	50%	5.00	5.00	50.00	-	40.00	-
	70%	3.00	7.00				
	30%	10.50	4.50				
MVN15	50%	7.50	7.50	40.00	-	45.00	-
	70%	4.50	10.50				
	0%	5.00	0.00				
	30%	3.50	1.50				
MVT5	50%	2.50	2.50	65.00	-	-	30.00
	70%	1.50	3.50				
	100%	0.00	5.00				
	0%	10.00	0.00				
	30%	7.00	3.00				
MVT10	50%	5.00	5.00	45.00	-	-	45.00
	70%	3.00	7.00				
	100%	0.00	10.00				
	0%	15.00	0.00				
	30%	10.50	4.50				
MVT15	50%	7.50	7.50	50.00	-	-	50.00
	70%	4.50	10.50				
	100%	0.00	15.00				

3.6.3 System Vinyl Chloride/Dichloroethane

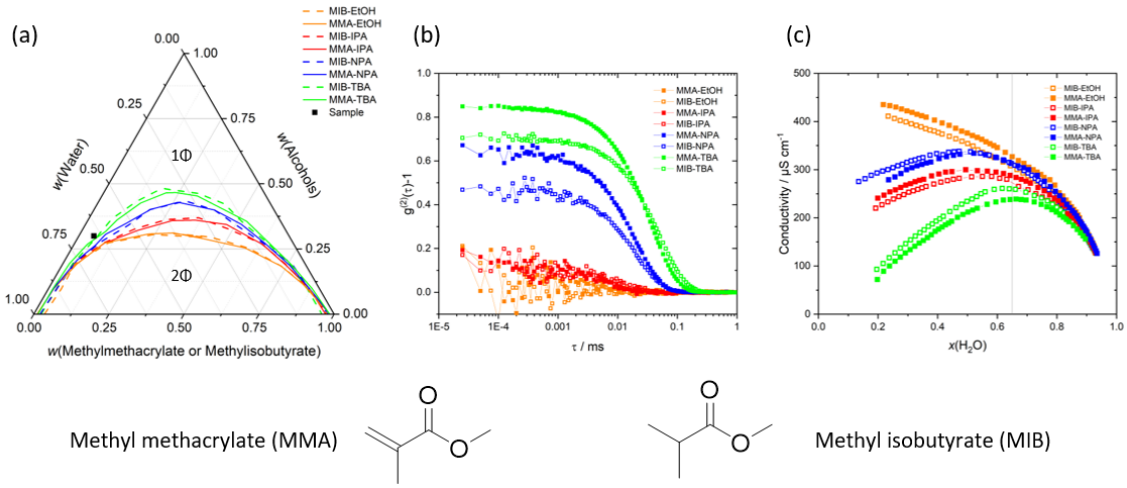

Figure S 3.2 *Comparison of the behaviour of the molecules methyl methycrylate (MMA) and methyl isobutyrate (MIB) in SFMEs consisting of MMA/MIB, water, and the hydrotropes EtOH, IPA, NPA, and TBA: (a) ternary phase diagrams, (b) autocorrelation fuctions derived by DLS, and (c) percolation curves, which intercut the samples at the black dashed lines. 0.2 wt% NaBr is added to the initial solution for conductivity measurements. All experiments are performed at 25 °C.*

Figure S 3.2 depicts the comparison of methyl methacrylate (MMA) and methyl isobutyrate (MIB) concerning their behaviour in an SFME. MMA and MIB differ only in the double bond found in MMA. The comparison is made as the question arised, if non-polymerizable substances such as MIB could be suitable as model substance for the investigation of its polymerizable double. The location of the binodal in ternary phase diagrams (cf. **Figure S 3.2 a**) is nearly identical in between MMA and MIB for all four hydrotropes, except for TBA, where MIB comprises a slightly higher biphasic region. The percolation cuvres (cf. **Figure S 3.2 c**) intercut the samples marked in the ternary phase diagram at the black dashed line, indicating the kind of structuring found in the SFME. 0.2 wt% NaBr is added to the initial solutions in order to ensure a sufficient number of charge carriers for conductivity measurements. The shape of the curves of MMA and MIB appear almost identical. Conductivity curves for EtOH show an steadily decreasing course, which suggests a pure dilution effect without relevant structuring for both oils. IPA, NPA, and TBA show the shape expected for percolation curves. The samples of the IPA and NPA systems intercut the percolation curve at the decreasing part, indicating an oil-in-water-like structure for both MMA and MIB. For TBA, the conductivity curve is intercutted pretty much at the peak of the curve, indicating a bicontinuous-like structuring. Autocorrelation functions show the biggest difference between MMA and MIB (cf. **Figure S 3.2 b**). However, this difference is mainly concerning the y-axis intercept and almost not the lag time, which is more relevant. The consistently lower y-axis intercept for MIB could possibly be explained by the single-bond, allowing more degrees of freedom due to the freely rotatable binding compared to the double bond of MMA,

which could make the structure more fluctuating. However, the behaviour of MMA and MIB is remarkably similar, making MIB to a surely suitable model molecule for MMA.

Table S 3.4 *Compositions of samples investigated in the system vinyl chloride with dichloroethane as model substance.*

Sample	*w*(DCE) / wt%	*w*(Water) / wt%	*w*(NPA) / wt%	*w*(TBA) / wt%
ND35/5	5.00	60.00	35.00	
ND45/5	5.00	50.00	45.00	
ND55/5	5.00	40.00	55.00	
TD35/5	5.00	60.00		35.00
TD45/5	5.00	50.00		45.00
TD55/5	5.00	40.00		55.00

3.6.4 System Poly(styene-co-acrylonitrile)

Table S 3.5 *Compositions of samples investigated in the system styrene-co-acrylonitrile.*

Sample	*w*(Styrene) / wt%	*w*(AN) / wt%	*w*(Water) / wt%	*w*(TBA) / wt%
T5-0	5.00	0.00	40.00	55.00
T5-30	3.50	1.50	60.00	35.00
T10-30	7.00	3.00	45.00	45.00
T5-50	2.50	2.50	65.00	30.00
T10-50	5.00	5.00	50.00	40.00
T10-70	3.00	7.00	60.00	30.00
T10-100	0.00	10.00	70.00	20.00

3.6.5 System with Glycolethers as Hydrotropes

Table S 3.6 *Compositions of samples with MMA as monomer and the glycolethers DEGME, DGB, and DPM as hydrotropes.*

Sample	*w*(MMA) / wt%	*w*(Water) / wt%	*w*(DEGME) / wt%	*w*(DGB) / wt%	*w*(DPM) / wt%
DEGME-1	0.03	0.60	0.37		
DEGME-2	0.04	0.49	0.47		
DEGME-3	0.05	0.45	0.50		
DEGME-4	0.05	0.34	0.61		
DEGME-5	0.14	0.33	0.53		
DGB-1	0.05	0.65		0.30	
DGB-2	0.05	0.55		0.40	
DGB-3	0.05	0.45		0.50	
DGB-4	0.11	0.50		0.39	
DGB-5	0.16	0.41		0.43	
DPM-1	0.05	0.55			0.40
DPM-2	0.05	0.45			0.50
DPM-3	0.12	0.43			0.45
DPM-4	0.20	0.33			0.47

Figure S 3.3 *Visual appearance of freeze-dried samples with glycol ethers after 7 h polymerization time at 45 °C with 0.4 mol% BCC as initiator.*

3.7 Bibliography

[1] U. Ali, K. J. B. A. Karim, and N. A. Buang, *Polymer Reviews* **2015**, *55,* 678–705.

[2] S. T. Camli, F. Buyukserin, O. Balci, and G. G. Budak, *J. Colloid. Interface Sci.* **2010**, *344,* 528–532.

[3] C. G. Dobie, and K. V. Boodhoo, *Chem. Eng. Process* **2010**, *49,* 901–911.

[4] M. F. Cunningham, *Polym. React. Eng.* **1999**, *7,* 231–257.

[5] B. M. Louie, G. M. Carratt, and D. S. Soong, *J. Appl. Polym. Sci.* **1985**, *30,* 3985–4012.

[6] P. Eastup, C. Howick, and M. Moss, *Plast.* **2005**, *34,* 148–154.

[7] R. N. Mead, and G. W. Poehlein, *Ind. Eng. Chem. Res.* **1988**, *27,* 2283–2293.

[8] F. M. Silva, E. L. Lima, and J. C. Pinto, *Ind. Eng. Chem. Res.* **2004**, *43,* 7324–7342.

[9] A. S. Brar, and Sunita, *Eur. Polym. J.* **1991**, *27,* 17–20.

[10] T. Learner, *The Conservator* **2000**, *24,* 96–103.

[11] S. Nishimura, K. Nishida, S. Shiomoto, and M. Tanaka, *Mater. Adv.* **2022**, *3,* 5043–5054.

[12] J. Glasing, P. G. Jessop, P. Champagne, W. Y. Hamad, and M. F. Cunningham, *Langmuir* **2020**, *36,* 796–809.

[13] J. Blahnik, S. Krickl, K. Schmid, E. Müller, J. Lupton, and W. Kunz, *J. Colloid. Interface Sci.* **2023**, *648,* 755–767.

[14] GESTIS-Stoffdatenbank, *Methylmethacrylat,* https://gestis.dguv.de/data?name=013350. **17.05.2023**.

[15] GESTIS-Stoffdatenbank, *Vinylacetat,* https://gestis.dguv.de/data?name=012720. **17.05.2023**.

[16] *Polymer handbook,* 4. Aufl., Wiley, New York, **1999**.

[17] M. I. Baker, S. P. Walsh, Z. Schwartz, and B. D. Boyan, *J. Biomed. Mater. Res. B. Appl. Biomater.* **2012**, *100,* 1451–1457.

[18] J. I. Jones, *Brit. Poly.J.* **1973**, *5,* 493–494.

[19] C. Luciani, and K. Y. Choi, *Can. J. Chem. Eng.* **2023**.

[20] W. R. P. Raj, M. Sasthav, and H. M. Cheung, *Langmuir* **1991**, *7,* 2586–2591.

[21] Y. Yao, C. Li, F. Liu, P. Zhao, Z. Gu, and S. Zhang, *Phys. Chem. Chem. Phys.* **2019**, *21,* 10477–10487.

[22] M. Dossi, K. Liang, R. A. Hutchinson, and D. Moscatelli, *J. Phys. Chem. B* **2010**, *114,* 4213–4222.

[23] T.-H. Kim, and N. A. Peppas, *Polym. Bull.* **1984**, *12,* 59–63.

[24] G. D. Azevedo, and J. C. Pinto, *J. Appl. Polym. Sci.* **2020**, *137,* 49298.

[25] Plastics Europe, *Plastics - the Facts 2022,* www.plasticseurope.org, **2022**.

[26] D. Braun, *J. Polym. Sci. A Polym. Chem.* **2004**, *42,* 578–586.

[27] K. Endo, *Prog. Polym. Sci.* **2002**, *27,* 2021–2054.

[28] J. Kielhorn, C. Melber, U. Wahnschaffe, A. Aitio, and I. Mangelsdorf, *Environ. Health Perspect.* **2000**, *108,* 579–588.

[29] H. Zhao, S. Chen, M. Guo, D. Zhou, Z. Shen, W. Wang, B. Feng, and B. Jiang, *ACS Omega* **2019**, *4,* 2081–2089.

[30] *PVC handbook,* 1. Aufl. (Hrsg.: C. E. Wilkes, J. W. Summers, C. A. Daniels und M. T. Berard), Hanser Gardner; Hanser, Cincinnati, Ohio, Munich, **2005**.

[31] R. F. Hankel, P. E. Rojas, M. Cano-Sarabia, S. Sala, J. Veciana, A. Braeuer, and N. Ventosa, *Chem. Commun. (Camb.)* **2014**, *50,* 8215–8218.

[32] J. Maul, B. G. Frushour, J. R. Kontoff, H. Eichenauer, K.-H. Ott, and C. Schade, in: *Ullmann's encyclopedia of industrial chemistry,* Wiley-VCH, Weinheim, Wiley online library, **2010**.

[33] *Modern plastics handbook,* McGraw-Hill Education; McGraw Hill, New York, N.Y., **2000**.
[34] S. Olivera, H. B. Muralidhara, K. Venkatesh, K. Gopalakrishna, and C. S. Vivek, *J. Mater. Sci.* **2016**, *51,* 3657–3674.
[35] *Styrenic copolymers,* Rapra Technology Ltd, Shawbury, U.K, **2002**.
[36] S. Koltzenburg, *Polymere: Synthese, Eigenschaften und Anwendungen,* Springer Spektrum, Berlin, Heidelberg, **2014**.
[37] R. Thier, J. Lewalter, and H. M. Bolt, *Arch. Toxicol.* **2000**, *74,* 184–189.
[38] GESTIS-Stoffdatenbank, *Styrol,* https://gestis.dguv.de/data?name=010110. **10.05.2023**.
[39] GESTIS-Stoffdatenbank, *Acrylnitril,* https://gestis.dguv.de/data?name=011410. **10.05.2023**.
[40] J. Blahnik, E. Müller, L. Braun, P. Denk, and W. Kunz, *COCIS* **2022**, *57,* 101535.
[41] T. Buchecker, S. Krickl, R. Winkler, I. Grillo, P. Bauduin, D. Touraud, A. Pfitzner, and W. Kunz, *Phys. Chem. Chem. Phys.* **2017**, *19,* 1806–1816.
[42] GESTIS-Stoffdatenbank, *Ethylacetat,* https://gestis.dguv.de/data?name=012040. **10.05.2023**.
[43] R. L. Smith, *Environ. Health Perspect.* **1984**, *57,* 1–4.
[44] C. A. Staples, R. J. Boatman, and M. L. Cano, *Chemosphere* **1998**, *36,* 1585–1613.
[45] S. T. Cragg, in: *Patty's Toxicology* (Hrsg.: E. Bingham, B. Cohrssen and C. H. Powell), John Wiley & Sons, Inc, Hoboken, NJ, USA, **2001,** 789–878.

4 Surfactant-free Microemulsions (SFMEs) as a Template for Porous Polymer Synthesis

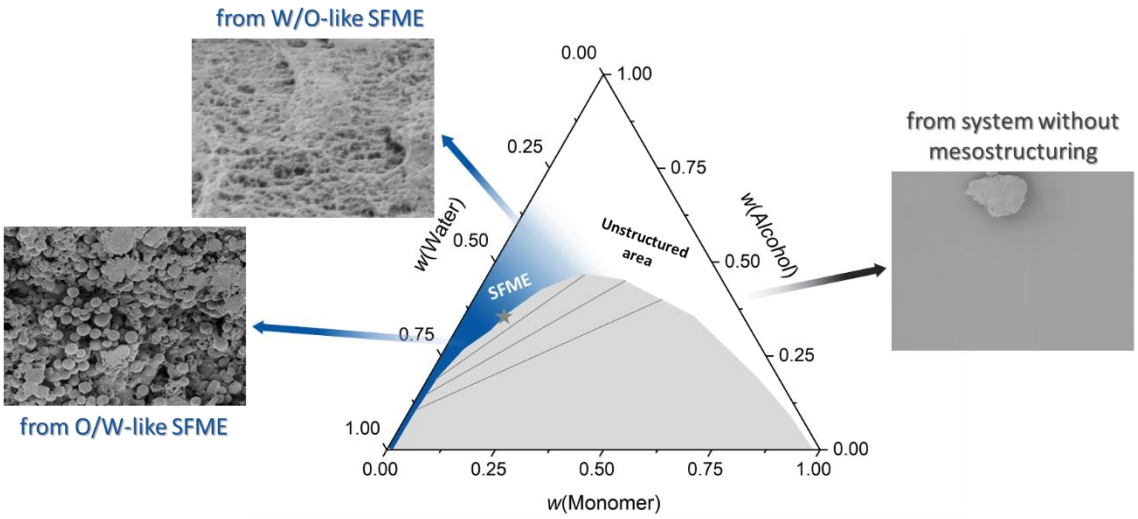

Figure 4.1 *The graphical abstract shows a typical phase diagram for a polymerizable SFME system. The area in which SFMEs can be expected is marked in blue. Three SEM images of polymers and their area of origin are given: droplet-like polymers from O/W-like SFME, sponge-like polymers from W/O-like SFME, and a polymer without observable nanostructures from the region where no mesostructures are found before polymerization.*

In the previous Chapters 2 and 3, the focus of the research is on the impact of the surfactant-free microemulsion (SFME) systems on polymerization kinetics, derived molar masses, and conversions. Chapter 2 did already show light microscopy images of derived polymers and teased that differently shaped polymers can be observed. In the following chapter, the focus will be on the interplay of the previous structuring and the derived polymer morphology.

This work comprises a systematic study to compare the morphology of poly(methyl methacrylate) (PMMA) monopolymers as well as PMMA-poly(2-hydroxyethyl methacrylate) (PHEMA)-copolymers with the expected nature of the SFME before polymerization. A surfactant-based microemulsion with nonionic surfactants is investigated as a reference system.

Simple SFME systems composed of water, a hydrotrope (*iso*-propanol (IPA) or *tert*-butyl alcohol (TBA)), and MMA as polymerizable oil as well as the more complex system comprising 2-hydroxyethyl methacrylate (HEMA) as an additional amphiphilic co-monomer, are investigated. A surfactant-based system using a mixture of Tergitol 15-S-12 and Synperonic A11-LQ-(TH) as surfactants, water, and MMA in the presence and absence of HEMA as polymerizable cosurfactant is investigated as a reference system. Structural analysis is done by recording pseudo-ternary phase diagrams, dynamic light scattering (DLS), and conductivity measurements. Polymerizations are performed using the oil-soluble initiator BCC at 45 °C for 24 h with adjacent lyophilization. The morphology of dried polymers is determined by light microscopy, scanning electron microscopy, and BET adsorption isotherms.

Porous polymers of different morphologies (from coagulations of droplet-like aggregates to sponge-like ones) in the size range of 200 nm up to some µm can be derived from previously mesostructured, surfactant-free mixtures. Previously unstructured, oil-rich regions lead to solid, transparent polymers without nanostructured morphologies. The surfactant-based reference system comprises remarkably similar phase behavior before polymerizations and similar polymer morphologies as the comparable surfactant-free system. This leads to the assumption that the hydrotropic behavior of HEMA and its interplay with MMA and water is the structure-giving factor in this system.

This chapter is published in *Journal of Colloids and Interface Science* (J. Blahnik, J. Schuster, R. Müller, E. Müller, and W. Kunz, *Surfactant-free microemulsions (SFMEs) as a template for porous polymer synthesis*, JCIS, **2023**, *655*, 371-382). [1]

Contributions to the experimental work:

- Jonas Blahnik: Conceptualization, experimental work, data evaluation
- Jennifer Schuster: Experimental work, data evaluation

4.1 Introduction

Many methods concerning the production of porous polymeric membranes have been published in the last decades. [2; 3] A much-discussed method makes use of the structuring of bicontinuous or lamellar microemulsions as templates. [3; 4; 2] The microemulsion breaks during polymerization due to the growing polymers and is no longer thermodynamically stable (excess of 7-10 k_BT) when using non-polymerizable surfactants. [5] Thus, the original structure is usually not present anymore. [5] However, polymers with morphologies similar to those of the previous microemulsion can be observed but by a factor of 100-1000 larger size range, usually in the nanometer to micrometer region. [5–7]

Methyl methacrylate (MMA) is a commonly used monomer that is reported to form microemulsions with non-polymerizable and polymerizable surfactants. [2] 2-Hydroxyethyl methacrylate (HEMA), which is completely water-miscible in contrast to MMA, is discussed as a polymerizable cosurfactant in literature and can influence the pore sizes of MMA/HEMA copolymers. [4; 8]

Ultra-flexible or surfactant-free microemulsions (SFME) are usually ternary, mesostructured liquids containing water, oil, and a hydrotrope instead of a surfactant. [9] Several studies in recent years established a more detailed understanding of the structural and mechanistic effects within SFMEs. [10–13] SFMEs are used as a reaction medium from the beginning. Indeed, enzymatic reactions in these ternary systems are even the reason to postulate that mesostructures must be present. [14; 15] Other examples, like organic reactions or inorganic nanoparticle synthesis, are rare up to now. [16–20] We recently published a contribution about surfactant-free microemulsion and microsuspension polymerization of PMMA with a focus on polymerization kinetics. [21] As an outlook, we could show that the nature of mesostructuring close to the binodal seems to impact the morphology of the latter PMMA polymer.

The present contribution comprises a proof-of-concept for the preparation of porous polymeric particles in surfactant-free microemulsions. We investigate SFME systems containing water, the monomer MMA, and *tert*-butyl alcohol (TBA), *iso*-propanol (IPA), or HEMA as hydrotropes. Pseudo-ternary systems containing both the hydrophilic monomer HEMA and TBA or IPA are further studied. A surfactant-based system containing a mixture of the surfactants Synperonic A11-LQ-(TH) and Tergitol 15-S-12 in the presence or absence of HEMA as a cosurfactant is investigated as a reference system. (Pseudo-)Ternary phase diagrams are recorded for all systems, and the critical point is determined for ternary systems. Further investigation on mesostructuring is done by dynamic light scattering (DLS) and conductivity measurements. Polymerizations are initiated by the oil-soluble peroxy dicarbonate BCC at 45 °C for 24 h. Polymers are dried using

freeze-drying, and full drying is ensured in a drying cabinet. The morphology of polymers is investigated using light microscopy, scanning electron microscopy (SEM), and nitrogen adsorption isotherms following the Brunauer-Emmett-Teller (BET) model.

4.2 Materials and Methods

4.2.1 Materials

Methyl methacrylate (MMA, 99% purity, stabilized with 4-methoxyphenol ≤ 30 ppm), 2-hydroxyethyl methacrylate (HEMA, 97% purity, contains ≤ 250 ppm monomethyl ether hydroquinone as inhibitor), Tergitol 15-S-12 (Tergitol, ≥ 90% concentration, alcohols C12-14-secondary, ethoxylated), sodium bromide (99% purity), CombiTitrant 5, methanol (anhydrous for analysis, max. 0.003% H_2O) and dimethyl sulfoxide-d_6 (DMSO-d_6, 99.5 atom % D) are obtained from Merck (Darmstadt, Germany). *Tert*-butyl alcohol (TBA, 99%) is purchased from Carl Roth (Karlsruhe, Germany). *Iso*-Propanol (IPA, 99.8%) is bought from Fisher Scientific (Schwerte, Germany). *Bis*-(4-*tert*-butylcyclohexyl)peroxydicarbonate (BCC, 95% is provided by PERGAN (Bocholt, Germany). Synperonic A11-LQ-(TH) (≥ 90% concentration, alcohols C12-15 ethoxylated) is obtained from Croda (Nettetal-Kaldenkirchen, Germany).

Prior to use, MMA is distilled at 40 °C and 60 mbars MMA to remove the stabilizer. HEMA used for polymerization is purified with a pre-packed inhibitor-removing column (Merck KGaA, Darmstadt, Germany). Aqueous solutions are prepared using deionized water with a resistivity of 18 MΩcm. All other chemicals are used without further purification.

4.2.2 Ternary Phase Diagrams

Phase diagrams are recorded at 25 °C ± 1 °C and 45 °C ± 1 °C according to the method of Clausse *et al.* [22] as described in section 2.3.2. For pseudo-ternary diagrams, the hydrotrope-mixture, surfactant/cosurfactant-mixture (instead of the hydrotrope), or monomer-mixture is handled like a single component. Hydrotrope or monomer mixtures are made with weight ratios of 1:1. The surfactant/HEMA mixture contained 62 wt% HEMA, 19 wt% Tergitol 15-S-12 and 19 wt% Synperonic A11-LQ-(TH). [23] The phase diagram of the surfactant-based reference system without cosurfactant (1:1 mixture of Tergitol and Synperonic by mass) at 25 °C is recorded by adding the surfactant mixture to binary mixtures of water/MMA, and the phase diagram at 45 °C is recorded by preparing individual samples in the one- and the two-phase region close to the phase border. Weight fractions are calculated from the masses of the individual components by precise weight measurements.

4.2.3 Critical Point Determination

Critical points are determined as described in section 2.3.3.

4.2.4 Compositions of Phases and Tie Lines

Tie lines of real ternary mixtures are determined as described in section 2.3.4. To determine the phase compositions of pseudo-ternary mixtures, ^{1}H-NMR and Karl Fischer titrations are established for both the water- and oil-rich phases.

4.2.5 Dynamic Light Scattering (DLS) of SFME Systems

DLS experiments are conducted as described in section 2.3.5.

4.2.6 Conductivity Measurements

Conductivity measurements are performed with the same setup as described in section 2.3.6. Due to the different position of the phase boundaries of the system MMA/HEMA/surfactant at different temperatures, the measurement is carried out at 45°C ± 0.2°C, which corresponds to the polymerization temperature. Binary MMA/alcohol, pseudo-binary MMA/HEMA/alcohol, and MMA/HEMA/surfactant mixtures are prepared with an addition of 0.2 wt% sodium bromide on the water-rich and, different to the experiments in section 2.3.6, 0.04 wt% sodium bromide on the oil-rich side to ensure a sufficient amount of charge carriers and a minimal amount of water necessary to ensure the complete dilution of the salt.

4.2.7 Polymerizations

8 ml of each reaction mixture, including 0.2 mol% BCC (referring to the monomer), are placed in 20 mL rolled-rim glasses and closed with aluminum crimp caps with polytetrafluoroethylene (PTFE) septum. After sealing the tube, the oxygen is replaced with nitrogen via a cannula for 45 seconds. The polymerizations are carried out for 24 hours at 45 °C in a heating bath. Polymerizations are stopped by freezing in liquid nitrogen and placed in a Modulyo 4K freeze dryer (Feldkirchen, Germany) and dried under reduced pressure (< 10 mbars) for 48h. After freeze-drying, the samples are stored in a drying cabinet at 110 °C until a constancy in weight.

4.2.8 Light Microscopy

Light microscopy images of dried microsuspension polymers are taken as described in section 2.3.12.

4.2.9 Scanning Electron Microscopy (SEM)

Field emission scanning electron microscopy (SEM) images are recorded on a Zeiss Leo 1530 scanning electron microscope (Carl Zeiss Microscopy GmbH, Oberkochen, Germany). Polymers are sputtered with Au/Pd for 30 s (2.45 kV, 22 mA) under an argon atmosphere using a Polaron E 510 Series II Sputter Coater (Polaron Instruments, London, UK).

4.2.10 BET Adsorption Isotherms

The specific surface areas of selected, dried polymer samples are determined by nitrogen adsorption following the Brunauer-Emmett-Teller (BET) adsorption model using an Accelerated Surface Area and Porosimetry System ASAP 2010 of Micromeritics (Norcross, GA, USA).

4.3 Results

4.3.1 Structural Investigations of Ternary and Pseudo-ternary SFME Systems

Ternary phase diagrams of systems containing water, MMA, and the hydrotropes IPA/TBA/HEMA are depicted in **Figure 4.2 a-c** (including reaction mixtures). We observe phase diagrams that can be expected for rather balanced SFME systems. [10]

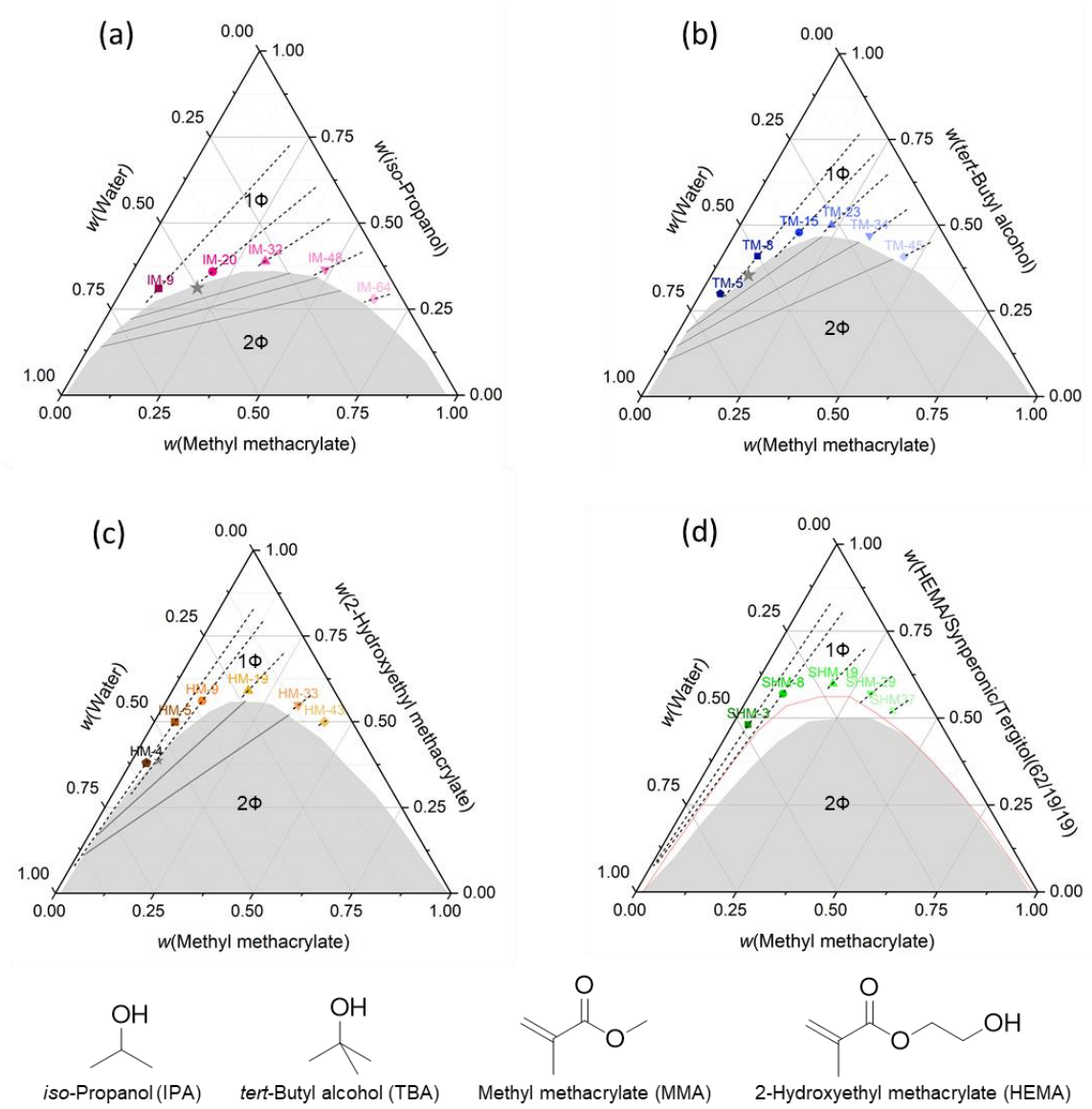

Figure 4.2 *Ternary phase diagrams of MMA, water, and the hydrotropes (a) iso-propanol (samples IM), (b) tert-butyl alcohol (samples TM), (c) 2-hydroxyethyl methacrylate (samples HM). The phase boundary is determined at 25 °C (grey area biphasic). (d) shows the pseudo-ternary diagram of the reference system MMA, water, and surfactant/cosurfactant mixture hydroxyethyl methacrylate, Synperonic A11-LQ-(TH), and Tergitol 15-S-12 at 25 °C (grey area) and 45 °C (red line). The dotted black lines describe the dilution curves for conductivity measurements. The critical point is marked as a dark grey star, and tie lines are drawn as dark grey lines in the ternary systems. The further studied compositions are marked with different symbols and their sample names. Structures of used chemicals are depicted on the bottom.*

The phase diagrams at 25 °C and 45 °C are nearly identical for the ternary systems. Thus it is not differentiated in-between temperatures. The phase diagrams of the systems containing IPA and TBA as hydrotropes were already investigated in a previous study (cf. chapter 2). [21]

The biphasic region increases in the order IPA < TBA < HEMA (cf. **Figure 4.2**). The system with HEMA has a relatively large two-phase region in the phase diagram given in mass fraction, especially when compared to IPA. The tilt of the tie lines is getting steeper and is shifted toward the water-rich side. Also, the critical point is shifted toward the water-rich side in the order IPA < TBA < HEMA. The same diagrams given in mol fractions instead of weight fractions are depicted in **Figure S 4.1** in the appendix. In molar fractions, the binodals look quite similar, with HEMA having even a slightly lower biphasic region compared to IPA and TBA.

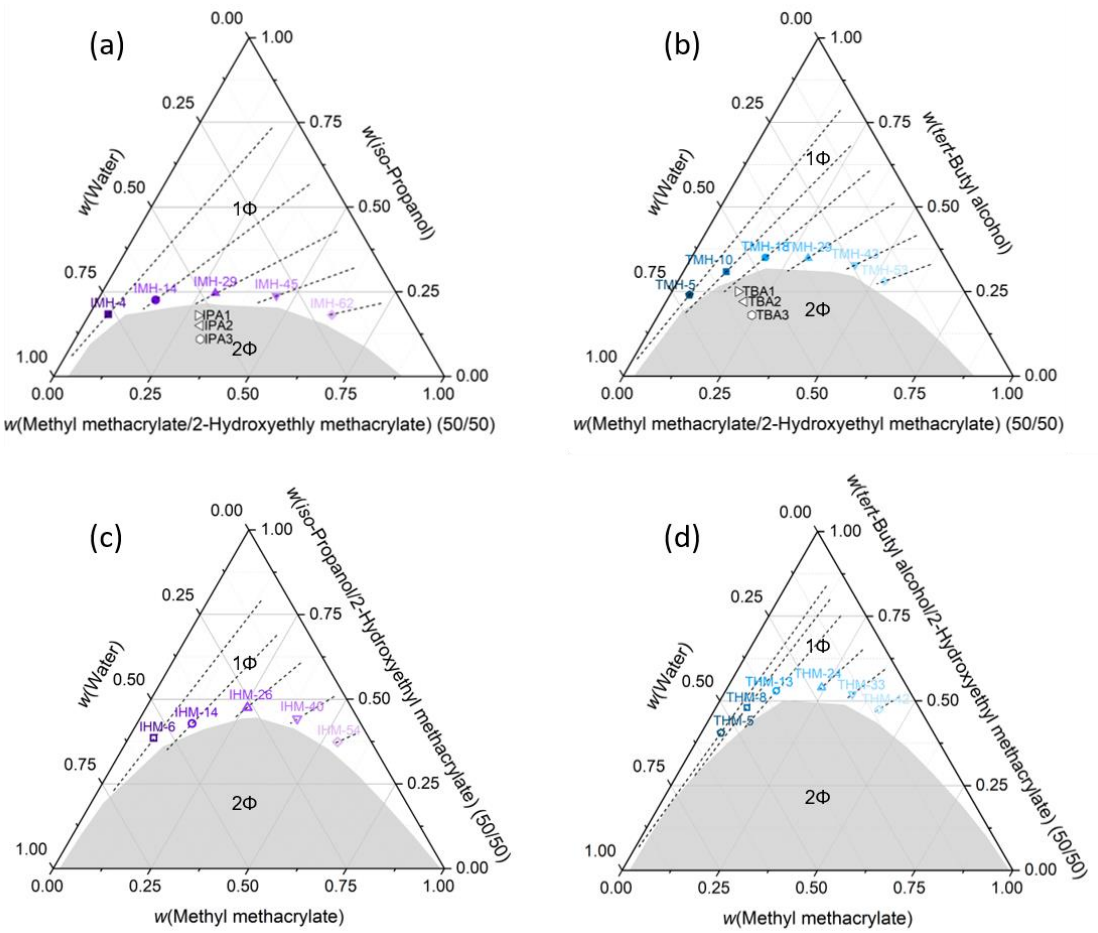

Figure 4.3 *Pseudo-ternary phase diagrams of water, the pseudo-ternary oil phase MMA/HEMA (50:50), and the hydrotropes (a) IPA (samples IMH), and (b) TBA/HEMA (samples TMH) as well as pseudo-ternary phase diagrams of water, MMA, and the pseudo-ternary hydrotrope mixtures (c) IPA/HEMA (samples IHM) and (d) TBA/HEMA (samples THM). The phase boundary is determined at 25 °C (grey area biphasic). The dotted black lines describe the dilution curves for conductivity measurements. The further studied compositions are marked with different symbols and their sample names. The black contoured points in the pseudo-ternary diagrams are studied regarding the composition of the two pseudo-phases*

Two different kinds of pseudo-ternary systems are investigated: HEMA as part of the hydrotrope phase or HEMA as part of the oil phase. As HEMA is already applied as hydrotrope in **Figure 4.2 c**, this might be the better choice from a colloid chemist's view. However, this has the disadvantage of different HEMA to MMA ratios across the phase diagram. The second variant of HEMA/MMA mixtures is applied in order to compare polymers resulting from identical HEMA to MMA ratios. The role of HEMA will be part of the discussion in section 4.4.1. The pseudo-ternary systems with MMA/HEMA as oil-phase (cf. **Figure 4.3 a** and **b**) comprise a significantly lower biphasic region compared to the ternary systems. The miscibility of the pseudo-ternary oil phase with water is clearly higher on the oil-rich side, making the phase diagram asymmetrical. The pseudo-ternary systems with HEMA as part of the hydrotrope mixture (cf. **Figure 4.3 c** and **d**) show quite symmetric biphasic regions, comparable to the ternary systems from **Figure 4.2**. The size of the biphasic region of the alcohol-HEMA mixtures is inbetween pure IPA and pure HEMA (or TBA and HEMA, respectively). All samples that are investigated further are marked in **Figure 4.2** (exact compositions can be found in **Table S 4.1** and **Table S 4.3** in the appendix).

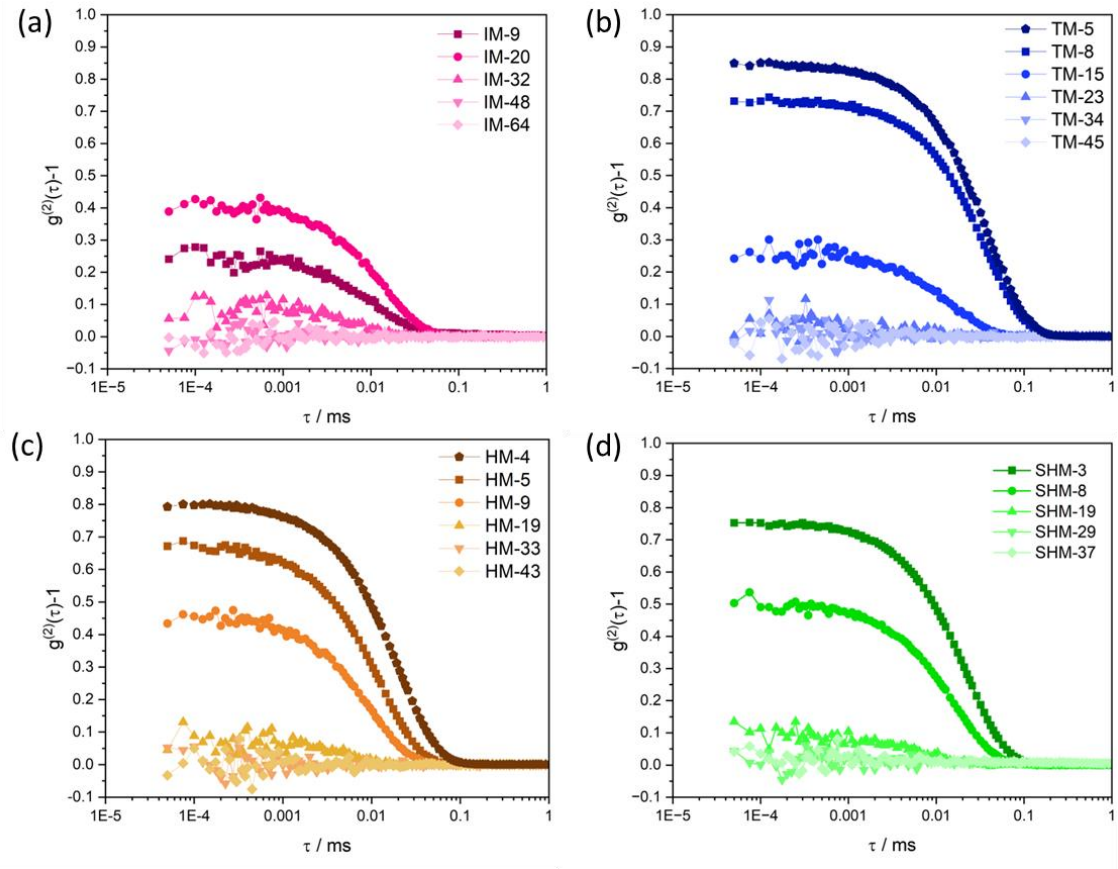

Figure 4.4 *Autocorrelation functions obtained by DLS measurements at 45 °C for the ternary systems with (a) IPA, (b) TBA, and (c) HEMA and (d) the surfactant-based reference system for reaction mixtures as marked in* ***Figure 4.2****.*

Figure 4.4 shows autocorrelation functions for the mixtures marked in **Figure 4.2**. The quality of the autocorrelation functions of the ternary systems of IPA and TBA increases around the critical point. However, distinct autocorrelation functions can still be found at a higher distance to the critical point. For the TBA and pure HEMA system, the most water-rich samples (TM-5 and HM-4) comprise the best structuring, while for IPA, the maximum can be found around 20 wt% MMA (sample IM-20). Overall, better-pronounced autocorrelation functions can be found on the more monomer-rich side of the critical point. Structuring is decreasing faster on the oil-rich side of the critical point. For samples with an MMA concentration of 48 wt% or higher in the case of IPA as hydrotrope, 34 wt% or higher for TBA, and 33 wt% or higher for HEMA, no autocorrelation function, but only noise can be observed.

Autocorrelation functions of the pseudo-ternary systems are depicted in **Figure S 4.2** in the appendix. The general trends are very similar compared to the ternary systems. The location of the most pronounced structuring seems to be mainly dependent on the MMA concentration within the alcohol systems, around 14 wt% for the IPA system, which corresponds to the samples IHM-14 and IMH-29 (where MMA is only half of the 29 wt% total monomer phase). In the pseudo-ternary TBA systems, the most pronounced structuring is observed at the lowest MMA concentrations, as in the ternary systems. Structuring can be observed up to around 25 wt% MMA for both alcohol systems.

Conductivity curves for ternary and pseudo-ternary systems are depicted in **Figure 4.5**. Please note that a tiny amount of NaBr is added to each sample to ensure a sufficient amount of charge carriers, as described in the experimental section. These tiny amounts (0.2 wt% or 0.04 wt%) are chosen as a compromise between not affecting the measurements and providing enough charge carriers for the measurement. Each dashed line intercuts the conductivity curve with the same color at the corresponding point marked in the respective phase diagram (cf. **Figure 4.2**). The systems IPA-MMA (IM), IPA-MMA/HEMA (IMH), and TBA-MMA/HEMA (TMH) include compositions at the rising part of the conductivity curve, the region around the maximum, and also the falling portion (see **Figure 4.5 a**, **b**, and **e**) with increasing water content. In the systems TBA-MMA (TM), HEMA-MMA (HM), and MMA-IPA/HEMA (IHM) (see **Figure 4.5 c**, **f**, and **g**), even the most water-rich sample is only at the region of the maximum. Thus, no samples on the falling portion of the conductivity curve are present. A large amount of all samples, including even the most water-rich sample of the system MMA-TBA/HEMA (THM, cf. **Figure 4.5 d**), lie on the rising part of the conductivity curves.

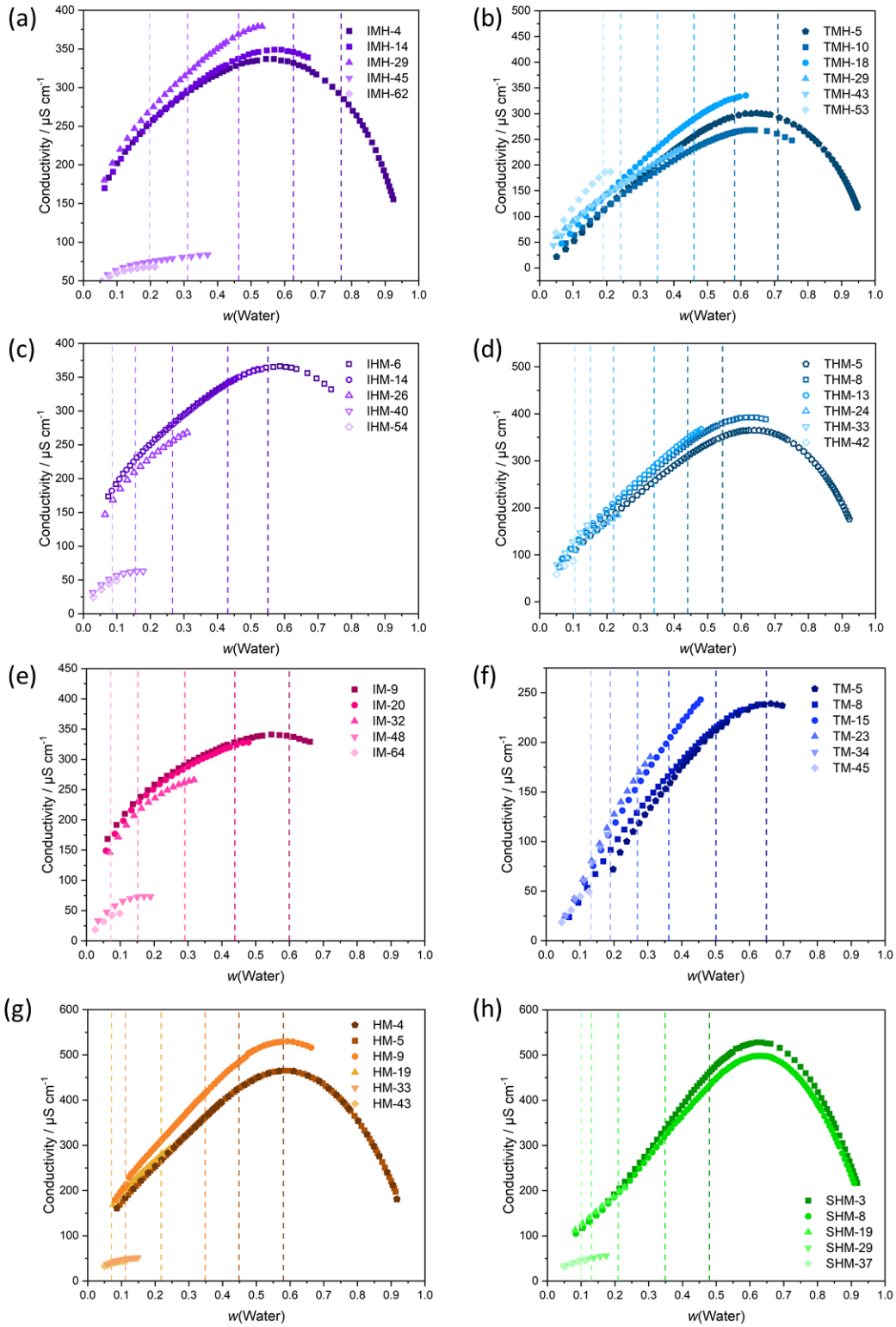

Figure 4.5 *Conductivity curves of the pseudo-ternary systems at 25°C containing HEMA as part of the oil phase, MMA, water, and the hydrotopes (a) IPA, (b) TBA, as well as HEMA as part of the hydrotrope phase and the alcohols (c) IPA and (d) TBA, and conductivity curves of ternary systems containing MMA, water, and the hydrotropes (e) IPA, (f) TBA, and (g) HEMA. (h) shows conductivity curves of the surfactant/HEMA-based reference system. Up to 0.2 wt% NaBr are added to the initial compositions to ensure enough charge carriers. Each dashed line intercuts the conductivity curve with the same color-marking exactly at the composition marked in* ***Figure 4.2*** *or* ***Figure 4.3****.*

4.3.2 Structural Investigations of the Reference Systems

Two different systems are investigated as reference: A surfactant-based system with MMA and Synperionic/Tergitol as well as a surfactant-cosurfactant-based system with MMA, HEMA, and Synperionic/Tergitol. [23]

The phase diagram of the latter cosurfactant/surfactant system is depicted in **Figure 4.2 d**. The two-phase region is quite high and increases from 25 °C to 45 °C. Autocorrelation functions behave similarly to the SFME systems (cf. **Figure 4.4**). The most pronounced function can be found for the most water-rich sample (SHM-3). For the two most oil-rich samples (SHM-29 and SHM-37), no mesostructuring can be observed. All intercuts with samples are on the increasing side of the conductivity curves. Concerning all three phase diagrams, autocorrelation functions, and conductivity curves, a very close similarity between the systems water/MMA/HEMA and water/MMA/surfactants/HEMA can be observed when comparing samples with similar locations in both phase diagrams (cf. **Figure 4.2 c** and **d**, **Figure 4.4 c** and **d**, and **Figure 4.5 g** and **h**).

The surfactant system without HEMA appears to have a smaller biphase range than the system with HEMA at both temperatures (phase diagram and correlation function can be found in **Figure S 4.4**, compositions in **Table S 4.2** in the appendix). Detection of the phase boundary in the system without HEMA as a cosurfactant is complicated by liquid crystal formation, so the phase boundary is only an approximate range. The system is overall very hard to handle due to very large areas of liquid crystalline behavior, which has not been studied in detail so far. The autocorrelation functions of the two possibly suitable mixtures in this system (SM-4 and SM-8) appear identical.

4.3.3 Investigation of PMMA Polymers

Figure 4.6 depicts SEM images of the system MMA/TBA/water. Macroscopic and light-microscopic images as well as more SEM images of polymers derived from the systems MMA/TBA/water and MMA/IPA/water can be found in **Figure S 4.5** and **Figure S 4.6** in the appendix. The appearance of the macroscopic morphology changes around the phase diagram. While samples derived from the most water-rich compositions (TM-5, IM-9) appear white, opaque, and powder- or sponge-like, PMMA derived from the most oil-rich samples (TM-45 and IM-64) appear transparent.

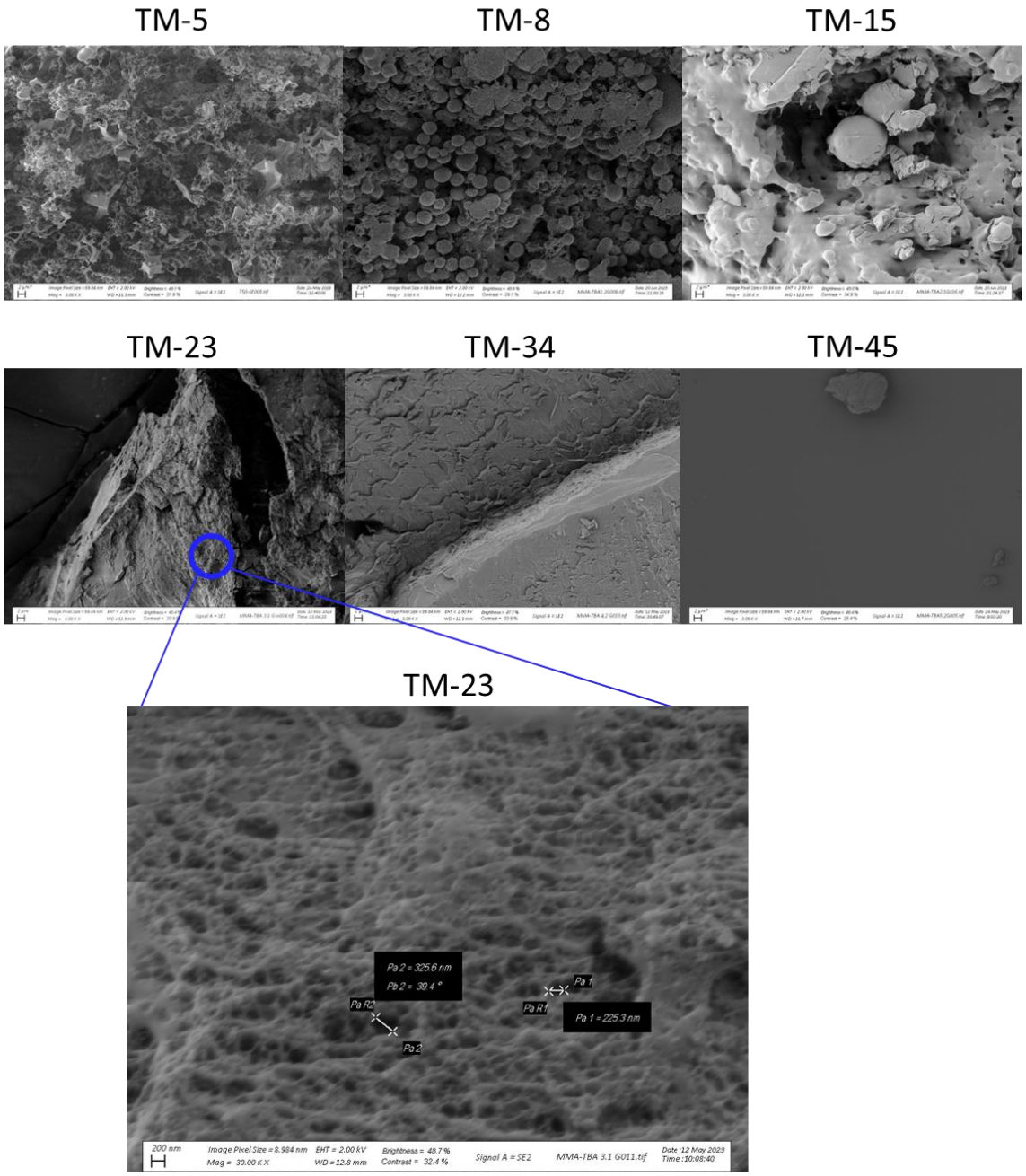

Figure 4.6 *SEM images of polymers derived from the system MMA/TBA/water at a magnification factor of 3,000 and a snapshot of the sample TM-23 at a magnification factor of 30,000.*

The microscopic morphology changes just like the macroscopic one. SEM images show polymers consisting of a coagulation of droplet-like aggregates (TM-5 and TM-8) changing to a sponge-like morphology with holes (TM-15 and TM-23). The sample TM-34 reveals some kind of layered structure on a fractured edge but otherwise looks unstructured, just like TM-45. A closer look at the sample TM-23 shows pores in the size range of 200-400 nm. (cf. **Figure 4.6**) Sizes of other samples from the TBA and IPA samples can be seen in **Figure S 4.7**, giving sizes of PMMA droplets in the area of 600 nm to some µm for TM-5 and 3-5 µm for TM-8, and pore sizes of 1.0-1.3 µm

for TM-15. In the IPA system, sizes for clearly structured systems range from 1-2 µm (IM-9) to 11 µm (IM-20).

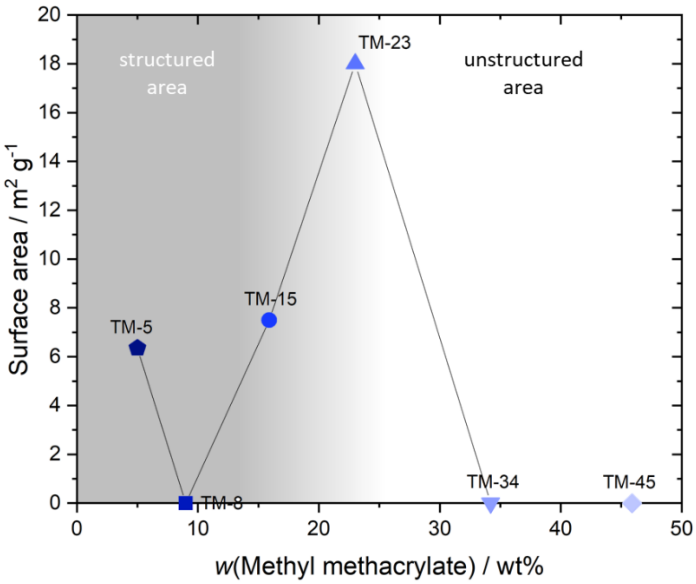

Figure 4.7 *Surface areas derived from nitrogen adsorption measurement (BET) of PMMA particles derived from the water/TBA/MMA system plotted against the MMA weight fraction. The grey shaded area represents the region in which distinct autocorrelation functions could be derived by DLS (marked "structured area"), and the white area represents the region where only noise could be found in DLS measurements (marked "unstructured area").*

Nitrogen adsorption measurements for the TBA system (cf. **Figure 4.7**) found specific surface areas of 6.3 $m^2\ g^{-1}$ (TM-5), 7.5 $m^2\ g^{-1}$ (TM-15), and 18 $m^2\ g^{-1}$ (TM-23), followed by a drop in the specific surface area below the detection limit. Using a simple, spherical model with the density of PMMA given in the literature, [24] this would correspond to particle sizes of 0.8 µm (6.3 $m^2\ g^{-1}$, TM-5) to 0.3 µm (18 $m^2\ g^{-1}$, TM-23), which fits the sizes of the pores measured in SEM images. For TM-8, where a size range of 3-5 µm is measured in SEM images, a specific surface of around 1 $m^2\ g^{-1}$ should theoretically be found, which might be too low for the experimental setup. The reference system with only surfactants and MMA without HEMA led to a very viscous, yellow-to-brown polymer paste and is not considered further (cf. **Figure S 4.14**).

4.3.4 Investigation of Poly(MMA-co-HEMA) Copolymers

Figure 4.8 depicts SEM images of selected porous polymers derived from the systems water-HEMA/surfactants-MMA, water-HEMA-MMA, and water-HEMA/TBA-MMA. Macroscopic, light microscopic, and SEM images of all investigated samples can be found in **Figure S 4.8**, **Figure S 4.9**, **Figure S 4.10**, **Figure S 4.11**, **Figure S 4.12**, **Figure S 4.13**, and **Figure S 4.14** in the appendix. Just like for pure PMMA samples, porous polymers can be observed for previously structured systems on the water-rich side and unstructured polymers for the previously molecularly dispersed systems.

For systems with MMA/HEMA mixtures and alcohols (cf. **Figure S 4.9** and **Figure S 4.10**), both IPA and TBA lead to comparable polymers like pure MMA (compare, *e.g.*, TM-5 to TM-23, **Figure 4.6** with TMH-5 and TMH-10, **Figure 4.8**). HEMA/alcohol mixtures, however, lead to less defined polymer morphologies (cf. **Figure S 4.11** and **Figure S 4.12**).

Both systems without alcohols but only HEMA or HEMA/surfactant mixtures show sponge-like morphologies with holes at very low MMA concentrations already, in contrast to samples from SFME systems with IPA or TBA (see **Figure 4.6** for TBA, samples with IPA are depicted in **Figure S 4.6 b**). Especially SMH-3 (with surfactant and HEMA) and HM-4 (without surfactant, but HEMA) seem to produce very similar morphologies but in a larger size range for samples without surfactant. The overall finest structure is observed for TMH-10 (see **Figure 4.8 f**) in the system water-MMA/HEMA-TBA.

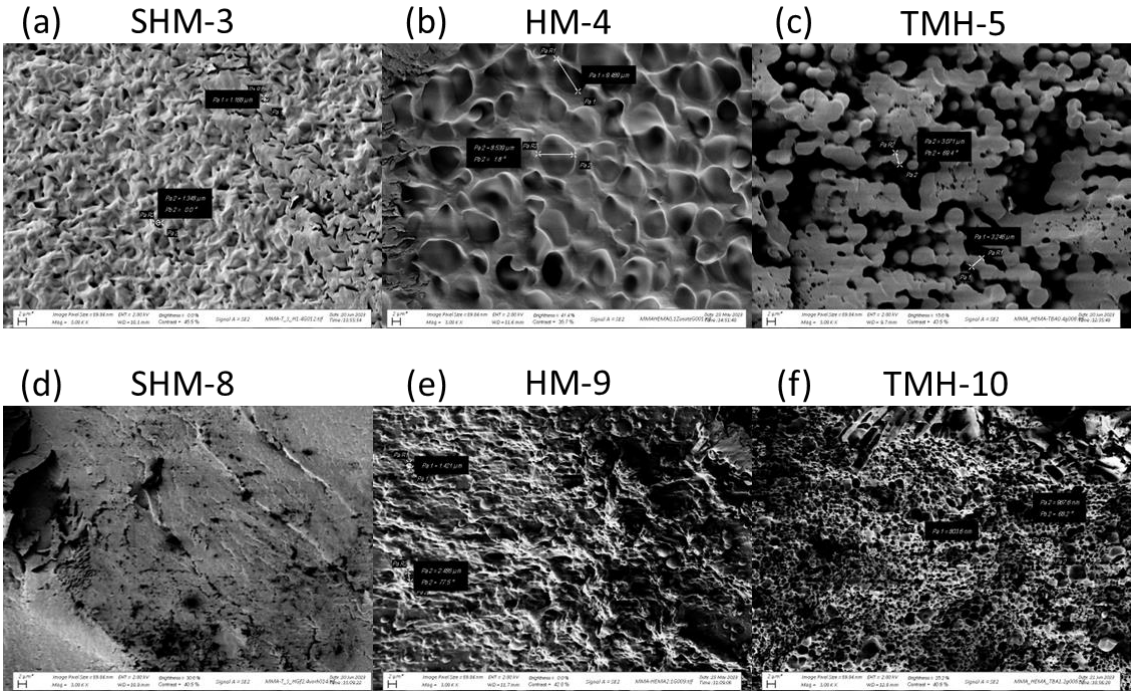

Figure 4.8 *SEM images of porous polymers from the systems with (a) and (d) MMA/HEMA/surfactant, (b) and (e) MMA/HEMA, and (c) and (f) TBA/HEMA/MMA with a magnification factor of 3,000.*

4.4 Discussion

4.4.1 The Role of HEMA in Pseudo-ternary Systems

While the ternary systems with MMA and IPA or TBA as hydrotropes have already been described previously [21], the question of how to treat HEMA in a pseudo-ternary system arises. While MMA is clearly defined in the literature as an (albeit relatively hydrophilic) oil, [25] HEMA is used as a cosurfactant in some systems, [4; 26] which, in combination with its complete miscibility with water, indicates the possibility of hydrotropic behavior. [10] One could consider two possibilities concerning pseudo-ternary systems: HEMA as part of the oil phase as a monomer together with MMA or as a hydrotrope with the alcohols IPA or TBA. **Figure 4.2 c** shows the phase diagram with water, MMA, and HEMA as a hydrotrope. Although the biphasic region is more extended than with IPA or TBA, the shape can still be expected for an SFME system. Also, quite pronounced structuring can be found in the pre-Ouzo region of the system by DLS (cf. **Figure 4.3 c**). Comparing the ternary systems with MMA and the hydrotropes IPA, TBA, and HEMA in molar fractions (cf. **Figure S 4.1**), HEMA performs even slightly better than IPA and TBA with a smaller biphasic region. Thus, HEMA must be considered as quite a good hydrotrope for SFME systems with the drawback of a high molar mass, enlarging the biphasic region in comparison to alcohols like TBA or IPA when considering mass fractions. However, investigating pseudo-ternary systems with HEMA as part of the hydrotrope phase only (which would be correct based on the behavior observed) has the disadvantage of different HEMA to MMA ratios across the phase diagram. This will change the polymer properties (especially the hydrophilicity) drastically, which is also a drawback of the surfactant-based reference systems with HEMA as a cosurfactant. [23]

Tie lines with HEMA are tilted strongly towards the water-rich side of the phase diagram (cf. **Figure 4.2 c**). That indicates that the oil-rich phase might be quite hydrotrope-rich compared to the water-rich phase, when expecting the mesoscale pseudo-phase separation to be similar to the one in the nearby Ouzo region. [21; 27] The investigation of the compositions of the separated phases in the biphasic region close to the binodal of the pseudo-ternary systems with HEMA/MMA mixtures as oil phase (cf.

Table S 4.4) approves this and shows that the major part of the HEMA in the system might be in the oil-rich phase, similar to TBA. Thus, to compare the systems best way possible, polymerizations are performed for both possibilities of pseudo-ternary systems: HEMA as hydrotrope, which is more correct from a colloid chemist's point of view, and HEMA as part of the oil phase,

leading to copolymers with similar MMA to HEMA ratios across the phase diagram and making the polymers thus more comparable.

4.4.2 Investigation of (Pseudo-)Ternary Systems Before Polymerization

DLS and conductivity curves observed by conductivity measurements are used to investigate the nature of the systems. When an impact on the polymer derived is expected, knowledge about structuring *per se* and the kind of structuring are relevant. In conventional microemulsion systems, conductivity curves are plotted, *e.g.*, against the volume fraction or the square root of the surfactant concentration in order to evaluate them on the basis of the Percolation or Effective Medium theories. [28; 29] Since the applicability of these models to SFMEs has not yet been discussed and proven, we only consider the position with respect to the maximum and compare the curves, which allows a plot of conductivity against the mass fraction that is also used for phase diagrams. [30] In the region around the maximum in conductivity, a bicontinuous-like structure is expected, while an O/W-like SFME can be expected on the falling partition of the curve, and a W/O-like SFME can be expected on the increasing part of the curve. In contrast to surfactant-based systems, we expect a continuous transition from molecular-disperse to structured systems. The distinction is made on the basis of autocorrelation functions from DLS measurements.

Concerning the ternary systems without HEMA, the first three samples from the water-rich side for both the IPA (IM-9, -20, and -32) and the TBA (TM-5, -8, and -15) system show distinct correlation functions indicating mesostructuring, TM-23 seems to be an in-between case, while only noise can be observed in the other cases (cf. **Figure 4.4**). The compositions IM-20, IM-32, TM-8, and TM-15 intercut the conductivity curves on the rising branch, indicating inverse (water in oil-like) structuring. However, especially IM-20 is not far from the turning point where bicontinuous structuring can be expected. TM-5 is located directly on top of the curve, indicating bicontinuous structuring. IM-9 intercuts the conductivity curve on the falling part of the curve just after the maximum, thus on the oil-in-water-like region. These samples around the maximum of the conductivity curves are in proximity to the critical point of the ternary systems, where phase transition can be expected. [30]

HEMA behaves mainly like a hydrotrope in the pseudo-ternary systems, as already discussed. While the autocorrelation function is the highest at the most water-rich sample in both TBA/HEMA systems, the best structuring sample seems to be shifted towards a more monomer-rich region for the IPA system, with HEMA being part of the oil phase (the most pronounced

autocorrelation functions are found for IMH-29 and IHM-14). However, when only MMA is considered as the oil, the highest structuring for both systems is around 14 wt% MMA. Thus, HEMA does not seem to influence the location of maximum structuring drastically.

The point of inflection of conductivity curves, however, appears to be shifted slightly towards the water-rich side with HEMA, being in between 9 and 20 wt% MMA (IM-9 and IM-20) for the IPA system without HEMA and between 6 and 14 wt% MMA for the pseudo-ternary systems (around IHM-6 and between IMH-14 and IMH-29). As the critical point of HEMA locates similarly to the TBA system in the ternary system in contrast to IPA (where the critical point is more oil-rich), it is not astonishing that the pseudo-ternary TBA/HEMA system differs less from the ternary systems than IPA/HEMA.

The HEMA/surfactant-based system (cf. **Figure 4.2 d**) is quite temperature-sensitive. The phase diagram at 45 °C, as well as the autocorrelation functions and conductivity curves, behave surprisingly similarly to the system with pure HEMA as a hydrotrope (cf. **Figure 4.2 c** and **d**, **Figure 4.4 c** and **d**, and **Figure 4.5 g** and **h**). The samples SHM-29 and SHM-37 show no distinct autocorrelation functions but only noise, which would not be expected at all for a surfactant-based system. All samples intercut the conductivity curves on the rising part of the curves, indicating only inverse microemulsions present in this system. This is contrary to the general idea of using bicontinuous microemulsion phases. [23] In this system, HEMA seems to play the dominant role in defining the nature of structuring. The two nonionic surfactants appear to incorporate into the existing pre-structure in the surfactant-free system at 45°C rather than pretending to have a different structure. A further stabilization or even a destabilization due to the surfactants cannot be excluded. However, as seen in the comparison between 25 °C and 45 °C, the system gets more temperature dependent due to the ethylene oxide groups of both surfactants. Since the pure surfactant-based system without cosurfactant (cf. **Figure S 4.4**) forms highly viscous phases in large parts of the phase diagram at 45 °C, only two very water-rich points could be selected for further investigation and polymerization.

4.4.3 PMMA Polymers

PMMA particles derived from ternary systems with IPA or TBA as hydrotrope show distinct differences across the phase diagram. This difference can already be seen macroscopically (cf. **Figure S 4.5** in the appendix). The change from opaque to transparent corresponds to the region where no structuring could be observed by DLS anymore. In the TBA system, nanostructured polymers can be seen in SEM images from samples TM-5 to TM-23 (see **Figure 4.6**). Counterintuitive, the finest structures cannot be observed for samples with previously most pronounced

autocorrelation functions (*i.e.,* TM-8) but on the edge regions where mesostructuring is just still present (*i.e.,* TM-5 and TM-23). According to conductivity curves, TM-5 should be bicontinuous, and the other samples (TM-8 to TM-23) should be inverse (cf. **Figure 4.5 f**). Indeed, the polymer derived from TM-5 has a morphology similar to what we expect from a bicontinuous microemulsion but with a pore size of some hundred nanometers to some micrometers. TM-23 has a sponge-like appearance with more holes, what we expect from a W/O-like microemulsion (cf. **Figure 4.6**). In between, larger and more drop-like shapes in a size range of 3-4 µm could be observed for TM-8 that remind of the shape of Ouzo aggregates. Polymers of a similar size but with more holes could be observed for TM-15 (for size evaluation, cf. **Figure S 4.7** in the appendix).

For IPA samples, results are similar: IM-9, which should form an O/W-like SFME, leads to droplet-like agglomerates in a size range of around 1 µm (cf. **Figure S 4.6 b**). Sample IM-20, which showed the most pronounced autocorrelation function before structuring, leads to larger, droplet-like agglomerates, just like the sample TM-5. Further samples with IPA are not really well structured anymore.

Overall, the sizes of polymers range from some hundred nanometers to a few micrometers, which is by a factor of 100 to 1000 larger than initial SFMEs. [10; 21] As already mentioned in the introduction, a destabilization of 7-10 k_BT is calculated to be caused by the growing polymer chains in investigated conventional microemulsions. [31; 5] The reason for this memory is discussed to lie in the repulsive force on the thermodynamically unstable polymer particles, [5] which might also be applicable to SFMEs. [21]

In literature, several studies on the use of Ouzo systems for polymerizations are known, mainly using a top-down nanoprecipitate technique of dissolved polymer [32] but also using in-situ polymerizations like in our case [33; 34]. Morphologies of those particles are mainly spherical, sometimes agglomerates of droplets, comparable to our systems TM-8, IM-20, and IM-9. As discussed in a previous paper, the SFME will get unstable during polymerization, leading to an Ouzo-like stabilizing effect. [21] This seems to be especially the case for samples close to the critical point (TM-8, TM-20, IM-9) and makes sense due to the fact that SFMEs and the Ouzo regime are closely linked. [27]

The novelty of using in-situ polymerizations in the SFME regime, however, is what happens when using the edge regions of the previously mesostructured area: Just like reported for surfactant-based microemulsions, [31; 5] one can observe a morphology similar to the one of the previous

SFME (*i.e.,* compare samples IM-9, TM-5, TM-23). Thus, not only droplet-like morphologies like for Ouzo-polymerizations but also bicontinuous and sponge-like morphologies could be obtained. The consistent sizes of SEM and calculations for BET adsorption isotherms (where adsorption is tested on much larger sample sizes) suggest that the structure does not only appear superficially but continues homogenously inside the polymer particles.

4.4.4 PMMA-HEMA-Copolymers

Starting with the most simple system using only water, MMA, and HEMA as a hydrotrope, things are not as straightforward as for pure PMMA at first sight. The polymer derived from HM-4 (see **Figure 4.8 b**), where the SFME should be bicontinuous due to the conductivity experiments (cf. **Figure S 4.3 g**), shows more of a morphology with holes, which would be expected for a W/O-like system.

Overall, the tendency to form inverse structures seems to increase in the order IPA < TBA < HEMA. The same order can also be found for the location of the critical point and the location of intercepts in the conductivity points. (cf. section 4.3.1) However, the system water/MMA/HEMA has the drawback of different MMA to HEMA ratios across the phase diagram. Furthermore, HEMA is known to build hydrogels, which might disturb the well-balanced behavior of SFMEs/Ouzo-domains. [35] The droplets embedded in the unstructured polymer matrix (cf. HM-5, HM-19, HM-33, **Figure S 4.8**) could indicate that phase separation occurred due to hydrogel formation, and polymers with significant MMA/HEMA enrichment are formed. However, this is not investigated further. The same might also be the case for pseudo-ternary mixtures with HEMA as part of the hydrotrope phase.

The most interesting MMA/HEMA copolymers are derived from samples with MMA/HEMA mixtures with a fixed MMA to HEMA ratio of 1:1 by mass as the oil phase (systems TMH, IMH). Due to the higher alcohol content in comparison to HEMA, the nature of the alcohols seems to dominate over HEMA, leading to droplet-like polymers for very water-rich samples for IPA (IMH-4, IMH-14, all SEM images of this system are depicted in **Figure S 4.10** in the appendix) and droplet- as well as bicontinuous/inverse-like polymers for TBA samples (TMH-5, TMH-10, see **Figure 4.8 c** and **f,** all samples of this system are depicted in **Figure S 4.10** in the appendix). Even though IPA/TBA dominates the structuring, the impact of HEMA might still be noticeable, shifting the areas of larger, Ouzo-like droplets but also the W/O-like structures more to the water-rich side of the phase diagram. The most interesting sample might be TMH-10, which shows pores in a size range of < 1 µm, comparably with those derived from surfactant-based microemulsions in the literature without polymerizable surfactants. [36; 7]

4.4.5 Comparison of Polymerizations in SFME and Surfactant-based Microemulsions

The similarities between the surfactant-based and the surfactant-free systems with HEMA before polymerizations have already been mentioned in section 4.4.2. Just like the ternary systems, also the polymers show quite similar behaviors. The samples SHM-3 and HM-4 show remarkably similar structures but in smaller size ranges for the surfactant-based system (1.0-1.5 µm for SHM-3 vs. 8-10 µm for HM-4, see **Figure 4.8 a** and **b**). SHM-8 (see **Figure 4.8 d**) has a slightly porous and overall much less defined structure, while no nanostructuring could be observed for polymers derived from more MMA-rich mixtures in the SEM, even after washing steps (images of all samples are printed in **Figure S 4.14**, before and after washing can be compared in **Figure S 4.15** in the appendix), what is surprising for a surfactant-based system.

It appears as if HEMA would dictate the structure both before and during polymerization in this system, while the surfactants incorporate and possibly stabilize the interphase, but without changing it. During polymerization, we expect additional stabilization to occur due to the presence of the surfactants. This appears to result in smaller overall pore sizes with an otherwise similar structure (compare **Figure 4.8 a** and **b).** There are some Ouzo-like systems described in the literature where additional surfactants have been added. [33; 37; 38] However, this was before the Ouzo effect was discussed in a broader scientific community. It was already mentioned in a review that in terms of precipitation in Ouzo systems, the characteristics of these systems seem to be nearly independent of the surfactant. [33] A similar case can be found in a publication about high alcohol contents in a nonionic microemulsion system. It is described that the alcohols dominate above the surfactants in those systems with high levels of solvents. [39] This publication dates from a time before surfactant-free (micro)emulsions are known to a broader community as well, [10] which leads to the assumption that it was not even thought of the possibility that this alcohol domination origins from a pre-structure without the surfactant.

Thus, in some systems, as in the present reference system, the added nonionic surfactants might only have an additional kinetic stabilizing effect but are not fundamentally necessary for the nature of the system. On the contrary, in the present example, the smallest pore sizes could be obtained both with and without HEMA in the surfactant-free system with the hydrotrope TBA (TM-5 and TMH-10).

4.5 Conclusions and Outlook

In the present contribution, we investigate the impact of the mesostructures in surfactant-free microemulsions (SFMEs) on the nanostructures of the dried polymers. While polymerizations in SFMEs have already reported in chapter 2, [21] we can clearly link the correlation between the mesostructure of the former SFME to the resulting polymer morphologies for the first time.

SFME systems with MMA are investigated with different hydrotropes (*iso*-propanol (IPA), *tert*-butyl alcohol (TBA), 2-hydroxyethyl methacrylate (HEMA)). Pseudo-ternary systems with both MMA/HEMA with and without IPA or TBA as additional hydrotropes are investigated and compared to a system with MMA/HEMA and the surfactants Tergitol 15-S-12 and Synperonic A11-LQ-(TH). [23] HEMA is discussed as a polymerizable cosurfactant in literature, [4; 26] but also shows more hydrotropic than co-solvent or cosurfactant behavior, in our opinion.

It is found that it is possible to achieve different kinds of mesostructured polymers that are linked to structures expected in previous SFMEs (droplet-like shapes coming from O/W-like SFMEs as well as sponge-like shapes derived from bicontinuous to W/O-like SFMEs). However, the size of the derived polymers is by a factor of 100 to 1000 higher than the mesostructures found in the initial SFMEs. [21; 10] Both the different morphologies as well as particles in the micrometer range behave like polymers derived from conventional microemulsion systems without polymerizable surfactants. [7; 36] Sizes found in scanning electron microscopy (SEM) images are in agreement with specific surface areas measured by nitrogen adsorption measurements following the Brunauer-Emmett-Teller (BET) model.

The difference between the MMA/HEMA systems with and without surfactants is surprisingly low and leads to the assumption that the interplay of MMA, HEMA (additional TBA/IPA, if present), and water defines the basic structure without the surfactants. The surfactant might only have an additional stabilizing effect on the growing polymer particles, leading to slightly smaller sizes, but without changing the basic morphology. However, the smallest pore size in sponge-like particles, both with and without HEMA, are observed in the surfactant-free system with TBA as a hydrotrope (around 200 nm for TM-23, < 1 µm for TMH-10). While the use of SFME for droplet-like polymer morphologies (*i.e.,* for encapsulation) was already discussed several times, [40; 41] we could show that also other morphologies are possible. This opens a field of possibilities, *e.g.*, for filtration applications.

4.6 Appendix

4.6.1 Compositions of Samples Investigated in this Work

Table S 4.1 *Composition of samples of ternary SFME systems investigated further in this study.*

System	Sample	Water / wt%	MMA / wt%	HEMA / wt%	IPA / wt%	TBA / wt%
MMA-IPA-water	IM-9	60.0	9.1		30.9	
	IM-20	43.7	20.2		35.1	
	IM-32	29.1	32.0		38.9	
	IM-48	15.2	48.3		34.5	
	IM-64	7.2	64.9		27.9	
MMA-TBA-water	TM-5	65.0	5.0			30.0
	TM-8	50.1	9.0			40.9
	TM-15	36.2	15.9			47.9
	TM-23	27.0	23.0			50.0
	TM-34	18.9	34.2			46.9
	TM-45	13.3	45.9			40.8
MMA-HEMA-water	HM-4	58.0	4.0	38.0		
	HM-5	44.8	5.2	50.0		
	HM-9	34.9	9.0	56.1		
	HM-19	21.7	19.2	59.1		
	HM-33	11.2	34.0	54.8		
	HM-43	7.0	43.0	50.0		

Table S 4.2 *Composition of samples of surfactant-based systems investigated further in this study.*

System	Sample	Water / wt%	MMA / wt%	HEMA / wt%	Synperonic/ Tergitol (50/50) / wt%
MMA-HEMA/Synperonic/ Tergitol-water	SHM-3	48.0	3.9	29.8	18.3
	SHM-8	34.9	8.1	35.4	21.6
	SHM-19	20.1	19.1	37.1	22.7
	SHM-29	13.0	29.9	35.4	21.7
	SHM-37	10.0	38.0	32.2	19.8
MMA-Synperonic/ Tergitol-water	SM-4	72.0	4.0		24.0
	SM-8	64.0	8.0		28.0

Table S 4.3 *Composition of samples of pseudo-ternary SFME systems investigated further in this study.*

System	Sample	Water / wt%	MMA / wt%	HEMA / wt%	IPA / wt%	TBA / wt%
MMA/HEMA-IPA-water	IMH-4	76.8	2.45	2.45	18.3	
	IMH-14	62.6	7.4	7.4	22.6	
	IMH-29	46.3	14.55	14.55	24.6	
	IMH-45	31.1	22.55	22.55	23.8	
	IMH-62	19.7	31.05	31.05	18.2	
MMA/HEMA-TBA-water	TMH-5	71.0	2.5	2.5		24.0
	TMH-10	58.1	5.5	5.5		30.9
	TMH-18	46.0	9.45	9.45		35.1
	TMH-29	35.1	15	15		34.9
	TMH-43	24.1	21.5	21.5		32.9
	TMH-53	19.0	26.5	26.5		28.0
MMA-HEMA/IPA-water	IHM-6	55.0	6.4	19.3	19.3	
	IHM-14	43.1	14.1	21.4	21.4	
	IHM-26	26.6	25.9	23.75	23.75	
	IHM-40	15.5	40.3	22.1	22.1	
	IHM-54	8.6	54.0	18.7	18.7	
MMA-HEMA/TBA-water	THM-5	54.4	5.0	20.3		20.3
	THM-8	44.0	8.0	24.0		24.0
	THM-13	34.1	13.0	26.5		26.5
	THM-24	22.0	24.0	27.0		27.0
	THM-33	15.1	32.9	26.0		26.0
	THM-42	10.6	42.0	23.7		23.7

Table S 4.4 *Distribution of the two phase-separated phases of the pseudo-ternary phase diagrams.*

	Phase	Water / wt%	HEMA / wt%	MMA / wt%	IPA or TBA / wt%
IPA1	oil-rich	28.96	34.50	15.08	32.71
	water-rich	74.34	9.00	2.16	14.50
IPA2	oil-rich	22.87	26.53	31.48	19.12
	water-rich	82.49	6.13	1.40	9.98
IPA3	oil-rich	17.69	30.47	37.83	14.01
	water-rich	82.88	6.97	1.55	8.60
TBA1	oil-rich	40.97	12.46	12.55	34.01
	water-rich	74.29	5.15	2.75	17.81
TBA2	oil-rich	30.83	15.51	19.76	33.90
	water-rich	79.21	5.14	1.74	13.90
TBA3	oil-rich	23.36	18.80	27.21	30.62
	water-rich	82.90	5.27	1.20	10.63

4.6.2 Ternary Phase Diagrams Given in Mol Fractions

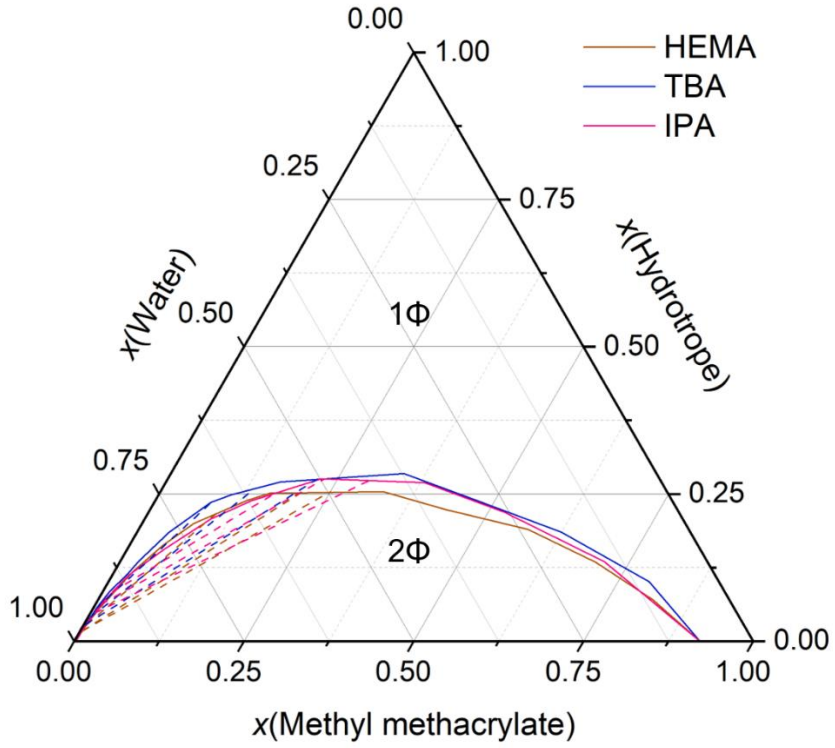

Figure S 4.1 *Phase diagram of the ternary systems water, MMA, and the hydrotropes HEMA (brown), TBA (blue), and IPA (pink) at 25 °C given in mol fractions. Tie lines are drawn as dashed lines.*

4.6.3 DLS and Conductivity Data of the Pseudo-ternary Systems with HEMA

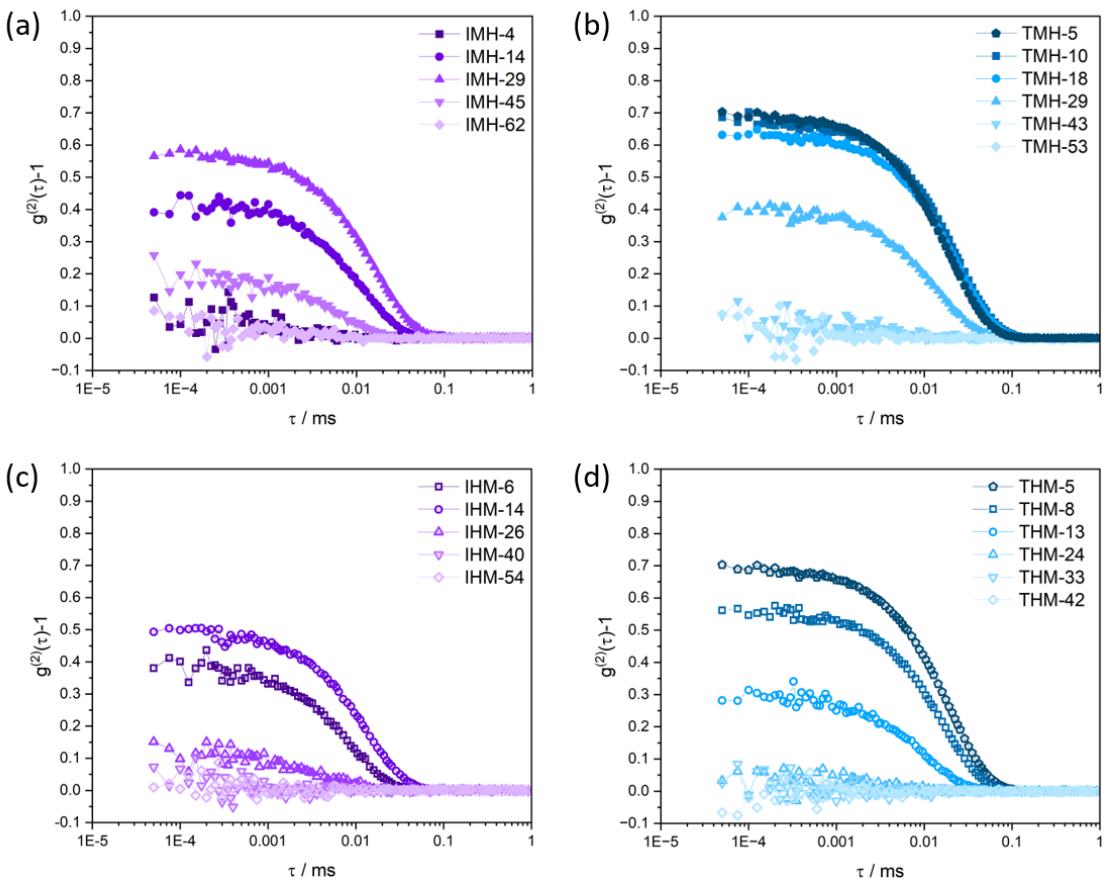

Figure S 4.2 *Autocorrelation functions obtained by DLS measurements at 45 °C for the pseudo-ternary systems with water, a mixture of MMA and HEMA (50:50 by weight) as oil phase and (a) IPA, or (b) TBA as hydrotrope, and pseudo ternary mixtures with water, MMA as oil phase, and a mixture of HEMA and (c) IPA, or (d) TBA, as hydrotropes, for reaction mixtures as marked in* ***Figure 4.2****.*

The most pronounced autocorrelation function in the pseudo-ternary system with a mixture of MMA and HEMA as oil phase and IPA as hydrotrope (cf. **Figure S 4.2 a**) can be found at a monomer content of 29 wt% for IPA (sample IMH-29), which is significantly higher than for the system with HEMA as part of the oil phase (IHM-14, thus 14 wt% oil phase, cf. **Figure S 4.2 c**) or the IPA system without HEMA. Considering only the MMA content as oil in both pseudo-ternary systems, the most pronounced autocorrelation function can be found at an MMA fraction of around 14 wt%. In the system, MMA/HEMA-TBA (with HEMA as part of the oil phase), autocorrelation functions for samples up to 18 wt% monomers (TMH-5, TMH-10, and TMH-18) are all quite identically well pronounced. All those samples contain up to 9.5 wt% MMA. The pseudo-ternary system with HEMA as part of the hydrotrope phase with TBA shows already more decreasing but still pronounced structuring at 8 wt% MMA (sample THM-8).

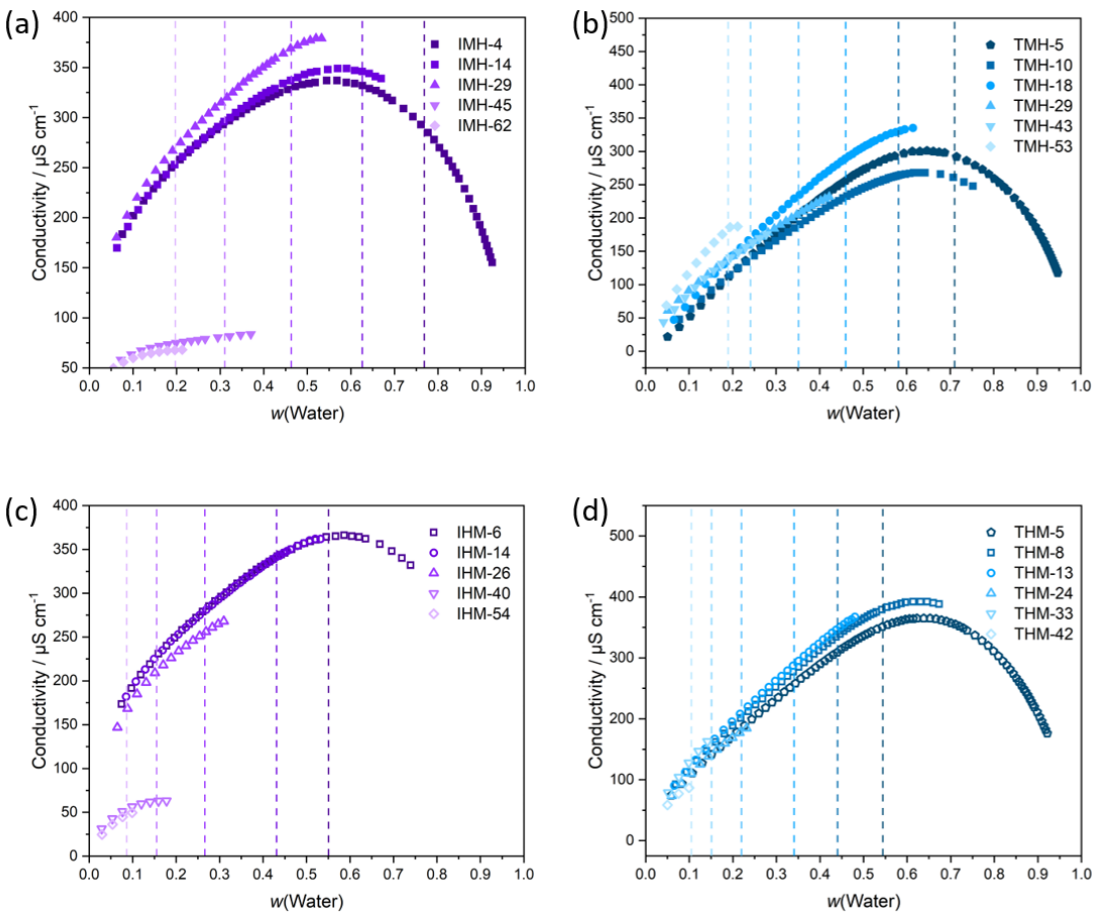

Figure S 4.3 *Conductivity curves obtained by electrical conductivity measurements at 25°C of the ternary systems containing MMA, Water and the hydrotophes (a) IPA, (b) TBA, and (c) HEMA. Each dashed line intercuts the conductivity curve with the same color-marking exactly at the composition marked in* ***Figure 4.2****.*

4.6.4 Investigation of the Reference System without HEMA

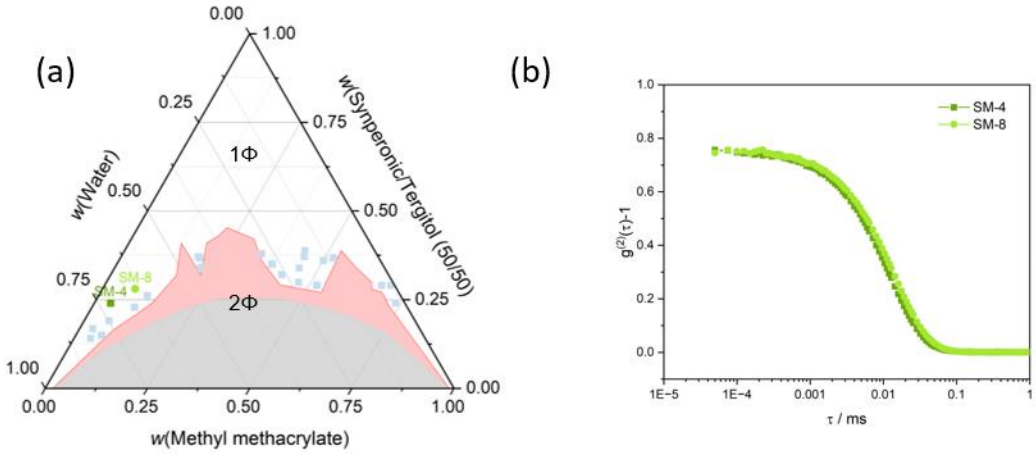

Figure S 4.4 *Investigation of the surfactant-based reference system without cosurfactant containing Water, MMA, Synperionic and Tergitol. (a) ternary phase diagram at 25 °C (grey) and 45 °C (red). Blue points mark compositions that are one-phasic and taken for determination of the phase diagram. (b) Autocorrelation functions derived by DLS at 45 °C.*

4.6.5 Polymers Derived from Ternary SFME Systems

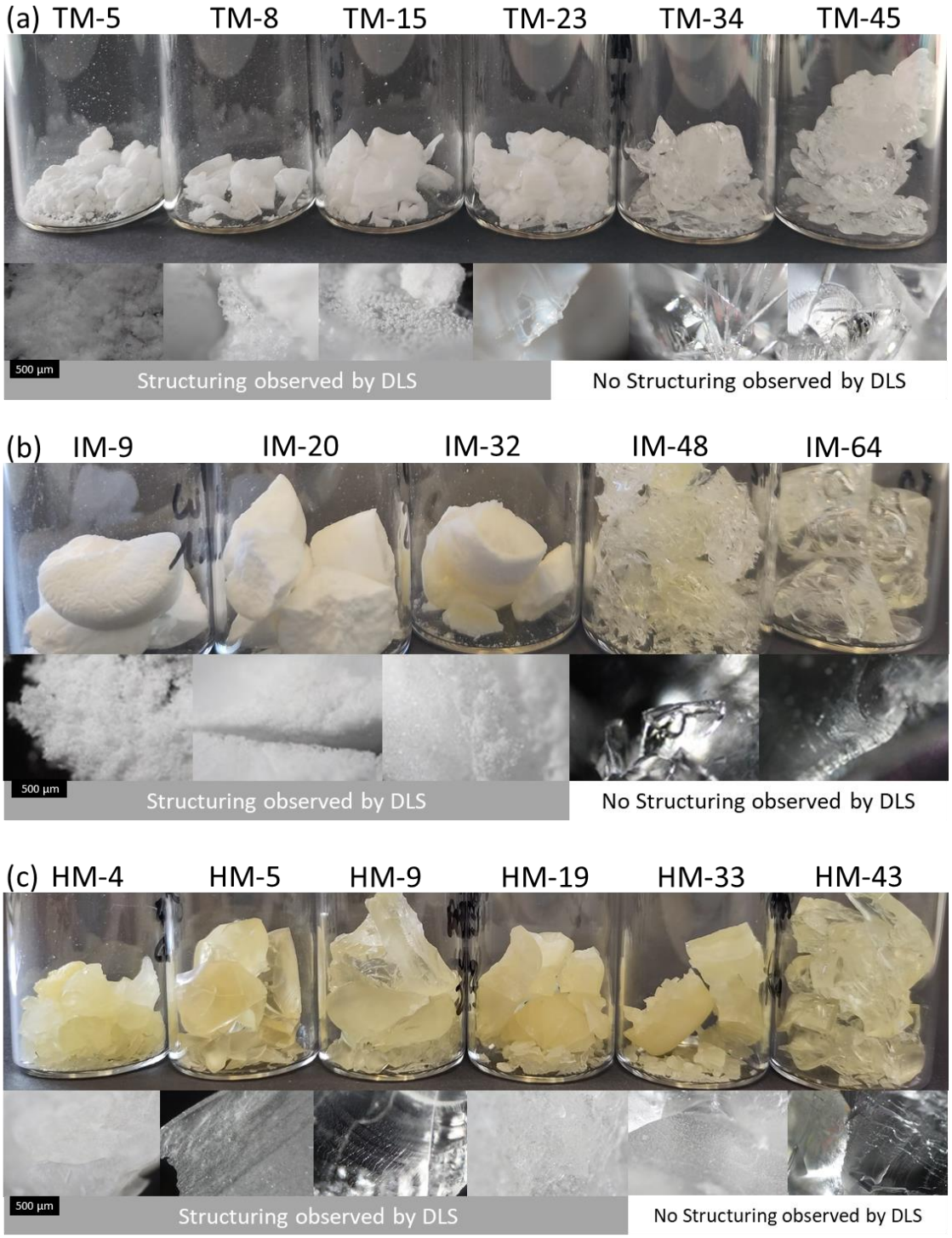

Figure S 4.5 *Macroscopic and microscopic pictures of freeze-dried polymers derived from the systems (a) water/TBA/MMA, (b) water/IPA/MMA, and (c) water/HEMA/MMA*

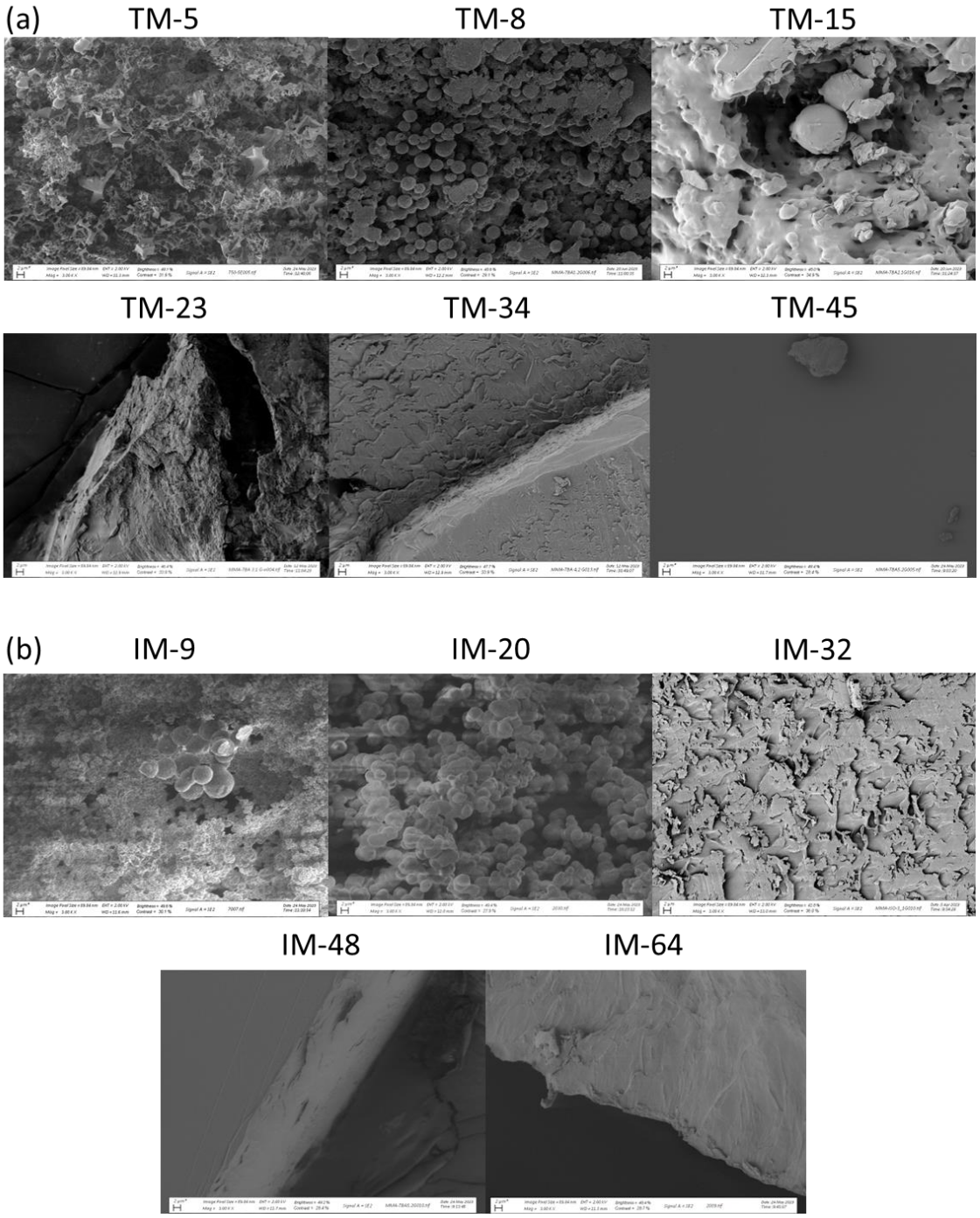

Figure S 4.6 *SEM images of freeze-dried polymers derived from the systems (a) water/TBA/MMA and (b) water/IPA/MMA.*

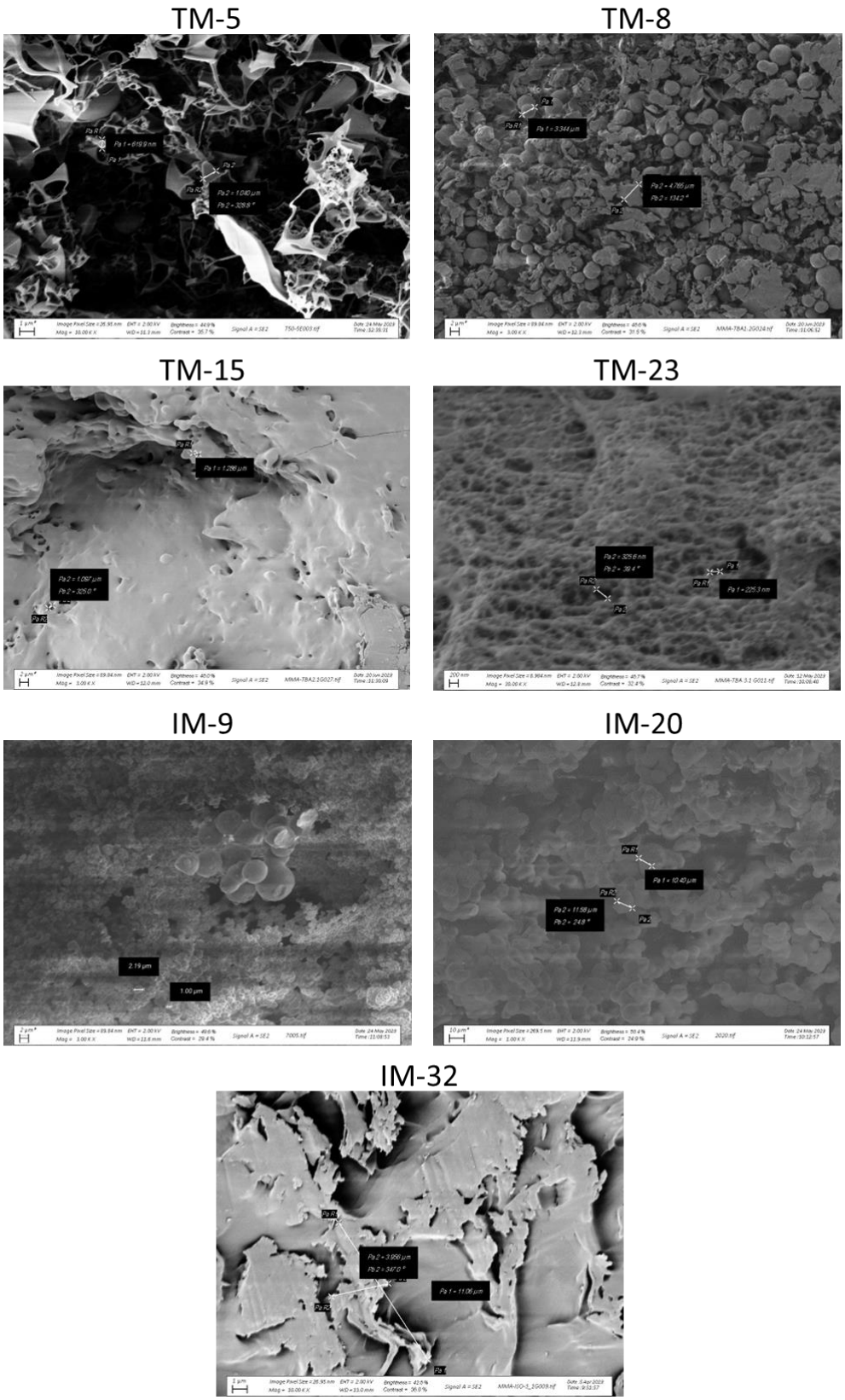

Figure S 4.7 *SEM images of selected, freeze-dried polymers derived from the systems (a) water/TBA/MMA and (b) water/IPA/MMA with manually measured pore/droplet sizes*

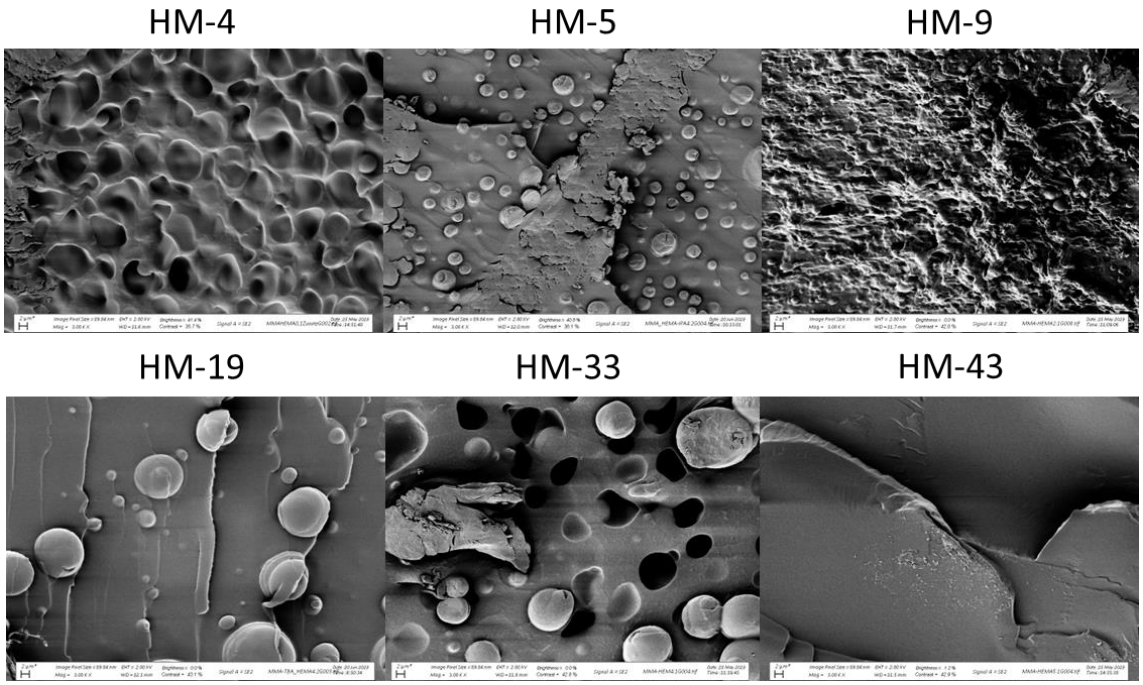

Figure S 4.8 *SEM images of freeze-dried polymers derived from the system water/HEMA/MMA.*

4.6.6 Polymers Derived from Pseudo-ternary SFME Systems

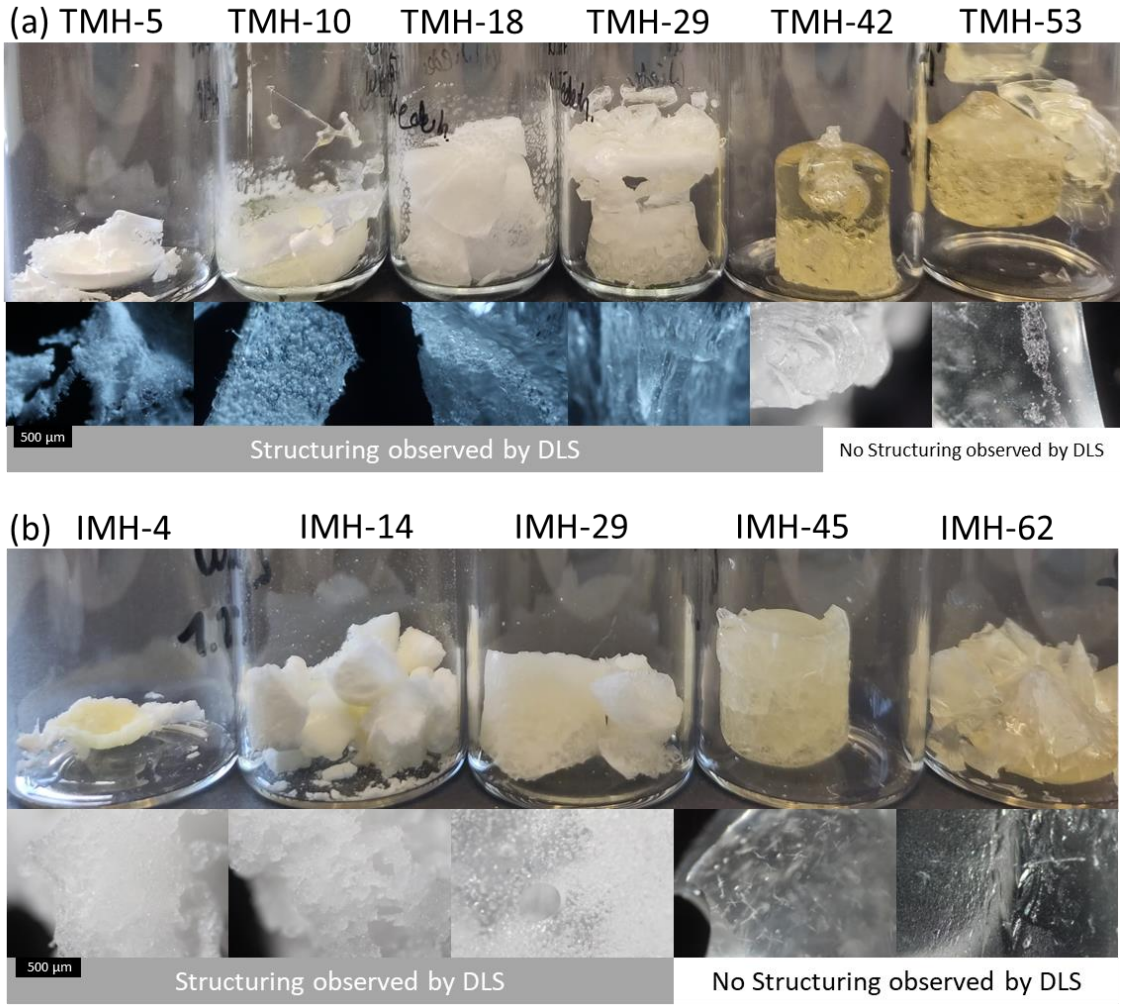

Figure S 4.9 *Macroscopic and microscopic pictures of freeze-dried polymers derived from the pseudo-ternary systems with MMA/HEMA (50:50) as oil phase, water, and (a) TBA and (b) IPA as hydrotropes.*

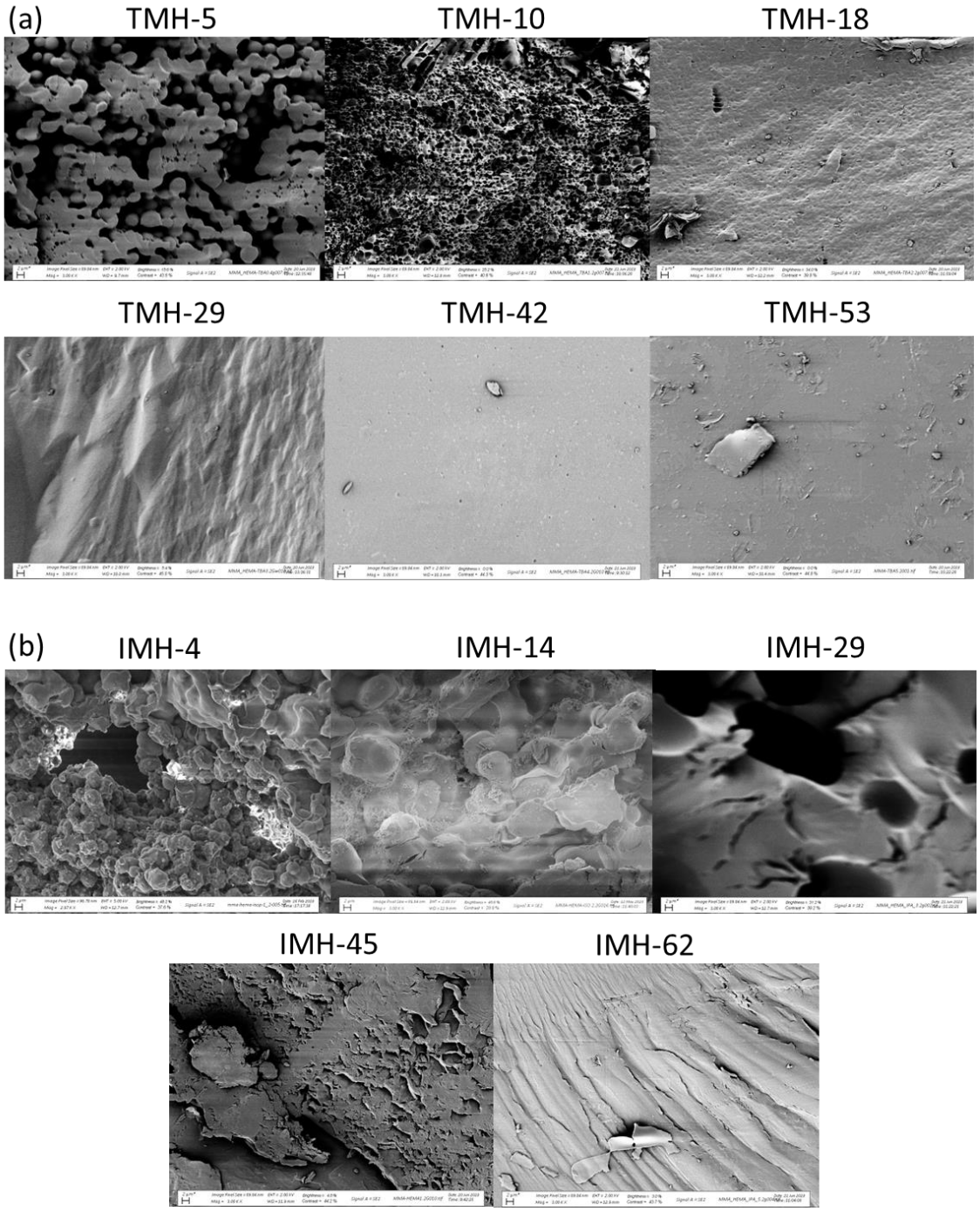

Figure S 4.10 *SEM images of freeze-dried polymers derived from the pseudo-ternary systems with MMA/HEMA (50:50) as oil phase, water, and (a) TBA and (b) IPA as hydrotropes.*

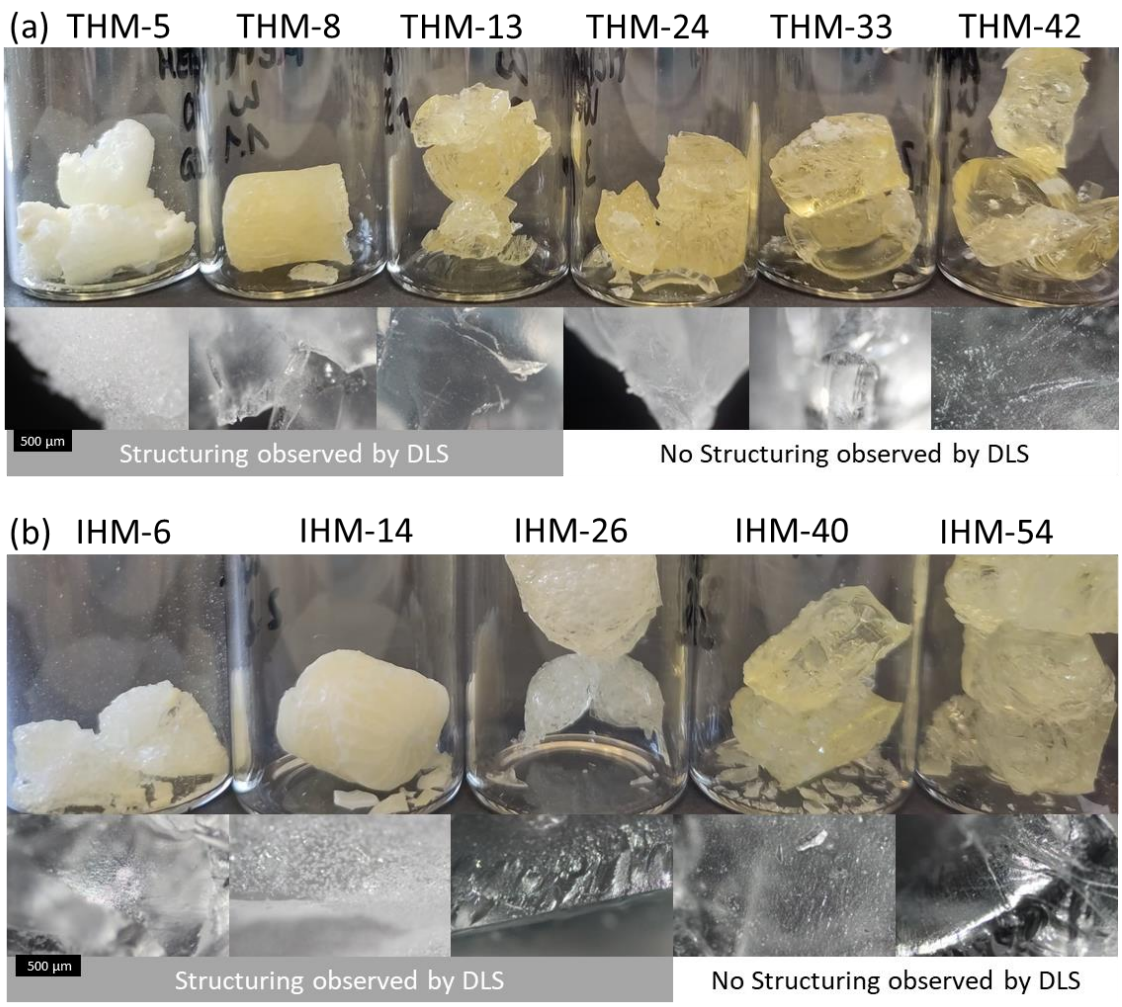

Figure S 4.11 *Macroscopic and microscopic pictures of freeze-dried polymers derived from the pseudo-ternary systems with HEMA/Alcohol (50:50) as hydrotrope phase, water, MMA and (a) TBA and (b) IPA as part of the hydrotrope phase.*

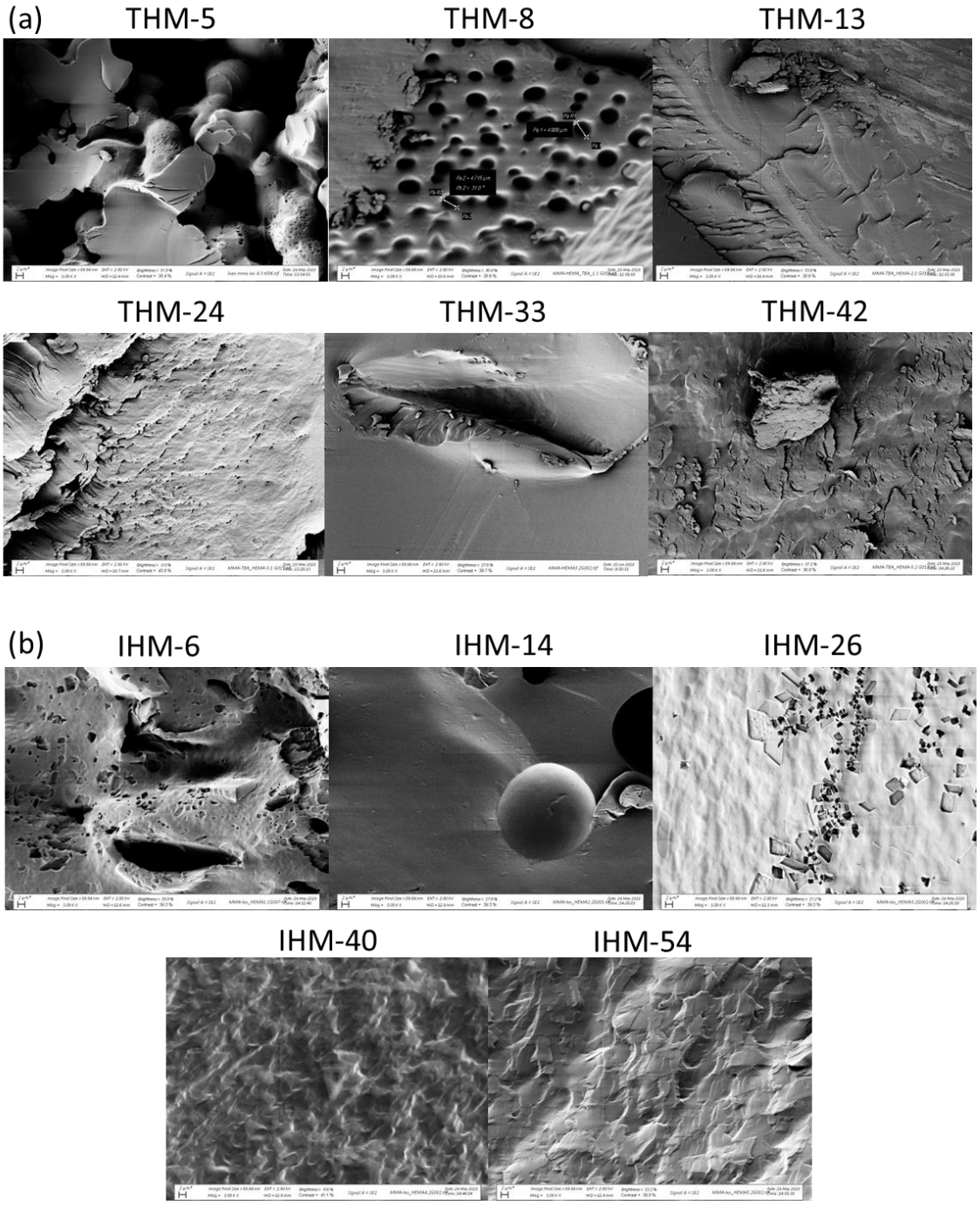

Figure S 4.12 *SEM images of freeze-dried polymers derived from the pseudo-ternary systems with HEMA/Alcohol (50:50) as hydrotrope phase, water, MMA and (a) TBA and (b) IPA as part of the hydrotrope phase.*

4.6.7 Polymers Derived from Surfactant-based Reference Systems

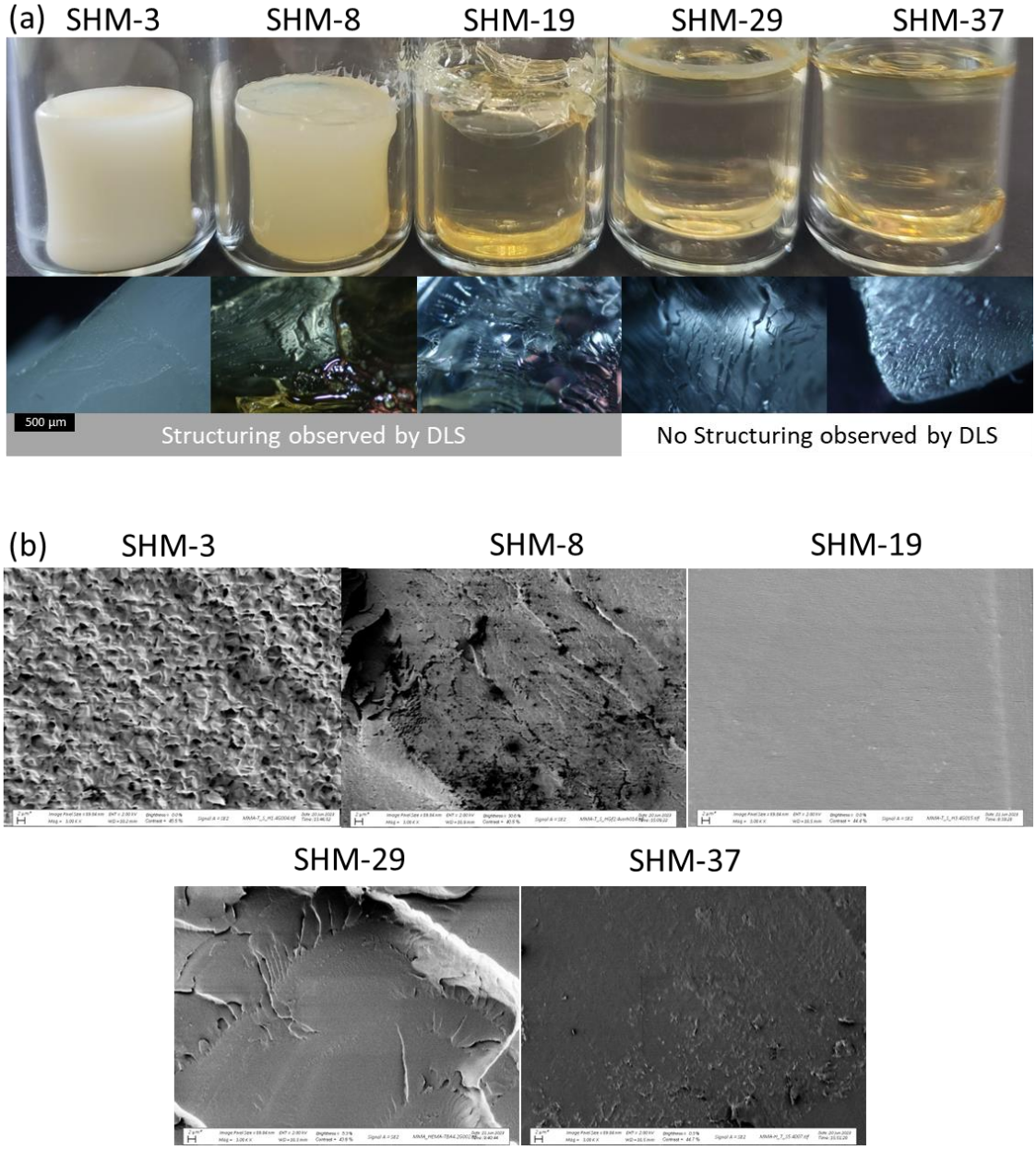

Figure S 4.13 *(a) Macroscopic and microscopic pictures and (b) SEM images of freeze-dried polymers derived from the surfactant-based reference system containing Hydroxyethyl methacrylate, Synperonic A11-LQ-(TH) and Tergitol 15-S-12.*

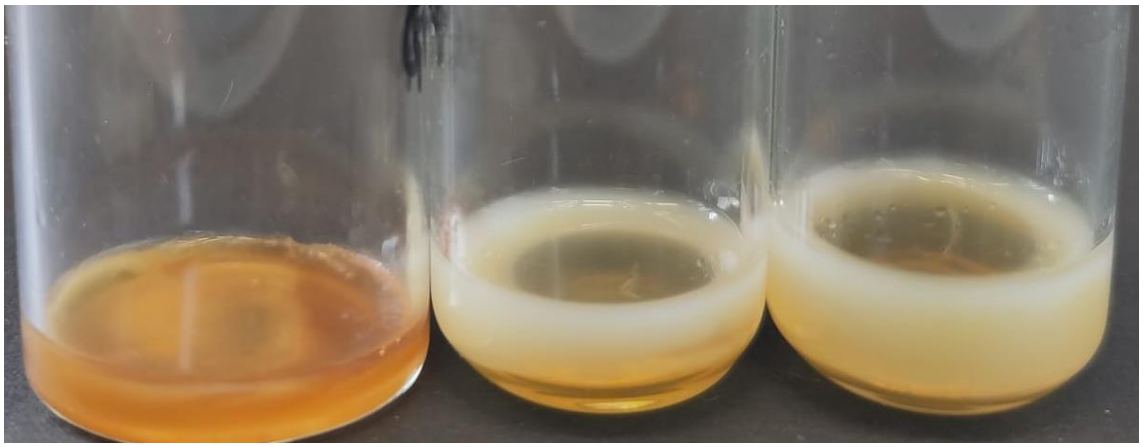

Figure S 4.14 *Macroscopic images of samples derived from the system Water, MMA, Synperonic A11-LQ-(TH) and Tergitol 15-S-12 without HEMA.*

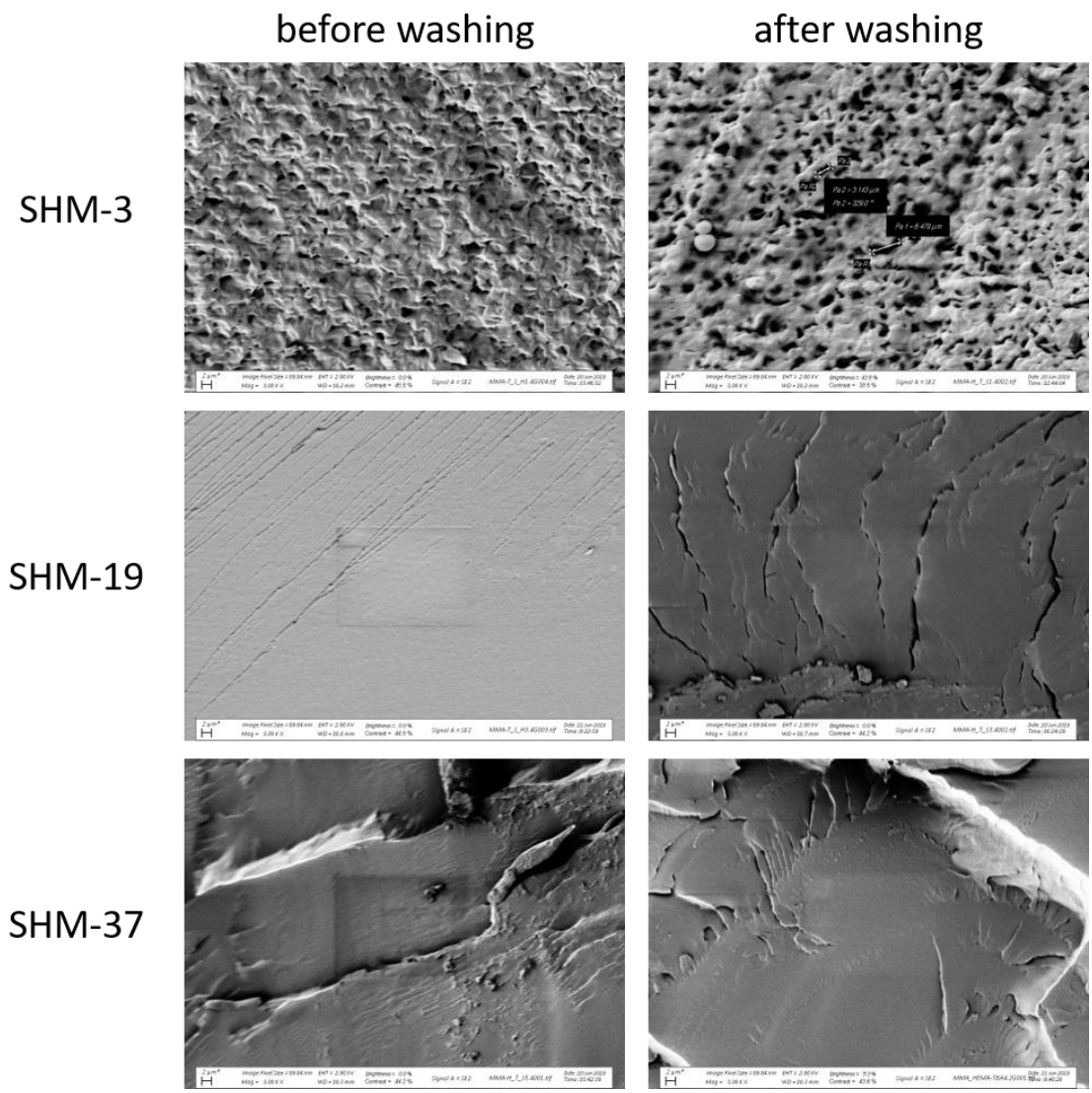

Figure S 4.15 *SEM images of polymers derived from the surfactant-based reference system containing Hydroxyethyl methacrylate, Synperonic A11-LQ-(TH) and Tergitol 15-S-12 before and after washing with water.*

4.7 Bibliography

[1] J. Blahnik, J. Schuster, R. Müller, E. Müller, and W. Kunz, *J. Colloid. Interface Sci.* **2024**, *655,* 371–382.

[2] T. D. Li, L. M. Gan, C. H. Chew, W. K. Teo, and L. H. Gan, *Langmuir* **1996**, *12,* 5863–5868.

[3] T. H. Chieng, L. M. Gan, W. K. Teot, and K. L. Pey, *Polymer* **1996**, *37,* 5917–5925.

[4] C. H. Chew, T. D. Li, L. H. Gan, C. H. Quek, and L. M. Gan, *Langmuir* **1998**, *14,* 6068–6076.

[5] M. Antonietti, R. Basten, and S. Lohmann, *Macremol. Chem. Phys.* **1995**, *196,* 441–466.

[6] F. Yan, and J. Texter, *Soft Matter* **2005**, *2,* 109–118.

[7] H. Hentze, and M. Antonietti, *Curr. Opin. Solid State Mater Sci.* **2001**, *5,* 343–353.

[8] J. H. Burban, M. He, and E. L. Cussler, *AIChE J.* **1995**, *41,* 907–914.

[9] O. Diat, M. L. Klossek, D. Touraud, B. Deme, I. Grillo, W. Kunz, and T. Zemb, *J. Appl. Crystallogr.* **2013**, *46,* 1665–1669.

[10] J. Blahnik, E. Müller, L. Braun, P. Denk, and W. Kunz, *COCIS* **2022**, *57,* 101535.

[11] M. Hahn, S. Krickl, T. Buchecker, G. Jošt, D. Touraud, P. Bauduin, A. Pfitzner, A. Klamt, and W. Kunz, *Phys. Chem. Chem. Phys.* **2019**, *21,* 8054–8066.

[12] S. Prevost, T. Lopian, M. Pleines, O. Diat, and T. Zemb, *J. Appl. Crystallogr.* **2016**, *49,* 2063–2072.

[13] T. N. Zemb, M. Klossek, T. Lopian, J. Marcus, S. Schöettl, D. Horinek, S. F. Prevost, D. Touraud, O. Diat, S. Marčelja, and W. Kunz, *Proc. Natl. Acad. Sci. U. S. A.* **2016**, *113,* 4260–4265.

[14] Y. L. Khmelnitsky, I. N. Zharinova, I. V. Berezin, A. V. Levashov, and K. Martinek, *Ann. N. Y. Acad. Sci.* **1987**, *501,* 161–164.

[15] Y. L. Khmelnitsky, R. Hilhorst, and C. Veeger, *Eur. J. Biochem.* **1988**, *176,* 265–271.

[16] S. Krickl, D. Touraud, P. Bauduin, T. Zinn, and W. Kunz, *J. Colloid. Interface Sci.* **2018**, *516,* 466–475.

[17] H. S. Tarkas, D. M. Marathe, M. S. Mahajan, F. Muntaser, M. B. Patil, S. R. Tak, and J. V. Sali, *Mater. Res. Express* **2017**, *4,* 25018.

[18] X. Cui, J. Wang, X. Zhang, Q. Wang, M. Song, and J. Chai, *Langmuir* **2019**, *35,* 9255–9263.

[19] S. Krickl, L. Jurko, K. Wolos, D. Touraud, and W. Kunz, *J. Mol. Liq.* **2018**, *271,* 112–117.

[20] E. Hofmann, P. Degot, D. Touraud, B. König, and W. Kunz, *Food chemistry* **2023**, *417,* 135944.

[21] J. Blahnik, S. Krickl, K. Schmid, E. Müller, J. Lupton, and W. Kunz, *J. Colloid. Interface Sci.* **2023**, *648,* 755–767.

[22] M. Clausse, L. Nicholas-Morgantini, A. Zradba, and D. Touraud, in: *Surfactant Science Series* (Hrsg.: M. Dekker), New York, **1987,** 15–62.

[23] C. Guzelot. Dissertation, École doctorale Mécanique, énergétique, génie civil et procédés Toulouse, **2022**.

[24] V. Ravi Raj, and B. Vijaya Ramnath, *Silicon* **2021**, *13,* 1925–1932.

[25] U. Ali, K. J. B. A. Karim, and N. A. Buang, *Polymer Reviews* **2015**, *55,* 678–705.

[26] L. M. Gan, T. H. Chieng, C. H. Chew, and S. C. Ng, *Langmuir* **1994**, *10,* 4022–4026.

[27] S. Prévost, S. Krickl, S. Marčelja, W. Kunz, T. Zemb, and I. Grillo, *Langmuir* **2021**, *37,* 3817–3827.

[28] M. Clausse, J. Peyrelasse, J. Heil, C. Boned, and B. Lagourette, *Nature* **1981**, *293,* 636–638.

[29] B. Lagourette, J. Peyrelasse, C. Boned, and M. Clausse, *Nature* **1979**, *281,* 60–62.

[30] T. Buchecker, S. Krickl, R. Winkler, I. Grillo, P. Bauduin, D. Touraud, A. Pfitzner, and W. Kunz, *Phys. Chem. Chem. Phys.* **2017**, *19,* 1806–1816.

[31] F. M. Pavel, *J. Dispers. Sci. Technol.* **2004**, *25,* 1–16.
[32] J. Aubry, F. Ganachaud, J.-P. Cohen Addad, and B. Cabane, *Langmuir* **2009**, *25,* 1970–1979.
[33] F. Ganachaud, and J. L. Katz, *ChemPhysChem* **2005**, *6,* 209–216.
[34] H. Kempe, and M. Kempe, *J. Colloid. Interface Sci.* **2022**, *616,* 560–570.
[35] D. Gulsen, and A. Chauhan, *Int. J. Pharm.* **2005**, *292,* 95–117.
[36] T. H. Chieng, L. Gan, C. Chew, L. Lee, S. Ng, K. Pey, and D. Grant, *Langmuir* **1995**.
[37] O. Thioune, H. Fessi, J. P. Devissaguet, and F. Puisieux, *Int. J. Pharm.* **1997**, *146,* 233–238.
[38] H. Murakami, M. Kobayashi, H. Takeuchi, and Y. Kawashima, *Int. J. Pharm.* **1999**, *187,* 143–152.
[39] S. Yamaguchi, *Colloid. Polym. Sci.* **1996**, *274,* 1152–1160.
[40] X. Yan, P. Alcouffe, G. Sudre, L. David, J. Bernard, and F. Ganachaud, *Chem. Commun. (Camb.)* **2017**, *53,* 1401–1404.
[41] Y. Yao, C. Li, F. Liu, P. Zhao, Z. Gu, and S. Zhang, *Phys. Chem. Chem. Phys.* **2019**, *21,* 10477–10487.

5 The Impact of Additives on Surfactant-free Microemulsions and Polymerizations in Those

5.1 Preface and Abstract

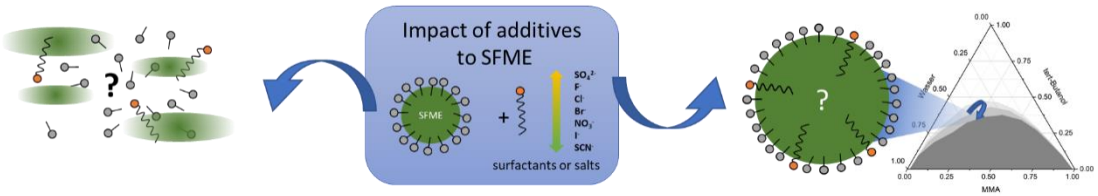

Figure 5.1 *Graphical abstract: Addition of sodium dodecyl sulfate (SDS) to surfactant-free microemulsions (SFMEs): strengthening, changing, or weakening the structure?*

In conventional polymerization processes, a lot of auxiliaries can be present – from surfactants to kinetically stabilize the product, to salts, *e.g.*, as part of common initiator systems for (micro)emulsion polymerization systems, *i.e.,* sulfates and persulfates. [1–3] The latter might influence not only the reaction *per se* but also the surrounding system, which might be taken into account rarely.

There are already some studies about the impact of salts and special electrolytes on surfactant-free microemulsions (SFMEs). [4–7] Of course, a lot of publications on the influence of cosurfactants on classical microemulsions are known. [8; 9] However, classical microemulsions were mainly studied in times when most colloid chemists would never have considered that mesostructuring could also exist in surfactant-free systems. [10] This assumption has already

been brought in chapter 4, based on the results comparing polymers derived from surfactant-free and surfactant-based systems.

The present chapter aims to understand the impact of surfactants and electrolytes in SFMEs. Instead of adding cosurfactants to conventional microemulsions, we approached this topic from the other side: Adding surfactants to surfactant-free microemulsions and investigating the change in their phase behavior.

Beginning with the well-investigated SFME system octanol, ethanol (EtOH), and water, [11; 7; 12; 13] nonionic and anionic surfactants are added, and their impact on the phase behavior is investigated. In the next step, other oils and hydrotropes are taken into account to generalize the concept before moving to our well-known polymerizable systems with methyl methacrylate (MMA). The impact of sodium dodecyl sulfate (SDS) and salts of the Hofmeister series on polymers derived from microsuspension polymerization is investigated in a final step.

Parts of this work are planned for future publication. Some more selected experiments including the phase behavior with other surfactants, supplemented by further scattering data, might help to fully understand this topic.

Contributions to the experimental work:

- Jonas Blahnik: Conceptionalization, experimental work, data evaluation
- Selina Reigl and Diana Funkner: Experimental work (pre-experiments with SDS)
- Sebastian Hof and Antonia Schmalhofer: Experimental work (polymerizations with SDS)
- Andreas Kanygin and Sebastian Hof: Experimental work (polymerizations with salts)
- Philipp Schmid: SWAXS experiments and data processing

5.2 Introduction

The impact of additives is always an interesting question in colloidal chemistry. Investigating the role of salts on macromolecules and living systems started back in the 19th century already. [14] A pioneer in the work of specific ion or salt effects is Franz Hofmeister, whose publications from the 1880s are still famous today. [15] Hofmeister is especially known for his research on the impact of different salts on the salting-in and salting-out of proteins, leading to the famous Hofmeister series for cations and anions (see **Figure 5.2**). [16]

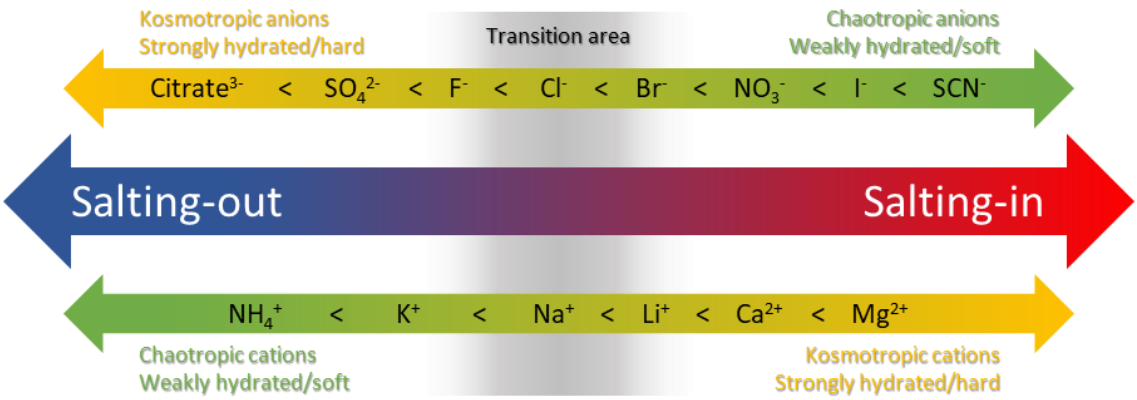

Figure 5.2 *Hofmeister series for anions and cations depicting their salting-in and salting-out effect for proteins according to their positions. Additionally, anions and cations are labeled according to their kosmotropic or chaotropic character. This figure is inspired by the work of Johannes Mehringer. [17]*

It seems counterintuitive that the tendency of cations and anions is different. While in the case of anions, the trend goes from hard, strongly hydrated ions (salting-out) to weakly hydrated, soft anions (salting-in), it is just the other way around for cations. In this context, it is necessary to note that Hofmeister investigated the impact of salts on proteins, which carry charges on their surface, influencing the effects. [16; 17] The terms chaotropic and kosmotropic, which were used for decades, are possibly misleading in their original meaning (structure-making and structure-breaking) due to the short range of the interactions of ions in water. [16] However, we will keep the terms for convenience, meaning the trends weakly hydrated/soft/low charge density versus strongly hydrated/hard/high charge density.

An important concept to understand the effect of salts is Collins' "concept of matching water affinities," meaning that two hard or two soft ions can build inner sphere ion pairs in an aqueous solution, while a combination of a hard and a soft ion is disadvantageous for building those. [18] This rule is very intuitive and can be compared to the rule "like seeks like" that every undergraduate student learns, *e.g.*, in the HSAB concept for acids and bases, dating back in the 1960s. [19; 20]

It was a question of many publications which kinds of interactions play essential roles for specific ion effects, *e.g.*, dispersion, hydration, polarizability, or charge density. [16] This might not be clarified generally, as the system itself plays a decisive role. In this context, especially the head groups of ionic substances and interfaces in the system need to be mentioned. [14; 17]

The roles of head groups of charged surfactants and their counterions were intensively investigated in the last decades. [21] The role of headgroups of charged hydrotropes was studied by Mehringer *et al*., adding the length of the hydrophobic side chain as a second axis to the head group series, resulting in a two-dimensional concept. [22]

There are already the first publications on the impact of salts and special electrolytes on surfactant-free microemulsions (SFMEs). [7] Many electrolytes, including the surfactant sodium dodecyl sulfate (SDS), were studied on their concentration-dependent influence on a single SFME composition by scattering experiments. However, the phase behavior was not studied yet. It is found that the weak aggregation of pre-Ouzo aggregates is very sensitive to the addition of electrolytes, and the pre-Ouzo domains increase as soon as ethanol is salted out of the water-rich pseudo phase. [4; 5] The impact of SDS as a true surfactant is less clear.

The impact of electrolytes and surfactants on SFME systems is of interest from different points of view:

- As different electrolytes may be present in a polymerization process (*e.g.*, as part of the initiator system for microemulsion processes, but also in the form of charged surfactants), it is important to know the role of salts on the SFME system and the polymerization kinetics in SFME systems.
- While the impact of SDS on SFMEs is not completely understood so far, [7] that of uncharged surfactants was not systematically investigated yet, to our knowledge. However, previous results of this work (cf. discussion of chapter 4) indicate that nonionic surfactants have a significantly low impact on SFMEs, in contrast to charged ones.
- Cosurfactants in conventional microemulsions may also be used as hydrotropes or even the oil phase in SFMEs. The impact of cosurfactants and high solvent concentrations on microemulsions was mainly investigated in times when hardly any colloid chemist was thinking about mesostructuring in surfactant-free systems. [8; 10; 9] Approaching this topic from the other side – adding surfactant instead of adding cosurfactants or solvents – might help to understand mechanisms in “conventional” microemulsions with

cosurfactants or high solvent ratios in more detail. This work might lead to a novel approach of formulating thermodynamically stable microemulsions with low surfactant concentrations.

In this contribution, we investigate the impact of adding the surfactant SDS to ternary systems consisting of water, various hydrophobic compounds (namely 1-octanol, ethyl acetate, limonene, citronellol, triacetin, and methyl methacrylate (MMA)), and simple alcohols such as ethanol (EtOH), *iso*-propanol (IPA), *n*-propanol (NPA) and *tert*-butyl alcohol (TBA) as hydrotropes. The surfactants sodium lauryl ether sulfonate (SLES) and polyethylene glycol-10 dodecyl ether (C12E10) are investigated as references. In contrast to previous works, we investigate the effect not only on specific composition but on the phase behavior in general. The impact on the phase behavior is studied by recording (pseudo-)ternary phase diagrams and the effect on mesostructures is investigated by dynamic light scattering (DLS) and small-angle X-ray scattering (SWAXS). Thermally activated, free-radical polymerizations initiated by BCC of MMA are performed in systems with the addition of different salts and surfactants. Freeze-dried polymers are evaluated according to their conversion and their weight average molar mass.

5.3 Materials and Methods

5.3.1 Materials

Methyl methacrylate (MMA, 99% purity, stabilized with 4-methoxyphenol ≤ 30 ppm), ethanol (EtOH, 99.8%), *n*-propanol (NPA, 99.5%), polyoxyl-10 lauryl ether (C12E10, technical grade), (R)-(+)-limonene (94%), citronellol (95%), *n*-octanol (99%), triacetin (99%), sodium bromide (99%), sodium chloride (99.5%), sodium sulfate (99%), ammonium chloride (99%), potassium chloride (99%), sodium fluoride (99.5%), sodium iodide (99.5%), and sodium ethyl sulfate (98%) are obtained from Merck (Darmstadt, Germany). *tert*-Butyl alcohol (TBA, 99%), calcium chloride dihydrate (99%), and magnesium chloride (98.5%) are purchased from Carl Roth (Karlsruhe, Germany). Tetrahydrofuran (THF, analytical reagent grade), ethyl acetate (99.8%), sodium *n*-pentyl sulfate (99%), sodium *n*-octyl sulfate (99%), sodium thiocyanate (98%), and *iso*-propanol (IPA, 99.8%) are bought from Fisher Scientific (Schwerte, Germany). Poly(methyl methacrylate) standards (ReadyCal-Kit PSS-mmkitr1) are obtained from PSS Polymer Standards Service (Mainz, Germany). *Bis*-(4-*tert*-butylcyclohexyl) peroxy dicarbonate (BCC, 95%) is provided by PERGAN (Bocholt, Germany). Sodium *n*-dodecyl sulfate (SDS, 99.8%) is purchased from AppliChem (Darmstadt, Germany). Sodium laureth sulfate (SLES, technical grade, trade name Marlinat 242/70) is provided by Sasol (Hamburg, Germany).

Prior to polymerization, MMA is distilled at 40 °C and 60 mbars to remove the stabilizer. Aqueous solutions are prepared using deionized water with a resistivity of 18 MΩcm. All other chemicals are used without further purification.

5.3.2 Ternary Phase Diagrams

Phase diagrams are recorded at 25 °C ± 1 °C (for all oils but MMA) and 45 °C ± 1 °C (in the case of MMA) as described by Clausse *et al.*, [23] compare section 2.3.2. For pseudo-ternary phase diagrams, the additive (surfactant or electrolyte) is used with a fixed weight ratio as part of the hydrotrope. Surfactants are used in weight fractions (corresponding to the hydrotrope) only, while all electrolytes are tested with a concentration of 13 mM, corresponding to 5 wt% SDS.

5.3.3 Dynamic Light Scattering (DLS)

DLS experiments are performed as described in section 2.3.5.

5.3.4 Critical Point Determination

Critical points (CPs) are determined as described in section 2.3.3.

5.3.5 Small-and-wide-angle X-ray Scattering (SWAXS)

Small-and-wide-angle X-ray scattering (SWAXS) measurements are performed on a bench-built XENOCS (Grenoble, France) using a Mo radiation X-ray source (λ = 0.0071 nm). A large online scanner detector (345 mm diameter) is used to record the scattered beam, covering a large *q*-range (0.2 – 40 nm^{-1}) with an off-center detection. The collimation is applied using a 12:∞ multilayer Xenocs mirror (for Mo radiation), connected to two sets of scatter-less FORVIS slits providing a 0.8 × 0.8 nm X-ray beam at the sample position. Pre-analysis of the data is performed with a FIT2D software. Scattered intensities are detected versus the magnitude of the scattering vector $q = \left[(4\pi)/\lambda \sin\left(\frac{\vartheta}{2}\right)\right]$ with a wavelength of the incident radiation λ and the scattering angle ϑ. The solutions are filled in 2 mm quartz capillaries. Usual corrections for background (empty cell and detector noise) subtractions and intensity normalization using high-density polyethylene film as a standard are applied. The experimental resolution is $\Delta q/q$ = 0.05. The scattering vector calibration standard is silver behenate in a sealed capillary. All measurements are carried out at room temperature. [14; 24]

5.3.6 Polymerizations and Yield Determination

Polymerizations are performed at 45 °C ± 1 °C using 0.2 mol% BCC as the initiator (referring to the monomer) for 7h and freeze-dried afterward as described in section 2.3.9. The mass of the additives is subtracted in the conversion determination.

5.3.7 Gel Permeation Chromatography (GPC)

Gel permeation chromatography is performed as described in section 2.3.10.

5.4 Results and Discussion

5.4.1 Impact of SDS on SFMEs

5.4.1.1 Impact of SDS on the System Octanol-Ethanol-Water

The ternary (or pseudo-ternary) phase diagram of the system water/EtOH (+SDS)/1-Octanol is depicted in **Figure 5.3 a**. The addition of small amounts of SDS in a fixed ratio in relation to EtOH leads to a continuous decrease of the liquid-liquid two-phase region with an increasing SDS amount. Simultaneously, the shape of the binodal changes and gets more symmetric as the maximum is slightly shifted to the octanol-rich corner. The liquid-solid two-phase region (leading back to the low solubility of SDS in EtOH) is increasing. This liquid-solid two-phase region is almost linear and continuously increasing with increasing SDS content. However, as this region is not of our main interest, the border to the two-phase liquid-liquid region is meant when only phase-border or two-phase region is written.

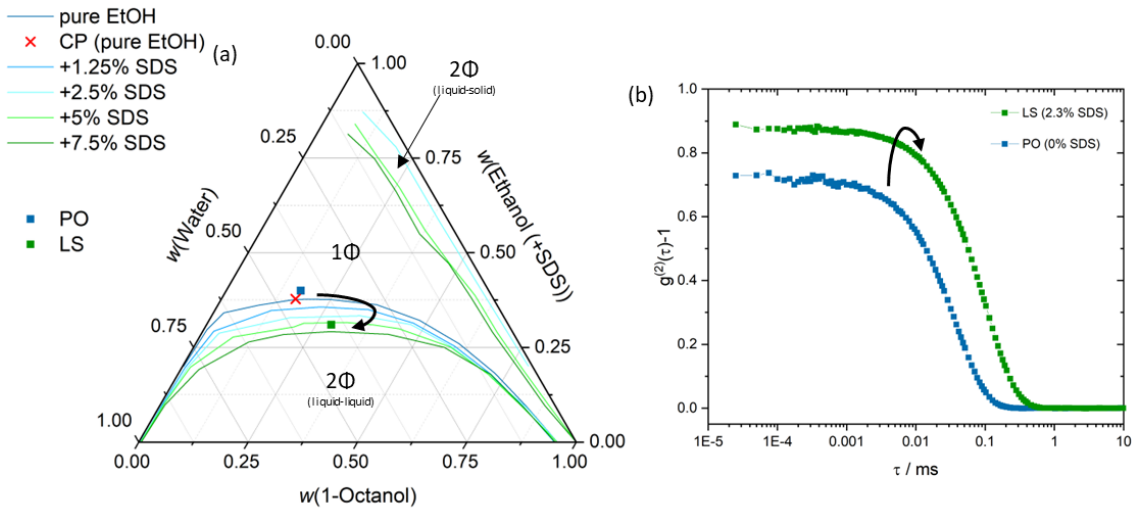

Figure 5.3 *(a) Impact of different SDS to ethanol ratios on (pseudo-)ternary phase diagrams of the system water, 1-octanol, ethanol (+SDS) and (b) autocorrelation functions of compositions in the region of maximal structuring in the surfactant-free system (blue) and the pseudo-ternary system with 7.5% SDS in EtOH (2.3% SDS in the overall composition, green).*

Figure 5.3 b depicts the autocorrelation functions of two points in similar distances to the phase border, one in the pre-Ouzo region of the surfactant-free microemulsion (called PO) and one in the corresponding area in the pseudo-ternary system with 7.5 wt% SDS in EtOH (which corresponds to a quite low surfactant concentration exactly 2.325 wt% SDS in this composition, called LS). The autocorrelation function of LS comprises a higher y-intercept and a higher lag time τ than the autocorrelation function of PO. Both compositions are in the region around the phase border, where the most pronounced autocorrelation function can be found, as **Figure 5.4** shows.

This point of the most pronounced autocorrelation functions is shifted towards higher octanol-ratios with increasing SDS content, comparable to the shift of the appearances of the two-phase region itself. However, also all other compositions in the "former" biphasic region (LS and S1-S4, cf. **Figure 5.4 a**) show at least as pronounced autocorrelation functions as PO, the sample of the highest structuring in the pre-Ouzo system (cf. **Figure 5.4 b** and **c**). Thus, the impact of surfactant is present in the whole former biphasic system, not only in the immediate vicinity of the pseudo-critical point.

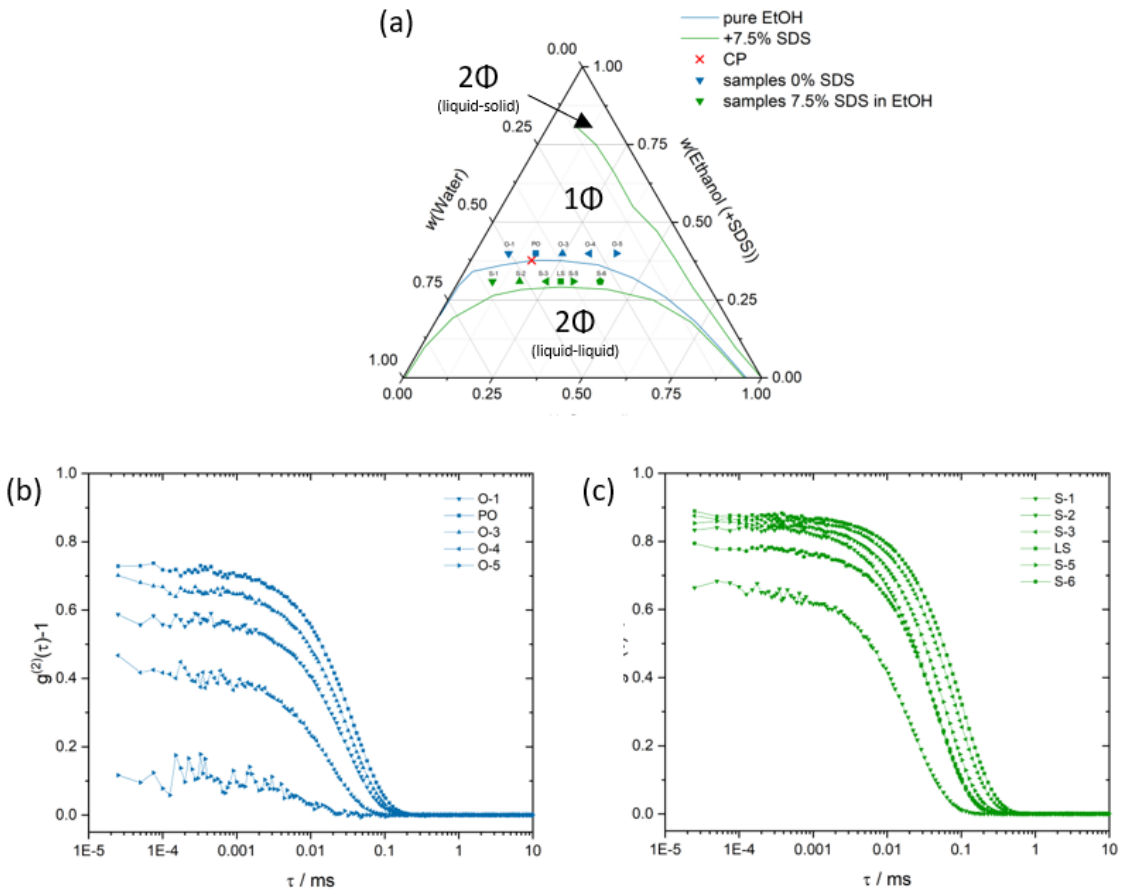

Figure 5.4 *(a) (Pseudo-)Ternary phase diagrams of the system water, 1-octanol, EtOH (+7.5 wt% SDS) and samples investigated by DLS (b) autocorrelation functions of compositions in the surfactant-free system (blue) and (c) the pseudo-ternary system with 7.5% SDS in EtOH (2.3% SDS in the composition, green).*

When SDS is added to PO, a steady decrease in the correlation functions is found (see **Figure 5.5 a**), as already published by Marcus *et al.* [7] The same can be observed for LS (see **Figure 5.5 c**), where SDS is added on top of the amount of approximately 2.3%, which are already present in the composition LS. Even though the absolute autocorrelation functions are higher, the same effect is present.

The absolute intensity of SWAXS (see **Figure 5.5 b** and **d**) at low *q*-values decreases with increasing SDS content. There is no real maximum at the compositions PO and LS but a continuous increase in intensity at $q \rightarrow 0$. When adding SDS to both mixtures, a maximum emerges and shifts towards higher *q*-values associated with repulsive aggregates, as already published by Marcus *et al.* [7] In the system LS, basically the same trend as in the system PO is observed. However, the absolute intensities are higher in the system LS, having overall higher slopes and shifting the maximum to even higher *q*-values.

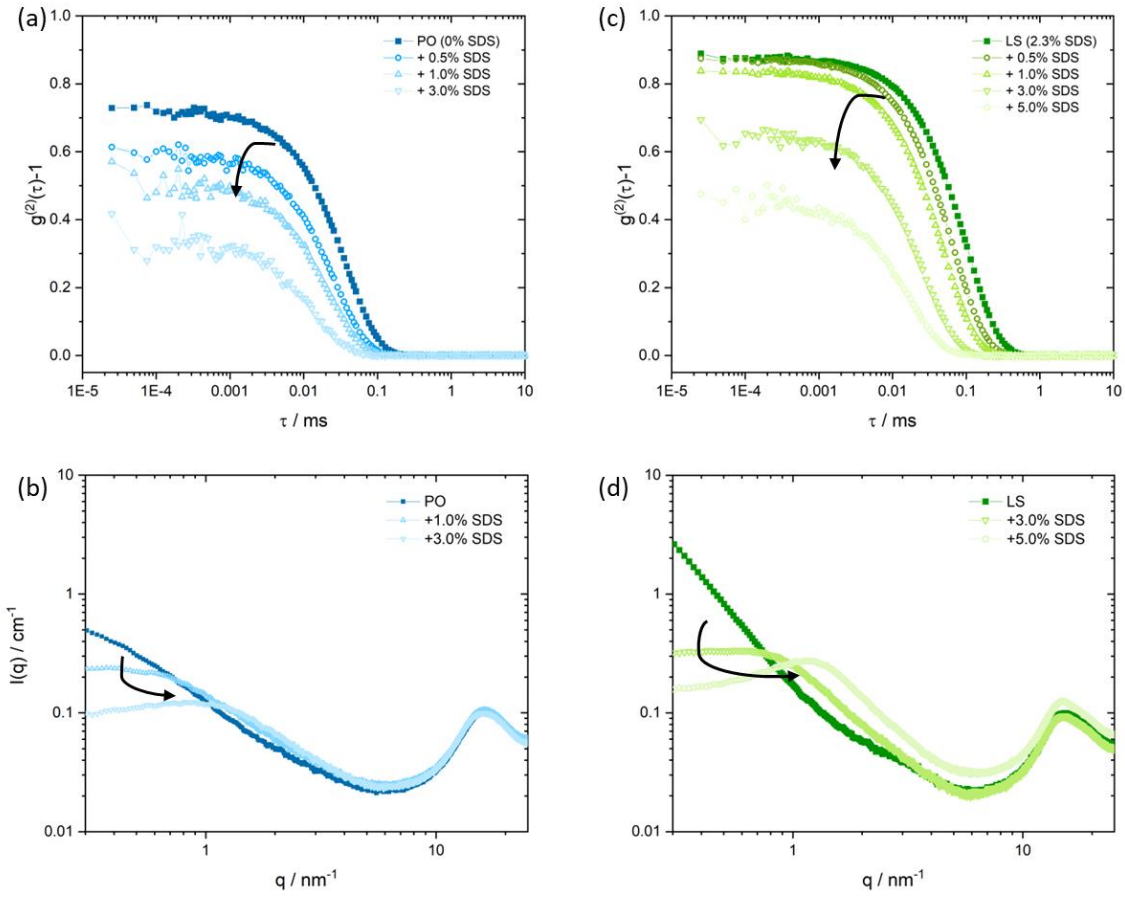

Figure 5.5 *(a) Autocorrelation functions derived by DLS and (b) SWAXS spectra of different additions of SDS to the composition PO in the pre-Ouzo region. (c) Autocorrelation functions and (d) SWAXS spectra of different additions of SDS to the composition LS in the pseudo-ternary 7.5% SDS/EtOH in the region, which is biphasic in the SDS-free system.*

A distance between aggregates can be estimated roughly by the location of the maximum intensity without determining structure or form factors. The distances range from 5 nm (LS+5% SDS) via 7 nm (PO+3% SDS), 10 nm (LS+3% SDS) to 16 nm (PO+1% SDS). It was calculated approximately that there should be between 30 (LS+5% SDS), 55 (PO+3% SDS), 165 (LS+3% SDS) and 420 (PO+1% SDS) SDS molecules per aggregate. [25] Pure SDS micelles are given with a *q*-vector of 1.55 nm^{-1} at similar concentrations in the literature (corresponding to a distance of 4.1 nm and

53-73 SDS molecules per micelle). [26; 27] These estimations suggest that mixed aggregates are formed instead of conventional SDS micelles.

5.4.1.2 Other Oils and Other Hydrotropes

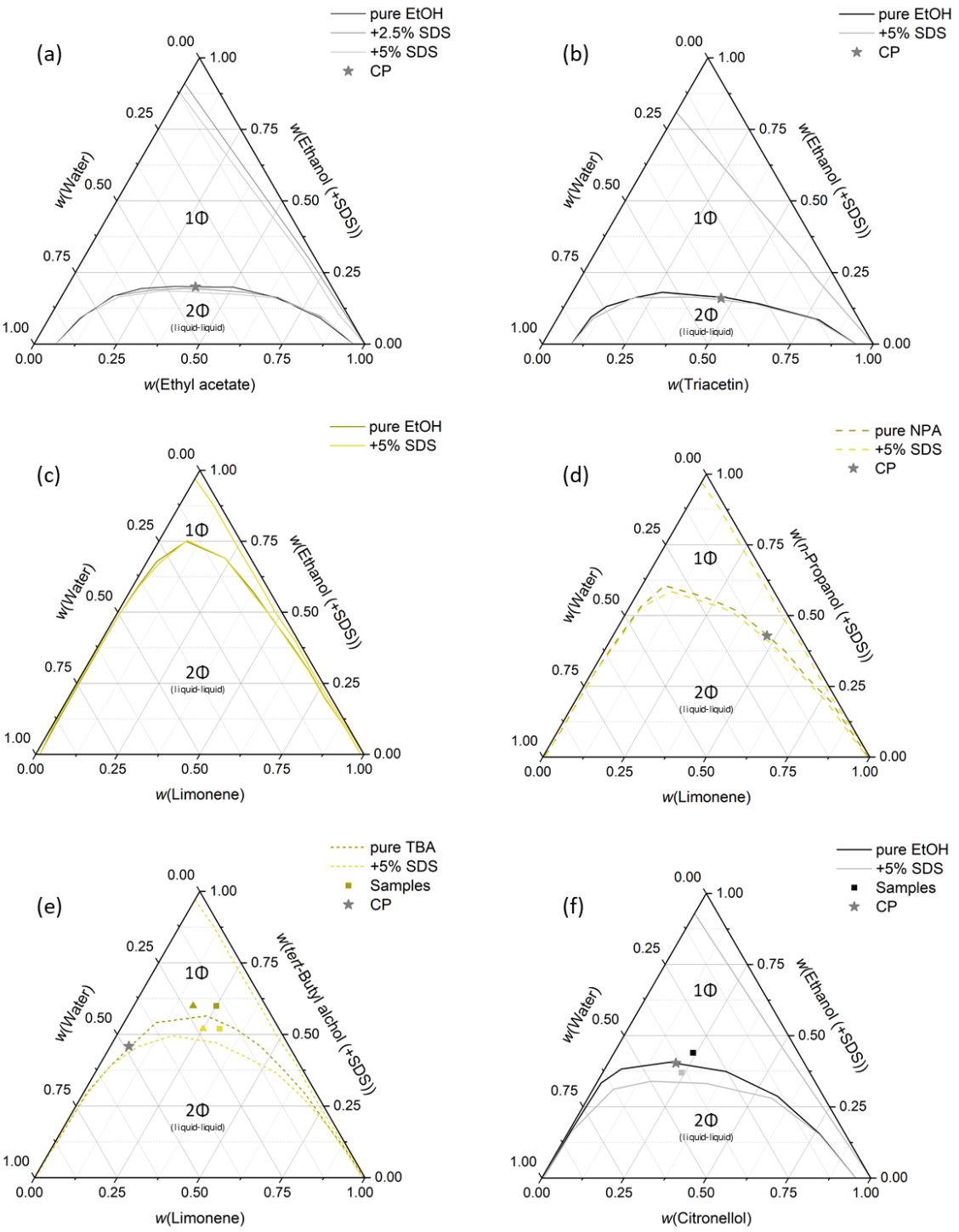

Figure 5.6 *(Pseudo-)Ternary phase diagrams of the systems water, (a) EtOH (+SDS) and ethyl acetate, (b) EtOH (+SDS) and triacetin, (c) EtOH (+SDS) and limonene, (d) NPA (+SDS) and limonene, (e) TBA (+SDS) and limonene, and (f) EtOH (+SDS) and citronellol at 25 °C.*

Further hydrotropes and hydrophobic compounds are tested. There is only little effect of SDS in the case of ethyl acetate and triacetin, which both have a quite low miscibility gap (see **Figure 5.6 a** and **b**). The system with limonene is interesting, as the behavior of the system is different with different alcohols (see **Figure 5.6 c-e**). Limonene-EtOH has a very high miscibility gap, and the addition of 5 wt% SDS (as a part of the EtOH phase) does not show any impact on the phase border at all. When adding SDS to limonene-NPA, which still has a quite large two-phase region, the two-phase region is decreased slightly, while the shape does not significantly change. When moving from NPA to TBA in the ternary systems, the maximum of the binodal is shifted to the limonene-rich side, while the CP is much more to the water-rich side. The addition of SDS leads to a significant decrease in the two-phase region, comparably to the octanol-EtOH system. The decrease due to SDS is stronger on the oil-rich side in this case. Also, in the system citronellol-EtOH (see **Figure 5.6 f**), a decrease due to SDS can be observed. The system behaves similarly to the octanol-EtOH system, with the maximum of the binodal being shifted to the oil-rich side, which is thus getting more symmetrical. The decrease is, in contrast to the limonene-TBA system, not different between the oil- and the water-rich side.

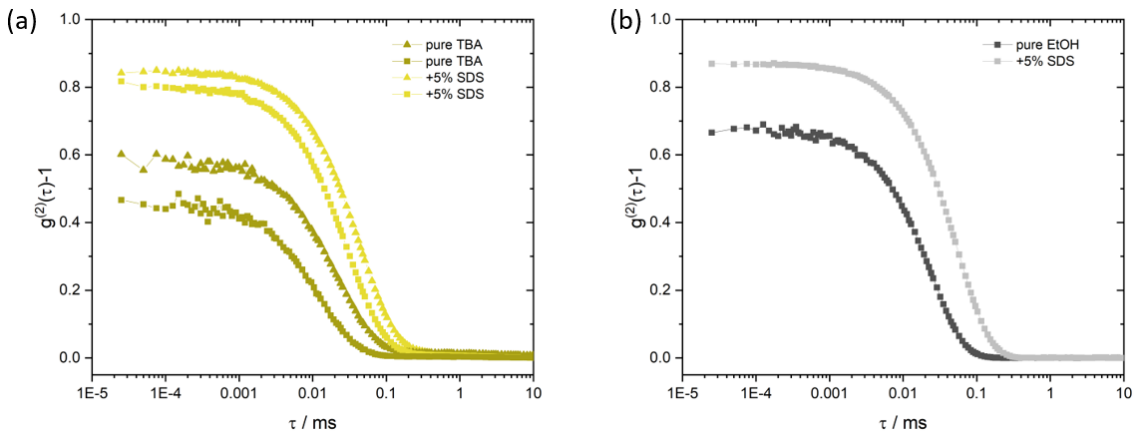

Figure 5.7 *DLS autocorrelation functions of samples of the systems (a) water, limonene, TBA (+SDS) and (b) water, citronellol, EtOH (+SDS). Samples with SDS are in the previous Ouzo region without additional SDS. Corresponding phase diagrams are depicted in* ***Figure 5.6****.*

Light scattering experiments are recorded in the systems limonene-TBA and citronellol-EtOH, which both show a reduced biphasic region due to SDS. Compositions are printed in the phase diagrams in **Figure 5.6 e** and **f**. Autocorrelation functions derived by DLS (see **Figure 5.7**) show basically the same trend as for the octanol-EtOH system. When moving from the surfactant-free pre-Ouzo region (marked as pure TBA or pure EtOH) to the novel one-phase system with SDS, a significant increase in the y-axis intercept as well as in the lag time can be observed.

5.4.1.3 Other Surfactants

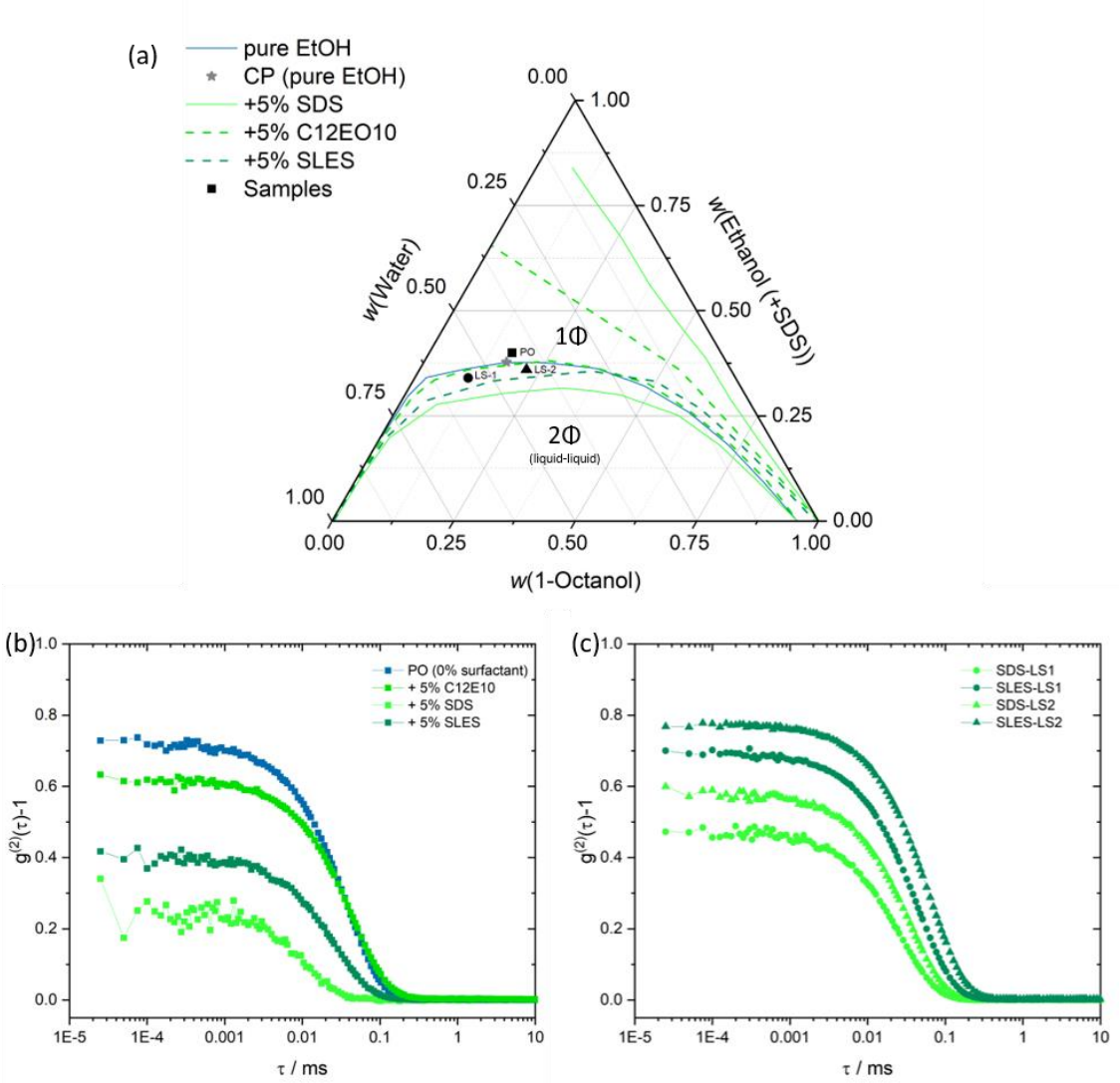

Figure 5.8 *(a) Ternary phase diagram of the system water, EtOH, octanol, and pseudo-ternary diagrams when adding 5 wt% SDS, SLES, and C12E10 to EtOH. (b) Autocorrelation functions when adding an absolute amount of 5 wt% SDS, SLES, and C12E10 to the composition PO in the pre-Ouzo region and (c) Autocorrelation functions of the pseudo-ternary systems with 5 wt% SDS and SLES in EtOH in the former two-phase region.*

The impact of the common ionic surfactant sodium lauryl ether sulfate (SLES, mixture of C12 and C14) and the nonionic surfactant polyethylene-10 laurate (C12E10) is depicted in **Figure 5.8**. The uncharged surfactant C12E10 does not significantly impact the phase behavior. The autocorrelation function when adding a total amount of 5 wt% surfactants to EtOH in the composition PO shows a slightly lower y-axis intercept and a slightly higher lag time compared to PO without additives. SLES, in contrast, acts as a mild variant of SDS. A difference to SDS is that the decrease of the binodal is more pronounced on the water-rich side, while on the oil-rich side, even a slight extension of the former two-phase region is deserved. The overall decrease in the liquid-liquid binodal is less pronounced. The liquid-solid two-phase region is much more pronounced

compared to SDS. In the former two-phase region (compositions LS-1 and LS-2, see **Figure 5.8 a** and **c**), the autocorrelation functions are, in all cases, more pronounced compared to the absolute addition to the composition PO (see **Figure 5.8 b**). However, in contrast to the results seen before, the increase in the DLS signal is lower.

5.4.2 Discussion – Impact of Surfactants on SFME

From scattering experiments on the system octanol/ethanol/water with the addition of different salts and also SDS, Marcus *et al.* [7] concluded that true surfactant micelles appear progressively within the addition of SDS to the composition of octanol/ethanol/water investigated in their research. The authors were, however, not sure what happens at low concentrations of SDS. It is possible that the addition of SDS destroys the surfactant-free clusters first before a micellar system is formed or that there is a transition in between. [7] Marcus *et al.* also concluded that pre-Ouzo aggregates are of overall weak aggregation and, thus, very sensitive to the addition of electrolytes. [7] The study investigated a lot of salts but at rather high salt concentrations. Furthermore, the phase behavior was not investigated at that time.

As shown in this work, the addition of even small amounts of SDS leads to a significant decrease in the biphasic region of the system octanol/ethanol/water (cf. **Figure 5.3** and **Figure 5.4**). The impact of SDS is surprisingly high for those relatively small concentrations (7.5 wt% in EtOH corresponds to an absolute concentration of 2.33 wt% or 80 mmol kg^{-1} of the absolute formulation of the sample LS without additional SDS). The decrease in autocorrelation function by DLS and the decrease in absolute intensity in SWAXS spectra, as well as the emerging maximum at higher q-values upon adding SDS for the composition in the pre-Ouzo region (PO) were already reported by Marcus *et al.* [7] The behavior in the previously biphasic region is however new. (cf. **Figure 5.5**). Comparing both DLS and SWAXS data, we observe that autocorrelation functions as well as the intensity of SWAXS diffractograms for $q \rightarrow 0$, are increased for LS. Interestingly, the SWAXS data for LS without additional SDS (which only contains an absolute SDS amount of 2.3 wt%) reminds us of that of an SFME [28], even though SDS is already present. When adding extra or further SDS, the effect is similar for both LS and PO.

Some thoughts must be considered to interpret this behavior:

- We expect SDS as a surface-active molecule to locate somewhere in the interphase of the surfactant-free aggregates. This surely happens at higher concentrations, where the repulsive forces due to charged aggregates can be seen in SWAXS spectra. It must be noticed that in SFMEs, no clear interface as in conventional surfactant-based microemulsions is present. [10] On the other side, it is proven that there is an interphase, in which enrichment of the hydrotrope can be observed. [29; 13] Thus, the term interphase should be preferred in the context of SFMEs.

- At higher surfactant concentrations, we would expect SDS/octanol micelles in these systems. [7] Thus, the ethanol would be somehow displaced from the interphase.

- Pre-Ouzo aggregates are very fluctuating, with a lifetime probably by a factor of 1000 lower than conventional microemulsions. [13; 30]
- There are pre-Ouzo aggregates present in the Ouzo region in a kind of equilibrium. [31]

In contrast to SDS, nonionic surfactants, like C12E10 in this system (cf. **Figure 5.8**), do not really affect the location of the binodal and do not really affect autocorrelation functions by DLS. The same is found in chapter 4 for the system water/TBA/HEMA/Tergitol/Synperonic, where the two nonionic surfactants did not seem to impact the binodal. Also, autocorrelation functions and conductivity curves seemed relatively unaffected by Tergitol and Synperonic in that chapter. Only the growing polymers seemed to have slightly smaller pore sizes but with the same morphology. We concluded, at this point, that there must be an additional stabilization of the nonionic surfactant during the polymerization process (cf. section 4.5). Thus, the fact that SDS is surface active alone does not explain the observed effects.

Investigating the effect of SDS on ternary systems with other oils and hydrotropes (cf. **Figure 5.6** and **Figure 5.9** for MMA at 45 °C) might help to understand the impact of SDS further. Ethyl acetate/ethanol does not form a mesostructured SFME (even though the system is sometimes called SFME in literature). [10] In this particular system, SDS only shows a very tiny impact which is neglectable. The same is the case for triacetin/ethanol, a system with a very small miscibility gap, that is considered an SFME system with weak structuring. (cf. **Figure 5.6 a** and **b**) [32] Thus, we can conclude that there is no impact of SDS when both the hydrotrope and the oil are quite hydrophilic, leading to a very small miscibility gap and no or only weak mesostructuring.

A very interesting system to investigate is with limonene as the oil phase. In contrast to triacetin, this oil is very hydrophobic. Limonene is tested with EtOH, NPA, and TBA as hydrotropes (cf. **Figure 5.6 c**, **d**, and **e**). Previous literature suggests that for this system, the pre-structuring of alcohols in water is essential for the formation of an SFME (like it is the case for TBA). [28] For EtOH, which comprises a very high miscibility gap, no effect at all can be observed on the ternary phase diagram when adding SDS. With NPA, a slight effect can be observed, while we observe an impact similar to that of octanol for the system limonene/TBA. The same is the case for citronellol/EtOH (cf. **Figure 5.6 f**). Autocorrelation functions for both systems are more pronounced in the previous biphasic region, just like for octanol (cf. **Figure 5.7**). For the system with MMA at 45 °C (cf. **Figure 5.9**), the effect increases from EtOH to TBA, just like the quality of mesostructuring.

These systems lead to a few conclusions. The presence of mesostructures in the system without surfactant seems to be a necessary condition for the reduction of the biphasic region. Otherwise, it cannot be explained why no effect of SDS is observed in the system with limonene and EtOH as a hydrotrope but with TBA. This presence, however, seems to be a necessary but not sufficient condition for lowering the biphasic region with SDS. As mentioned above, a system with very hydrophilic oil and very hydrophilic hydrotrope (*e.g.*, ethyl acetate/ethanol or triacetin/ethanol) with a small miscibility gap is hardly influenced by SDS. Even though structuring can be observed in the system with triacetin, [32] no distinct effect can be observed with SDS. This might have two reasons: on the one side, the miscibility gap is already extremely small, so it can hardly be reduced further. On the other side, it is possible that in addition to the mesostructuring, either the hydrotrope or the oil must be suitable to serve as a cosurfactant for SDS. Triacetin is sterically demanding and, thus, probably not a very suitable cosurfactant. In summary, we probably need a balanced SFME system which is not too hydrophilic and with a sufficiently large biphasic region to observe an impact by adding ionic surfactants like SDS.

The next question that arises is what exactly happens within the addition of SDS to the previous biphasic region when the system is suitable. In the biphasic region just below the pre-Ouzo region, the so-called Ouzo effect occurs. [11] In a recent contribution, it is proven that Ouzo emulsions and pre-Ouzo aggregates always coexist in bulk in a dynamic equilibrium. [31] The energy barriers in the Ouzo domain are quite low, just in the region of a few k_BT. [33] Thus, the energy required to bring the system into a thermodynamic equilibrium is not very large. Even though no calculations are done for this particular system, a stabilization in the range of 1-2 k_BT is thinkable for the adsorption of molecules onto a surface and reported, *e.g.*, for antagonistic salts. [34] Both the Ouzo and the pre-Ouzo aggregates were shown to be only present above the minimal hydrotropy concentration (MHC). [31] This is possibly the minimal concentration to where the phase diagram might be reduced. This would support the thesis that in the system with triacetin, a further reduction is hardly possible.

In conventional studies on the effect of ethanol on SDS (instead of the other way around, like done here), it is written that the critical micellar concentration (CMC, which is around 8 mM in pure water at room temperature [35]) is at first slightly decreasing up to an ethanol concentration of 15% and afterward increasing upon the addition of ethanol. [36] This is explained as ethanol follows both cosolvent and cosurfactant behavior. [36] With an SDS concentration of 80 mmol kg^{-1} at the sample LS, we are in the same order of magnitude as the CMC in a water or water/alcohol mixture might be. However, as an interphase is already present in the system, it might be more beneficial for SDS to incorporate into the already existing interphase instead of

forming micelles. As we do not see the typical peak for a repulsive aggregate for LS in the SWAXS spectrum (on the contrary, the spectrum looks more like that of a very pronounced SFME, cf. **Figure 5.5**), the impact of SDS at these rather low concentrations seems to be more like that of a co-hydrotrope (like the case for facilitated hydrotrope [37; 38]) or of antagonistic salts. [39] With an augmenting amount of SDS, its impact increases, and the structure changes towards a swollen SDS micelle. [7] As we remember that the mean lifetime of an SFME is by a factor of approximately 1,000 smaller than a conventional microemulsion, [30; 10] we can expect a stabilization of the pre-Ouzo domains by the addition of SDS, slowing down the fluctuations and leading thus to a less pronounced signal in DLS. By adding more SDS, the character changes, and SDS will dominate the properties of the aggregates (*i.e.*, shape and size) more and more. Starting from a previous metastable Ouzo domain (in balance with pre-Ouzo domains), the addition of small amounts of SDS is able to shrink the size of the Ouzo droplets until a probably stable system is reached, even before classical micellar systems can be observed. Even though DLS and SWAXS spectra for these systems (*i.e.*, the composition LS without additional SDS, cf. **Figure 5.4** and **Figure 5.5**) are significantly more pronounced than in the pre-Ouzo domain (*e.g.*, the composition PO, cf. **Figure 5.4** and **Figure 5.5**), we are currently not sure if we can interpret the data as aggregates that are also larger in size. This would have to be proven in further experiments.

The influence of sodium (alkyl) sulfates (from sodium sulfate to ethyl, pentyl, and octyl to dodecyl sulfates) shows a continuous trend from salting-out (sodium sulfate) to salting-in (SDS) (see **Figure 5.16**). The binodal, as well as the autocorrelation functions for ethyl sulfate, are more or less similar to that of pure TBA. With a longer alkyl chain length, the decrease is getting more pronounced. With increasing chain length, there is a shift from a specific ion effect via a hydrotrope effect to a surfactant behavior. [40] Please note that sulfate as a head group is considered rather soft and less hydrated, while sulfate as a counterion is very hard and hydrated. [40; 21; 16] Thus, it would also be of interest to test not only other nonionic surfactants or SLES (which showed a similar effect, see **Figure 5.8**) but also ionic surfactants with other head groups (*i.e.*, carboxylates or phosphates) for further understanding this effect.

Summarizing things up so far, we can conclude that the impact of SDS on SFMEs is a very balanced effect.

- The impact of SDS can only be seen in ternary systems, which comprise mesostructuring and a miscibility gap, which is not too small.

- The fact that SDS is a surfactant alone does not explain the behavior, as nonionic surfactants show no impact on the ternary phase diagram at all, even though they should also be adsorbed at the interphase of pre-Ouzo aggregates, but obviously without changing the characteristics.
- The large impact of salts on SFMEs (cf. chapter 5.4.4.2 and literature [7; 5; 4]) strengthens the hypothesis that the ionic character of SDS is the relevant factor. As conventional salts do only show a significant salting-out effect for kosmotropes but not really a salting-in effect for chaotropes, the combination of the surface-active and the ionic character of SDS seems to be the crucial factor.

5.4.3 Impact of SDS and Electrolytes on Polymerizations in SFME

5.4.3.1 Impact of SDS on the System MMA-Alcohols-Water

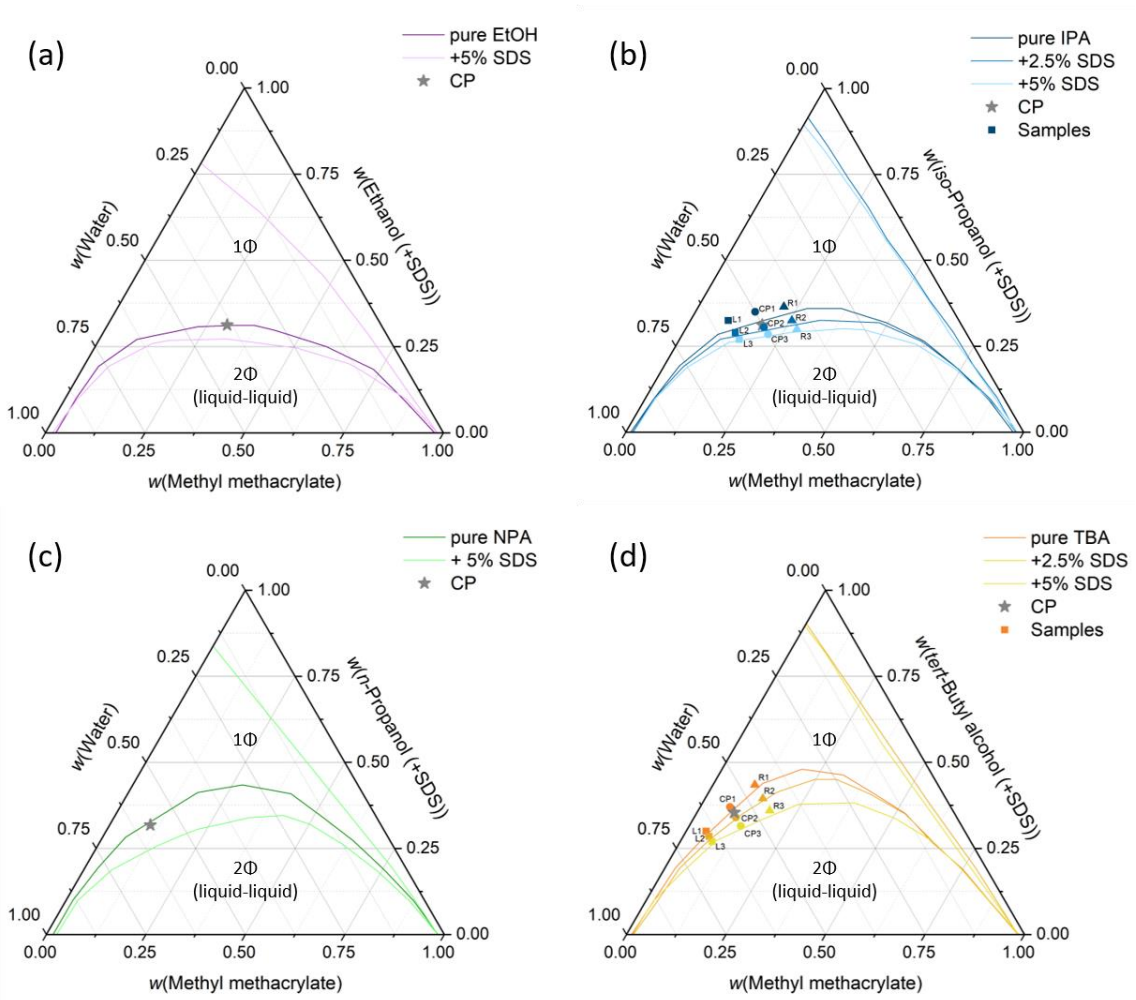

Figure 5.9 *(Pseudo-)Ternary phase diagrams at 45 °C of systems containing Water, MMA, and the hydrotropes (a) EtOH (+SDS), (b) IPA (+SDS), (c) NPA (+SDS), and (d) TBA (+SDS). Samples investigated further are shown in the systems IPA and TBA. Critical points of the ternary systems without SDS at 25 °C are marked as grey stars.*

Phase diagrams with MMA and (a) EtOH, (b) IPA, (c) NPA, and (d) TBA at 45 °C are depicted in **Figure 5.9**. The impact of SDS is increasing in the order from EtOH to TBA, in which also the autocorrelation functions get more pronounced (cf. chapter 2). The region of highest SDS impact is shifted from the more MMA-rich in the case of EtOH, over the middle in the case of IPA, to the water-rich two-phase area in the case of NPA and TBA. The CP (marked as grey star in the phase diagrams) is shifted in the same order and range. The systems with the hydrotropes IPA and TBA are investigated further. Examined compositions are shown in **Figure 5.9 b** and **d**. For each system (without additional SDS, as well as with an additional amount of 2.5 wt% and 5.0 wt%), samples close to the CP (called "CP"), on the water-rich side (called "L") and on the oil-

rich side (called “R”) are chosen in approximate equidistance to the binodal. L1, CP1, and R1 contain no SDS at all before the addition of further SDS, while samples with numbers 2 or 3 are pseudo-ternary with a small SDS concentration.

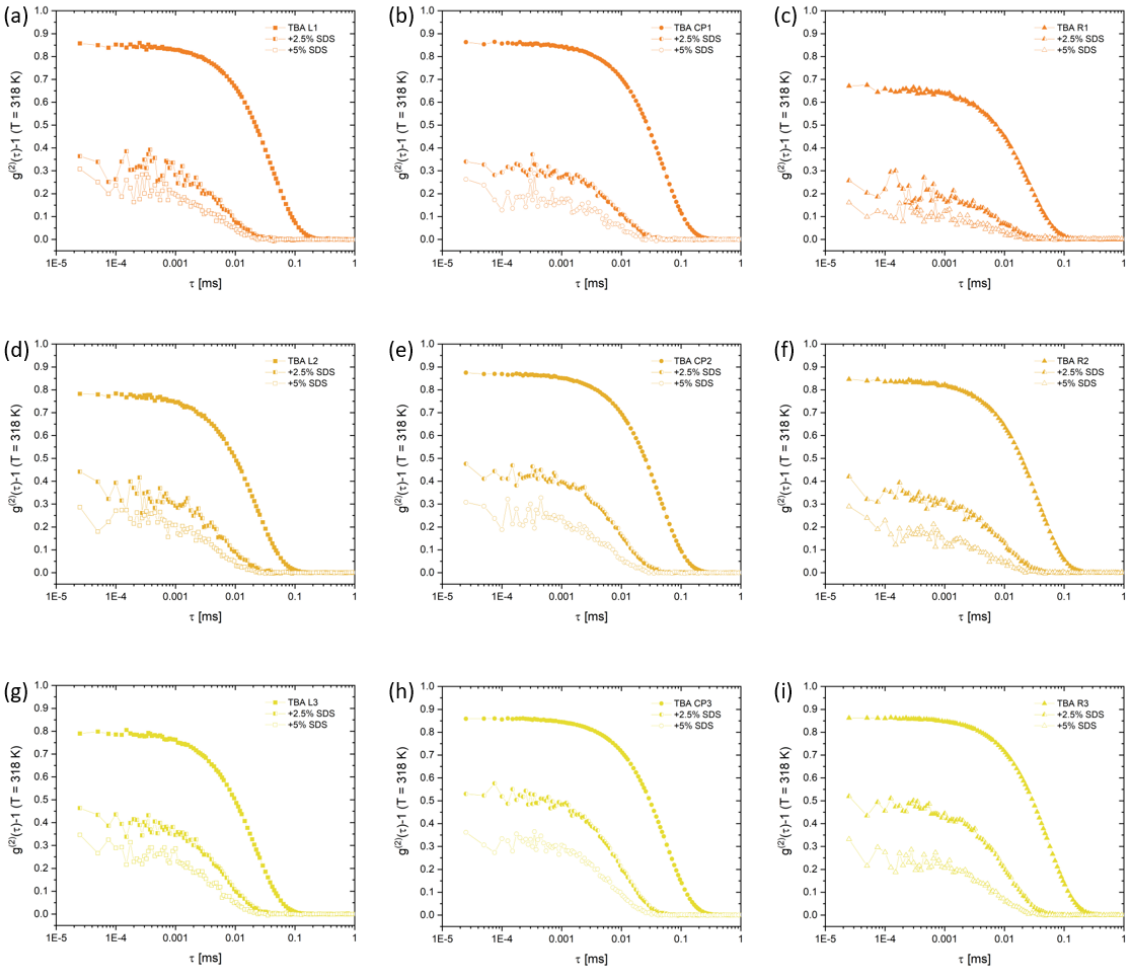

Figure 5.10 *DLS autocorrelation functions of samples of the TBA system, each without additional SDS (fully painted), and with an additional amount of 2.5 wt% (half colored) and 5 wt% SDS (framed), as marked in the phase diagrams in* ***Figure 5.9****.*

Light scattering experiments of the TBA system are depicted in **Figure 5.10**. They are performed without additional SDS (fully painted), as well as with an additional amount of 2.5 wt% (half painted) and 5.0 wt% SDS (framed). For samples in the pre-Ouzo region (TBA L1, CP1, and R1, see **Figure 5.10 a**, **b**, and **c**), autocorrelation functions are quite pronounced on the water-rich side of the CP (L1) and close to the CP (CP1) with a lag time > 0.1 ms and a y-axis intercept of 0.8 to 0.9. The autocorrelation function of R1 on the oil-rich side is less strong compared to L1 and CP1 but still indicates good structuring. Samples in the former two-phase region but without additional SDS (L2, CP2, R2, as well as L3, CP3, R3) show all distinct autocorrelation functions in the case of CP2 and CP3, comparably to the sample CP1. On the oil-rich side, autocorrelation

functions get more pronounced when moving from R1 to R3, while on the water-rich side, autocorrelation functions are slightly less strong for L2 and L3 compared to L1 (see **Figure 5.10 d** to **j** compared to **a** to **c**). When adding an additional amount of 2.5 wt% or even 5.0 wt% SDS, the quality of autocorrelation functions decreases drastically, as already seen in the Octanol system (cf. section 5.4.1.1).

Autocorrelation functions for the IPA systems are only recorded without additional SDS (just the amount necessary for the pseudo-ternary system) and are shown in **Figure 5.11**. Structuring on the oil-rich side (IPA R1) is more pronounced than on the water-rich side (IPA L1), in contrast to the TBA system. As a parallel to the TBA system, the impact of SDS when moving to the former two-phase region is most pronounced on the oil-rich side (IPA R2, R3) than on the water-rich side (IPA L2, L3).

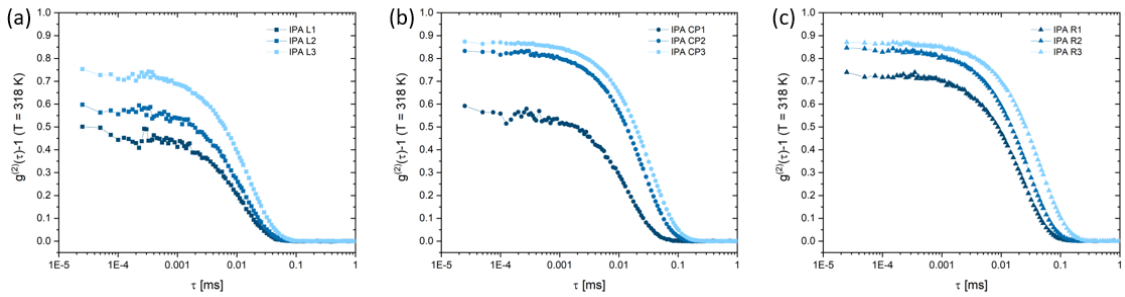

Figure 5.11 *DLS autocorrelation functions of samples of the IPA system without additional SDS, as marked in the phase diagram in* ***Figure 5.9****.*

Polymerizations are performed in the TBA and IPA systems and stopped after 7 hours. **Figure 5.12** depicts the weight average molar mass and the conversion of samples in the TBA system (cf. **Figure 5.9** and **Figure 5.10** for the corresponding phase diagrams and DLS measurements). For all individual samples, the mean molar mass and the conversion increase drastically with the addition of SDS to the primary composition. Whereas weight average molar masses range between 280 kDa (R1) to 470 kDa (L1) in samples without any SDS, they reach almost 2 MDa in the composition L3(+5% SDS). Comparing the location in the phase diagram, the trend of decreasing average molar mass when moving to higher monomer contents can be observed. This finding has already been described in chapter 2 and is consistent, even when adding SDS. Conversions range in the region of 60 wt% for samples without SDS and are increasing to over 90 wt% for samples with additional SDS. The same results, but plotted as a function of the absolute SDS concentration (concentration of the base samples plus addition of 2.5 or 5.0 wt%, if applicable), are shown in **Figure 5.13**. The conversion (**Figure 5.13 b**) shows a quite clear trend of increasing

conversion with increasing SDS concentration as a function that runs into saturation. It is noticeable that the samples L1, CP1, and R1 with an additional amount of 2.5 wt% and 5.0 wt% SDS, which are in the monophasic pre-Ouzo region before the addition of SDS, show a slight downward deviation compared to the overall trend. The weight average molar mass shows the same trend of increasing M_w-values with increasing SDS concentration, but with a significantly higher spread.

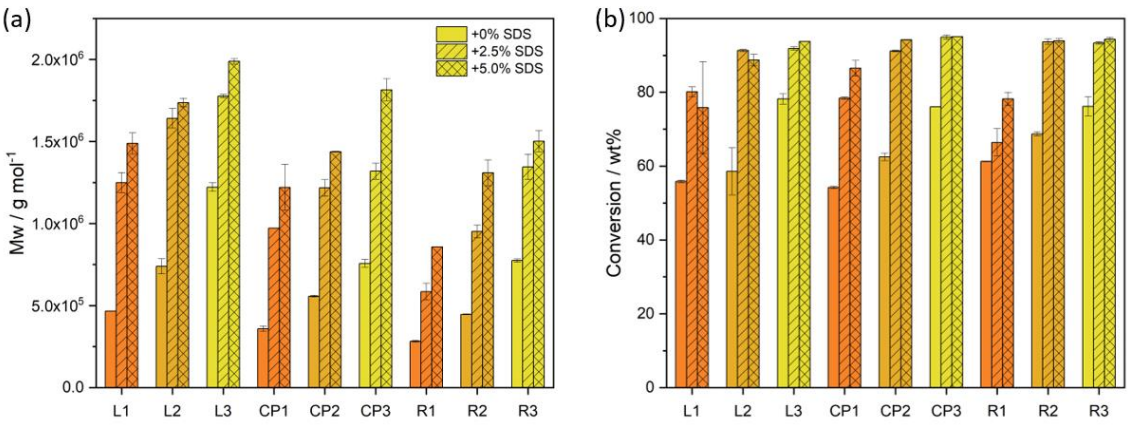

Figure 5.12 *Data of polymers derived from samples of the TBA system (cf.* ***Figure 5.9****) without additional SDS (clear), 2.5 wt% SDS (dashed) and 5 wt% SDS (chequered): (a) weight average molar mass and (b) conversion after 7 hours.*

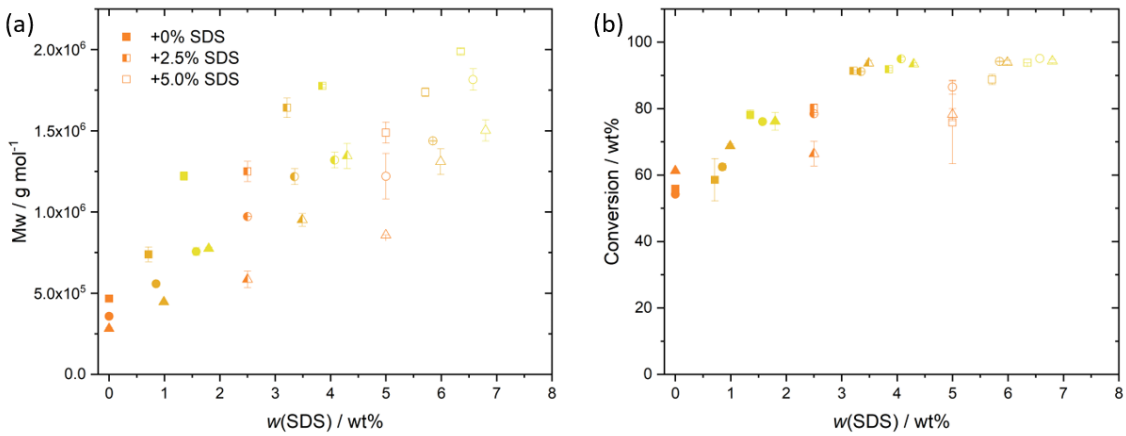

Figure 5.13 *Data of polymers derived from samples of the TBA system (cf.* ***Figure 5.9****) without additional SDS (fully painted), 2.5 wt% SDS (half painted) and 5 wt% SDS (only framed) : (a) weight average molar mass and (b) conversion after 7 hours, plotted against the absolute SDS concentration.*

The results of weight average molar masses and conversions of the IPA system are depicted in **Figure 5.14**. As in the TBA system (cf. **Figure 5.12**), weight average molar masses increase with increasing SDS amount. In contrast, polymerizations are only performed in samples without additional SDS (with only the amount given from the pseudo-ternary phase diagrams, without

additional amounts of 2.5 or 5.0 wt%). The absolute molar masses of comparable samples are higher in the IPA system compared to the TBA system (*e.g.*, 470 kDa for TBA L1 and 1.22 MDa for TBA L3 vs. 940 kDa for IPA L1 and 1.35 MDa for IPA L3). Furthermore, the effect of decreasing weight average molar mass with increasing MMA concentration of the sample can be found again. The impact of SDS on the conversion is way less pronounced compared to the TBA system, with all conversions being higher than 80 wt%.

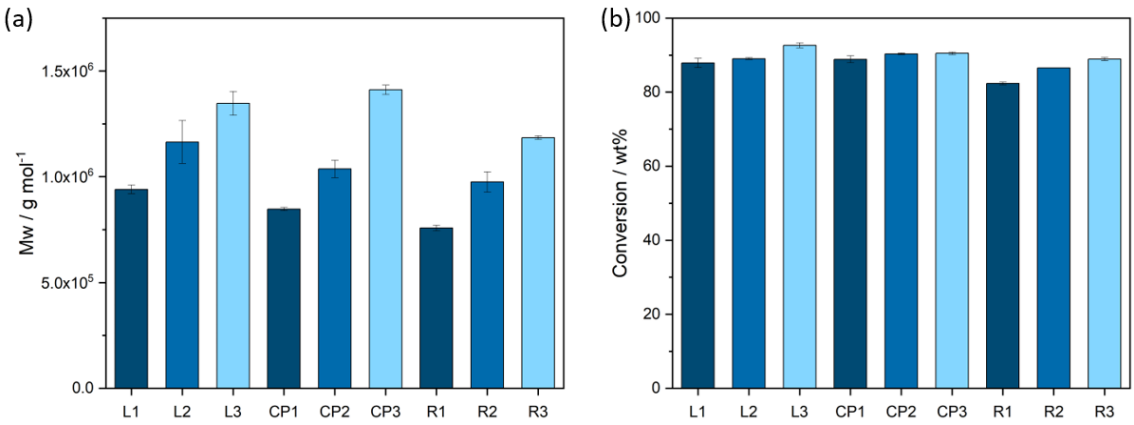

Figure 5.14 *Data of polymers derived from samples of the IPA system (cf.* ***Figure 5.9****) without additional SDS: (a) weight average molar mass and (b) conversion after 7 hours.*

The same data plotted against the SDS concentration are depicted in **Figure 5.15**. As seen in the TBA system, the weight average molar mass increases with increasing SDS concentration. For each composition, the trend seems to be quite linear. Concerning the conversion, no significant change can be observed due to the overall good conversion.

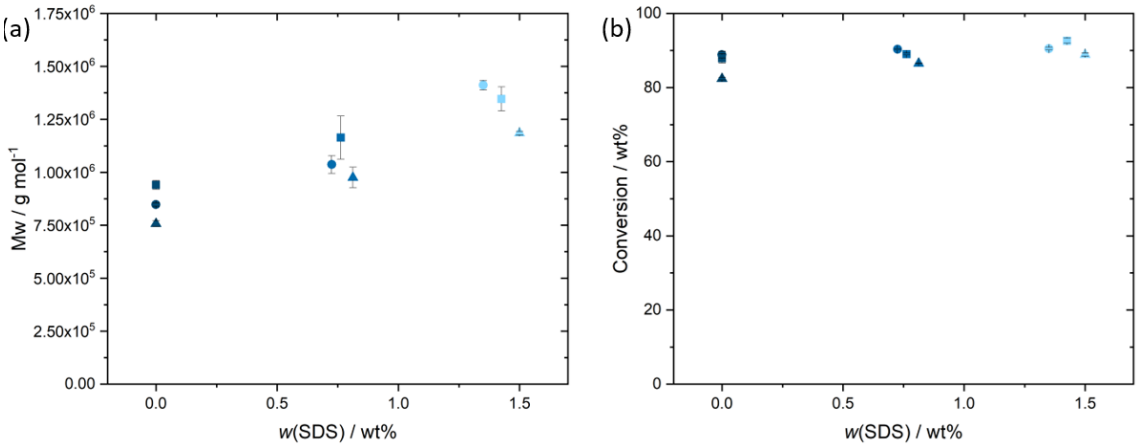

Figure 5.15 *Data of polymers derived from samples of the IPA system (cf.* ***Figure 5.9****) without additional SDS: (a) weight average molar mass and (b) conversion after 7 hours, plotted against the absolute SDS concentration.*

5.4.3.2 Between Surfactant, Hydrotrope and Salt: Different Length of Sodium Salts

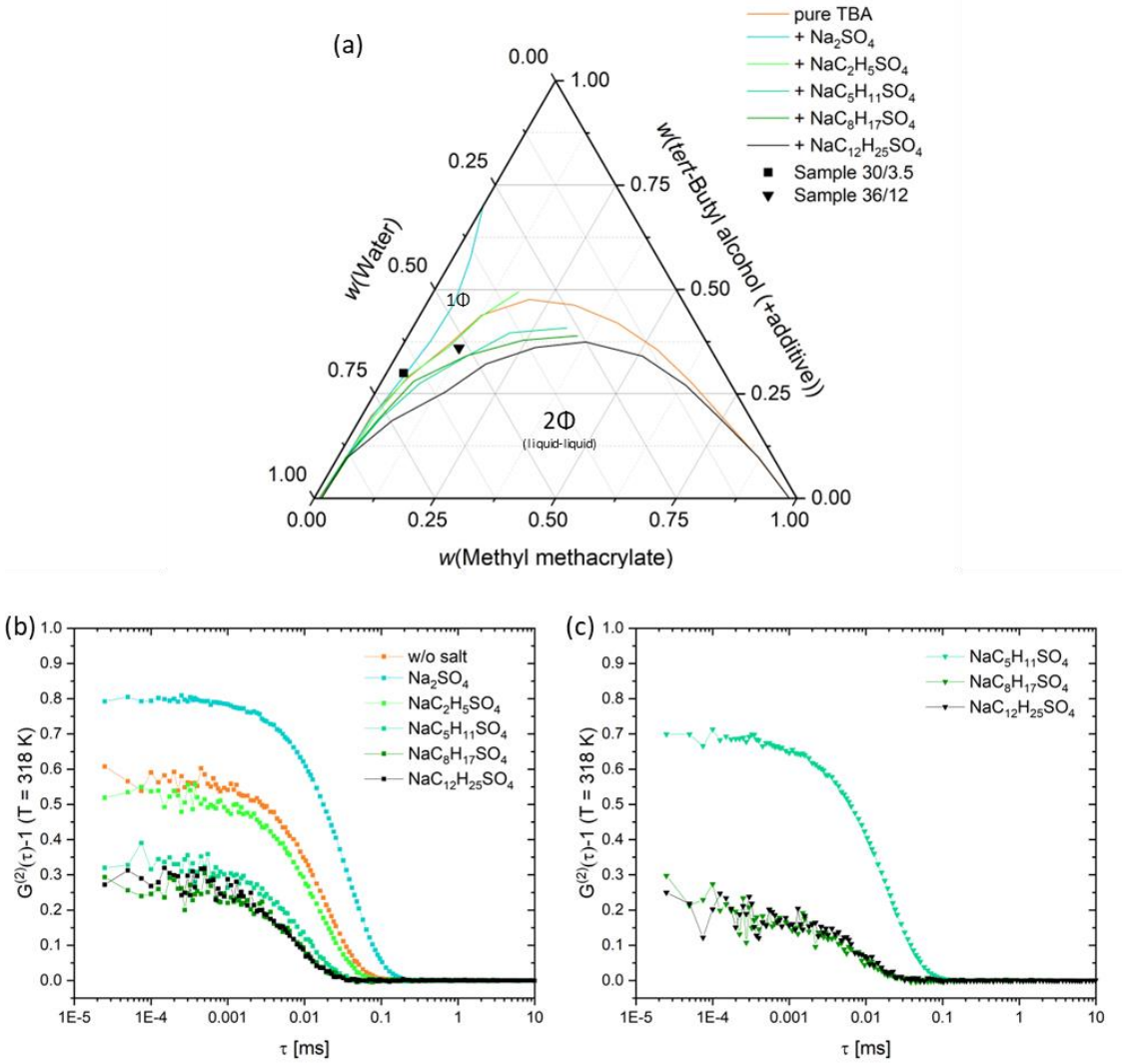

Figure 5.16 *(a) Pseudo-ternary phase diagrams as well as (b) and (c) DLS measurements of the system water/MMA/TBA with 0.013 mol% sodium sulfate in TBA or 5 wt% of sodium alkyl sulfates with different chain lengths at 45 °C, as marked in the phase diagram.*

Sodium alkyl sulfates with different chain lengths starting from pure sodium sulfate, via ethyl sulfate up to dodecyl sulfate (SDS), are tested as additives in order to get a better insight into the role of the additive at 45 °C, at which temperature the latter polymerization will take place. While the alkyl sulfates are used in a ratio of 5 wt% of the hydrotrope phase in TBA, Na_2SO_4 is used in a ratio of 0.013 mol% referring to TBA, which is just the same molar ratio as 5 wt% SDS in TBA (corresponding to around 60 mmol kg^{-1} additive for the composition 30/3.5). The same molar ratio is applied for other salts as well (see following chapters 5.4.3.3 and 5.4.3.4).

While Na_2SO_4 has a remarkably strong salting-out effect for such a low salt concentration (0.06 mmol g^{-1} for the sample 30/3.5, close to where the first deviation from the binodal from pure TBA can be observed, see **Figure 5.16 a**), the binodal for sodium ethyl sulfate in TBA is more

or less similar to that of pure TBA. From sodium pentyl sulfate via sodium octyl sulfate to sodium dodecyl sulfate, the salting-in behavior increases with a decreasing biphasic region. The auto-correlation functions at sample 30/3.5 show a more pronounced autocorrelation function for the addition of Na_2SO_4. For the ethyl sulfate, the autocorrelation function can be compared to that of pure TBA, while the quality decreases with increasing chain length (see **Figure 5.16 b** and **c**).

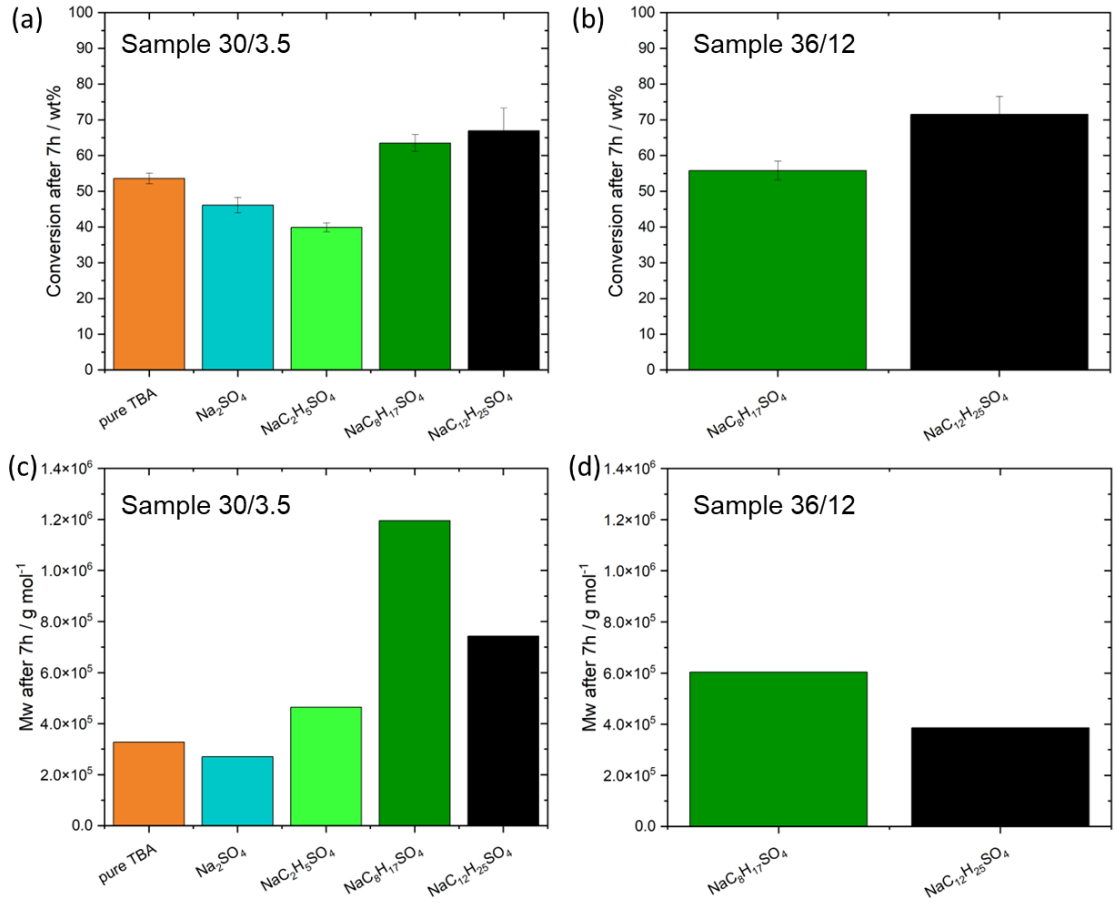

Figure 5.17 *(a) Conversion (N=2) and (c) weight average molar mass of polymers derived from the samples 30/3.5, and (b) conversion (N=2) and (d) weight average molar mass of polymers derived from the samples 36/12 after 7 h with the addition of different (alkyl) sulfates in comparison to pure TBA.*

The mean conversion after 7h in sample 30/3.5 (see **Figure 5.17 a**) decreases from TBA (53%) via Na_2SO_4 until ethyl sulfate (40%) and increases afterward via octyl sulfate (63%) to dodecyl sulfate (67%). Both latter additives lead to higher conversions compared to pure TBA. The trend in the mean molar mass is less clear (see **Figure 5.17 c**). M_w decreases within the addition of sodium sulfate from 320 kDa to 270 kDa, and is increased for ethyl sulfate already (460 kDa). The maximum, however, can be found for octyl sulfate (1.2 MDa), while dodecyl sulfate is in-between (740 kDa).

In sample 36/12, only polymerization with octyl and dodecyl sulfate is performed, as pure TBA, sodium sulfate, and also ethyl sulfate mixtures are already biphasic for this region. Samples with pentyl sulfate could not be performed due to a lack of substance. The conversion after 7h (see **Figure 5.17 b**) is higher than with pure TBA in sample 30/3.5 and higher for dodecyl sulfate than for octyl sulfate, just like for the sample 30/3.5. The weight average molar mass (see **Figure 5.17 d**) decreases from 600 kDa for octyl sulfate to 385 kDa for dodecyl sulfate.

5.4.3.3 Polymerizations with Different Anions and Sodium as the Counterion

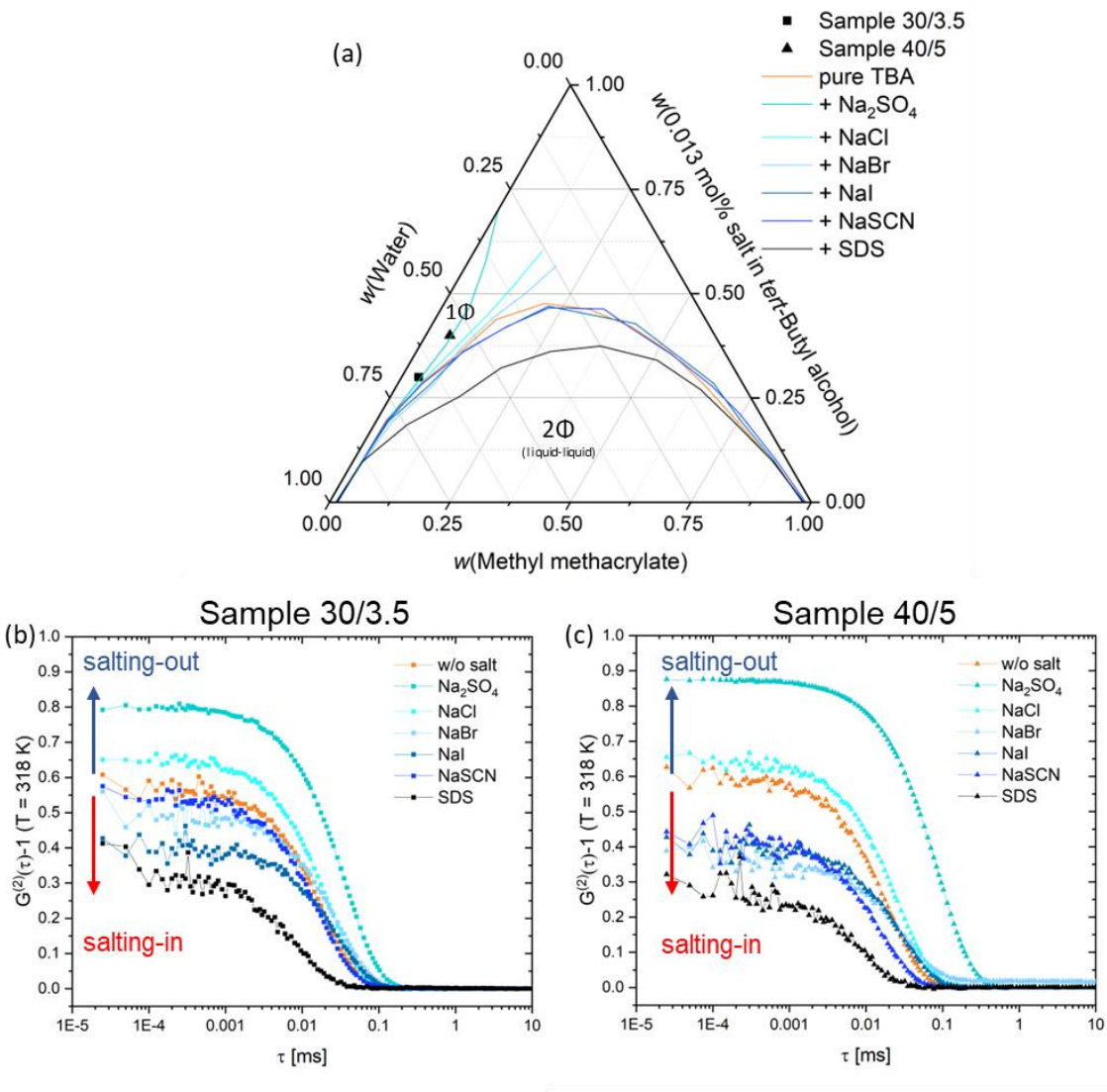

Figure 5.18 *(a) Pseudo-ternary phase diagrams as well as (b) and (c) DLS measurements of the system water/MMA/TBA with 0.013 mol% of salts in TBA with different anions and sodium as counterion at 45 °C (corresponding to 60 mmol kg^{-1} for sample 30/3.5 and 80 mmol kg-1 for 40/5).*

A series of salts with different anions and sodium as counterion is tested on their influence on the system water/TBA/MMA. A concentration of 0.013 mol% referring to TBA is chosen, which corresponds to 5 wt% SDS in TBA. **Figure 5.18 a** depicts the pseudo-ternary phase diagram with

the tested anions at 45 °C. The chaotropic salts NaI and NaSCN comprise a miscibility gap quite similar to that of pure TBA. The binodal might be shifted slightly to the oil-rich side for both salts, which, however, is not a strong effect. With the harder ions Br^-, Cl^-, and SO_4^{2-}, the binodal is continuously shifted upwards. For Na_2SO_4, only a very narrow strip with little MMA contents along the water-TBA-line is still monophasic. Only SDS leads to a significant decrease in the bi-phasic region, not comparable to any of the "normal" salts. Note that for NaBr and NaCl, the diagram is not recorded completely. The solid-liquid biphasic region is not determined for any of the ions. Autocorrelation functions derived by DLS are depicted in **Figure 5.18 b** (Samples 30/3.5) and **Figure 5.18 c** (Samples 40/5). Both sample compositions are chosen to be in the one phasic region for all tested additives. For salting-out salts (NaCl, Na_2SO_4), we can observe a more pronounced autocorrelation function compared to pure TBA without additives.

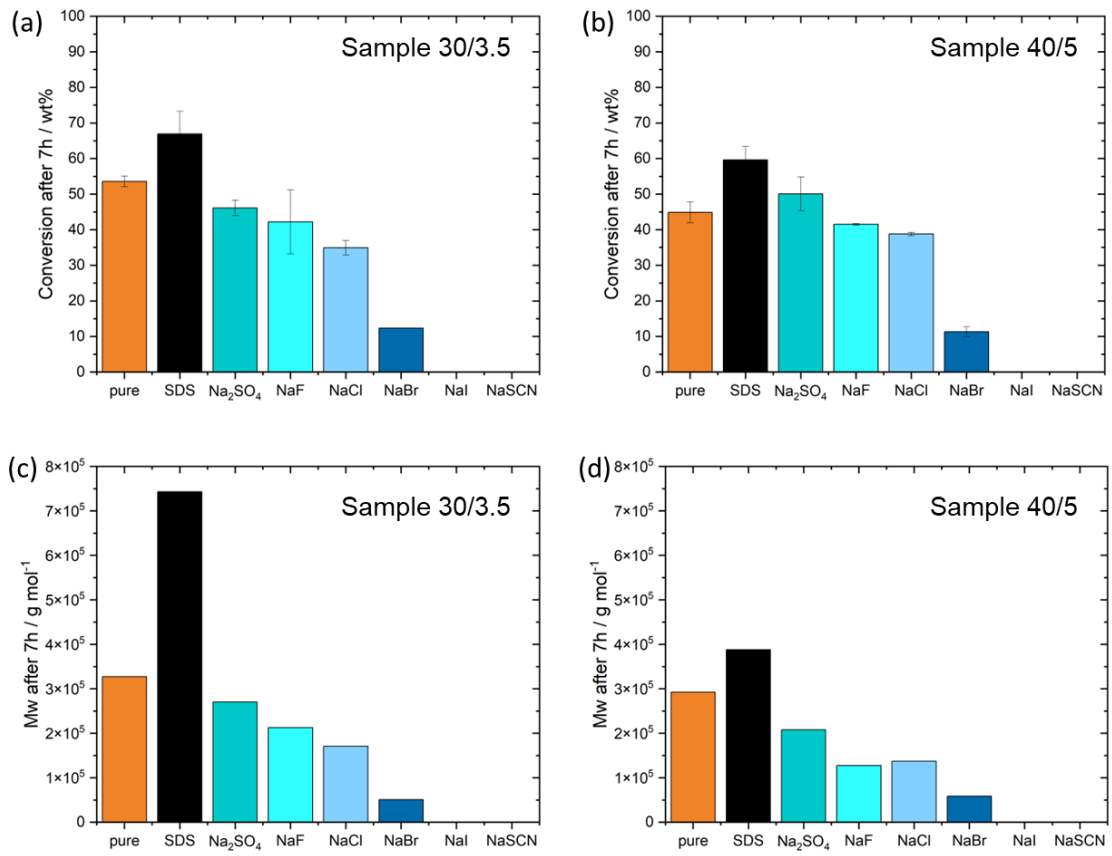

Figure 5.19 *(a) Conversion and (c) weight average molar mass of polymers derived from the samples 30/3.5, and (b) conversion and (d) weight average molar mass of polymers derived from the samples 40/5 after 7 h with the addition of 0.013 mol% in comparison to pure TBA of salts composed of different anions and sodium as counterion.*

In contrast to the biphasic region of the (pseudo-)ternary phase diagram, which did not get significantly smaller with chaotropic anions, we observe a decrease in the quality of the autocorrelation functions starting from NaBr already. The quality further decreases to NaI and NaSCN.

The addition of SDS to this sample leads to the least pronounced autocorrelation function, similar as described in section 5.4.3.1 already.

Figure 5.19 depicts conversions and molar masses for polymers after 7h polymerization times for the compositions 30/3.5 (**Figure 5.19 a** and **c**) and 40/5 (**Figure 5.19 b** and **d**). Both conversion and weight average molar mass behave mainly similarly independently of both compositions. The conversion decreases from TBA without additive steadily via Na_2SO_4 and NaF to NaCl for the sample 30/3.5. For 40/5, the conversion with Na_2SO_4 is slightly higher than with pure TBA and decreases afterward. The weight average molar mass decreases in the same order from pure TBA to NaCl. For both compositions, the conversion, as well as the weight average molar mass, is significantly lower with NaBr than with NaCl. Composition with NaI and NaSCN do not lead to a measurable amount of polymer. Compositions with NaI turned from clear to yellowish just after adding the initiator (dissolved in MMA) to the water/alcohol/salt mixture, indicating a kind of reaction. SDS leads to significantly higher conversions and molar masses for both compositions.

5.4.3.4 Polymerizations with Different Cations and Chloride as the Counterion

The impact of different cations on the phase behavior of the system water/TBA/MMA is tested with chloride as the counterion. Chloride is chosen, even though it showed salting-out behavior in the series of anions. Bromide, which would be the next ion in the Hofmeister's series, led to a significant drop in both conversion and weight average molar mass in previous experiments, which cannot be explained only by a physical ion effect (cf. section 5.4.3.3).

The impact of cations on the phase-diagram and autocorrelation functions derived by DLS is depicted in **Figure 5.20**. We observe a salting-out tendency with an increased biphasic region for all salts, starting with NH_4^+, which showed the lowest effect, via K^+, Na^+, and Mg^{2+}, to Ca^{2+}. This order is from soft, polarizable ions with little charge to hard ions with a high charge like for anions (cf. section 5.4.3.3) and thus reversed from the Hofmeister's series of cations for proteins. [15] Concerning autocorrelation functions derived by DLS (see **Figure 5.20 b** and **c**), the trend is not so clear. NH_4^+, which showed the least effect on the ternary phase diagram, leads to less pronounced autocorrelation functions compared to TBA. The same is the case for KCl at composition 30/3.5. The lag time, however, seems quite similar. For sample 40/5, the autocorrelation function of KCl is more pronounced than pure TBA. Na^+, Mg^{2+}, and Ca^{2+} show an increase in the autocorrelation function, but with differences between both compositions. Especially Mg^{2+} leads to a significantly higher autocorrelation function in the composition 40/5, while Ca^{2+} leads to the highest function for 30/3.5.

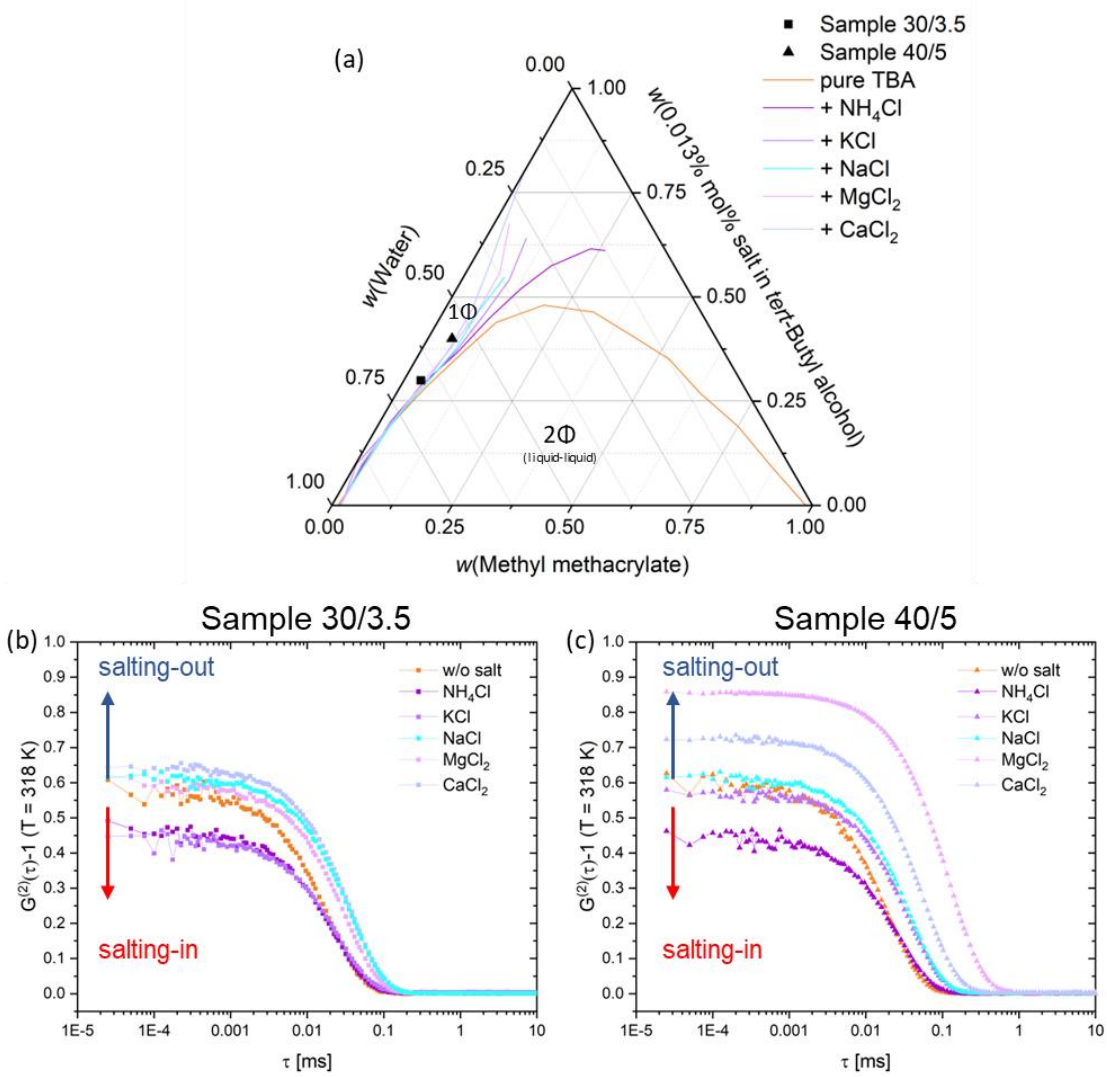

Figure 5.20 *(a) Pseudo-ternary phase diagrams as well as (b) and (c) DLS measurements of the system water/MMA/TBA with 0.013 mol% of salts in TBA with different cations and chloride as counterion at 45 °C (corresponding to 60 mmol kg^{-1} for sample 30/3.5 and 80 mmol kg^{-1} for 40/5).*

Polymerization data after 7h are depicted in **Figure 5.21**. For both compositions, all salts decrease the conversion and the weight average molar mass after 7h. Especially for 40/5, no real differences, and thus no trend can be given in between the ions. For sample 30/3.5, one might see a trend in the conversion, with NH_4Cl leading to the lowest conversion, increasing via KCl to NaCl. $MgCl_2$, however, shows a lower conversion again. Concerning the weight average molar mass at the composition 30/3.5, all masses are quite similar, except KCl, which comprises a slightly higher average molar mass. In contrast to the anions (cf. section 5.4.3.3), the differences within the cations are significantly smaller.

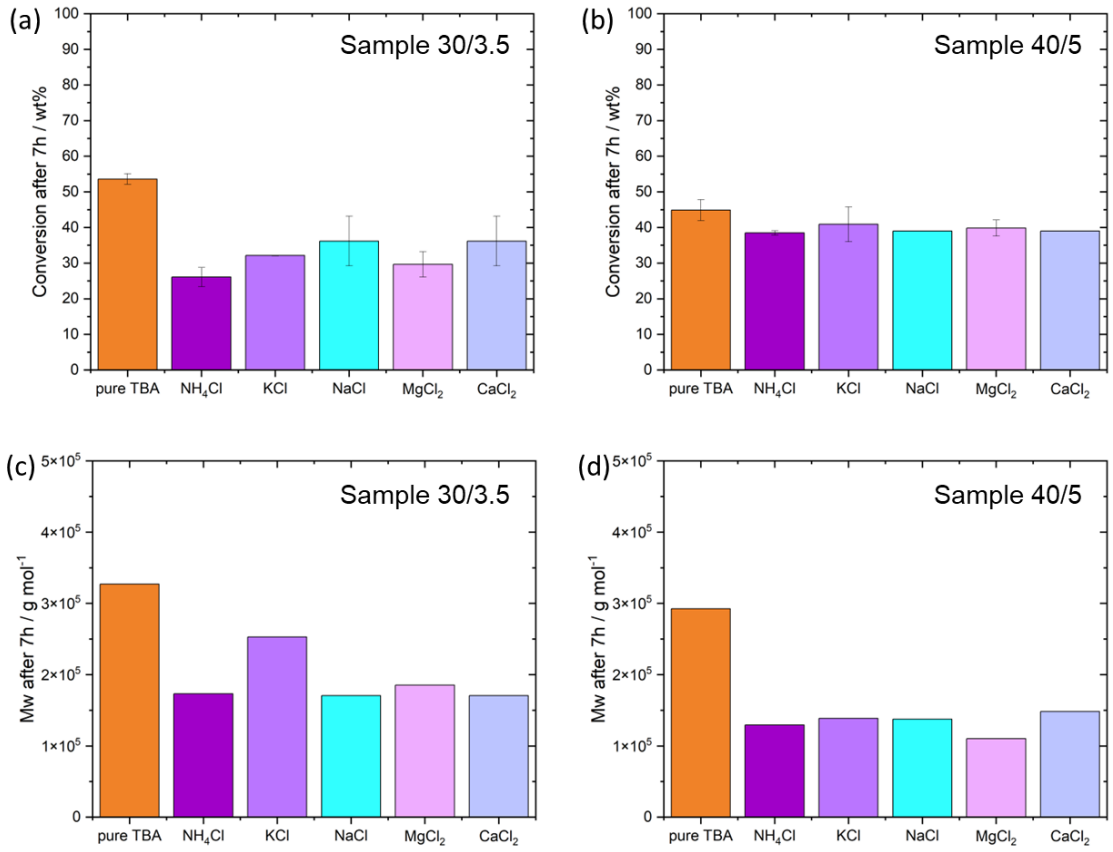

Figure 5.21 *(a) Conversion and (c) weight average molar mass of polymers derived from the samples 30/3.5, and (b) conversion and (d) weight average molar mass of polymers derived from the samples 40/5 after 7 h with the addition of 0.013 mol% in comparison to pure TBA of salts composed of different cations and chloride as counterion.*

5.4.4 Discussion – Impact of SDS and Electrolytes on Polymerizations in SFME

5.4.4.1 Impact of SDS on Microsuspension Polymerizations of MMA

The impact of SDS on the polymerizable systems with MMA at 45 °C is similar to what was described before (see section 5.4.1). The impact increases from EtOH to TBA (see. **Figure 5.9**). In the same order, the biphasic region and also the quality of mesostructuring increase (cf. chapter 2). Autocorrelation functions derived by DLS (cf. **Figure 5.10** for TBA and **Figure 5.11** for IPA) show a similar behavior to the system with octanol, as well. Upon the addition of SDS, both conversion and weight average molar mass increase drastically for any sample in the TBA system (cf. **Figure 5.12**). Also when moving into the previous biphasic region (with only the amount of SDS necessary for the pseudo-ternary system, thus without additional SDS, *e.g.*, from L1 to L2 and L3), both molar mass as well as the weight average molar mass increases for any sample upon the addition of SDS. However, just like found for polymerizations in SFME (cf. chapter 2), the average mass decreases with increasing MMA content. [1] When plotting both molar mass as well as the conversion just as a function of the SDS concentration (cf. **Figure 5.13**), especially the trend of the conversion is clearly dependent on the SDS concentration, independent of the location in the ternary phase diagram. The weight average molar mass seems to be more dependent on the position in the phase diagram (higher for samples with lower MMA content and lower for samples with higher MMA content). However, also M_w increases drastically with increasing SDS concentration, and within similar samples (L, CP, R), a less fluctuating trend is observed. Samples derived from systems with IPA (cf. **Figure 5.14** and **Figure 5.15**) behave quite similarly. Obviously, SDS is significantly involved in the polymerization process. As the system gets unstable during polymerization, [1–3] it is assumed that SDS will adsorb onto the growing polymer particle, providing better kinetic stabilization. The same was already postulated for other polymerization processes upon the addition of SDS. [41] Additionally, SDS might shield the growing polymer particle from contact with water and possibly also lead to less EtOH in very close proximity. Both together should lead to fewer termination reactions, resulting in both higher conversions and higher weight average molar masses (cf. discussion in section 2.5). [1]

5.4.4.2 Impact of Salts on the Ternary System MMA-TBA-Water and Polymerizations in Those

As described by Marcus *et al.* [7] and Schöttl *et al.*, [5] we observe a significant impact of salts on SFMEs. While we can observe an increase in the quality of autocorrelation functions derived by DLS for hard, highly charged anions or cations, the opposite happens upon adding soft, weakly charged cations or anions (cf. **Figure 5.18** and **Figure 5.20**). Having a look at the pseudo-ternary

phase diagrams, no real salting-in effect by chaotropic ions can be observed (the binodal upon addition of NaBr or NaI is quite similar to that of pure TBA, cf. **Figure 5.18**). The adsorption of these ions on the interphase, as reported in the literature, [7; 5] obviously influences the fluctuations seen in the autocorrelation curves but not the phase behavior, in contrast to SDS (cf. discussion in section 5.4.2 above). Kosmotropic ions, on the other side, lead to a drastic reduction of the onephasic region by salting-out ethanol from the water-rich pseudo phase, which is essential for the stability of SFMEs. [5; 13] The fact that all cations seem to have a (more or less pronounced) salting-out effect has probably two reasons: at first, the specific ion effect of cations is generally smaller than for anions. [16] Additionally, chloride is used as a counterion, which is shown to have a salting-out effect in the series of anions (cf. **Figure 5.18**). However, as our main aim is to perform polymerizations, ions on the more chaotropic side of the Hofmeister's series (*e.g.,* Br^- or I^-) seem to interfere with the radical polymerization reaction itself, as a drop in both conversion and weight average molar mass happens in between chloride and bromide (cf. **Figure 5.19**, this is already a signal that something else than just an ion effect occurs). Even more relevant is the fact that no conversion at all can be observed in the presence of iodide or thiocyanate. The observation of the iodide solution turning yellowish upon adding the initiator (cf. results in section 5.4.3.3) leads to the assumption that elementary iodine is present in small concentrations. [42] The only possible explanation for this is that the ions, from bromide onwards, but certainly iodide and thiocyanate, react with the free radicals formed by the initiator. Thus, less initiator is available for the polymerization process itself. The inhibiting effect of I_2 and Br_2 on free-radical polymerizations is known in the literature. [41] The continuous decrease in both conversion and weight average molar mass from pure TBA via hard anions like sulfate to chloride leads to the assumption that any adsorption of ions on the interphase of the growing polymer domains and probably even ionic strength *per se* is unfavorable. The low impact of cations on the polymerizations corresponds to the overall lower specific ion effect of cations in contrast to anions. [16] First publications on the effect of salts on polymerizations have already been published for both microemulsion and microsuspension processes and called retarding effect. [41] Unfortunately, the vast majority of publications on polymerization provide little information about the system in which the polymerization takes place. For this reason, it is difficult to conclude from the literature whether the retarding effect originates from an influence of the salts on the reactivity or from a salt effect on the system. [41] However, weakly hydrated ions will adsorb at the interphase in closer proximity to the polymerization taking place in the monomer-rich pseudo-phase. In contrast, hard, highly hydrated ions will surely stay in the water-rich phase, leading to a salting-out of ethanol into the monomer-rich pseudo-phase. Thus, if an

interference of the ions with the free-radical polymerization reaction itself would be the relevant factor, specific ion effects surely lead to higher concentrations of chaotropic salts in proximity to the reaction process than of kosmotropic one. The same would be the case if only ionic strength would play a role. Thus, it cannot be finally concluded what exactly leads to the retarding effect of ions. However, specific ion effects will surely play a role.

5.5 Conclusion and Outlook

In this chapter, we investigated the impact of surfactants and salts on surfactant-free microemulsions (SFMEs) and on free-radical microsuspension polymerization processes in those. The impact of sodium dodecyl sulfate (SDS) is tested on several SFME systems with different alcohols (from ethanol (EtOH) to *tert*-butyl alcohol (TBA)) as hydrotropes and different oils.

It is found that adding SDS in rather small amounts (up to 2.5 wt% absolute in the mixture) can lead to a significant decrease in the biphasic region. For this effect, the Ouzo region in close proximity to the binodal on the biphasic side might be relevant, which exists in equilibrium with pre-Ouzo aggregates. Pre-structuring (*i.e.*, the appearance of pre-Ouzo domains, and thus probably also the appearance of an Ouzo domain) seems necessary for the reduction of the biphasic region. Furthermore, the biphasic region must be sufficiently large for the reduction. In other words, the reduction might just be possible from the minimum hydrotropic concentration (MHC) upwards. Nonionic surfactants, on the other side, do not seem to impact the location of the binodal at all. In the previous biphasic region, the intensity of both autocorrelation functions by dynamic light scattering (DLS) as well as small/wide angle x-ray scattering (SWAXS) spectra is higher than for samples in the real pre-Ouzo region. The impact of adding further SDS leads, in both cases (pre-Ouzo and previously biphasic region), to a decrease in the quality of DLS spectra as well as the formation of a peak in the SWAXS spectrum due to repulsive aggregates. It cannot be clarified yet whether this increased intensity has something to do with larger aggregates or a different nature of aggregates. This particular region might be interesting for further research. Investigating the change in the exact composition of the water- and oil-rich pseudo phase might help in understanding the effects. Further scattering experiments, maybe even neutron scattering with isotope variation, could help to understand what happens in the transition from pre-Ouzo to a micellar system and in the previous Ouzo region. Variation of the head groups of the surfactant (*i.e.,* phosphates or carboxylates would be of interest), as well as testing other nonionic surfactants, could help to further understand and predict effects.

Understanding these effects might give a novel view into the role of cosurfactants and surfactants in conventional microemulsions. Thus, one could think of formulating microemulsions with really low surfactant concentrations.

The effect could also be beneficial for reducing solvent concentrations. Replacing 10-15 wt% of alcohols with only 1-2 wt% charged surfactants and still gaining a transparent, thermodynamically stable system might be beneficial for the formulation of several systems, *e.g.*, perfumes.

Reducing the amount of volatile organic compounds (VOCs) might also be an aim in industrial processes.

While ionic surfactants have a huge impact on previously mesostructured, surfactant-free systems, nonionic surfactants do not seem to have any impact at all. The not existing impact of nonionic surfactants on SFME systems strengthens the conclusion in the chapter on porous polymers (cf. chapter 4) that the interaction of the oil and the hydrotrope might direct the nature of structures in nonionic microemulsions with high solvent/cosurfactant ratios. To further confirm this thesis, it would be of interest to investigate the impact of different nonionic surfactants on different SFME systems, including scattering and conductivity experiments in order to compare the nature of structuring (oil-in-water, bicontinuous, or inverse) with and without surfactants.

Polymerizations show overall higher conversions and higher weight average molar masses upon the addition of SDS. We expect that SDS will adsorb onto growing polymer domains as soon as they appear and lead to further kinetic stabilization of growing polymer domains, reducing termination reactions. This effect is remarkably dependent on the SDS concentration and might be an easy tool for tuning molar masses.

Concerning the impact of salts, it is found that hard, highly hydrated ions lead to a strong salting-out effect due to the salting-out of EtOH from the water-rich domain. Soft, weakly hydrated ions do not really impact the position of the binodal, even though changes can be observed in autocorrelation functions by DLS. Also, changes in the SWAXS spectra were found by Marcus *et al.*, [7] coming from the adsorption of weak ions to the interphase.

Free-radical microsuspension polymerizations in SFMEs are extremely influenced by the addition of salts. The addition of any salt leads to a decreased conversion and average molar mass. However, the decrease is lower for hard, very hydrated ions (which will stay in the water-rich phase and thus at a higher distance to the polymerization reactions in the oil-rich phase). The decrease is stronger for softer ions, which will preferentially go to the interphase, resulting in a locally higher concentration in proximity to where polymerizations take place. Even softer anions (Br^-, I^-, and SCN^-) interfere with the radical polymerization process directly and quench it. [41] Even though the absolute reason for the impact of salts cannot be clarified from this work, specific ion effects will surely play a role. The impact of cations is way less pronounced than for anions. The study shows clearly that specific ion effects must be considered when choosing the counterions for redox initiator systems or even charged monomers.

5.6 Bibliography

[1] J. Blahnik, S. Krickl, K. Schmid, E. Müller, J. Lupton, and W. Kunz, *J. Colloid. Interface Sci.* **2023**, *648,* 755–767.

[2] F. M. Pavel, *J. Dispers. Sci. Technol.* **2004**, *25,* 1–16.

[3] M. Antonietti, R. Basten, and S. Lohmann, *Macremol. Chem. Phys.* **1995**, *196,* 441–466.

[4] S. Schöttl. Dissertation, Universität Regensburg, **2019**.

[5] S. Schöttl, and D. Horinek, *J. Chem. Phys.* **2018**, *148,* 222818.

[6] J. Marcus. Dissertation, Universität Regensburg, **2016**.

[7] J. Marcus, D. Touraud, S. Prévost, O. Diat, T. Zemb, and W. Kunz, *Phys. Chem. Chem. Phys.* **2015**, *17,* 32528–32538.

[8] J. Klier, C. J. Tucker, T. H. Kalantar, and D. P. Green, *Adv. Mater.* **2000**, *12,* 1751–1757.

[9] D. Langevin, *Annu. Rev. Phys. Chem.* **1992**, *43,* 341–369.

[10] J. Blahnik, E. Müller, L. Braun, P. Denk, and W. Kunz, *COCIS* **2022**, *57,* 101535.

[11] O. Diat, M. L. Klossek, D. Touraud, B. Deme, I. Grillo, W. Kunz, and T. Zemb, *J. Appl. Crystallogr.* **2013**, *46,* 1665–1669.

[12] S. Prevost, T. Lopian, M. Pleines, O. Diat, and T. Zemb, *J. Appl. Crystallogr.* **2016**, *49,* 2063–2072.

[13] T. N. Zemb, M. Klossek, T. Lopian, J. Marcus, S. Schöettl, D. Horinek, S. F. Prevost, D. Touraud, O. Diat, S. Marčelja, and W. Kunz, *Proc. Natl. Acad. Sci. U. S. A.* **2016**, *113,* 4260–4265.

[14] P. Schmid. Dissertation, Universität Regensburg, Regensburg, **2022**.

[15] W. Kunz, J. Henle, and B. W. Ninham, *COCIS* **2004**, *9,* 19–37.

[16] W. Kunz, *COCIS* **2010**, *15,* 34–39.

[17] J. Mehringer. Dissertation, Universität Regensburg, Regensburg, **2021**.

[18] K. D. Collins, *Methods* **2004**, *34,* 300–311.

[19] R. G. Pearson, *J. Am. Chem. Soc.* **1963**, *85,* 3533–3539.

[20] J. Lyklema, *Chem. Phys. Lett.* **2009**, *467,* 217–222.

[21] N. Vlachy, B. Jagoda-Cwiklik, R. Vácha, D. Touraud, P. Jungwirth, and W. Kunz, *Adv. Colloid Interface Sci.* **2009**, *146,* 42–47.

[22] J. Mehringer, and W. Kunz, *Adv. Colloid Interface Sci.* **2021**, *294,* 102476.

[23] M. Clausse, L. Nicholas-Morgantini, A. Zradba, and D. Touraud, in: *Surfactant Science Series* (Hrsg.: M. Dekker), New York, **1987,** 15–62.

[24] E. Hofmann. Dissertation, Universität Regensburg, Regensburg, **2023**.

[25] S. H. Chen, E. Y. Sheu, J. Kalus, and H. Hoffman, *J. Appl. Crystallogr.* **1988**, *21,* 751–769.

[26] O. G. Us'yarov, *Colloid J.* **2016**, *78,* 698–704.

[27] K. D. Danov, P. A. Kralchevsky, and K. P. Ananthapadmanabhan, *Adv. Colloid Interface Sci.* **2014**, *206,* 17–45.

[28] T. Buchecker, S. Krickl, R. Winkler, I. Grillo, P. Bauduin, D. Touraud, A. Pfitzner, and W. Kunz, *Phys. Chem. Chem. Phys.* **2017**, *19,* 1806–1816.

[29] S. Schöttl, D. Touraud, W. Kunz, T. Zemb, and D. Horinek, *Colloids Surf. A.* **2015**, *480,* 222–227.

[30] S. Krickl. Dissertation, Universität Regensburg, Regensburg, **2021**.

[31] S. Prévost, S. Krickl, S. Marčelja, W. Kunz, T. Zemb, and I. Grillo, *Langmuir* **2021**, *37,* 3817–3827.

[32] P. Degot, V. Huber, E. Hofmann, M. Hahn, D. Touraud, and W. Kunz, *Food chemistry* **2021**, *336,* 127660.

[33] R. Botet, and K. Roger, *COCIS* **2016**, *22,* 108–112.

[34] T. Zemb, and W. Kunz, *COCIS* **2016**, *22,* 113–119.

[35] F. I. El-Dossoki, E. A. Gomaa, and O. K. Hamza, *SN Appl. Sci.* **2019**, *1*.
[36] P. C. Griffiths, N. Hirst, A. Paul, S. M. King, R. K. Heenan, and R. Farley, *Langmuir* **2004**, *20,* 6904–6913.
[37] M. Durand, A. Stoppa, V. Molinier, D. Touraud, and J.-M. Aubry, *J. Solution Chem.* **2012**, *41,* 555–565.
[38] M. L. Klossek, D. Touraud, and W. Kunz, *Phys. Chem. Chem. Phys.* **2013**, *15,* 10971–10977.
[39] R. Winkler, T. Buchecker, F. Hastreiter, D. Touraud, and W. Kunz, *Phys. Chem. Chem. Phys.* **2017**, *19,* 25463–25470.
[40] J. Mehringer, E. Hofmann, D. Touraud, S. Koltzenburg, M. Kellermeier, and W. Kunz, *Phys. Chem. Chem. Phys.* **2021**, *23,* 1381–1391.
[41] A. S. Sarac, *Prog. Polym. Sci.* **1999**, *24,* 1149–1204.
[42] N. Wiberg, A. F. Holleman, E. Wiberg und G. Fischer, *Inorganic Chemistry,* 102. Aufl., De Gruyter, Inc, Berlin/Boston, **1995**.

6 Natural Photoinitiator Systems for Polymerizations in SFMEs

6.1 Preface and Abstract

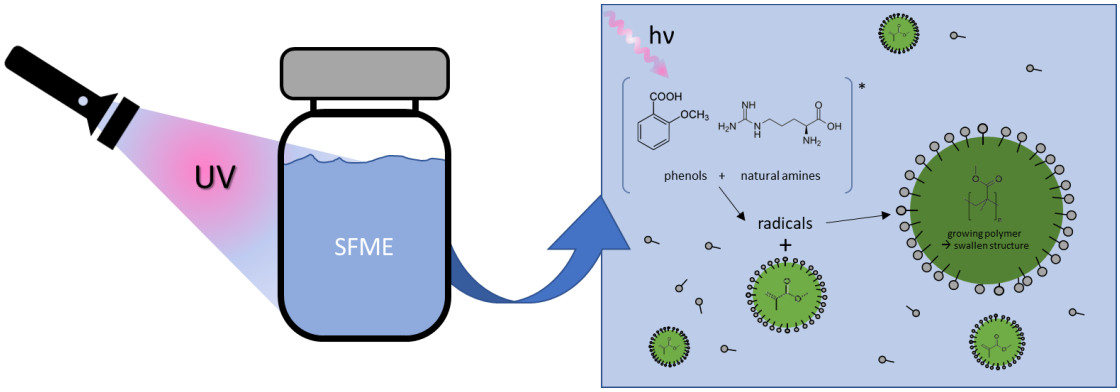

Figure 6.1 *Graphical abstract: Using natural photoinitiators for UV-initiated polymerizations in SFMEs.*

This chapter comprises a pre-study of the suitability of natural phenols and amines as natural photoinitiator systems using UV light. This work is a pre-study for the ZIM project "BIOINIT" from the network "go2green," aiming to reduce toxic materials in the coatings industry.

Photopolymerization, or UV curing, is a method recently used in industry, especially for coatings. High-performance initiators are extremely quick but pose health and environmental concerns. Many photoinitiators are considered of being harmful to health, but some of them have not been adequately tested. A big problem can be the migration of unreacted initiators, which can diffuse out of the coating or the polymer matrix. This is particularly relevant in the case of food contact.

This work studies natural phenols and amines for their suitability as photoinitiators in our simple surfactant-free microemulsion (SFME) systems comprising water, methyl methacrylate (MMA)

as the monomer, and *tert*-butyl alcohol (TBA) or *iso*-propanol (IPA) as hydrotropes. UV-LEDs (λ=365 nm) are used to initiate the polymerizations. The conversion of dried polymers are investigated, and average molar masses are determined by gel permeation chromatography (GPC).

Trans-o-coumaric acid, o-anisic acid, 2,3-dimethoxybenzoic acid, 2,4-dimethoxybenzoic acid and 3,5-dihydroxybenzoic acid show interesting results, but also other phenols, especially in combination with amines (like proline, arginine or histidine). The different performance of phenols and phenol/amine mixtures can neither be linked to the maximum of absorption in their UV/VIS spectra nor to their bond dissociation enthalpies.

Contributions to the experimental work:

- Jonas Blahnik: Conceptualization, experimental work, data evaluation
- Chiara Schmid: Experimental work, data evaluation

6.2 Introduction

Photoinitiators are a fast and easy-to-control method to initiate polymerizations. These two properties make them especially interesting for coatings. Viscous, polymerizable varnish can be applied to a substrate and be polymerized in less than one second by UV irradiation. [1] This procedure is also called "UV curing." [2] Technical relevant photoinitiators are, amongst others, benzoin derivates, benzilketals, acetophenone derivates, aromatic ketones, or ionic ones like phenyl sulfonium or phosphonium derivates. [3; 4] Many of these photoinitiators themselves or their cleavage products are of health or environmental concern. This is especially a problem when the cleavage products can migrate. [4; 5] The list of initiators with low migration potential and low toxicity, which are suitable, *e.g.*, for food contact, is quite small. [4] Up to now, there is only one real natural photoinitiator that is applied on the market: camphorquinone. [4]

Photoinitiators are generally divided into two groups: Type I and type II photoinitiators. The nomenclature follows the Norrish-type reactions: [6] Type I generates reactive radicals, which can start a polymerization directly. Type II initiators, on the other side, will abstract a hydrogen atom from a donor molecule, building a reactive radical on the donor molecule, which will then start the polymerization process. [4] The donor takes a very important role in a type II initiation process and is called a synergist in an industrial context. [5] Due to the fact that most industrial-relevant synergists comprise a (ternary) amine functionality, they might also be called amine synergists. [4] But also thiols or even amino acids are reported for their use as synergists. [4]

Increasingly stricter regulations are creating a need for new, bio-based, and non-hazardous initiators. Examples of molecules being tested are, *e.g.,* riboflavin, carotene, curcumin, flavones, or α-ketoesters. [7–13] The scientific community is working particularly intensively on photoreactions in visible light. [14] The initiators used must therefore be colored *per se* in order to absorb in the visible spectrum. This has the disadvantage that the final product (coating or polymer) also inevitably takes on a color. For this reason, the following chapter will focus on natural monophenols, which also occur as building blocks in larger molecules discussed, such as curcumin or flavones. Most monophenols are colorless and absorb exclusively in the UV range. Many different monophenols occur in nature as phytochemicals and can also be synthesized natural-based, making them suitable for industrial use. [15–17]

In this chapter, a large screening on the suitability of phenolic compounds for polymerization of methyl methacrylate (MMA) in surfactant-free microemulsions (SFMEs) is done. The substances are studied as type I initiators andt type II initiators by adding natural amines, and conversion and the weight average molar mass of derived polymers are investigated.

6.3 Materials and Methods

6.3.1 Materials

Azobisisobutyronitrle (AZDN, ≥ 98%) is gratefully received from Pergan GmbH (Bocholt, Germany). *tert*-Butyl alcohol (TBA, 99%) and ethanol (EtOH, ≥ 99.8%) is purchased from Carl Roth GmbH & Co. KG (Karlsruhe, Germany). Curcumin (≥ 97%), 2,3-dihydroxybenzoic acid (> 98%), 2,4-dihydroxybenzoic acid (> 98%), 3,4-dihydroxybenzoic acid (> 98%), 2,3-dimethoxybenzoic acid (> 98%), 2,4-dimethoxybenzoic acid (> 98%), 3,4-dimethoxybenzoic acid (> 98%), 3,5-dimethoxybenzoic acid (> 98%), 3,4-dimethoxycinnamic acid (> 98%), 3-(4-hydroxyphenyl)propionic acid (> 98%), 4-hydroxy-3-methoxybenzoic acid (> 98%), m-anisic acid (> 98%), 4-methoxycinnamic acid (> 98%), o-anisic acid (> 98%), p-anisic acid (> 99%), riboflavin, sodium 3-hydroxybenzoate (> 99%), sodium 4-hydroxybenzoate (> 99%), sodium 4-hydroxy-3-methoxybenzoate (> 98%), and trans-o-coumaric acid (> 98%), are provided by TCI Deutschland GmbH (Eschborn, Germany). Riboflavin tetraacetate are synthesized and gratefully received from the chair of Prof. König (Regensburg, Germany). [18] 3,4-Dihydroxycinnamic acid (> 99%) are purchased from Acros Organics (Geel, Belgium). 3,5-Dihydroxybenzoic acid (> 98%) is provided by Fluka Analytical (Seelze, Germany). DL-Pyroglutamic acid (99%), 4-hydroxybenzoic acid (≥ 99%), p-coumaric acid (≥ 98%), sodium salicylate (≥ 99.5%), (±)-α-tocopherol (≥ 96%), trans-cinnamic acid (≥ 99%), and trans-2-methoxy cinnamic acid (98%) are obtained from Sigma-Aldrich Chemie GmbH (Steinheim, Germany). Ferulic acid is purchased from Alexmo Cosmetics GmbH (Stuhr, Germany). Gallic acid (≥ 98%), L-arginine (for biochemistry), L-histidine (for biochemistry), L-proline (≥ 99%), methyl methacrylate (MMA, 99%, stabilized with 4-methoxyphenol ≤ 30 ppm), N-methyl urea (97%), salicylic acid (≥ 99%), triethanolamine (≥ 99%), and urea (≥ 99.5) are provided by Merck KGaA (Darmstadt, Germany). *iso*-Propanol (IPA, 99.8%) and tetrahydrofuran (THF, anal. grade) are bought from Fisher Scientific GmbH (Schwerte, Germany). Poly(methyl methacrylate) standards (ReadyCal-Kit PSS-mmkitr1) are obtained from PSS Polymer Standards Service (Mainz, Germany).

Prior to polymerization, MMA is distilled at 40 °C and 60 mbars to remove the stabilizer. Aqueous solutions are prepared using deionized water with a resistivity of 18 MΩcm. All other chemicals are used without further purification.

6.3.2 Polymerizations

Samples of each 6 g are prepared in crimp-cap vials, consisting of 65 wt% water, 30 wt% IPA, and 5 wt% MMA (composition I30/5, see section 2.7.1 chapter 2), and the photoinitiators being

part of the water phase. The vials are closed with an aluminum cap with PTFE septum and flushed for 30 s with nitrogen to displace oxygen (air outlet via a second cannula). Samples are irradiated for 2 h in a home-built thermostatted gadget containing six UV-LEDs CUN66A1B (λ=365 nm, each 0.9 W, mounted on a star plate, LED-Tech.de, Mouers, Germany)) at 25 °C, whereby each LED irradiates one vial from the bottom. Polymerizations are stopped in liquid nitrogen after 2 h and freeze-dried afterward. Conversions are determined by weighing the dried polymers.

6.3.3 UV/Vis Spectroscopy

UV/Vis spectra are recorded with a Perkin Elmer Lambda 18 UV/Vis-spectrometer (Waltham, MA, USA). 3 mmol L^{-1} of each initiator is dissolved in ethanol, and samples with benzoic acid derivates are diluted further by a factor of 1:20. Cinnamic acid derivates and curcumin are further diluted by a factor of 1:25. Due to the low solubility of riboflavin in ethanol, a concentration of 0.83 mmol L^{-1} is used, filtered and further diluted to achieve the same concentration as for curcumin. Spectra are recorded from 250-450 nm in 70 µL UV-cuvettes micro from Brand GmbH + Co. KG (Wertheim, Germany).

6.3.4 Gel Permeation Chromatography (GPC)

Gel permeation chromatography (GPC) is executed and evaluated as described in section 2.3.10.

6.3.5 Bond Dissociation Enthalpies (BDE)

Bond dissociation enthalpies (BDE) are calculated using the increment tables from Guitard *et al.*, [19] if not found in literature. [20]

6.4 Results and Discussion

6.4.1 Screening of Different Phenols and Amines

As we observed fluctuations in performances in between different experiments, each setup consists of five different samples and one blank irradiated with the UV LEDs at the same time. In the blank, a polymerization occurs even in the absence of a photoinitiator to a small degree (5-15 wt% conversion). For more effective auto-photopolymerizations, radiation with higher energy/shorter wavelength than 365 nm (approx. 220-240 nm) would be necessary. [21] Chemical formulas of all tested substances are depicted in **Figure S 6.2**, **Figure S 6.3**, and **Figure S 6.4** in the appendix.

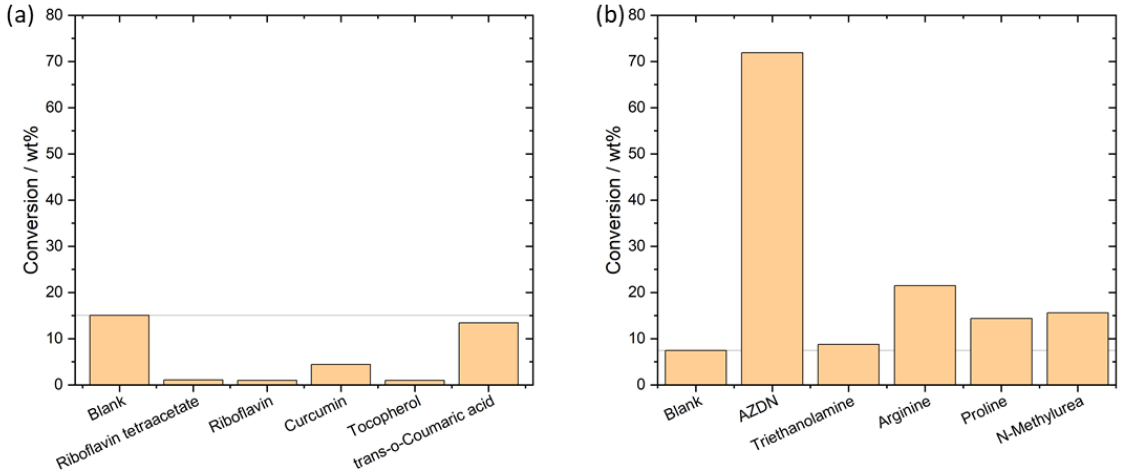

Figure 6.2 *Conversion of photoinitiated, freeze-dried polymers irradiated for 2 h. (a) Mono- and polyphenols (0.5 mol% referring to the monomer), (b) amines and AZDN as a second reference (2 mol%).*

Figure 6.2 depicts the conversions of the first tests with (a) 0.5 mol% mono- and polyphenols and (b) 2 mol% (both referring to the monomer) of different amines and AZDN as a second reference next to the blank. The results in **Figure 6.2** show that all mono- and polyphenols produce lower conversions than the blank without additives. Thus, the phenols have more of an antioxidant effect and scavenge the few radicals formed rather than initiating new ones. Most amines increase the conversions slightly (to 10-20 wt%), but only AZDN leads to relevant conversions (approx. 70 wt%). This may have different reasons: possibly, the phenols work more as a type II instead of a type I initiator. To check this, the phenols will be tested alone and with a synergist in a next step. However, also the system and the exact wavelength will have an impact. Except for coumaric acid, all substances tested in **Figure 6.2 a** are mentioned in the literature in the context of photoreactions. [7; 8] While for riboflavin, either a synergist or another wavelength might help for better performance, curcumin is reported as a type I photoinitiator at 365 nm. A

closer look into this work reveals conversions of 1-2%, while no reference without curcumin was made, which calls the whole study into question. [9]

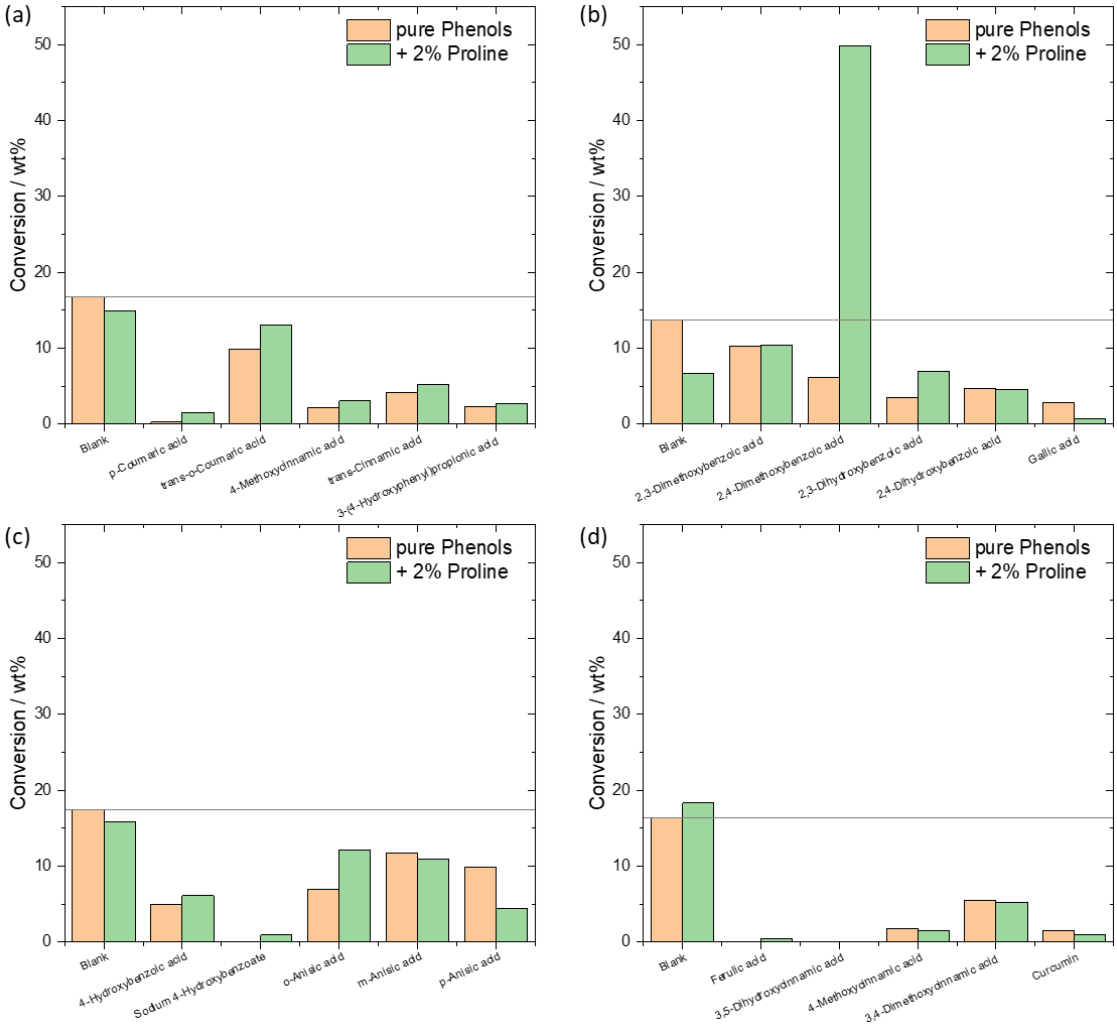

Figure 6.3 *Screening of the performance of different phenols as photoinitiators (2 mol% referring to the monomer) with and without 2 mol% proline as a synergist. The conversion after 2h irradiation time is depicted.*

Figure 6.3 and **Figure 6.4** depict the results of screenings of different phenols (2 mol% referring to the monomer each, except for **Figure 6.4 c**, where 0.5 mol% are used due to the low availability of riboflavin tetraacetate) with and without 2 mol% proline as a synergist. It must be noted that these experiments are only done once, and fluctuations in the results cannot be ruled out. However, a blank is measured in each experiment. Weight average molar masses for these systems can be found in **Table S 6.1** in the appendix. However, some results can be clearly drawn. At first, most sodium salts performed rather badly, *e.g.,* sodium 4-hydroxybenzoate (cf. **Figure 6.3 c**), sodium 3-hydroxybenzoate and sodium 4-hydroxy-3-methoxybenzoate (cf. **Figure 6.4 b**). On the other side, sodium salicylate (cf. **Figure 6.4 b**) lead to a conversion comparably with the blank. Gallic acid (cf. **Figure 6.3 b**), ferulic acid (cf. **Figure 6.3 d**), as well as curcumin, riboflavin,

and tocopherol (cf. **Figure 6.4 c**), which are all antioxidants, [19] performed badly. Also, the position of substituents seems to make a huge difference. Comparing p-coumaric acid and o-coumaric acid (cf. **Figure 6.3 a**), the para form leads to quite low conversions, while ortho-coumaric acid performs significantly better.

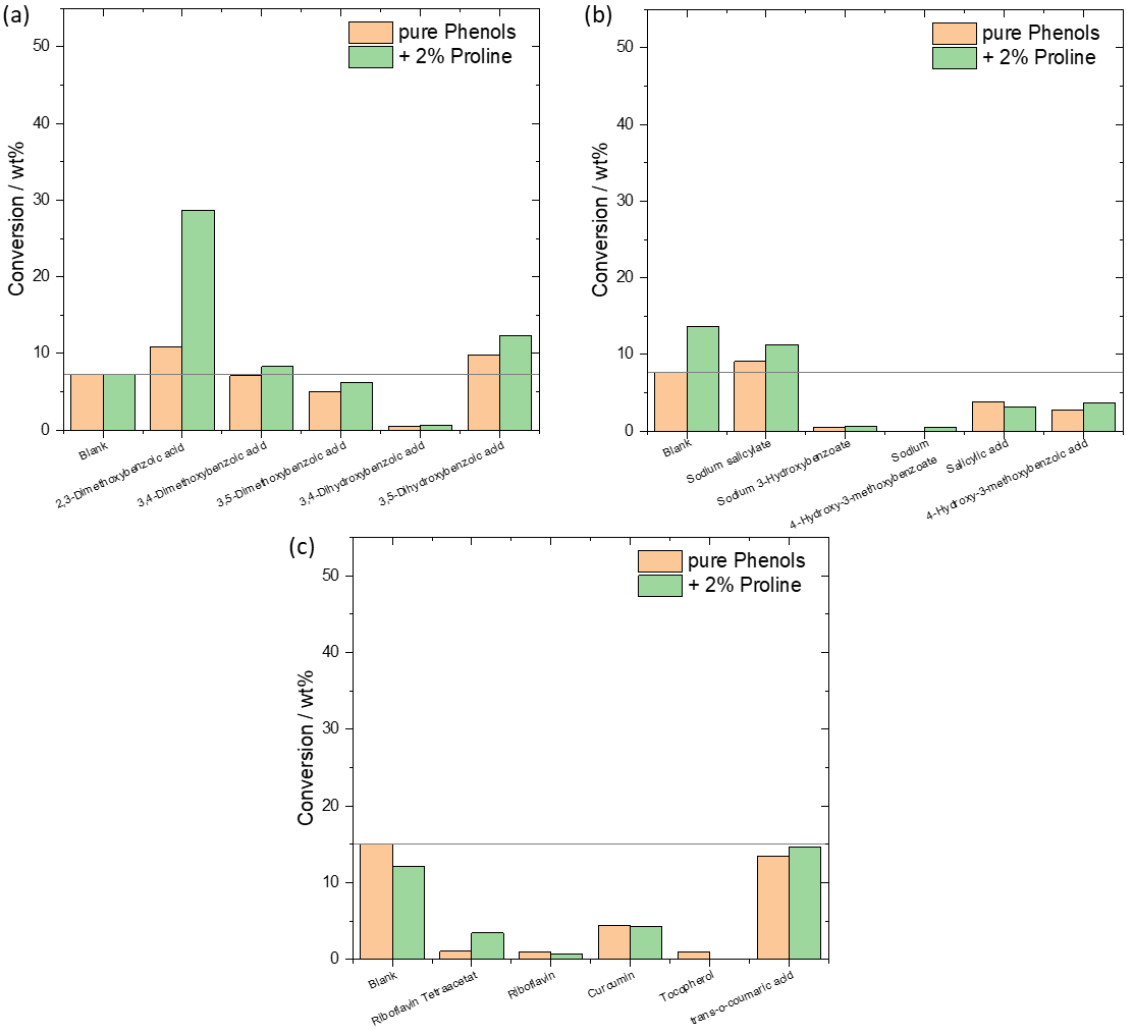

Figure 6.4 *Screening of the performance of different phenols as photoinitiators (2 mol% referring to the monomer for (a) and (b), 0.5 mol% referring to the monomer for (c)) with and without 2 mol% proline as synergist. The conversion after 2h irradiation time is depicted.*

The difference for anisic acid is lower, but the same trend might be seen (cf. **Figure 6.3 c**). Best performances are observed for 2,3- and 2,4-dimethoxybenzoic acid (**Figure 6.3 b** and **Figure 6.4 a**) and 3,5-dihydroxybenzoic acid (**Figure 6.4 a**). All three substances perform significantly better with proline as a synergist, indicating a type II mechanism. 3,5-Dihydroxybenzoic acid as well as o-coumaric acid and o-anisic acid, are chosen for further experiments, varying the synergists (cf. section 6.4.3). **Figure S 6.5** in the appendix depicts UV/VIS spectra of used photoinitiators. Even though most initiators do not have their absorption maximum around 365 nm, most still slightly

absorb in this area. No clear correlation can be drawn between the absorption and the photoinitiator performance.

6.4.2 Irradiation of Curcumin and Riboflavin with Visual Light

Riboflavin and curcumin, which both absorb in the visible light range (cf. **Figure S 6.5** in the appendix), are tested at a wavelength of 455 nm as well. **Figure 6.5** depicts conversions of riboflavin, curcumin, and riboflavin tetraacetate after 2h.

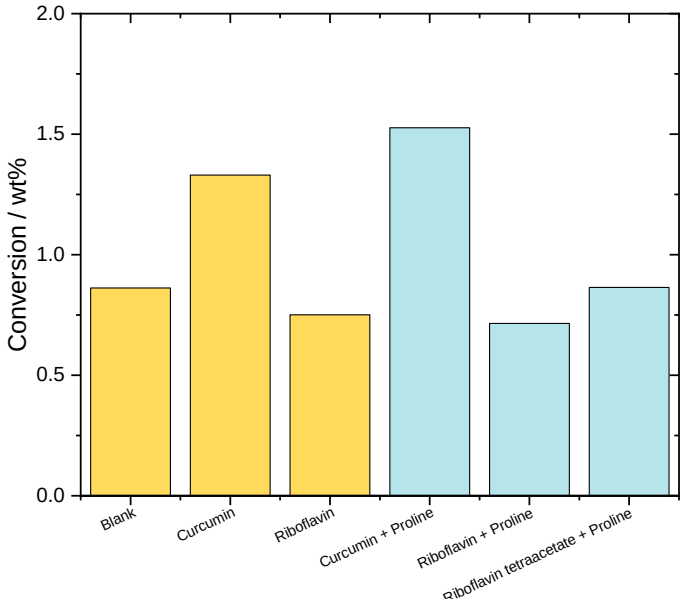

Figure 6.5 *Screening of the performance of 0.5 mol% curcumin, riboflavin, and riboflavin tetraacetate (referring to the monomer) with and without 2 mol% proline as synergist irradiated for 2h at 455 nm. The conversion after 2h irradiation time is depicted.*

Even though curcumin performs better than the blank both with and without proline, the conversion is less than 2 wt% after 2h irradiation time, showing that these substances are not suitable for light-initiated polymerizations in the SFME systems tested.

6.4.3 Further Investigation of More Effective Initiators with Different Amines

Figure 6.6 depicts conversions of 0.5 mol% of the phenols o-coumaric acid, o-anisic acid, and 3,5-dihydroxybenzoic acid with different amounts of the amine synergists proline, arginine, and histidine. o-Anisic acid does not really perform well for all three amines (cf. **Figure 6.6 b**). o-Coumaric acid and 3,5-dihydroxybenzoic acid, however, show different conversions with different amines. For o-coumaric acid, the conversion decreases with increasing histidine content, while the conversion increases beginning from 1 mol% arginine (cf. **Figure 6.6 a**). For 3,5-hydroxybenzoic acid, where arginine is not tested, histidine has the opposite effect and increased the conversion to over 70 wt% for 1 mol% histidine and to over 80 wt% for 5 mol% histidine.

These two examples show that the initiator-synergist system must be extremely balanced to obtain suitable results. It is especially interesting that histidine works well as a synergist for 3,5-dihydroxybenzoic acid, while it even declines the conversion in the case of o-coumaric acid.

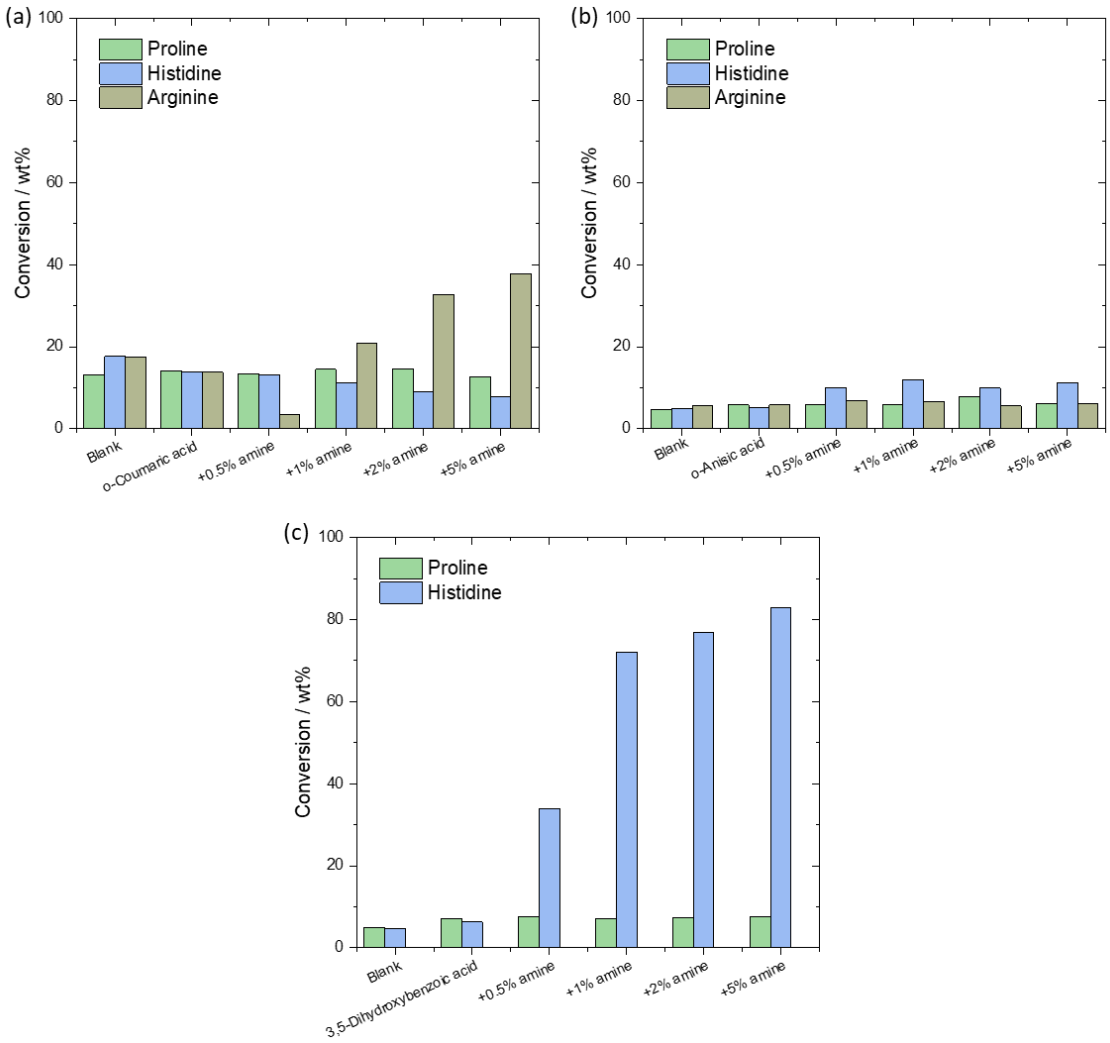

Figure 6.6 *Screening of the performance of 0.5 mol% (a) o-coumaric acid, (b) o-anisic acid, and (c) 3,5-dihydroxybenzoic acid (referring to the monomer) with different amounts of the synergistic amines proline, histidine, and arginine for 2h at 365 nm. The conversion after 2h irradiation time is depicted.*

6.4.4 Comparison of Bond Dissociation Enthalpies (BDE)

The question arises whether bond dissociation enthalpies (BDE) can somehow be correlated with the photoinitiator performance. Guitard *et al*. [19] found that the antioxidant power can be correlated directly to the BDE (lower BDE corresponds to better antioxidant power). One can think about two possibilities: a higher rate of radical forming with lower BDE or higher reactivity when the former bond had a higher BDE. **Table 6.1** shows BDEs of different phenols which performed good (+), neutral (o), or bad (-) in the screening experiments in section 6.4.1. The BDEs vary between 69 and 95 kcal mol^{-1}. trans-o-Coumaric acid and 2,5-dihydroxybenzoic acid have a

BDE of 80.1 and 83.5 kcal mol^{-1}, respectively. p-Coumaric acid, for example, also has a BDE of 80.5 kcal mol^{-1}, which, however, is very poor in the screening experiments. Both the neutral and the bad phenols cover almost the entire range of BDEs. Thus, the BDEs do not seem to have an impact on the photoinitiator performance.

Table 6.1 *BDEs of phenolic compounds compared to their photoinitiator performance based on the screening tests in section 6.4.1. BDEs marked with a star are calculated using the increment table of Guitard et al., [19] BDEs without a star are taken from the literature. [20]*

Phenolic compound	**BDE** / kcal mol^{-1}	**Photoinitiator performance**
trans-o-Coumaric acid	80.1	+
3,5-Dihydroxybenzoic acid	83.5*	+
2,3-Dihydroxybenzoic acid	86.4*; 75.7*	o
Salicylic acid	95.2	o
p-Coumaric acid	80.5	-
3-(4-Hydroxyphenyl)propionic acid	77.3*	-
Ferulic acid	79.7	-
3,4-Dihydroxycinnamic acid	72.1; 74.7*; 68.5*	-
4-Hydroxybenzoic acid	84.7	-
2,4-Dihydroxybenzoic acid	94.2*; 83.7*	-
Gallic acid	70.2; 74.7*; 67.1*	-
3,4-Dihydroxybenzoic acid	75.5; 75.9*; 75.7*	-
4-Hydroxy-3-methoxybenzoic acid	83.1	-
α-Tocopherol	69.1	-

6.5 Conclusion and Outlook

Different phenolic acid derivates with and without amino acids as synergists are investigated regarding their performance as UV photoinitiators. trans-o-Coumaric acid, o-anisic acid, 2,3-dimethoxybenzoic acid, 2,4-dimethoxybenzoic acid, and 3,5-dihydroxybenzoic acid show interesting results, but also other phenols, especially in combination with amines (like proline, arginine or histidine). The different performances of phenols and phenol/amine mixtures can neither be linked to the maximum absorption in their UV/VIS spectra nor to their bond dissociation enthalpies. [19; 20]

Both dimethoxybenzoic acids show good results with proline, while o-coumaric acid works with arginine, and 3,5-dihydroxybenzoic acid leads to conversions of more than 80 wt% with histidine. The different behavior of different amines is very interesting but cannot be explained so far. Possibly some specific interactions between the natural phenol and amine might play a role. It is known that some phenols and amino acids can form natural deep eutectic solvents (NADES). [22; 23]

Even though the mechanisms are not yet revealed, natural systems based on phenols and amino acids seem promising as photoinitiators for further research, which will be done in the ZIM project “BIOINIT” in the next two years. Next to phenolic compounds, also α-ketoacids and -esters could be promising natural UV photoinitiators. [13] Just like reported for the α-ketoacids, also phenolic acid esters could be promising. Further investigations concerning the radical species and intermediates could be done using electron paramagnetic resonance spectroscopy and ultrafast laser spectroscopy techniques, which might help in understanding the different performances of different systems. Next to their performance in polymerizable surfactant-free microemulsion (SFME) systems, also transfer and comparison of the results to water-based and water-free coating systems will be interesting. Especially the water-free systems might become challenging due to solubilization problems. However, especially NADES forming phenol-amine pairs might be interesting in overcoming solubility problems. [24]

6.6 Appendix

6.6.1 Structures of Phenols and Amines Tested as Photoinitiators

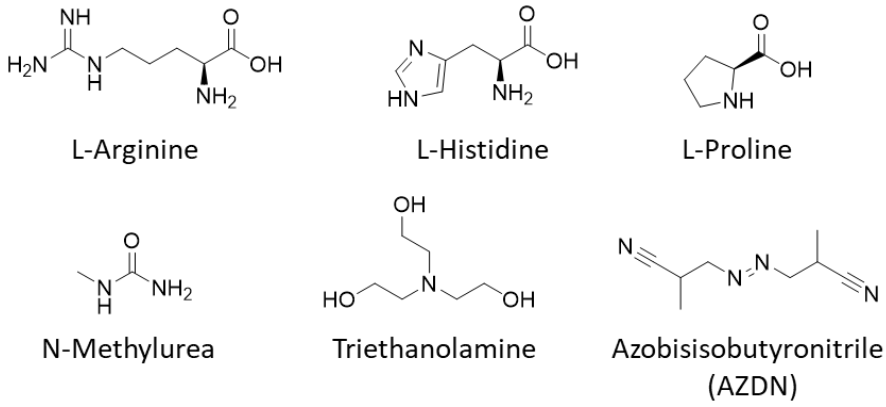

Figure S 6.1 *Structures of amines and the commercial initiator AZDN used in this chapter.*

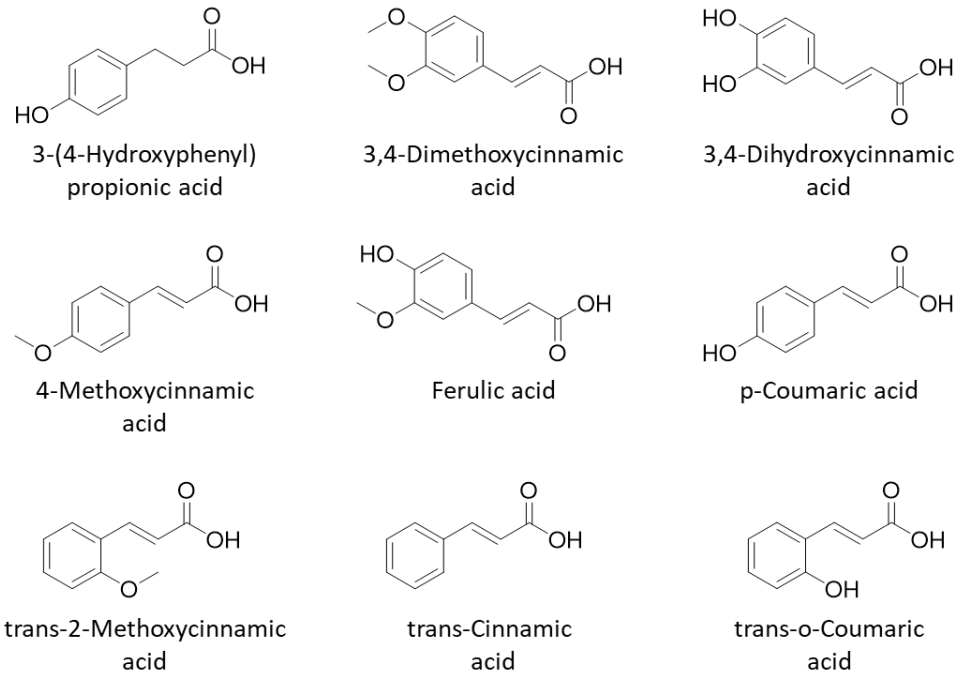

Figure S 6.2 *Structures of cinnamic acid derivates used in this chapter.*

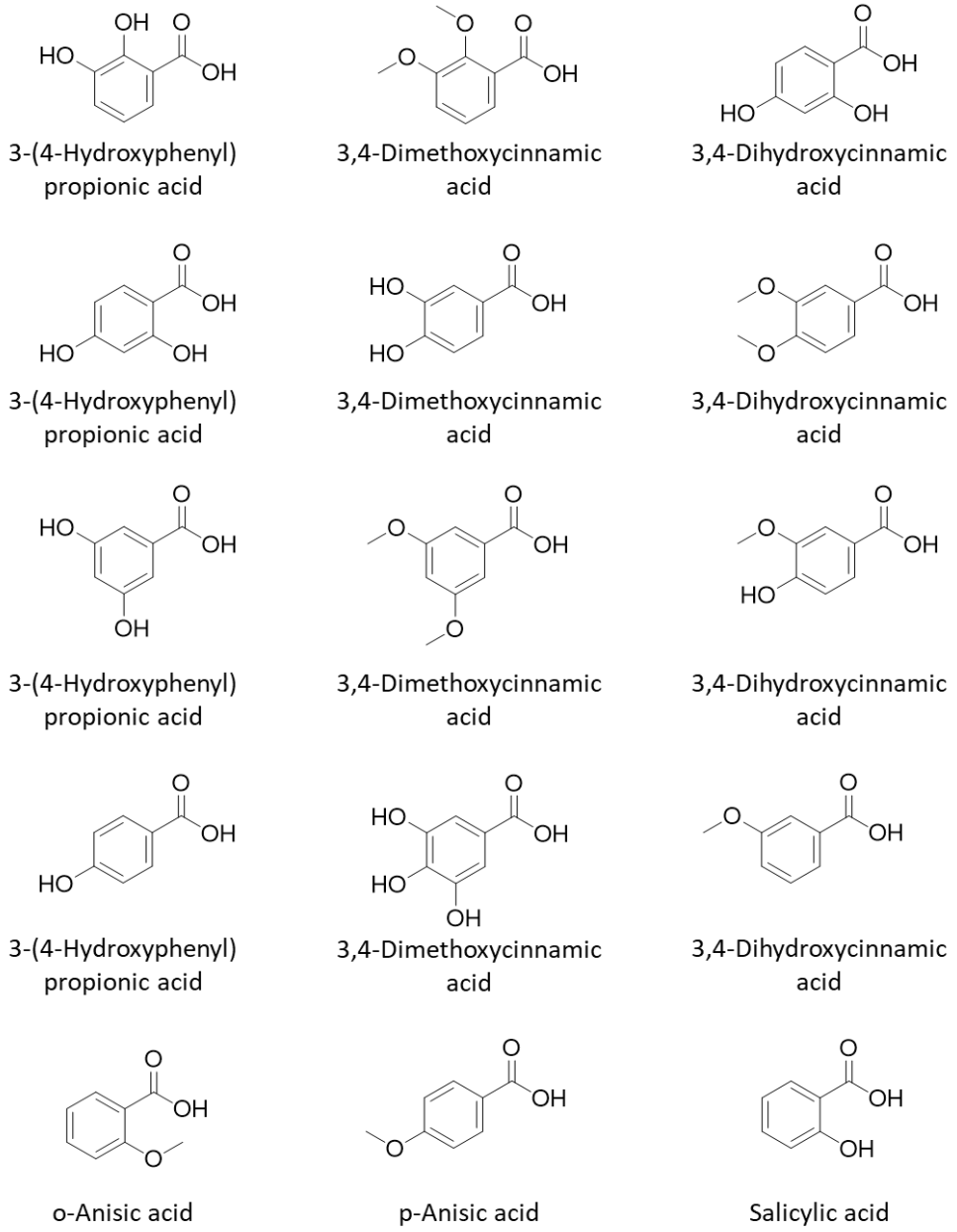

Figure S 6.3 *Structures of benzoic acid derivates used in this chapter.*

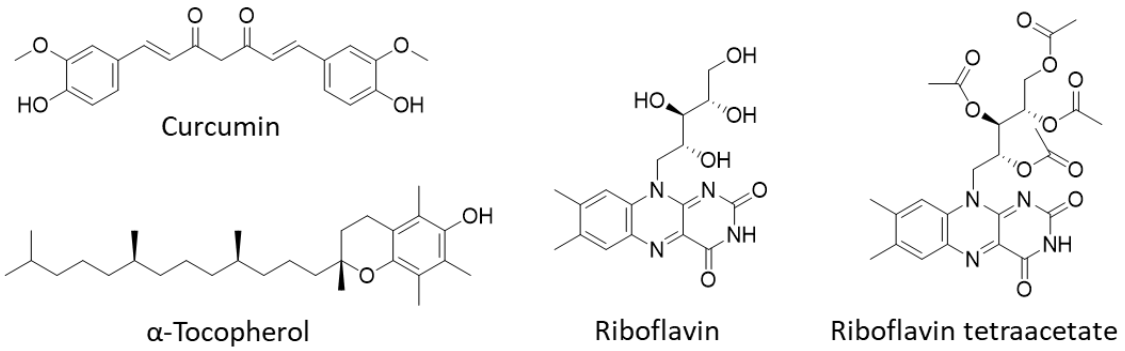

Figure S 6.4 *Structures of polyphenols and vitamins used in this chapter.*

6.6.2 UV/Vis Spectra of Investigated Phenols, Polyphenols, and Vitamins

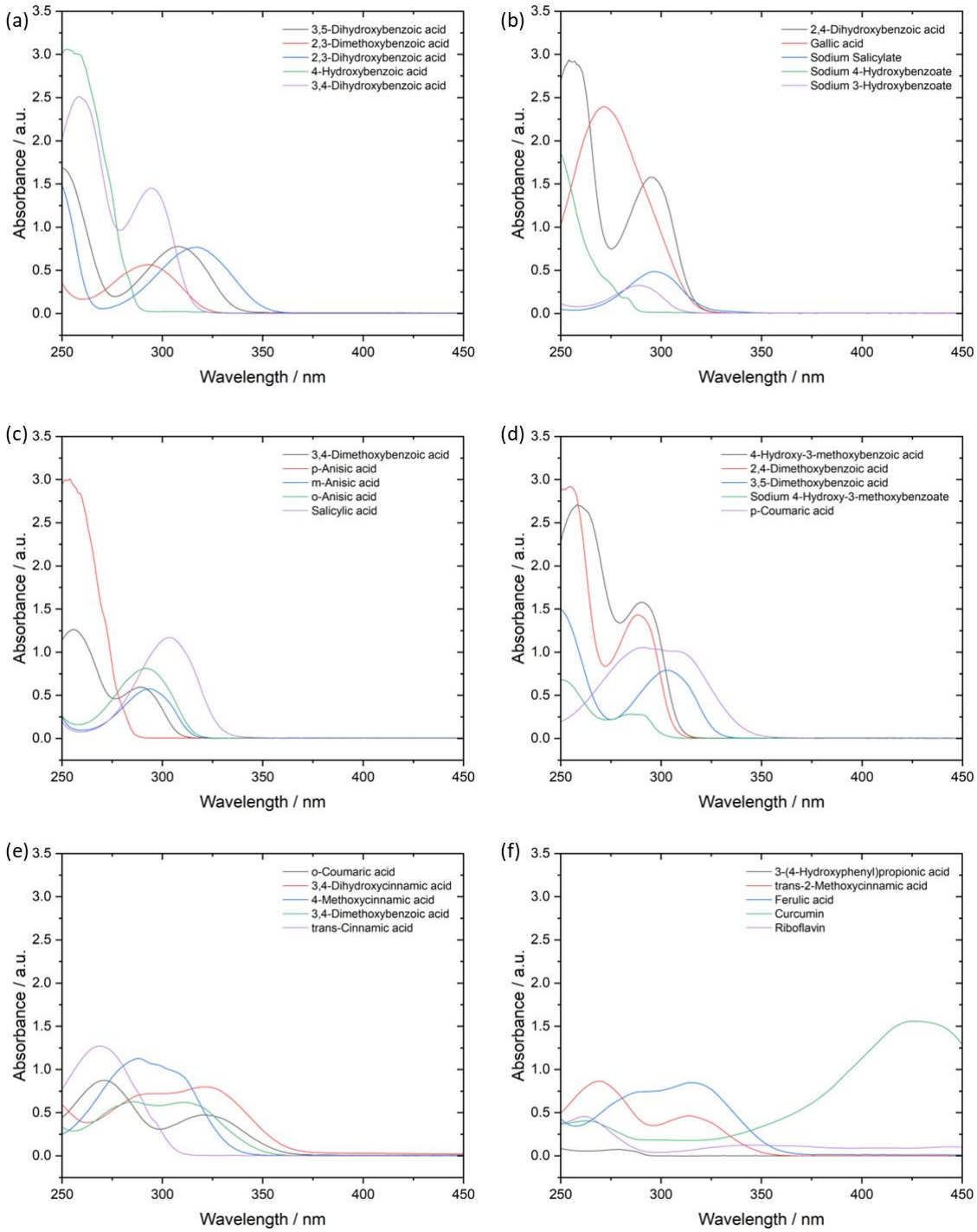

Figure S 6.5 *UV/Vis spectra of investigated phenols, polyphenols, and vitamins diluted in ethanol.*

Table S 6.1 *Weight average molar mass derived from GPC and conversion data of polymers depicted in* ***Figure 6.3*** *and* ***Figure 6.4****.*

Figure	Initiator	pure phenols		+ 2 mol% Proline	
		M_w / g mol^{-1}	Conversion / wt%	M_w / g mol^{-1}	Conversion / wt%
Figure 6.3 a	Blank	1,629,360	16.8	1,619,158	14.9
	p-Coumaric acid	-	0.3	-	1.6
	trans-o-Coumaric acid	315,406	10.0	270,183	13.1
	4-Methoxycinnamic acid	712,408	2.2	685,607	3.1
	trans-Cinnamic acid	1,085,422	4.1	1,120,168	5.2
	3-(4-Hydroxyphenyl)propionic acid	838,693	2.4	960,632	2.8
Figure 6.3 b	Blank	1,441,711	16.3	1,587,865	18.4
	Ferulic acid	-	0.0	-	0.5
	3,5-Dihydroxycinnamic acid	-	0.0	-	0.0
	4-Methoxycinnamic acid	456,564	1.8	538,810	1.5
	3,4-Dimethoxycinnamic acid	733,872	5.5	835,007	5.3
	Curcumin	-	1.5	102,354	1.0
Figure 6.3 c	Blank	1,434,892	17.4	1,589,716	15.9
	4-Hydroxybenzoic acid	-	5.0	-	6.1
	Sodium 4-Hydroxybenzoate	-	0.1	-	1.0
	o-Anisic acid	981,717	6.9	n.d.	12.2
	m-Anisic acid	932,785	11.8	1,008,561	11.0
	p-Anisic acid	1,084,805	10.0	1,103,954	4.4
Figure 6.3 d	Blank	1,502,207	13.8	1,413,282	6.6
	2,3-Dimethoxybenzoic acid	889,313	10.3	876,665	10.4
	2,4-Dimethoxybenzoic acid	1,081,434	6.2	n.d.	49.8
	2,3-Dihydroxybenzoic acid	369,983	3.5	625,571	6.9
	2,4-Dihydroxybenzoic acid	1,019,655	4.7	816,676	4.6
	Gallic acid	563,287	2.8	-	0.7
Figure 6.4 a	Blank	1,057,268	7.2	1,100,992	7.3
	2,3-Dimethoxybenzoic acid	860,059	10.9	1,011,077	28.7
	3,4-Dimethoxybenzoic acid	910,162	7.1	965,835	8.3
	3,5-Dimethoxybenzoic acid	907,422	5.1	1,011,823	6.3
	3,4-Dihydroxybenzoic acid	-	0.4	412	0.6
	3,5-Dihydroxybenzoic acid	879,876	9.8	927,319	12.3
Figure 6.4 b	Blank	1,121,550	7.6	1,324,944	13.6
	Sodium salicylate	n.d.	9.1	859,248	11.3
	Sodium 3-Hydroxybenzoate	-	0.5	-	0.6
	Sodium 4-Hydroxy-3-methoxyben-zoate	-	0.0	-	0.5
	Salicylic acid	676,091	3.8	639,360	3.2
	4-Hydroxy-3-methoxybenzoic acid	825,640	2.8	837,894	3.7
Figure 6.4 c	Blank	1,374,484	15.1	1,314,772	12.1
	Riboflavin Tetraacetat	-	1.1	n.d.	3.5
	Riboflavin	-	1.0	-	0.7
	Curcumin	316,539	4.4	n.d.	4.3
	Tocopherol	-	1.0	-	0.0
	trans-o-coumaric acid	651,885	13.4	n.d.	14.6

6.7 Bibliography

[1] C. Decker, *Polym. Int.* **1998**, *45,* 133–141.

[2] V. Shukla, M. Bajpai, D. K. Singh, M. Singh, and R. Shukla, *Pigment Resin Technol.* **2004**, *33,* 272–279.

[3] H. J. Hageman, *Prog. Org. Coat.* **1985**, *13,* 123–150.

[4] W. A. Green, *Industrial photoinitiators,* CRC Press, Boca Raton, **2010**.

[5] N. S. Allen, *J. Photochem. Photobiol., A* **1996**, *100,* 101–107.

[6] B. Marchetti, T. N. V. Karsili, and M. N. R. Ashfold, *Phys. Chem. Chem. Phys.* **2019**, *21,* 14418–14428.

[7] I. Ahmad, K. Iqbal, M. A. Sheraz, S. Ahmed, T. Mirza, S. H. Kazi, and M. Aminuddin, *ISRN Pharm.* **2013**, *2013,* 958712.

[8] G. Noirbent, and F. Dumur, *Eur. Polym. J.* **2021**, *142,* 110109.

[9] A. Mishra, and S. Daswal, *J. Macromol. Sci. A* **2005**, *42,* 1667–1678.

[10] B. Orellana, A. M. Rufs, M. V. Encinas, C. M. Previtali, and S. Bertolotti, *Macromolecules* **1999**, *32,* 6570–6573.

[11] I. Zaborniak, and P. Chmielarz, *Eur. Polym. J.* **2021**, *142,* 110152.

[12] I. Zaborniak, P. Chmielarz, and K. Wolski, *Eur. Polym. J.* **2020**, *140,* 110055.

[13] P. Gauss, M. Griesser, M. Markovic, A. Ovsianikov, G. Gescheidt, P. Knaack, and R. Liska, *Macromolecules* **2019**, *52,* 2814–2821.

[14] B. König, *Eur. J. Org. Chem.* **2017**, *2017,* 1979–1981.

[15] M. Fache, B. Boutevin, and S. Caillol, *ACS Sustainable Chem. Eng.* **2016**, *4,* 35–46.

[16] E. Hofmann, P. Degot, D. Touraud, B. König, and W. Kunz, *Food chemistry* **2023**, *417,* 135944.

[17] N. Ruwizhi, and B. A. Aderibigbe, *Int. J. Mol. Sci.* **2020**, *21*.

[18] E. Hofmann. Dissertation, Universität Regensburg, Regensburg, **2023**.

[19] R. Guitard, V. Nardello-Rataj, and J.-M. Aubry, *Int. J. Mol. Sci.* **2016**, *17*.

[20] R. Guitard, J.-F. Paul, V. Nardello-Rataj, and J.-M. Aubry, *Food chemistry* **2016**, *213,* 284–295.

[21] A. Jagtap, and A. More, *Polym. Bull.* **2022**, *79,* 8057–8091.

[22] A. Maimulyanti, I. Nurhidayati, B. Mellisani, F. Amelia Rachmawati Putri, F. Puspita, and A. Restu Prihadi, *Arabian Journal of Chemistry* **2023**, *16,* 104634.

[23] V. Huber. Dissertation, Universität Regensburg, **2022**.

[24] V. Huber, L. Muller, P. Degot, D. Touraud, and W. Kunz, *Food chemistry* **2021**, *355,* 129624.

7 Epilogue

7.1 Conclusion and Outlook

Microemulsion systems comprise an interesting reaction medium for polymerizations, allowing precise control of the polymerization kinetics and morphologies. In this work, the applicability of surfactant-free microemulsions (SFMEs) for free-radical polymerizations is studied.

Chapter 1 (General Background) gives an introduction to the topic, important fundamental knowledge for this topic as well as the current state of the art.

Chapter 2 (Surfactant-free Microemulsion and Microsuspension Polymerization of Methyl Methacrylate) is a proof-of-concept for polymerizations in SFME. A new method for the preparation of poly(methyl methacrylate) (PMMA) in surfactant-free microemulsions is presented. Using simple mesostructured systems comprising of water, a short-chain alcohol as the hydrotrope (ethanol (EtOH), *n*-propanol (NPA), *iso*-propanol (IPA), or *tert*-butyl alcohol (TBA)), and the monomer as the oil phase allows to gain control over polymer size, molar masses, kinetics, and macroscopic polymer morphologies without the help of any surfactants. The method is likely to be applicable to a large number of acrylic monomers. In contrast to surfactants, all auxiliaries (water, alcohols) can be completely removed after the polymerization, *e.g.*, by distillation and re-used. The method is different from the classifications of polymerization reactions in conventional (surfactant- or protective colloid- or solution-based) reaction media. Molar masses and conversions range in the same size region as PMMA particles derived from conventional microsuspension polymerizations. As expected, ethanol-based reaction mixtures, in which no mesostructures could be found in the initial starting mixture, lead to much higher molar masses and lower yields compared to the SFME systems used. It is found that the composition of the MMA-rich pseudo-phase and its repulsive force play a decisive role in conversion and the weight average molar mass.

Chapter 3 (Industrially Relevant (Co)polymers and Hydrotropes for Use in SFME Polymerization) extends the method presented in the previous chapter. Further, industrial-relevant monomers like acrylonitrile (AN), styrene, vinyl chloride (VC), vinyl acetate (VAc), and acrylic acid (AA) are considered. Furthermore, glycol ethers are used as hydrotropes in the system with MMA. All systems are investigated concerning their phase behavior with different hydrotropes. Since VC is gaseous at standard conditions, its industrial precursor, dichloroethane, is used for experiments. For all monomers and some of the glycol ethers, SFMEs can be formed, and structuring is found in dynamic light scattering (DLS) experiments. Polymerizations are done in the systems VAc/MMA and VAc/AA. While the polymerization of VAc-AA copolymers work well, VAc-MMA copolymers do not yield promising results at first sight. VAc is known to be a monomer with rather low reactivity, causing these problems. Nevertheless, the results are very interesting: The choice of the system has an influence on the reaction kinetics, the properties of the polymer, and the monomer ratios in the resulting copolymer. Thus, even though the example VAc-MMA does not work well, using an SFME as a reaction medium might give access to copolymers that are hardly formed due to bad copolymerization rates.

Chapter 4 (Surfactant-free Microemulsions (SFMEs) as a Template for Porous Polymer Synthesis) focuses on morphologies derived from polymerizations in SFME. The systems water, IPA or TBA, MMA (which has already been studied in Chapter 2), as well as a copolymer system with 2-hydroxyethyl methacrylate (HEMA) and MMA are investigated. The phase behavior is investigated in equidistance to the binodal from the water-rich to the monomer-rich corner of the phase diagrams. A nonionic surfactant-based system using ethoxylated alcohols and HEMA as a copolymer is used as a reference. It is found that it is possible to achieve different kinds of mesostructured polymers linked to structures expected in previous SFMEs (droplet-like shapes coming from W/O-like SFME, as well as sponge-like shapes derived from bicontinuous or O/W-like SFMEs). Sizes of polymer particles are in the range of 200 nm to > 1 µm, dependent on the system used. Polymers derived from the surfactant-free system and the surfactant-based reference system seem very similar, showing that surfactants are not necessary for template synthesis in microemulsions. It seems as if not the nonionic surfactant but the interaction of water, MMA, and HEMA is responsible for the kind of structuring observed.

The impact of surfactants on SFMEs is the topic of **Chapter 5** (The Impact of Additives on Surfactant-free Microemulsions and Polymerizations in Those). In the first part of this chapter, the impact of sodium dodecyl sulfate (SDS) and other anionic and nonionic surfactants on the phase behavior of different SFME systems are investigated. It is found that the addition of SDS in rather

small amounts can significantly decrease the biphasic region. Probably, SDS is incorporated into the already existing interphase of pre-Ouzo aggregates, leading to the stabilization of the fluctuations and decrease in the autocorrelation function derived from DLS. When adding even more SDS, a shift toward a conventional, micellar system can be observed. In the region where the biphasic region is decreased (former Ouzo region), very intense structuring can be observed. Here, SDS is obviously able to stabilize quite pronounced fluctuations. The existence of a pre-Ouzo system, which is linked to the Ouzo effect, seems to be necessary. Nonionic surfactants, on the other side, do not impact the location of the binodal, as already found for the system in chapter 4. The nonionic surfactants will surely incorporate into the existing interphase, as well. Thus, electrostatics must be the relevant driving force for the effect observed. In the second part of this chapter, the impact of SDS and various electrolytes is tested on the polymerizable SFME system water, *iso*-propanol or *tert*-butyl alcohol, and MMA. The same effect as described for other SFME systems occurs upon the addition of SDS. The conversion and molar mass are both extremely dependent on SDS and increase quite proportionally to the SDS concentration. Concerning salts, it is found that hard, highly hydrated ions lead to a strong salting-out effect due to the salting-out of the alcohols from the water-rich domain. Soft, weakly hydrated ions do not really impact the position of the binodal. Free-radical surfactant-free microsuspension polymerizations are extremely influenced by the addition of salts. Overall, the impact of anions is significantly higher than that of cations. The addition of any salt decreases the conversion and average molar mass. However, the decrease is lower for hard, very hydrated ions (which will stay in the water-rich phase and thus at a higher distance to where the polymerization reactions take place). Even softer anions (Br^-, I^-, and SCN^-) can react with the radicals themselves, quenching the polymerization. This study shows that specific ion effects should be considered when choosing cations and anions for polymerization processes, *e.g.*, the counterions of persulfates used in microemulsion polymerizations.

The last **Chapter 6** (Natural Photoinitiator Systems for Polymerizations in SFMEs) comprises a first study of the use of natural phenols, polyphenols, vitamins, and amino acids as UV photoinitiators in the SFME system with water, IPA, and MMA. The results of this pre-study reveal that the combination of some monophenols and amino acids can be promising type II photoinitiators. A more detailed study of these initiator systems as well as the transfer to industrial-relevant UV curing coating systems, will be done in the ZIM project “BIOINIT” in the next years.

The present work focuses on the usage of SFMEs for free-radical polymerizations and allows answering first questions. It can surely be proven that the weak structuring of SFMEs is sufficient for use in free-radical polymerizations. Not only the polymerization kinetics, conversions, and

average molar masses but also the morphologies can be fine-tuned in these systems without the need for surfactants. The submitted patent underlines the novelty and economic relevance of this work. The advantages are clear: The use of low-cost, non-critical chemicals, the ability to separate all process chemicals (*e.g.*, by distillation), and the ability to derive ultrapure polymers from the process. However, there are also disadvantages that need to be mentioned: A lower space-time yield due to limited monomer quantities (depending on the system) and the use of volatile organic compounds (VOCs), which may place higher demands on process safety. Therefore, the method might be particularly interesting for special applications that require very pure polymers, for example, medical technology. Subtle structuring may also provide access to copolymers that are otherwise difficult to synthesize due to very different monomer solubilities and poor copolymerization parameters.

It could be proven that many industrially relevant monomers are suitable for polymerizations in SFME. On the way to scale up and even to an application, especially relevant polymers or copolymers have to be identified in the next step. Afterward, the target properties of the polymer must at first be defined in order to be able to really compare the results of surfactant-free and conventional microemulsion or microsuspension polymers. These properties are mostly hidden as know-how in the industry and require an industrial partner for further research.

From a scientific point of view, it would surely be interesting to gain a deeper insight into what exactly happens during the polymerization process. Especially spectroscopic in-situ methods could be interesting tools. A better understanding of the systems might not only help to further separate the impacts of alcohols, initiators, temperature, and mesostructuring on polymerizations in SFME. The results could also be relevant for the understanding of conventional polymerization processes and a better insight into the Ouzo and pre-Ouzo effect.

A deeper understanding of the interaction of surfactant-free, mesostructured systems, and surfactants might not only be interesting for polymerizations. Understanding the impact of these distinct interactions could completely change the view on conventional microemulsion systems with high cosurfactant or solvent ratios.

Microemulsions, in general, are an indispensable part of industrial processes. Comparing SFMEs and conventional microemulsions for application can help to get an insight into the requirements for the system: Do we require a distinct interface? Is subtle, surfactant-free compartmentation sufficient? Or is it just a question of solubility? As this thesis shows, SFMEs can be a promising alternative as a reaction medium for free-radical polymerizations. Obviously, a subtle,

surfactant-free mesostructuring is sufficient for controlling polymerization kinetics, conversion, molar mass, and morphology. However, classical surfactant-based microemulsions will still be mandatory when a reaction medium with a well-defined and well-stabilized interface is required. In the near future, we expect that applications of surfactant-free and conventional microemulsions will develop in parallel, depending on the real requirements of the system and the latter product.

7.2 List of Scientific Contributions

7.2.1 List of Publications and Patents

(1) **J. Blahnik**, E. Müller, L. Braun, P. Denk, and W. Kunz: *Nanoscopicmicroheterogeneities or pseudo-phase separations in non-conventional liquids,* COCIS, **2022**, *57*, 101535

(2) W. Kunz, S. Krickl, **J. Blahnik**, and K. Schmid: *Microemulsion or microsuspension process for the production of a polymer dispersion, and polymer particles obtained by the process,* **2022**, WO2022112481A1

(3) **J. Blahnik**, S. Krickl, K. Schmid, E. Müller, and W. Kunz: *Microemulsion and microsuspension polymerization of methyl methacrylate in surfactant-free microemulsions (SFME*), JCIS, **2023**, *648*, 755-767

(4) **J. Blahnik**, J. Schuster, R. Müller, E. Müller, and W. Kunz: *Surfactant-free microemulsions as templates for porous polymer synthesis*, JCIS, **2024**, *655*, 371-382

7.2.2 List of Conference Contributions

(1) *Free-radical Polymerizations in Surfactant-Free Microemulsions*, Poster presentation, Zsigmondy-Colloquium of the German Colloidal Society, **2022**, Aachen, Germany.

(2) *The Impact of Surfactant-Free Mesostructured Liquids on Free-Radical Polymerization in Those*, Poster presentation, European Colloid and Interphase Society Conference, **2022**, Chania, Greece.

7.3 Eidesstattliche Erklärung

(1) Ich erkläre hiermit an Eides statt, dass ich die vorliegende Arbeit ohne unzulässige Hilfe Dritter und ohne Benutzung anderer als der angegebenen Hilfsmittel angefertigt habe; die aus anderen Quellen direkt oder indirekt übernommenen Daten und Konzepte sind unter Angabe des Literaturzitats gekennzeichnet.

(2) Die zu Beginn eines Kapitels aufgeführten Personen haben meine Arbeit in der beschriebenen Weise unentgeltlich unterstützt.

(3) Weitere Personen waren an der inhaltlich-materiellen Herstellung der vorliegenden Arbeit nicht beteiligt. Insbesondere habe ich hierfür nicht die entgeltliche Hilfe eines Promotionsberaters oder anderer Personen in Anspruch genommen. Niemand hat von mir weder unmittelbar noch mittelbar geldwerte Leistungen für Arbeiten erhalten, die im Zusammenhang mit dem Inhalt der vorgelegten Dissertation stehen.

(4) Die Arbeit wurde bisher weder im In- noch im Ausland in gleicher oder ähnlicher Form einer anderen Prüfungsbehörde vorgelegt.

Regensburg, 26.09.2023

Jonas Blahnik